University of Southern Queensland
Faculty of Engineering & Surveying

Fast-Response Piezoresistive Pressure Transducers For Thermofluids Experiments

A dissertation submitted by

Peter Hockings

in fulfilment of the requirements of

ENG4112 Research Project

towards the degree of

Bachelor of (Mechanical Engineering)

Submitted: October, 2004

Abstract

Thermofluids experiments often require the use of fast-response pressure transducers that maintain their accuracy over a wide range of operating temperatures. Existing pressure sensing technologies are available which suit these demanding applications, however these transducers are usually relatively expensive. This project investigates the use of inexpensive piezoresistive pressure transducers in the measurement of transient fluid pressures.

A temperature compensation routine was developed which improved the accuracy of the piezoresistive pressure transducers over a substantial range of operating temperatures. A dynamic response analysis indicated that the diaphragm resonant frequency of these sensors was 246.7 kHz (without the addition of latex or grease) and that the response times could be improved from approximately 12.5 μs to 0.38 μs with simple case modifications. These results demonstrated the suitability of piezoresistive pressure transducers for use in fast-response thermofluids experiments.

A piezoresistive pressure transducer produced very similar results to a piezoelectric sensor when both devices were tested simultaneously in the USQ Gun Tunnel. This indicated that the piezoresistive sensor was capable of accurately recording rapid fluctuations in pressure levels. The cylinder pressures of an internal combustion engine recorded by a piezoresistive and piezoelectric sensor also compared well. The high operational temperatures of the engine verified the success of the piezoresistive sensor temperature compensation routine.

University of Southern Queensland

Faculty of Engineering and Surveying

ENG4111/2 *Research Project*

Limitations of Use

Prof G Baker

Dean

Faculty of Engineering and Surveying

Certification of Dissertation

I certify that the ideas, designs and experimental work, results, analyses and conclusions set out in this dissertation are entirely my own effort, except where otherwise indicated and acknowledged.

I further certify that the work is original and has not been previously submitted for assessment in any other course or institution, except where specifically stated.

Peter Hockings

Q11219289

Signature

Date

Acknowledgments

I would like to sincerely thank the following individuals for their assistance in my work. Without the support of these people this project could not have reached completion.

Dr. David Buttsworth for his guidance and patience. Even with such a large number of project students, David was still able to find the time to lend assistance when it was needed.

Dr. Ahmad Sharifian for his assistance in the last few weeks of semester 2, once David had left for England.

The staff from the mechanical and electrical workshops for their vital contributions of supplying and manufacturing various components.

Finally, a special thankyou to my family, college friends and my girlfriend Emily. The understanding and support of these people was invaluable to the successful completion of this dissertation.

Peter Hockings

University of Southern Queensland

October 2004

Contents

List of Figures

List of Tables

Chapter 1

Introduction

This project investigates the performance characteristics of piezoresistive pressure transducers under high temperature operation and transient pressure measurement. Static calibrations and temperature compensation will be investigated as well as the dynamic response characteristics of the piezoresistive pressure transducers. These sensors will be applied to measurement of the cylinder pressures of an internal combustion engine and pressures within the USQ Gun Tunnel. The measurements taken with these pressure sensors can then be analysed and compared with similar data produced from other available types of transducers and various theoretical methods. The performance and suitability of piezoresistive pressure sensors for these applications can then be evaluated.

1.0.1 Project Aims and Objectives

This project aims to identify the frequency and temperature response characteristics of low cost piezoresistive pressure transducers and provide accurate calibration to allow these pressure sensors to be used with a high degree of confidence in fast-response thermofluids experiments.

The specific objectives of the project are as follows -

1. Review existing techniques for temperature measurement and compensation in

piezoresistive pressure measurement devices.

2. Devise appropriate electrical circuits to implement such techniques.
3. Devise suitable apparatus for quasi-static calibration of pressure transducers for both pressure and temperature sensitivity.
4. Perform calibrations on selected transducers.
5. Investigate the dynamic response of sensors of various configurations (added grease, modified cases etc.) using a shock tube calibration.
6. Obtain pressure measurements in a Gun Tunnel.
7. Analyse the measurements from the Gun Tunnel and compare with data obtained from a piezoelectric sensor.
8. Obtain pressure measurements in an IC engine.
9. Analyse the measurements from the IC engine and compare with data obtained from a piezoelectric sensor.

   as time permits -

10. Compare the measurements from the Gun Tunnel with predictions based on a computational model (Lagrangian quasi one dimensional).
11. Compare the measurements from the IC engine with predictions based on a computational model (thermodynamic engine simulation).

1.1 Overview of the Dissertation

This dissertation is organized as follows:

Chapter 2 covers the literature review, background and assessment of consequential effects.

Chapter 3 introduces the Design Methodology for this project.

Chapter 4 discusses static sensor calibration and temperature compensation techniques for piezoresistive sensors.

Chapter 5 covers the testing and analysis of the dynamic response characteristics of the piezoresistive sensors.

Chapter 6 investigates the application of measuring pressures within the Gun Tunnel using piezoresistive pressure sensors.

Chapter 7 examines the use of piezoresistive pressure transducers in the measurement of cylinder pressures of an IC engine

Chapter 8 draws conclusions for this dissertation and suggests possible further work.

Chapter 2

Background, Literature Review and Assessment of Consequential Effects

2.1 Project Background

Experimental testing facilities (including Gun Tunnels and Shock Tubes) and common machinery (such as the internal combustion engine) may require the measurement of internal pressures (both static and dynamic). This allows an analysis of their performance and provides further understanding of the thermofluids process that occur.

Measurement of pressures in the cases outlined above requires fast-response sensors that are able to withstand extreme operational conditions (such as high operating temperatures and fast fluctuations of pressure). While some expensive pressure sensors have been developed that are capable of responding to fast-response situations (such as high-end piezoelectric pressure sensors), the piezoresistive pressure transducer possibly offers a low cost solution. Generally, a low cost piezoresistive pressure sensor costs \$100 to \$200. A piezoelectric sensor may cost approximately \$2000. If a pressure measurement experiment also risks sensor damage, the use of an accurate low cost pressure sensor would be ideal.

Typically, piezoresistive pressure transducers have been used for the measurement of static or quasi-static pressure levels. This project aims to test the dynamic response characteristics of the sensors and investigate the feasibility of using these piezoresistive sensors for fast response measurements. The temperature effects on the sensors will also be analysed. This will ultimately allow a temperature compensation technique that maintains accurate pressure measurements in a wide variety of harsh operational environments.

2.2 Literature Review

2.2.1 Background - Piezoresistive Pressure Transducers

The typical fast-response piezoresistive pressure transducer relies on accurately measuring the deflection of a diaphragm (typically silicon) that is caused by fluid pressures. These sensors are generally low cost and can be implemented in a wide variety of applications. A diagram of a typical piezoresistive pressure transducer is shown in figure 2.1.

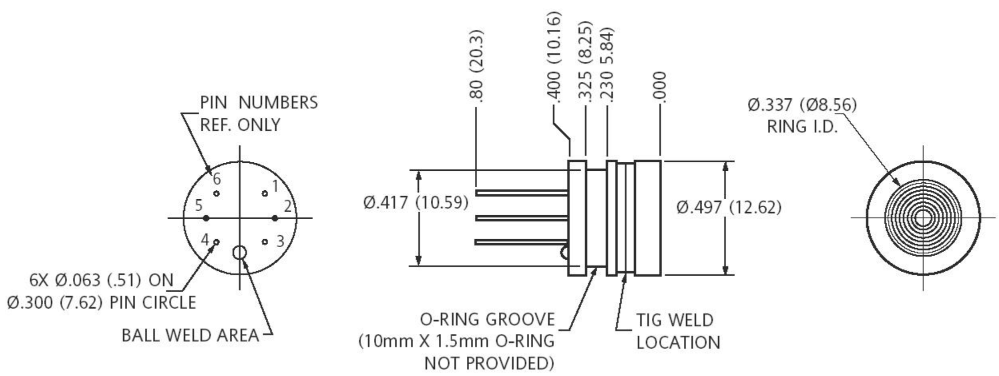

Figure 2.1: The Sensym 13U Stainless Steel Pressure Transducer (Honeywell/Sensym)

Some advantages associated with the piezoresistive pressure transducer are (Microsystems),

- Low-cost sensor fabrication opportunity.
- Mature processing technology.

- Different pressure levels can be achieved according to the application.
- Wide range of pressure sensitivities.
- Read-out circuitry can be either on-chip or discrete.

There are also some disadvantages of piezoresistive pressure sensors (MAXIM 2001),

- Strong nonlinear dependence of the full-scale signal on temperature (up to 1%/kelvin)
- Large initial offset (up to 100% of full scale or more)
- Strong drift of offset with temperature

The disadvantages associated with temperature dependance can be overcome (or at least, greatly reduced) using the temperature compensation techniques discussed in later sections.

The basic construction of the piezoresistive pressure transducer is shown in figure 2.2.

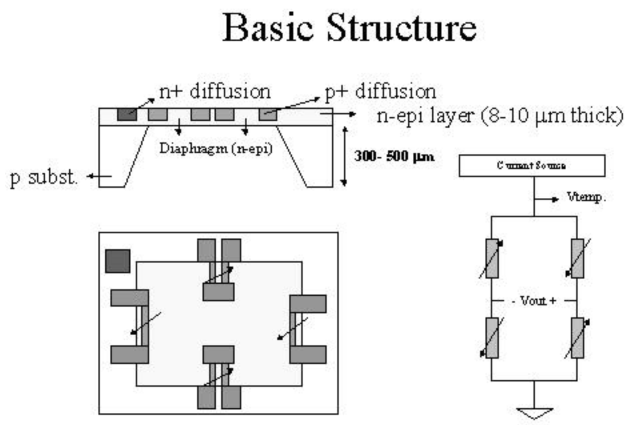

Figure 2.2: Basic Structure of Piezoresistive Pressure Transducer (MAXIM 2001)

Using diffusion methods, 4 piezoresistive elements are positioned on the top surface of the diaphragm. The elements change their resistance according to the level of strain. Therefore, as the diaphragm deflects (due to the fluid pressure), the resistance of each of the elements change.

The typical electrical circuit of a piezoresistive pressure transducer can be seen in figure 2.3. The design of the silicon diaphragm causes two resistive elements to be placed under compression and two to be placed under tension as the diaphragm deflects. This causes the resistance to increase in two elements, and decrease in the remaining two. This change in resistance is represented by ΔR in figure 2.3. The shift in the values of resistance causes a voltage difference between V1 and V2. This voltage difference is measured as the value of V_{out}. The value of V_{out} is linearly related to the applied fluid pressure.

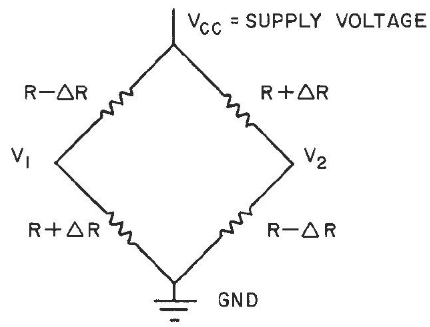

Figure 2.3: Wheatstone Circuit of the Pressure Transducer (Honeywell)

The transducer sensitivity can be determined through a static calibration process. The value of V_{out} may then be used to calculated the fluid pressure applied to the transducer.

Advances in production technology, such as the rapid developments in the semiconductor industry in the 1960s (Ainsworth et al. 2000), have enabled piezoresistive pressure transducers to become more compact, improved the quality of construction and minimizing the cost of production.

2.2.2 Temperature Compensation

One major issue in the use of piezoresistive pressure transducers is their temperature sensitivity. The output of the sensor may therefore require compensation for temperature effects. Temperature related errors may severely compromise the sensor accuracy under operation in extreme hot or cold environments.

Figure 2.4 displays temperature compensated and uncompensated sensor outputs. These plots demonstrate the high degree of temperature sensitivity of a piezoresistive pressure transducer.

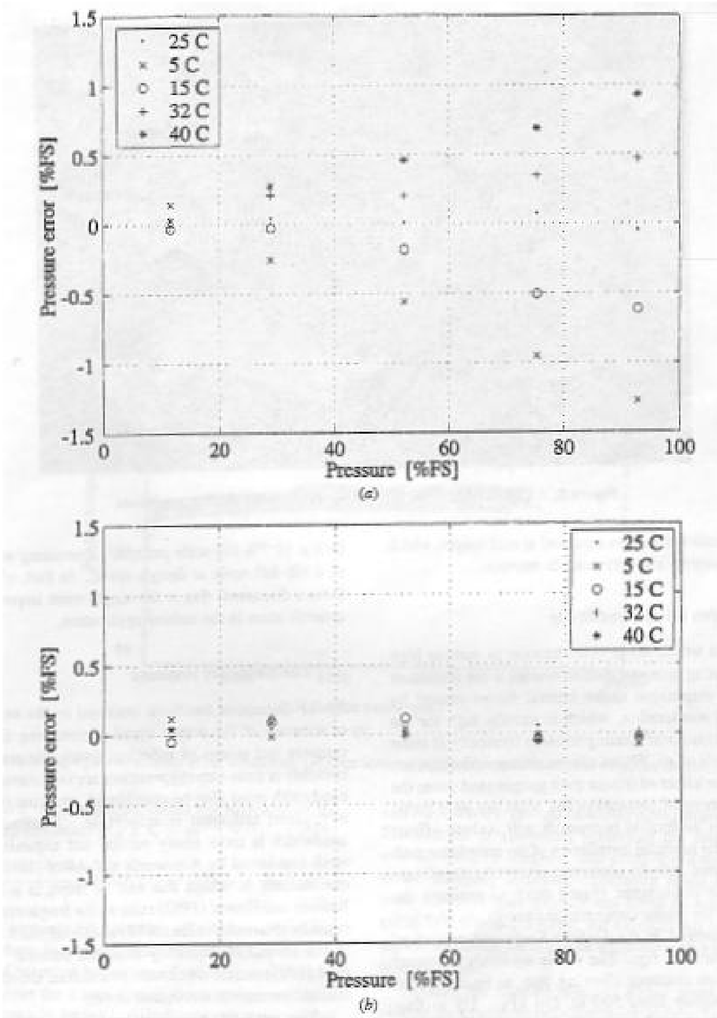

Figure 2.4: The comparison of outputs between an uncompensated pressure sensor (a) and a sensor compensated for temperature changes (b) (Ainsworth et al. 2000)

The output from a piezoresistive pressure transducer relies on two basic characteristics, the sensor Span (or sensitivity) and the sensor Offset (the sensor output at zero absolute pressure) (Ainsworth, Miller, Moss & Thorpe 2000, Denos 2002, Clark 1992). The values for Span and Offset change with temperature therefore errors are introduced when taking pressure measurements from relatively hot or cold environments. Compensation methods have been developed to take the temperature sensitivity of Span and Offset into account. These techniques allow a more consistent accuracy from the pressure transducers.

The temperature compensation method developed by (Clark 1992) assumes a linear relationship between Offset and operational temperature and correlates transducer sensitivity and temperature with a third-order polynomial function. Ainsworth et al. (2000)

and Denos (2002) assumed a linear relationship between sensor Offset and Span with temperature, however these investigations incorporated a much smaller temperature range. Each of these temperature compensation methods allows a post-experimental routine, where the recorded sensor output voltage and temperature can be used to accurately determine fluid pressure.

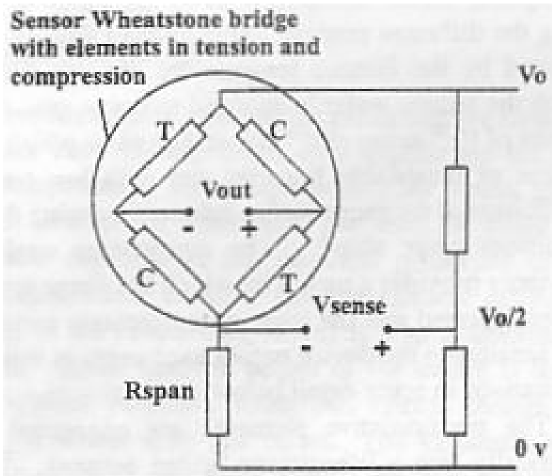

Figure 2.5: Basic circuit to determine V_{sense} (Ainsworth et al. 2000)

To indicate the temperature of the sensor (and allow the temperature correction to be applied), the conditioning circuit shown in figure 2.5 was implemented by both Ainsworth et al. (2000) and Denos (2002). This circuit incorporates the pressure transducer into a Wheatstone bridge. The overall resistance of the pressure transducer will vary with temperature, and the temperature of the other resistors in the external circuit will remain constant (causing the resistance of the external circuit to remain constant). A change in the sensor temperature will therefore result in a change in the voltage, V_{sense}. The value of V_{sense} is then used to calculate the temperature of the sensor. A temperature compensation routine can ultimately be applied to the pressure sensor output (demonstrated by Ainsworth et al. (2000) and Denos (2002)).

Temperature sensitivity compensations created by Denos (2002) also investigate calibrations under a temperature transient. This experimental process involved exposing the piezoresistive pressure transducers to a rapidly applied high temperature test fluid. While these experiments provided useful insight into the behavior of the pressure sensors, the time span involved in the transient temperature calibrations is much longer than typically encountered in a thermofluids experiment (such as a shock tube test).

Temperature calibrations conducted by Ainsworth et al. (1991) assumed that with short experimental run times, only minor temperature changes would be expected. For experimental situations with a significant and sustained operational temperature (eg. testing in-cylinder engine pressures), the static temperature compensation methods mentioned previously can be applied.

2.2.3 Dynamic Response Calibration

The dynamic response characteristics of the piezoresistive pressure transducer determine it suitability for use in fast-response thermofluids experiments.

Shock tubes can be used in experimental testing for the analysis of the dynamic response of the pressure transducers (eg. Ainsworth et al. 1991). The results from these tests reveal that certain frequencies become dominant in the response of the pressure sensor (these are the resonant frequencies of the pressure transducer). A typical sensor response to a step input can be observed in figure 2.6 and the related power spectrum demonstrating the resonant frequency is given in figure 2.7.

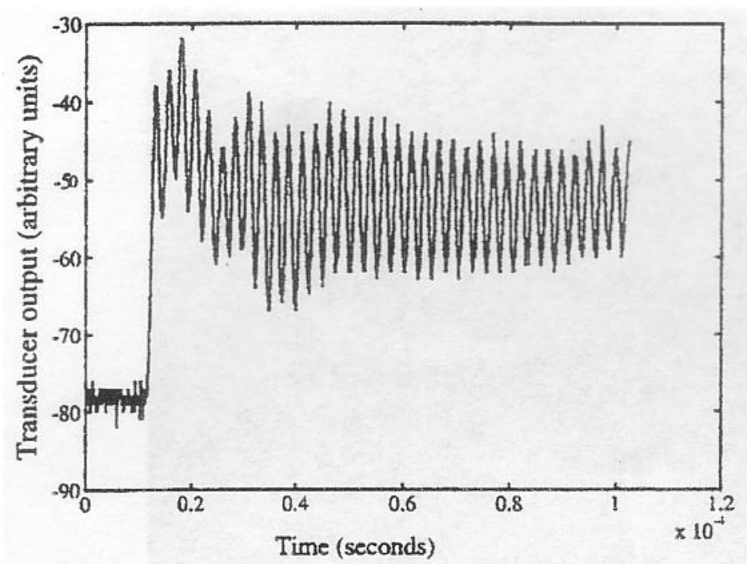

Figure 2.6: Output of a piezoresistive pressure transducer after a step input pressure signal (Ainsworth et al. 2000)

Another method developed for testing the sensor resonant frequency involves exposing the piezoresistive sensor to a constant noise source and measuring the response (Boerrigter & Charbonnier 1997). The noise source, created by an impinging air jet,

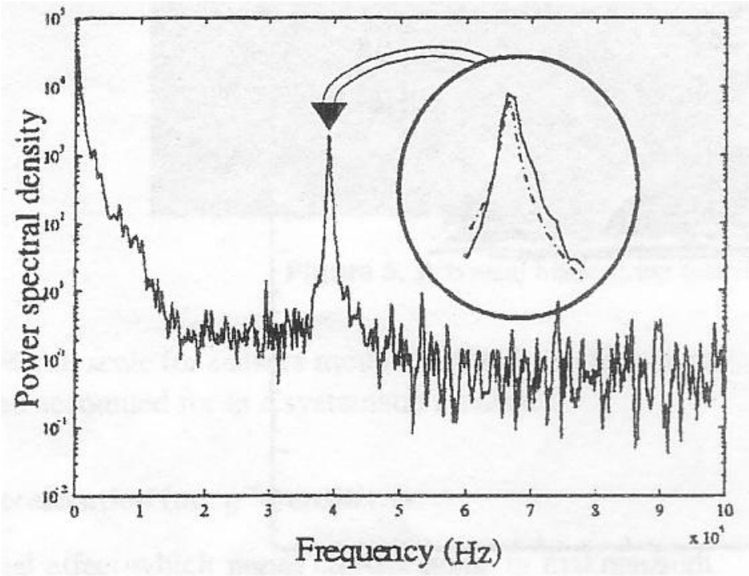

Figure 2.7: The power spectrum from a typical step response, showing the resonant frequency at the dominant peak on the graph (Ainsworth et al. 2000)

creates sounds waves of variable frequency. These sound waves then cause pressure variations at the pressure transducer. This allows the amplitude response and phase shift of the transducer to be analysed over a wide range of operational frequencies. As stated by Boerrigter & Charbonnier (1997), this has advantages over a shock tube tests since this technique easily identifies the resonant frequencies of other bodies (such as the air adjacent of the transducer) and the pressure and temperature of the test are known (the precise shock conditions in a shock tube test are difficult to determine).

Analytical techniques for the calculation of dynamic response were also demonstrated by Ainsworth et al. (2000) and Boerrigter & Charbonnier (1997). Ainsworth et al. (2000) have taken the approach of approximating the piezoresistive pressure transducer with a transfer function, which provides data about the expected frequency response of the system. This approach gives theoretical simulations for the transducer phase shift and amplitude. Boerrigter & Charbonnier (1997) developed an analytical model from key dynamics and fluid mechanics formulas that can also ultimately be used to predict the frequency response of a pressure measurement system.

From the work of Boerrigter & Charbonnier (1997), it appears that the frequency response of a pressure transducer may have two critical points - the resonant frequency of the air around or within the transducer, and the resonant frequency of the diaphragm of the transducer itself. Articles from Boerrigter & Charbonnier (1997) investigate the use of analytical calculations to determine the resonant frequency of the air in front of the diaphragm. Once the resonant frequencies of the piezoresistive pressure transducer have been measured, it can be determined whether these frequencies are related to the resonance of the air around the sensor or the resonance of the silicon diaphragm.

A layer of grease or a flexible compound may be used to cover the diaphragm on the pressure sensor. This procedure is designed to protect the pressure sensor from particles that may impact on the diaphragm and damage the sensor (Ainsworth et al. 2000, Buttsworth & Jacobs 2000). Experiments involving sensors with and without silastomer demonstrated that the silastomer layer significantly increased the damping ratio of the sensor response (Ainsworth et al. 2000).

2.3 Assessment of Consequential Effects

While this project focuses largely on short term results and immediate outcomes, long term effects of this research must also be considered. These effects include the aspects of sustainability, ethical responsibility and safety issues.

2.3.1 Substantiality

Environmental sustainability is of continually increasing importance to modern engineering practices. The short, medium and long term environmental consequences of an engineering task (such as the work undertaken on this project) must be anticipated. Where negative effects are apparent, actions need to be taken to minimize or remove any environmental damage.

While this project has a minimal environmental impact in terms of direct pollution created or environmental degradation caused, there are other non-direct environmental impacts associated with this research topic, including -

- The use of finite resources for the construction of the testing equipment

- The resource requirements for experimental testing

The components used in this project (the pressure sensors and the developed testing apparatus) make use of finite resources for their production (metals and plastics). Fortunately these products are mostly recyclable. The pressure sensors themselves can be reused for different pressure measurement applications and offer a reasonable service life (depending on the severity of the testing environment). The other materials used for the construction of the testing apparatus are readily recyclable (plastics, metals and electrical components) therefore the waste from this project can be minimized.

Some of the experimental testing procedures may require non-renewable resources. This project will require the use of internal combustion engines (for use in pressure testing and for powering other experiments) which use fossil fuels and produce harmful emissions. While these are negative environmental effects, these experiments will only be conducted over a short period during the experimental stages of the project.

The results from this project may ultimately contribute to environmental sustainability. If these pressure sensors are widely available at low cost, machinery and manufacturing process could be more readily monitored and their efficiency could be maximized. This could lead to a reduction of pollutants created and contribute towards a cleaner environment.

2.3.2 Ethical Responsibility

Most new technologies have associated ethical implications related to the particular outcomes of that development. Therefore an ethical responsibility exists where the engineer must consider the people who are affected.

This project makes heavy use of relatively new technologies and the possible outcomes of this research may also bring further advancement to the area of piezoresistive pressure sensor technology. The range of possible ethical consequences were considered before commitment to this project.

It is possible that some people may be disadvantaged if the piezoresistive sensor technology becomes widely implemented. Ultimately this project may allow a reduction in the use of highly expensive pressure transducers. This may adversely affect some suppliers and sensor producers. Fortunately the suppliers and manufacturers typically use a wide range of products, therefore if a small number of items became obsolete due to the piezoresistive technology, the consequences would be minimal.

One positive outcome that relates to ethical responsibility is the production of a reliable low-cost technology. This allows the advancements of this modern technology to become available to a wider range of the community.

2.4 Chapter Summary

This chapter has investigated background knowledge and previous research related to the field of piezoresistive pressure transducers. Past experiments and models used to test the dynamic characteristics and temperature compensations for piezoresistive sensors provide possible techniques that could be used for this project or similar research.

The assessment of consequential effects has drawn attention to the critical aspects of this project that could possibly lead to unwanted ethical, social or environmental damage. Now that these factors have been identified, steps can be taken to ensure that any negative effects of this project are eliminated or minimized.

Chapter 3

Design Methodology

3.1 Static Calibrations and Temperature Compensation for Pressure Sensors

The pressure and temperature sensitivity of piezoresistive pressure transducers can be determined through a series of static calibrations. These calibrations allow accurate results to be obtained from experimental testing.

The static calibration process will initially begin by testing the pressure sensitivity of the pressure transducers at room temperature (approximately 25°C). These static tests will be conducted using the 'Dead Weight' tester (shown in figure 3.1). The Dead Weight testers allows precise levels of pressure to be applied to the pressure sensor.

During the static calibration process, each pressure sensor was attached to the hydraulic fitting on the Dead Weight tester. A particular mass was placed on one of two hydraulic cylinders (shown in figure 3.1). The wheel of the Dead Weight Tester is turned inwards until the mass is freely suspended by the pressure of the hydraulic oil. Since the oil pressure suspends a mass of known value, the pressure of the oil can be accurately determined. Each mass for the Dead Weight tester has predetermined corresponding pressure values. To avoid any effects of temperature sensitivity within the The Dead Weight tester, this apparatus remained at approximately room temperature during all

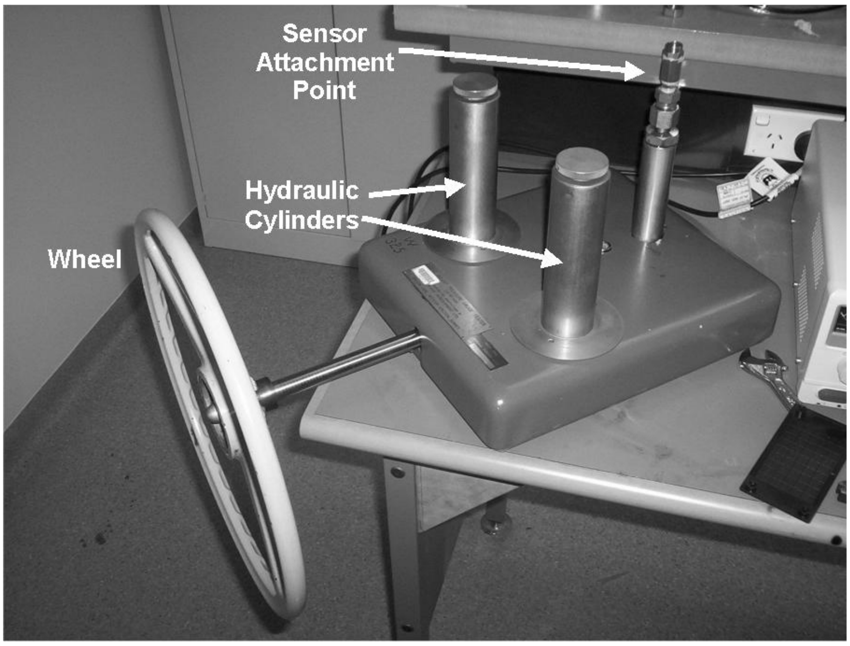

Figure 3.1: The 'Dead Weight' tester used for the static calibrations

calibration experimentation.

The output voltage of the pressure transducer(V_{out}) relates directly to the applied pressure. This typically results in a highly linear relationship between these two variables. The output of the transducer can be correlated to pressure using the equation 4.1 (Ainsworth et al. 2000, Denos 2002),

$$V = SP + O \tag{3.1}$$

In equation 4.1, 'V' is the output voltage (or V_{out}), 'S' is the senor span (or sensitivity) and 'O' is the sensor offset (the voltage output, V_{out}, at zero absolute pressure). This function can be used to accurately determine the pressure from the sensor output voltage while the pressure transducer is at room temperature.

As the temperature of the sensor changes, the values for Span and Offset also change. It is critical to determine the how these characteristics change with temperature. High temperature thermofluids experiments (such as testing the in-cylinder pressures on the IC engine) will produce inaccurate results if no temperature corrections are applied.

The operational temperature of the sensor must be determined to perform the temperature calibration process. One method is to incorporate the pressure sensor into a circuit as shown in figure 3.2. This electrical circuit is adapted from the work of Ainsworth et al. (2000).

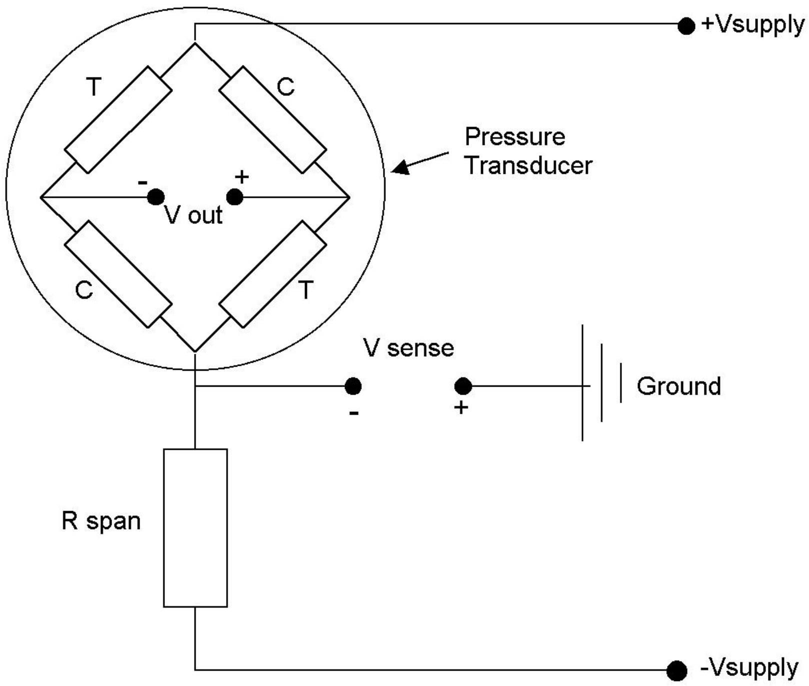

Figure 3.2: Conditioning Circuit to determine V_{sense}
(Ainsworth et al. 2000)

As the overall resistance of the pressure transducer changes with temperature, the value for V_{sense} will also shift.

A range of different pressures can be applied to the pressure transducer while it is held at selected constant temperatures (approximately ranging from room temperature to 150°C). This will be achieved by placing the pressure transducer in the oven shown in figure 3.3, and attaching a remote connection to the Dead Weight tester (figure 3.1).

The relationship between sensor output voltage, and applied pressure, allow values for Span and Offset to be calculated at a range of different testing temperatures. The rate of change of sensor Span and Offset with temperature can then be determined.

One particular method, developed by Ainsworth et al. (2000), applied the temperature correction directly to the value of V_{out}. A function was developed that uses the values of V_{out} and V_{sense} to provide a correction to V_{out} based on the temperature of the

Figure 3.3: Oven used for temperature calibrations

sensor. The temperature of the sensor is determined by the corresponding value for V_{sense}. This corrected value for V_{out}, known as V^*_{out}, is the predicted output that the sensor would produce if it were at room temperature. This function is shown in equation 3.2.

$$V^* = V\left(1 - \frac{1}{S_{25}}\frac{dS}{dT}\Delta T\right) - O_{25}\left(1 - \frac{1}{S_{25}}\frac{dS}{dT}\Delta T\right) - \frac{dO}{dT}\Delta T\left(1 - \frac{1}{S_{25}}\frac{dS}{dT}\Delta T\right) \quad (3.2)$$

The value of V^* (or V^*_{out}) can then be used with the room temperature values of span (S_{25}) and offset (O_{25}) to allow the true experimental pressure to be determined (equation 3.3).

$$V^* = S_{25}P + O_{25} \quad (3.3)$$

3.2 Testing of Dynamic Response Characteristics

The dynamic response characteristics of the piezoresistive pressure transducers determines the behavior of the pressure sensors under high frequency changes in fluid pressures. Dynamic response testing allows the maximum operational frequencies of the pressure transducers to be deduced. As experimental pressure fluctuation frequencies reach the maximum operational frequency of the pressure transducer, errors begin to occur in the output of the sensor.

The dynamic response properties of the piezoresistive pressure transducers will be tested using a shock tube (as shown in figure 3.4).

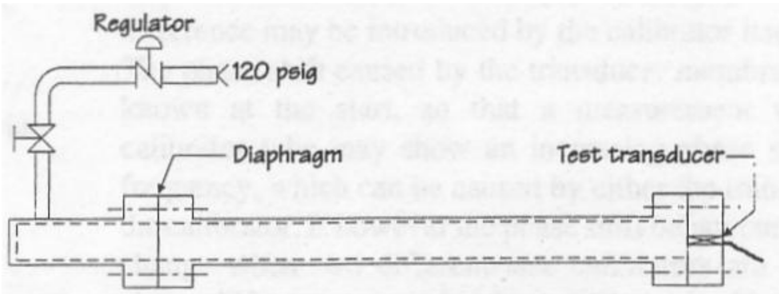

Figure 3.4: Basic Shock Tube design, similar to the apparatus used for this project (Boerrigter & Charbonnier 1997)

A shock wave is produced within the tube when a diaphragm is ruptured. This wave of pressure travels at high speed along the tube and reflects off the end face. The pressure transducer, mounted level with the end face of the tube, undergos an approximate step input (since the change in pressure is very rapid). The response of the transducer to this input then allows the dynamic response characteristics to be determined. These characteristics include values such as response time and resonant frequency.

A power spectrum of the sensor response can be derived from the shock tube test results. This indicates the dominant frequencies, allowing the resonant frequency of the pressure transducer to be identified. This resonant oscillation is due to the vibration of the silicon diaphragm of the sensor. Significant errors in the piezoresistive sensor output (possibly upwards of 10%) will occur if the measured fluid pressures begin to fluctuate at a level near the resonant frequency of the sensor (within the same order of magnitude).

The test results from the shock tube can also be used to find the response time of the pressure transducers. This will determine the suitability and general accuracy of the pressure sensors under fast response testing applications. In these transient pressure measurement applications short response times are essential for recording an accurate set of readings.

Shock tube tests can also be conducted to test the dynamic response characteristics of modified pressure sensors. Various configurations of sensors, including sensors with modified cases and added grease or silastomer, will be tested to investigate the effects of these changes on the sensor response. These modifications are expected to provide protection to the silicon diaphragm of the sensor (with the addition of grease or silastomer) and possibly improve the response time of the sensors (with case modifications).

3.3 Pressure Testing with the USQ Gun Tunnel

The static calibration operations and dynamic response analysis lead to testing in facilities such as the USQ Gun Tunnel. This apparatus (shown in figure 3.5) (Buttsworth n.d.) is capable of producing a high speed, short duration gas flow.

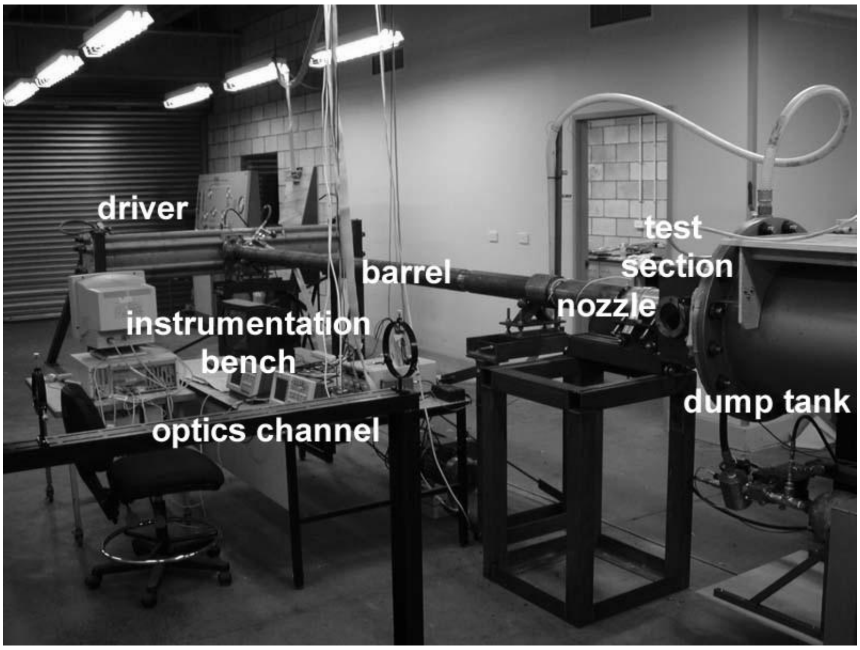

Figure 3.5: The USQ Gun Tunnel used for experimental testing

The short period of the actual test flow (typically milliseconds) demands that the pressure sensors used to analyse the test gas has a very short response time. It is assumed that thermal effects from the hot gases on the sensor are negligible, since the short test times will not allow the pressure transducer to significantly change temperature while results are being recorded.

The results obtained from the Gun Tunnel with the piezoresistive pressure sensor are then able to be compared to the output from a piezoelectric pressure transducer (an expensive sensor, well suited to this measurement application). This gives an indication of the accuracy of the static calibration of the piezoresistive sensors and also shows a comparison between the dynamic characteristics of the two sensors.

If time permits, a theoretical analysis of the Gun Tunnel may also be conducted, using computational methods. This allows a comparison between theoretical pressures and the results from the output from the piezoresistive pressure transducer.

3.4 Pressure Testing with an IC Engine and Theoretical Analysis

Pressure measurement within an internal combustion engine tests the effectiveness of the static calibrations and the sensor dynamic response characteristics. This application also tests the temperature compensation techniques for the piezoresistive sensors. The engine (specifications shown in table 3.1) has been modified to allow pressure transducers to be mounted in the head of the engine block.

In-cylinder pressure measurements can be taken from the engine during motored (unfired) and fired runs. To allow the pressure measurements to be coordinated with the position of the cylinder, a basic shaft-encoder can be attached to the drive shaft of the engine. The signal from the encoder can be combined with the corresponding pressure sensor outputs to determine the pressure of the engine at different stages of operation.

Computational calculations, consisting of a thermodynamic engine simulation, can verify the experimental results from the engine. A comparison between the results from

Specifications	**Details**
Make	Kubota
Model	GS200
Type	Four Stroke, air cooled, spark ignition,single piston, side valve, horizontal shaft
Rated Power	3.9 kW @ 3600 rpm (max), 2.8 kW @ 3600rpm (continuous)
Rated Torque	10.5 Nm @ 3000 rpm
Bore	69 mm
Stroke	54 mm
Compression Ratio	6:1
Swept Volume	201 cc
Conrod Length	93.9 mm

Table 3.1: Engine Specifications for the Kubota GS200 Petrol Engine

this theoretical approach and the measured pressure levels provides an indication of the accuracy of the piezoresistive pressure sensor.

3.5 Chapter Summary

The design methodology has introduced the various experiments and calculations that will provide the analytical data for this project. The results obtained from static calibrations and temperature compensations, dynamic response characteristics, testing in the USQ Gun Tunnel and testing of an internal combustion engine are discussed in the following chapters.

Chapter 4

Static Calibration and Temperature Compensation

4.1 Chapter Overview

This chapter investigates the static calibrations of the various piezoresistive pressure transducers that are used for this project. Temperature calibrations are also investigated, since the operating temperature of the sensor also effects the transducer sensitivity and other characteristics. The calibrations and temperature compensation techniques developed in this chapter form the basis for the following sections, as this allows an accurate means of converting the sensor output voltage to fluid pressures.

4.2 Initial Static Calibrations

The initial static (or quasi-static) pressure calibrations were conducted using the Dead Weight pressure tester (figure 3.1). These calibrations were conducted for all pressure transducers to determine their related values for Span and Offset.

The static calibrations were conducted at room temperature (approx 25°C) since this would be the approximate sensor operating temperature for the thermofluids experiments conducted in the Shock Tube and the USQ Gun Tunnel. While the actual gas temperatures during these experiments may have significantly exceeded room temperature values, the poor heat transfer properties of air and the very short time span over which the piezoresistive sensors were exposed to this flow allows a negligible increase in overall sensor temperature. The calibration temperature may not have precisely match the testing temperatures, however this small temperature variation would cause minimal variation in the properties of the pressure sensors.

The static calibrations for each type of piezoresistive pressure transducer were conducted in a similar manner. As introduced in the Design Methodology section (Chapter 3), the output of a typical piezoresistive pressure transducer is quantified by the voltage level V_{out}. The basic relationship between sensor output (V_{out} or V) and pressure (P) is shown in equation 4.1.

$$V = SP + O \tag{4.1}$$

The values for Span (S) and Offset (O) can be determined from the coefficients derived from a linear regression of data points of pressure against V_{out}. For equation 4.1, the units for V_{out} or V are mV, the units for Span are mV/Pa and the unit for Offset are mV. The values determined for Span and Offset for each of the pressure sensors were divided by the supply voltage to the sensor (15V for 13U3000 and 13U0500 and 12V for SX150AHO). These values would need to be multiplied by the supply voltage in order to use equation 4.1 with the experimental data.

The values for span and offset were determined for various pressure transducers that were used during the course of this research. The three types of transducers used in this project are as follows,

- Sensym, SX150AHO (150 psi piezoresistive pressure sensor)
- Sensym, 13U3000 (3000 psi piezoresistive pressure sensor)
- Sensym, 13U0500 (500 psi piezoresistive pressure sensor)

(The full specification sheet for each of these sensors can be seen in Appendix B)

4.2.1 Detailed Experimental Design

The sensor was attached to the Dead Weight Tester and a range of pressures were applied. The sensor output (V_{out}) was recorded for each pressure value. While during the initial experimentation stage, V_{sense} was recorded (a value that can be used to determine the operating temperature of the sensor), it served no use in the room temperature calibrations (the value of V_{sense} is used extensively for the temperature calibrations in later sections). As expected, the values for V_{sense} remained relatively constant for each the quasi-static room temperature calibrations (due to constant temperatures).

A basic block diagram in figure 4.1 demonstrates the process by which the values of V_{out} and V_{sense} were recorded.

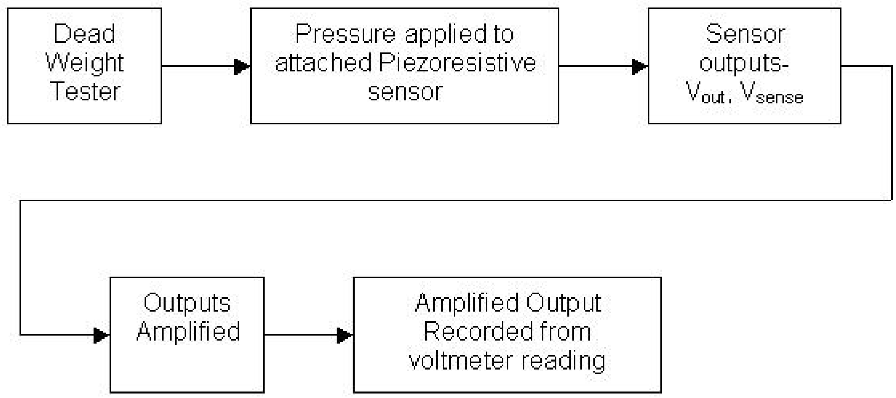

Figure 4.1: A block diagram, showing the approached used for the static calibrations

The conditioning circuit (figure 3.2) provides the output signals from the sensor, these signals were then directed through an Instrumental Amplifier (INA114 - specifications in Appendix B). The gain (amplification) was set to 1, however the amplifier circuit enables greater values of gain for future experiments. A photograph of the circuit used is shown in figure 4.2.

The circuit shown in figure 4.2 indicates the power supply points, ground, the connecting wires to the sensor, the amplifier integrated circuits (one for V_{out} and one for V_{sense}), and the connectors for the output signals (V_{out} and V_{sense}). This circuit also featured a potentiometer to allow V_{sense} to be trimmed close to 0V at room temperature.

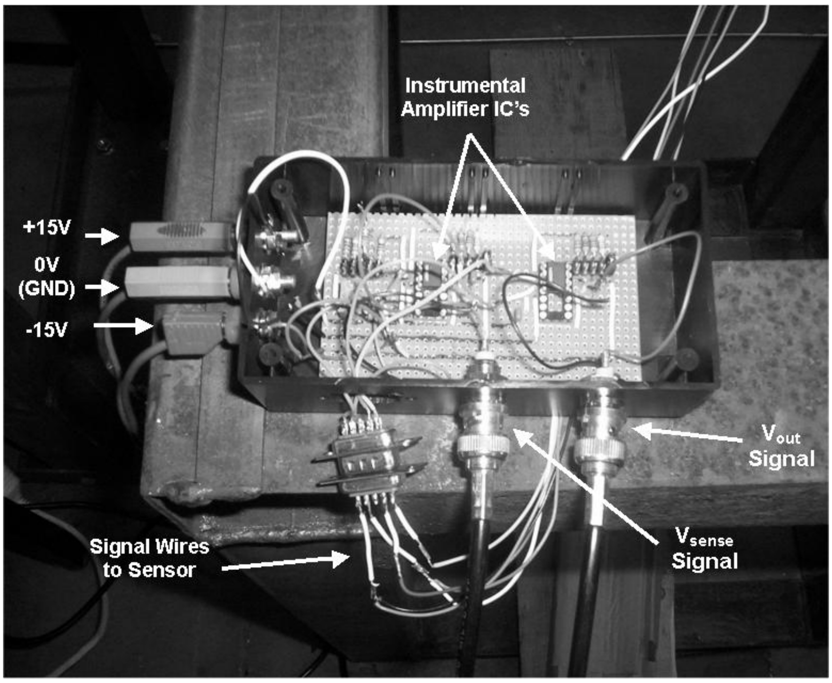

Figure 4.2: A photograph of the electrical circuit used to produce the sensor outputs, V_{out} and V_{sense}

Each sensor was tested over a range of pressures that incorporated the majority of the pressure range for each particular sensor. Once the output values of the sensor had been recorded for each pressure value, MATLAB (version 6) was used to perform a simple linear regression of V_{out} (y-axis) against absolute applied pressure (x-axis). The MATLAB function used for this process, 'load_cal2', is displayed in Appendix C. A general first order equation (linear) is in an equivalent form to the equation used to relate pressure and sensor output voltage (equation 4.1). This allows the values for Span and Offset to be determined directly from the coefficients derived from the first order regression.

The results of the static calibrations for each of the sensors are discussed in the following subsections.

4.2.2 Static Calibration of Unmodified SX150AHO

This particular sensor was used extensively in shock tube testing. Various different modified forms of this sensor were utilized (with modified cases, added grease and added latex compounds). The results from the unmodified sensor are shown in this section, purely demonstrating the techniques used for the static calibration at room temperature. The values configurations and calibrations for other modified SX150AHO sensors will be introduced in the Chapter 5, where these sensors are tested in the shock tube apparatus.

To allow the SX150AHO sensor to be attached to the Dead Weight tester, a unique part was constructed. The detail drawing for this part (SX150AHO Pressure Attachment) is shown in Appendix D.

The relationship between output voltage V_{out} and applied pressure is shown in figure 4.3. The supply voltage to the sensor was 12V.

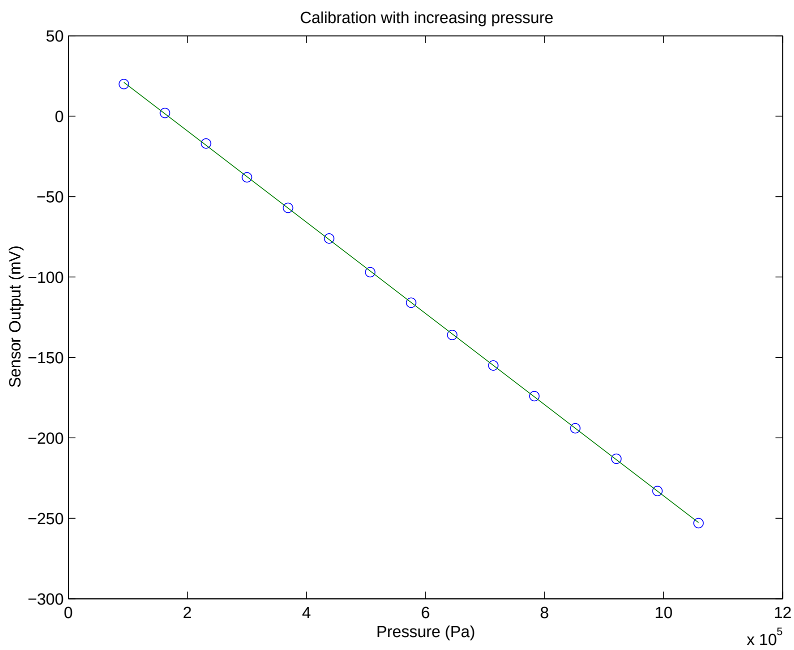

Figure 4.3: Static calibration of Sensym SX150AHO sensor

The negative slope shown in figure 4.3 is simply due to the polarity of the connection to the pressure sensor (by reversing the electrical connection, the plot would show a positive trend). For this particular data set, the room temperature values for Span and Offset were determined as follows (per unit supply voltage),

- Span = -2.29e-5 mV/V.Pa
- Offset = 3.83 mV/V

4.2.3 Static Calibration of 13U3000

The Sensym 13U3000 piezoresistive pressure transducer was used for pressure measurement in the USQ Gun Tunnel (Chapter 6). Since it was used in previous research for engine testing, this particular sensor had a layer of silastomer (approximately 2mm thick) on the diaphragm to protect it from high gas temperatures and foreign particles in the test fluid. The Span and Offset determined by this stage of experimentation were used to determine the pressures from the sensor output recorded from the Gun Tunnel Test.

Output voltage V_{out} and applied pressure are shown in figure 4.4. The supply voltage to the sensor was 15V.

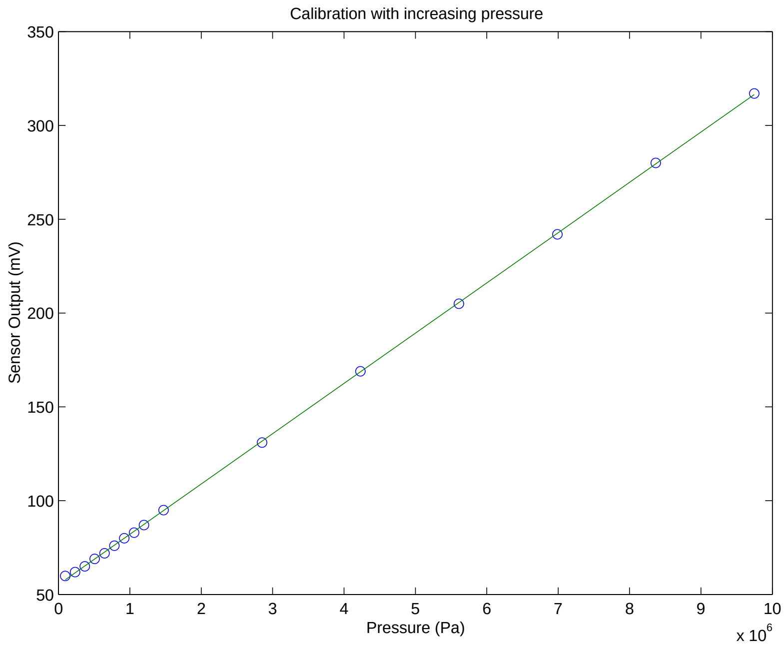

Figure 4.4: Static calibration of Sensym 13U3000 sensor

For these data points, the room temperature values for Span and Offset were determined as follows -

- Span = 1.19 e-7 mV/V.Pa
- Offset = 0.246 mV/V

4.2.4 Static Calibration of 13U0500

The Sensym 13U0500 pressure sensor was used to determine in-cylinder pressure for an internal combustion engine (Chapter 7). Similar to the 13U3000 sensor, this sensor also had a layer of silastomer (approximately 3mm thick) on the diaphragm for added insulation and protection.

Since this sensor was primarily used in the engine testing, it mainly operated at high temperatures. The room temperature static calibration for this sensor simply allows for a comparison of the values for Span and Offset for when the sensor is at higher temperatures during temperature compensation calibrations (discussed in the following section).

For the room temperature calibration, the output voltage V_{out} against absolute pressure is shown in figure 4.5. The supply voltage to the sensor was 15V.

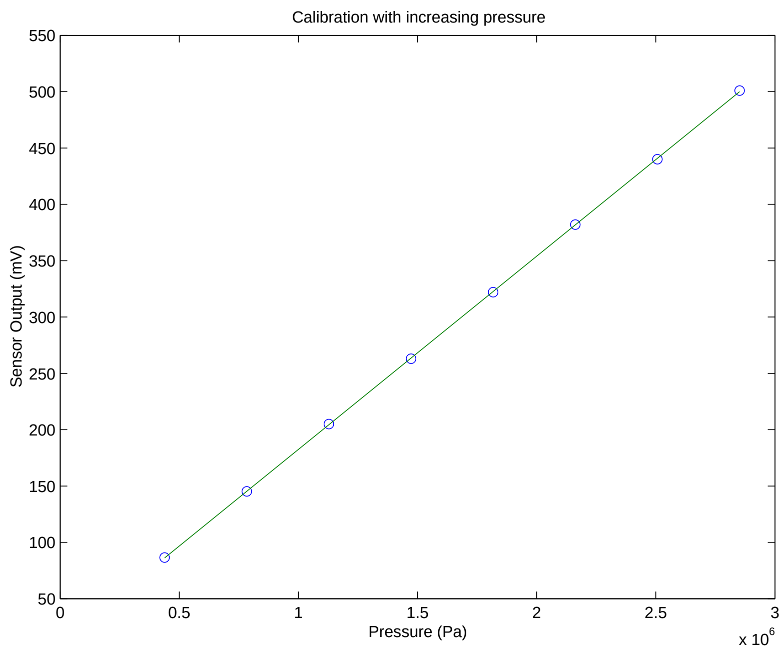

Figure 4.5: Static calibration of Sensym 13U0500 sensor

The related values for Span and Offset were then determined -

- Span = 1.15e-5 mV/V.Pa
- Offset = 0.74 mV/V

4.3 Temperature Compensation Calibrations

During thermofluids experiments, a range of different temperatures will be encountered. Piezoresistive pressure transducers must be calibrated for temperature effects to improve the accuracy of their results. Changes in temperature will alter the coefficients for sensor Span and Offset, therefore the effect of temperature on these values must be quantified.

The sensor used for the temperature calibrations is the Sensym, 13U0500, as this sensor is used for testing the pressures inside the cylinder of the internal combustion engine (discussed in Chapter 7). While the other thermofluids experiments may encounter a range of temperatures (shock tube and Gun Tunnel experiments), the 13U0500 is the only sensor where the actual sensor operating temperature significantly exceeded room temperature. A layer of silastomer was placed over the pressure sensitive diaphragm to protect the sensor from particles in the test fluid and high gas temperatures (encountered during engine testing - Chapter 7)

4.3.1 Detailed Experimental Design

To determine how Span and Offset were related to sensor temperature, the sensor was held at a range of constant temperatures (room temperature to approximately 150°C) while quasi-static pressure tests were conducted. Span and Offset were subsequently determined for a range of operating temperatures.

To allow the sensor to be held at a variety of steady temperatures while applying a range pressures to the sensor, a testing apparatus was developed. A small oven was modified to allow the pressure sensor to be heated by the oven while also being remotely connected to the Dead Weight tester. This setup can be observed in figure 4.6.

A thermocouple was situated immediately behind the pressure sensor to indicated the temperature of transducer (the temperature dial on the oven itself was found to be highly inaccurate). Pressure testing at each temperature was only conducted once the temperature reading from the thermocouple became steady.

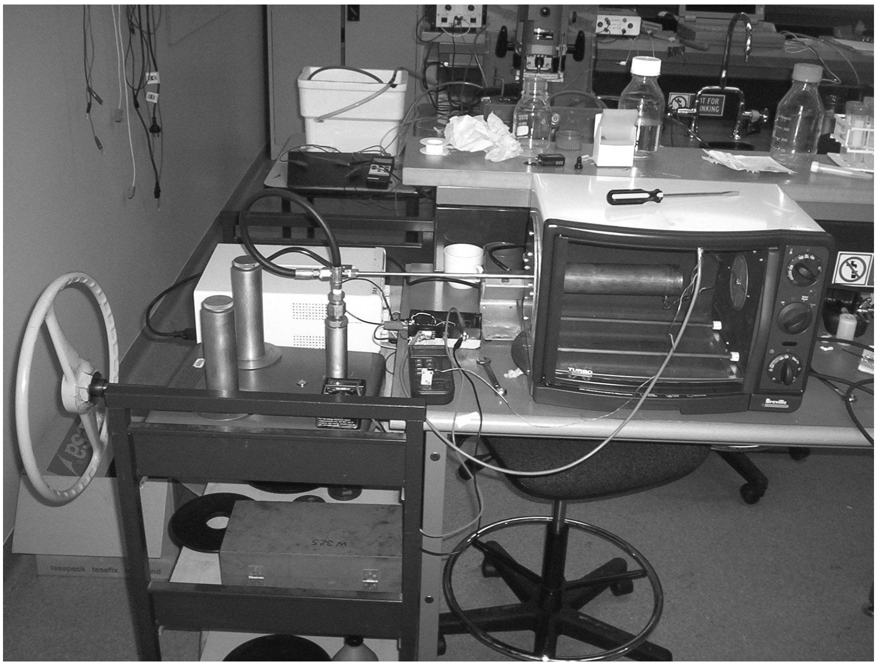

Figure 4.6: The modified oven (right) and the Dead Weight tester (left) used for temperature calibrations

Since the thermostat control for the oven continuously switched the heating elements on and off, temperature fluctuations were present within the oven. To overcome this temperature variation, the sensor was positioned within an insulted copper tube inside the oven (visible inside the oven in figure 4.6), effectively smoothing the temperature fluctuations and providing steady temperatures for experimental testing. Detailed drawings of the insulating tube assembly and individual parts are shown in Appendix D.

A stainless steel tube, providing the hydraulic connection between the Dead Weight tester and the pressure transducer inside the oven, was deliberately designed to allow a reasonable length of the tubing inside the oven. The length of tubing inside the oven allowed the hydraulic oil to be raised to the oven temperature at the point where it came in contact with the pressure sensor. This ensured that the sensor was held at a predictable temperature. Exposing the sensor to cool hydraulic fluid may have adversely affected the accuracy of the temperature calibration.

As discussed in the Design Methodology section (Chapter 3) the value for V_{sense} can be used to indicate the temperature of the pressure transducer (see figure 3.2). This value was recorded at each different sensor temperature. The voltage supplied to the complete conditioning circuit was 30V (approximately 15V being supplied to the sensor). The values recorded for V_{sense} were adjusted for the circuit supply voltage (divided by 30V), causing the unit of V_{sense} to be mV/V.

To test for temperature effects, the pressure transducer was held at 4 different temperatures, while a range pressures were applied at each temperature. The first temperature test was conducted at approximately room temperature (the pressure test was performed with the oven switched off). Ideally a larger range of temperatures could be tested, however due to the insulation around the pressure sensor, a considerable amount of time (about $1\frac{1}{2}$ hours) was required for the sensor to reach a new steady temperature. This restricted temperature testing to a range of only 4 different temperatures.

The maximum temperature for testing was limited below 150°C, since above this temperature the plastic insulation on the electrical wires begins to melt. At temperatures approaching 200°C, there is also a risk of melting the electrical soldering on the pressure sensor.

4.3.2 Analysis of Temperature Effects

After conducting pressure tests at a range of different temperatures, the changes in Span and Offset with temperature were investigated. For each set of data at a particular temperature (values for V_{out}, V_{sense} and the applied pressure values) an analysis was conducted to determine the values for Span and Offset (the process for determining Span and Offset was identical to that discussed in the Static Calibration section). Span, Offset and V_{sense} were then related to the operating temperature of the pressure sensor at each of the four tested temperatures (the operating temperature of the sensor was the steady temperature value displayed from the thermocouple instrumentation). A MATLAB script 'temp_cal2', developed to analyse the temperature effects on the sensors is displayed in Appendix C.

The plot shown in figure 4.7 demonstrates a highly linear relationship between V_{sense} and temperature. For each particular temperature V_{sense} remained relatively constant during the static calibration process, therefore the average V_{sense} at each testing temperature was used.

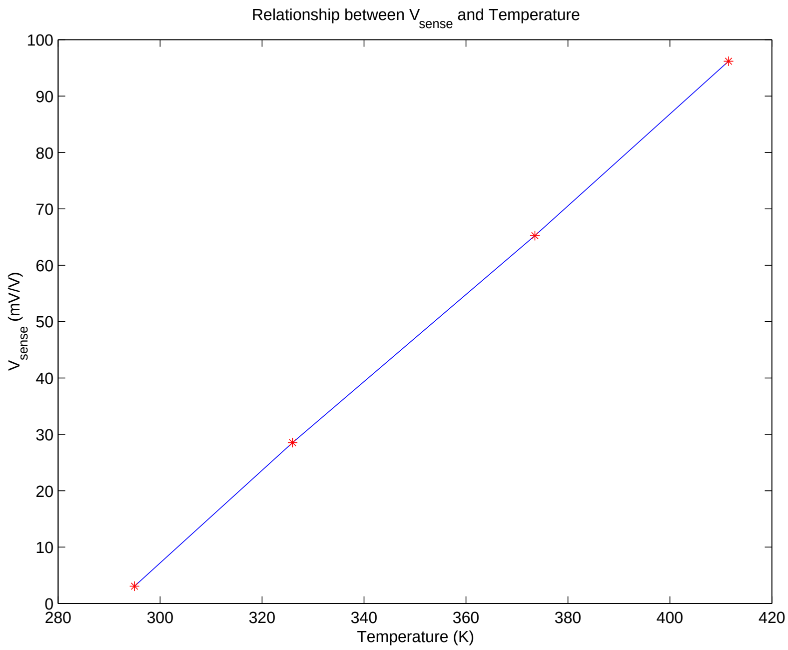

Figure 4.7: The Positive Linear Relationship between V_{sense} and Sensor Temperature

A linear regression of these results (via MATLAB version 6) provides a temperature coefficient for V_{sense}. This is listed in table 4.1. This demonstrates that V_{sense} can reliably be used to determine the operating temperature of the pressure sensor. This technique is necessary where a direct measurement (such as that previously provided by the thermocouple) isn't possible.

The relationship between sensor Span and temperature is displayed in figure 4.8. This also demonstrates a linear trend. The gradient of a linear regression provides the value for change in Span with change in temperature ($\frac{dS}{dT}$). Ainsworth et al. (2000) utilized a fractional span sensitivity, where the rate of change of Span with temperature is divided by the value of Span at room temperature ($\frac{1}{S_{25}}\frac{dS}{dT}$). This matches the format of the temperature coefficient of Span specified by the manufacturer. The value for fractional Span sensitivity is listed in table 4.1.

The association between sensor Offset and temperature demonstrates a higher order relationship (figure 4.9). While it is certainly possible to fit a second order curve to this data, for the purposes of this project, future values for Offset will simply be determined by a process of linear interpolation between these experimental data points. Both the manufacturer's specifications (see Appendix B) and Ainsworth et al. (2000) recognize

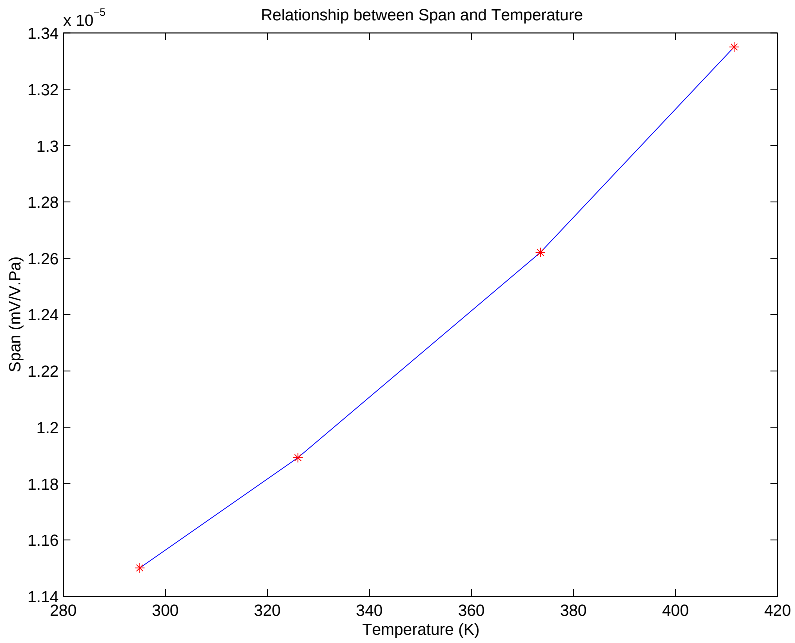

Figure 4.8: The Positive Linear Relationship between Span and Sensor Temperature

a linear rate of Offset change with temperature. This is may be accurate for this set of results when considering a linear regression of the temperature range of approximately 300K to 370K (or 27°C to 97°C).

The basic circuit for determining V$_{sense}$ can be analysed to allow the temperature coefficient of resistance of the pressure sensor to be determined (allowing a comparison with the manufacturers specifications). Equation 4.2 (Ainsworth et al. 2000) can be used to associate V$_{sense}$ and the temperature coefficient of resistance with the temperature changes of the pressure sensor. 'V$_0$' is the supply voltage to the conditioning circuit (figure 3.2), 'ΔT' is the change in sensor temperature, 'α' is the temperature coefficient of resistance.

$$\Delta T = \frac{1}{\alpha} \frac{4V_{sense}}{V_0 - 2V_{sense}} \tag{4.2}$$

By substituting the full temperature change of the experiment, and the change of V$_{sense}$ over this temperature, into equation 4.2 (since this equation assumed that V$_{sense}$ was zero at room temperature), the value for the temperature coefficient of resistance of the sensor can be determined (for this particular equation, the units for V$_{sense}$ must be kept as Volts). The temperature coefficient of resistance is compared with the

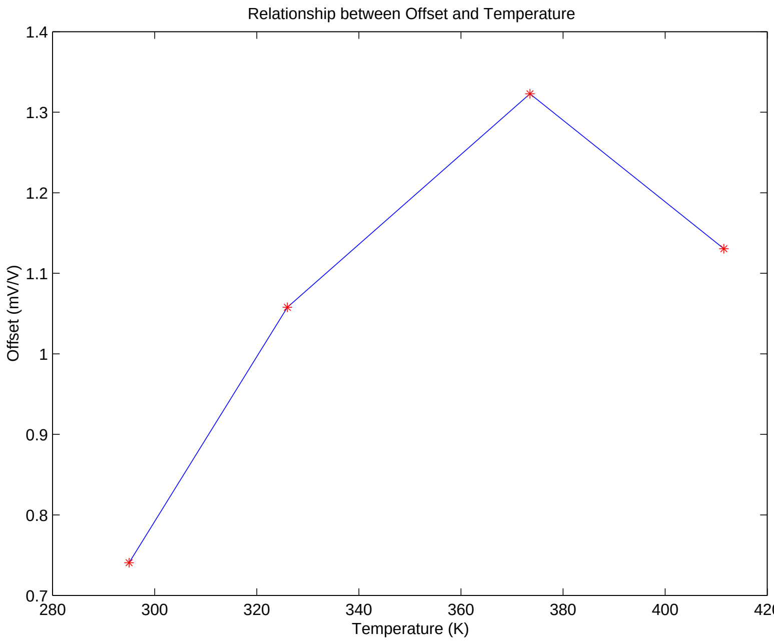

Figure 4.9: The Relationship between Offset and Sensor Temperature

Manufacturer's specifications in table 4.1.

In table 4.1 the temperature coefficients for Span and Offset are given proportional to the sensor supply voltage, however the specific supply voltage to the sensor was dependant on the value of V_{sense} (refer to figure 3.2). In these cases, the value of V_{sense} was subtracted from 15V to give the actual sensor supply voltage. The values of Span and Offset were then divided by this value (15V - V_{sense}). The values given for V_{sense} (in mV/V) were divided by the voltage supply to the original circuit (30V).

Sensor Characteristics	**Experimental Values**	**Manufacturer's Spec. (0 to 82°C)**
Temp. Coefficient of V_{sense}	0.795 mV/V.°C	N/A
Temp. Coefficient of Resistance	3928 ppm/°C	3420 ppm/°C (Typical)
Temp. Coefficient of Span	1371 ppm/°C	720 ppm/°C (Typical)
Temp. Coefficient of Offset	7.26 μV/V.°C	30 μV/V.°C (Typical)

Table 4.1: Sensor Characteristics for Sensym 13U0500 Piezoresistive Pressure Transducer - Experimental Values and Manufacturer's Specifications (Experimental Offset coefficient for 27 to 97°C, Manufacturer's Spec. Offset coefficient for 0 to 82°C)

The results shown in table 4.1 offer a direct comparison to the manufactures specifications. While there are some differences between these results, the manufacturer's performance characteristics are taken at a supply voltage of 5V (the experiments conducted for this research used a sensor supply voltage of approximately 15V). Other causes for the differences between the experimental results and the manufacturer's specifications may be due to the silastomer that was applied to the diaphragm of the sensor. While the silastomer should not effect the temperature coefficient of resistance, it may have effected the temperature coefficients of Span and Offset. The differences in these results reinforces the need for conducting the temperature calibrations to determine the sensor characteristics, instead of relying on the manufacturer's specifications. This is especially necessary if modifications (such as adding silastomer to protect the diaphragm) have been made.

4.3.3 Application of Temperature Calibrations

The experimental data provided by the previous subsection provides a means of determining an accurate values from a pressure transducer as it operates over a wide range of temperatures.

Initially, the operating temperature of the pressure sensor can be determined with calculations involving the value of V_{sense}. Once V_{sense} at room temperature has been recorded, equation 4.3 can be used to determine the operating temperature of the sensor.

$$\Delta T = \frac{V_{sense} - V_{sense(25)}}{\frac{dV_{sense}}{dT}} \tag{4.3}$$

'$V_{sense(25)}$' is the value of V_{sense} at room temperature (originally trimmed to be close to 0V), 'ΔT' is the change in room temperature from 25°C

Once the temperature of the sensor has been determined, the particular values of Span and Offset related to this temperature can then be calculated or interpolated from the range of known experimental values.

The basic formula for determining pressure from the output of a piezoresistive pressure transducer (V_{out}) is shown in equation 4.4 (derived from equation 4.1).

$$P = \frac{V - O}{S} \tag{4.4}$$

The basic equation for determining pressure (equation 4.4) does not take any changes in Span and Offset into account, therefore it cannot be used if the sensor is operating at temperatures other than room temperature. This equation must be modified to allow for the temperature sensitivity of Span and Offset.

If the temperature is less than approximately 370K, giving a constant rate of change in sensor offset (as displayed in table 4.1), equation 4.5 (Ainsworth et al. 2000) can be used to calculate an accurate pressure reading.

$$P = \frac{1}{S_{25} + \left(\frac{dS}{dT}\right)\Delta T}\left[V - \left(O_{25} + \frac{dO}{dT}\Delta T\right)\right] \tag{4.5}$$

In equation 4.5, 'S_{25}' and 'O_{25}' are the span and offset of the sensor at room temperature (25°C).

If the sensor operational temperatures reach the region where Offset temperature sensitivity becomes non-linear (above 370K), equation 4.5 must be modified. This results in equation 4.6, where the value for offset (O_{interp}) will be determined by linearly interpolating from the existing experimental data points.

$$P = \frac{1}{S_{25} + \left(\frac{dS}{dT}\right)\Delta T}\left[V - O_{interp}\right] \tag{4.6}$$

While the Design Methodology (Chapter 3) introduced a different equation for determining the temperature effects (equation 3.2), due to the non-linear behavior of Offset above approximately 370K, equations 4.5 and 4.6 will be used.

4.3.4 Temperature Compensation Effectiveness

To test the effectiveness of the temperature compensation routine, the errors between the compensated and uncompensated signals were compared. The experimental data collected for the temperature calibration process was used to indicate the effects of the sensor temperature compensation.

The quasi-static pressure tests, conducted at a range of temperatures, provided a range of sensor outputs to test the temperature compensation techniques. This allowed a comparison between the calculated fluid pressure (determined from the sensor output) and the actual applied pressure (from the Dead Weight tester).

To simulate an uncompensated pressure sensor, the Span and Offset at 25°C were applied to the sensor outputs for each tested operational temperature. These values were compared to the actual applied pressure for each quasi-static calibration. The error associated with the uncompensated sensor is shown in figure 4.10.

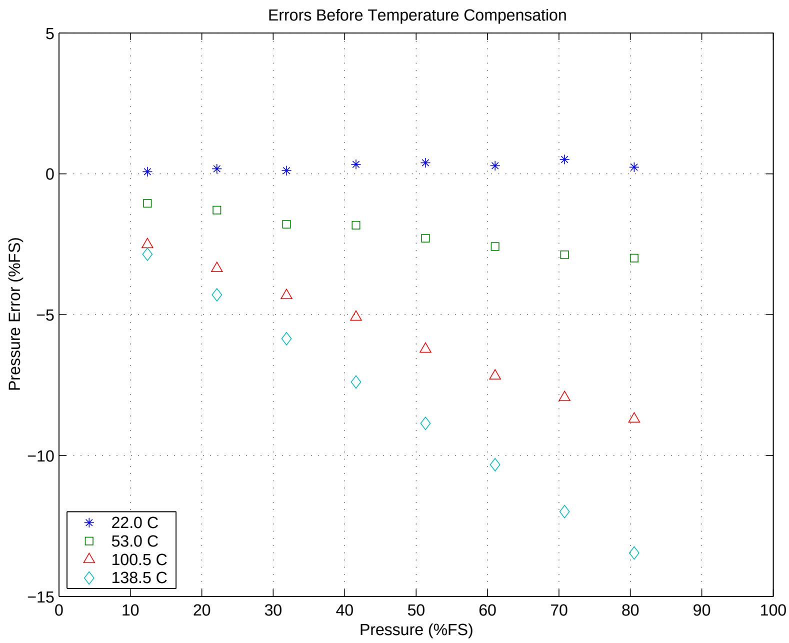

Figure 4.10: Error from an uncompensated piezoelectric sensor

The temperature compensation routine was applied to the experimental data. The values for applied pressure were determined using equation 4.6. The error associated with the compensated sensor is displayed in 4.11

The figures for the uncompensated and compensated sensor error demonstrate the capabilities of the temperature compensation routine. The pressure error was reduced from a maximum of 13.5% to less than 1%. While the magnitude of the compensated error is greater than the error determined in other similar experiments (see figure 2.4), the temperature range used for this experimentation was relatively large, reducing the accuracy of the temperature compensation.

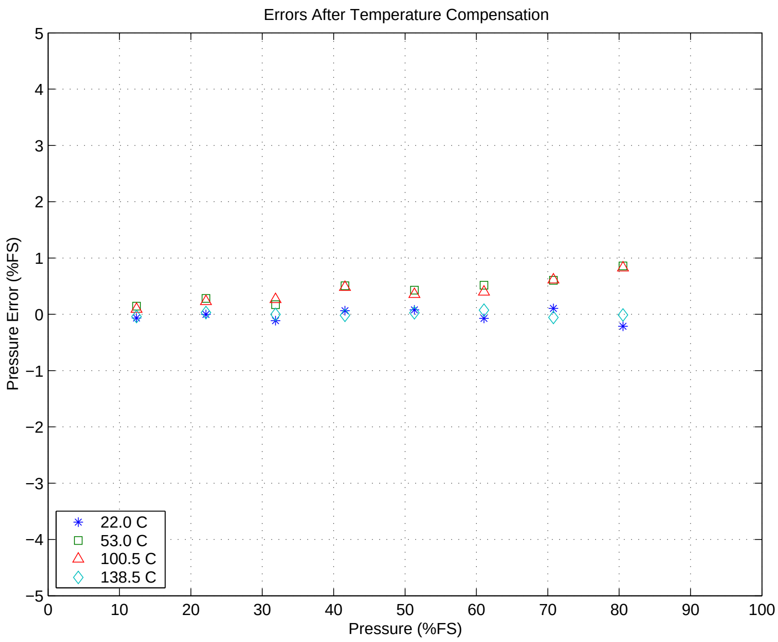

Figure 4.11: Error from a compensated piezoelectric sensor

4.4 Chapter Summary

Static Calibrations for are vital to ensure the accuracy of pressure tests using piezoresistive pressure transducers. Room temperature static calibrations were conducted for each of the piezoresistive pressure transducers used during this project, providing values of sensor Span and Offset. These room temperature calibrations are sufficient for experimental testing in the Shock Tube and the Gun Tunnel since the sensor temperature in these experiments remains relatively close to room temperature during the actual measurement of pressures.

Temperature calibrations become necessary once the piezoresistive pressure sensor operates at temperatures significantly different to room temperature (this will be the case for the pressure sensor used for testing pressures within the cylinder of the internal combustion engine). The temperature calibrations identified the relationship between the sensor characteristics (Span and Offset) and temperature. This allowed these sensor properties to be determined according to the particular operating temperature. To identify the operating temperature of the sensor, the value of V_{sense} was correlated to temperature, allowing the temperature of the sensor to be determined if V_{sense} was recorded.

Overall, these calibrations form the foundation of the work conducted in later sections of this dissertation. This chapter has provided an accurate means of determining the pressures measured by the sensor over a range of static conditions and operating temperatures. Other characteristics, such as the sensor dynamic response, can be now be thoroughly investigated in the following chapters.

Chapter 5

Dynamic Response Characteristics

5.1 Chapter Overview

This chapter explores the dynamic response characteristics of the piezoresistive pressure transducers. Using USQ's shock tube facility, various aspects of sensor response will be investigated, including sensor resonant frequency and response time. These characteristics reveal the capabilities of the pressure sensors under transient fluid pressures and dictate the level overall performance of the piezoresistive pressure transducers during fast-response thermofluids experiments.

5.2 Shock Tube Testing

The shock tube (introduced in the Design Methodology section (Chapter 3)) allows the sensor response to be analysed in detail. A photograph of the shock tube used for these experiments can be seen in figure 5.1

The particular piezoresistive pressure sensor used to test the dynamic response characteristics, was the Sensym SX150AHO sensor. Ideally, the dynamic response characteris-

Figure 5.1: Photograph of the shock tube used to test the sensor dynamic characteristics

tics for all three types of sensors could be investigated, however due to time constraints, only one type of sensor was tested with the shock tube. The dynamic characteristics of the SX150AHO sensor can however be generally related to the behavior of the other types of piezoresistive sensors.

5.2.1 Detailed Experimental Design

The SX150AHO pressure sensor is mounted to a plate that is attached to the end of the shock tube (the foreground of the picture in figure 5.1). The top surface of the sensor was level with the interior side of the plate (this positioned the pressure sensitive chip of the transducer approximately 3mm from the interior face of the mounting plate). Details of the shock tube mounting plate and the related mounting screw are shown in Appendix D.

Piezoelectric sensors are fitted along the tube at known locations. These sensors were used to determine shock speeds along the tube (by determining the shock speed, a theoretical analysis of the shock wave can be applied). The positioning of the piezoresistive and piezoelectric pressure transducers are shown in figure 5.2.

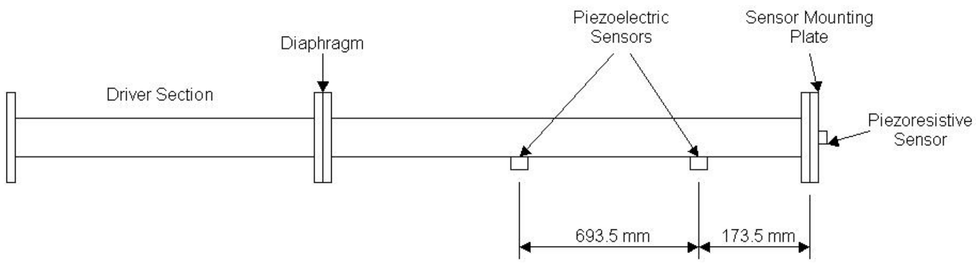

Figure 5.2: Schematic diagram of Shock Tube showing positions of pressure sensors

In all shock tube experiments, air was the test gas used. The diaphragm placed in the shock tube consisted of four sheets of common Cellophane (with the exception of the first shock tube test that used only three sheets).

For each shock tube test, pressure was increased in the driver section of the tube until the diaphragm burst. The rupture of the diaphragm caused a shock wave to propagate down the tube towards the sensor. The shock wave then hit the end of the tube where the sensor was mounted (reflecting back up stream), causing an approximate 'step' input of pressure to the pressure sensor. The response of the sensor to this input was then analysed.

A block diagram of the shock tube experiments demonstrates how the data was collected (figure 5.3).

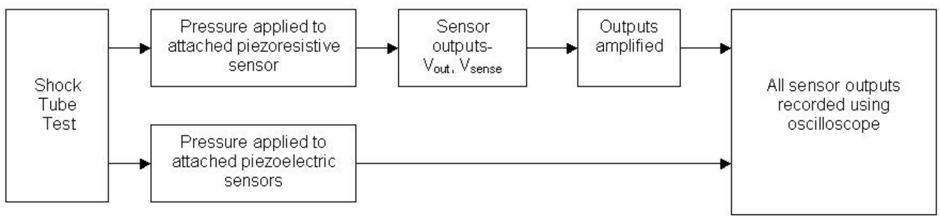

Figure 5.3: A block diagram, showing the method of pressure measurement for shock tube tests

5.2.2 Modification of Pressure Sensors

The stock SX150AHO sensor had a relatively small opening in its case, therefore the top of the case was removed in many instances to improve the filling time of the sensor (refer to figure 5.4. The filling time is the time taken for a higher pressure gas to fill the sensor.

Removing the top of the case further exposed the silicon diaphragm of the sensor to the test fluid. In these cases, to prevent foreign particles in the test gas from damaging the sensor, grease or latex were added (see figure 5.4) . Epoxy resin was also added to the sensors in some configurations to protect the gold connecting leads on the chip (the electrical connections). The use of Margarine (thinned with additional Canola oil) to protect the silicon chip was also trailed. This provided a readily available low viscosity grease-like compound, however Margarine was later found to deliver inconsistent results.

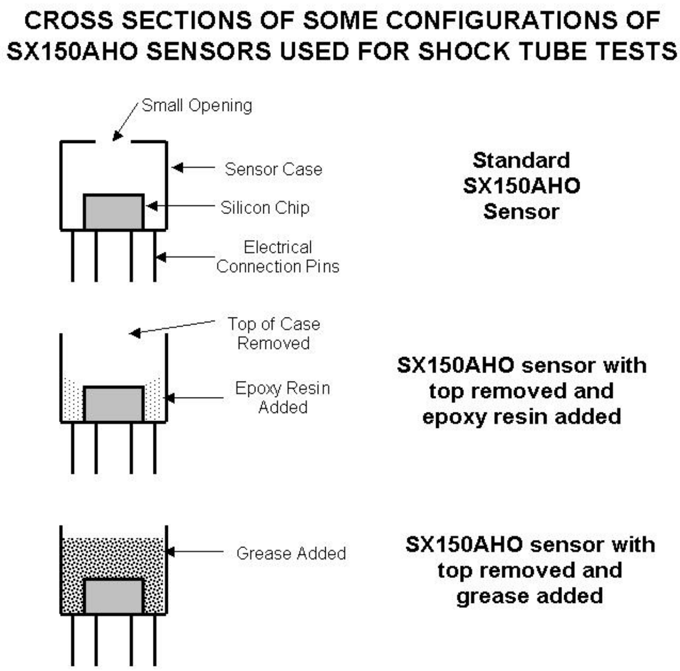

Figure 5.4: Modification of SX150AHO sensors

Once a sensor was modified or a new sensor was required, a static calibration (at room temperature) was conducted to redetermine the values of Span and Offset for that particular transducer (the static calibration process described in Chapter 4). A summary of these sensor modifications and their related calibration number can be viewed in table 5.1.

Calibration Number	Sensor Modification
1	Unmodified
2	Top of sensor removed
3	Top removed, Epoxy added around chip (wires and diaphragm exposed)
4	Top removed, Epoxy added around chip (wires covered, diaphragm exposed)
5	Sensor from (4), approx 1mm layer grease added over diaphragm
6	Sensor from (5), approx 3mm layer grease added over diaphragm (grease up to sensor lip)
7	Sensor from (2), thin layer latex (<1mm) added over diaphragm
8	Sensor from (7), grease added up to sensor lip over diaphragm
9	Sensor, top removed, approx 3mm of Margarine added over diaphragm (up to sensor lip)

Table 5.1: Summary of sensor modifications used for shock tube tests

The analysis of the Shock Tube tests for each of the sensor configurations displayed in table 5.1 is detailed in the next section.

5.3 Analysis of Results

The summary shown in table 5.2 displays the type of sensor used for each Shock Tube test. The atmospheric pressure and temperature at the time of each test were also recorded to allow for analysis of the Shock Tube results. The MATLAB script associated with the analysis of the Shock Tube tests, '‘shock_analysis2’ is shown in Appendix C.

The outputs recorded for each Shock Tube test can be seen in graphs in Appendix E. This includes short and long time span sensor responses, graphs of reflected shock pressures, graphs for each sensor response showing 10 and 90% response lines and a power spectrum analysis for each Shock Tube test.

Shock Test Number	Related Calibration	Notes
1	1	
2	1	
3	2	
4	2	
5	3	
6	3	
7	4	
8	5	
9	5	Sensor had approx 2mm layer grease (cal. for 1mm layer of grease used)
10	6	
11	7	
12	7	Sensor had approx 1mm layer grease added (cal. for no grease used)
13	8	Sensor had approx 1mm layer grease added (cal. for no grease used)
14	8	
15	8	
16	9	
17	9	

Table 5.2: Shock Tube tests and corresponding sensors used

5.3.1 Reflected Shock Pressures

A theoretical analysis was used to calculate the fluid characteristics of the shock wave generated in the Shock Tube. This analysis, consisting of basic gas equations, was provided in a series of MATLAB scripts produced by Dr. David Buttsworth. The program code for running this analysis 'p_T_reflected' is displayed in Appendix C.

By determining the inbound shock speed and inputting the ambient temperature and pressure, the reflected shock conditions of the test gas could be determined. This allowed the theoretical reflected shock pressure to be compared with the value indicated by the piezoresistive pressure transducer.

To determine the inbound shockwave speed, the time taken for the shock wave to travel along the tube was calculated. Two piezoresistive pressure transducers were located at known positions along the tube (figure 5.2). The silicon chip of the piezoresistive sensor was located 3mm behind the surface of the mounting plate, therefore 3mm was added to the original measurement from the piezoelectric sensor to the end of the

Shock Tube (173.5 mm in figure 5.2) (the distance between the second piezoelectric transducer and the piezoresistive transducer was therefore actually 176.5 mm). As the shock wave passed these sensors, a sudden increase in pressure occurred. A rapid increase in pressure also occurred in the piezoresistive pressure transducer (mounted at the end of the Shock Tube). By measuring the time between the sudden pressure changes in the sensors, the shock wave speed could be determined.

The measurement of shock speed between the three different sensors allowed three different shock speeds to be determined -

- Shock speed between the piezoelectric sensors
- Shock speed between the piezoelectric and piezoresistive sensor
- Estimated shock speed at the piezoresistive sensor

To estimate the shock speed at the piezoresistive sensor, a uniform deceleration of the shock wave was assumed. Therefore, given the time and location of the shock wave at the two piezoelectric sensors and the piezoresistive sensor, a third shock speed was calculated (the shock speed at the piezoresistive sensor). A second order polynomial was fitted to the points of time and displacement at each of the sensors. The gradient of this polynomial at the point of the piezoresistive sensor determined the shock speed at that point.

Since there was some degree of error in identifying the precise shock arrival times at each of the pressure transducers, a reflected shock pressure was determined from each of the calculated shock speeds.

To give a comparison between the theoretical analysis and the pressure sensor performance, an average pressure was taken from the piezoresistive sensor response after the signal had appeared to have settled sufficiently from the step input of the shock wave (the reflected shock pressure). A typical comparison between the theoretical and measured shock pressures can be observed in figure 5.5 ('P5' is the reflected shock pressure, 'US1' is the shock speed between the piezoelectric sensors, 'US2' is the shock speed between the piezoelectric and piezoresistive sensor and 'USP' is the estimated shock speed at the piezoresistive sensor).

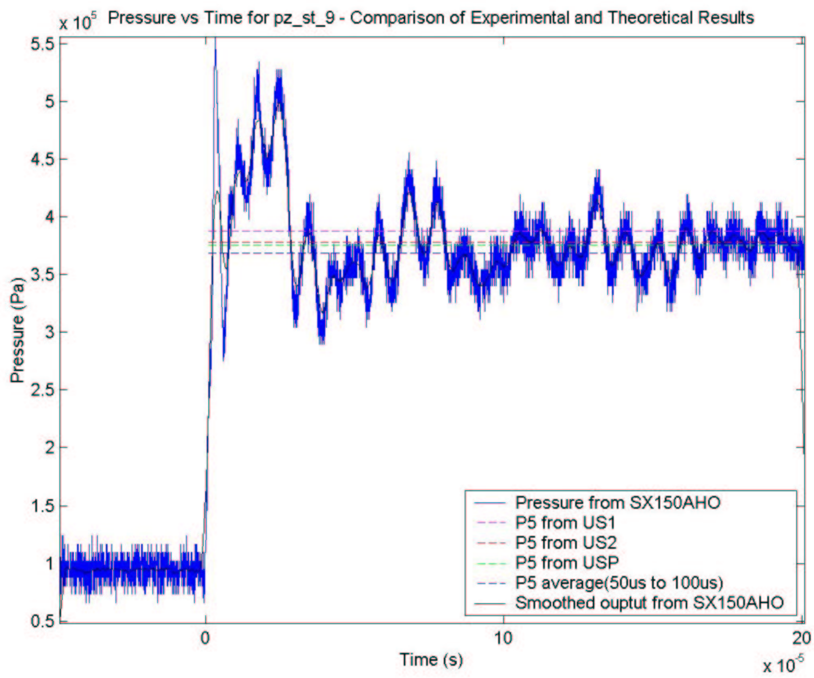

Figure 5.5: A typical sensor response and a comparison between measured and predicted reflected shock pressures.

Each sensor response was also recorded over a longer time scale. An average shock pressure was determined for each set of long time scale data from 0.5ms to 1.5 ms (graphs shown in Appendix E). This pressure average was also compared to the theoretical reflected shock pressures. For most Shock Tube tests, the sensor response had settled well before this time window, therefore the average shock pressures determined over the long time scale were generally not accurate. A plot of a typical long time sensor response (showing theoretical and measured pressures) can be observed in 5.6.

A comparison between the theoretical and measured shock pressures (short time scale) for all Shock Tube tests are shown in table 5.3.

- 'P5 1' is the reflected shock pressure based on the shock speed between the piezoelectric sensors
- 'P5 2' is the reflected shock pressure based on the shock speed between the piezoelectric and piezoresistive sensors
- 'P5 P' is the reflected shock pressure based on the estimated shock speed at the

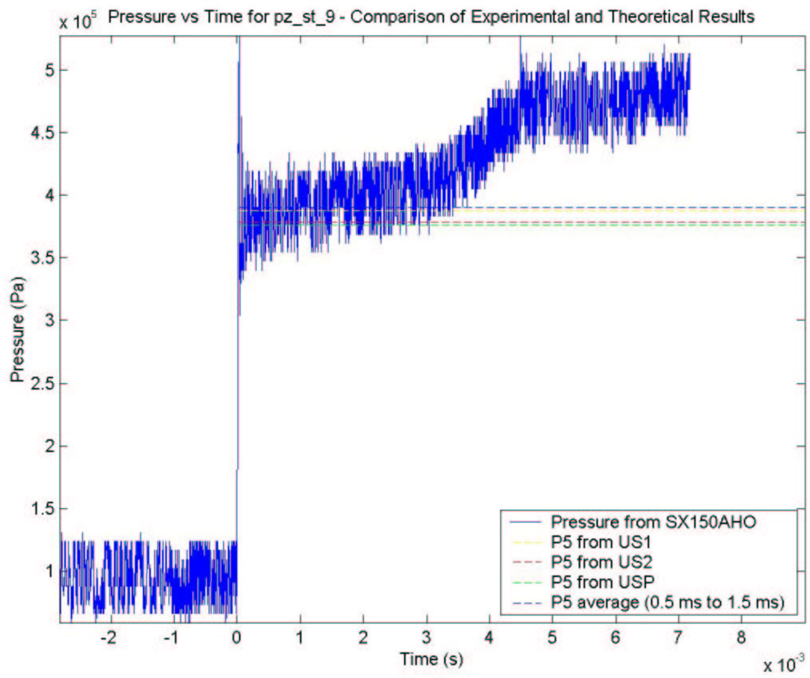

Figure 5.6: A typical long time scale sensor response and a comparison between measured and predicted reflected shock pressures.

piezoresistive sensor

- 'P5 measured' is the measured reflected shock pressure from the piezoresistive sensor output.

A comparison between the theoretical and measured reflected shock pressures in table 5.3 reveals some differences in results, however in most cases, the estimated shock pressure at the piezoresistive pressure transducer (P5 P) provided a reasonable estimation of the experimental value. It may also be noted that for some shock tests the shock speed (and therefore the shock pressure) appeared to increase along the Shock Tube. This scenario can obviously not occur and appears purely as a result of errors from the estimation the shock arrival times at the sensors.

The estimated reflected shock pressures for the Shock Tubes tests 1 and 2 were the average pressures taken from 300 to 400 μs (this was taken from the long time span data). This time window was selected due to the estimated filling time of the sensor. Filling time equations developed by Dr. David Buttsworth (derived from basic gas and energy conservation equations) were used to calculate the filling time of the unmodified

Shock Test Number	**P5 1 (kPa)**	**P5 2 (kPa)**	**P5 P (kPa)**	**P5 measured (kPa)**
1	354.0	324.5	318.7	316.6
2	411.5	383.7	378.1	375.0
3	417.1	384.6	378.1	421.1
4	340.0	353.5	356.3	338.3
5	417.5	410.5	409.1	402.4
6	387.1	377.3	375.3	371.9
7	422.0	410.5	408.2	405.7
8	413.9	394.4	390.4	394.8
9	388.8	378.1	376.1	368.8
10	375.7	378.1	378.6	382.0
11	406.3	403.9	403.4	411.0
12	353.4	341.4	339.0	339.0
13	361.0	355.9	354.9	355.0
14	353.4	355.9	356.4	358.3
15	368.8	355.9	353.3	366.0
16	419.8	355.9	343.3	442.2
17	349.7	327.5	323.1	369.0

Table 5.3: Comparison between theoretical and measures reflected shock pressures)

SX150AHO sensor (the equations, contained in a MATLAB script, involved calculation of sonic and subsonic flow through a converging diverging nozzle). To use the filling time equations with the shock tube data, the MATLAB script 'Fill_time' was written (shown in Appendix C). A comparison was made between the theoretical internal pressure as the sensor fills, and the recorded sensor output (converted to pressure). This revealed that the true reflected shock pressure may not be recorded by the sensor until approximately 300 μs after the arrival of the shock (hence taking the average reflected shock pressure from 300 to 400 μs). The relationship between the theoretical filling pressure and the sensor output can be observed in figure 5.7.

Since the internal pressure of the sensors in shock tests 1 and 2 do not appear to closely follow the results derived from the filling equations, the effect of the shock wave entering the sensor may have introduced additional air mass or pressure into the sensor (the filling equations don't take the effect of the shock wave into account). While the gas flow processes during the period of the shock wave entering the unmodified sensor are not exactly known, if the internal pressure of the pressure sensor increased significantly due to the effects of the shock wave, it is possible that the remainder of the sensor response is still governed by the filling equations. The graph shown in figure

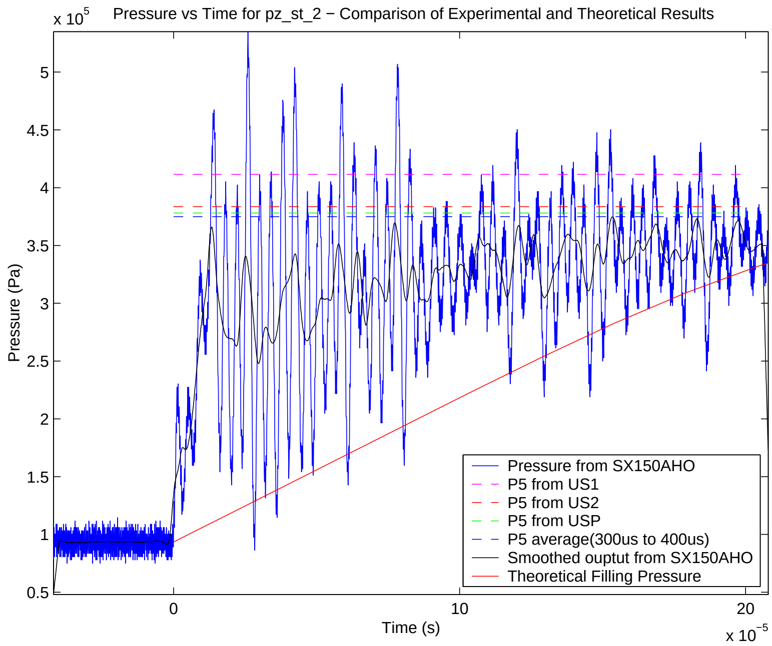

Figure 5.7: Comparison of sensor response and theoretical internal pressure over time for shock test 2

5.8 gives a possible theoretical filling situation, In this case, the shock wave is assumed to rapidly increases the sensor pressure to 250 kPa before the theoretical filling process is applied.

The point in time at which the average reflected shock pressure was taken, may account for some of the discrepancy between the practical and theoretical results. The windows of time used to determine the average pressures were only based on estimations that the sensor response had sufficiently settled. Shock tests 1 and 2 measured the average reflected shock pressures from 300 to 400 μs. Shock tests, 3 to 13, measured the average reflected shock pressures from 50 to 100 μs after the arrival of the shock wave. Shock tests 14 to 17 measured the average reflected shock pressure from 160 to 210 μs due to the longer settling time of these sensor responses. By taking an average pressure over slightly different windows of time, a variety of values for the measured reflected shock pressure could be obtained, introducing some error into the results.

The differences between the actual and predicted results may also be due to the idealized assumptions used in the theoretical analysis.

The general similarity demonstrated between the average reflected shock pressure mea-

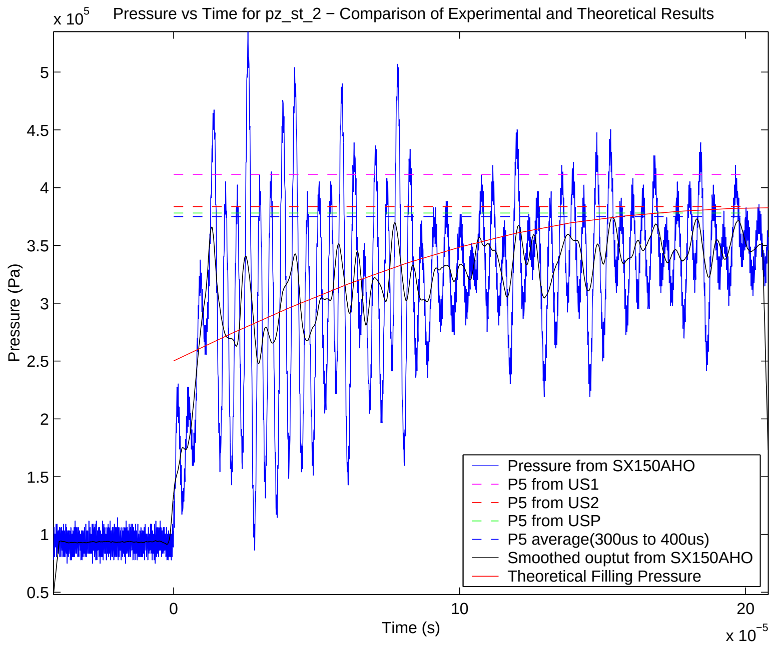

Figure 5.8: Comparison of sensor response and a possible theoretical model of internal pressure over time for shock test 2, given that the shock wave increases the internal pressure of the sensor to 250kPa

sured and the predicted shock pressure (taking the estimated shock speed at the piezoresistive sensor), suggests high reliability and accuracy from the piezoresistive pressure transducers.

5.3.2 Identification of Resonant Frequencies

The resonant frequency of the silicon diaphragm of the piezoresistive pressure transducer is a factor which determines the maximum operational frequency of the pressure sensor. If these sensors are to be used in fast-response thermofluids experiments, such as pressure measurement in an internal combustion engine, the errors associated with various frequencies of pressure fluctuations should be determined.

The oscillations of the output signal from the pressure transducers are due the vibration of the silicon diaphragm and the resonance of other bodies (such as the air) adjacent to the sensor. The sensor output from Shock Tube test number 4 (figure 5.9) demonstrates the existence of multiple modes of vibration.

The high frequency oscillations visible in figure 5.9 were found to be due to the os-

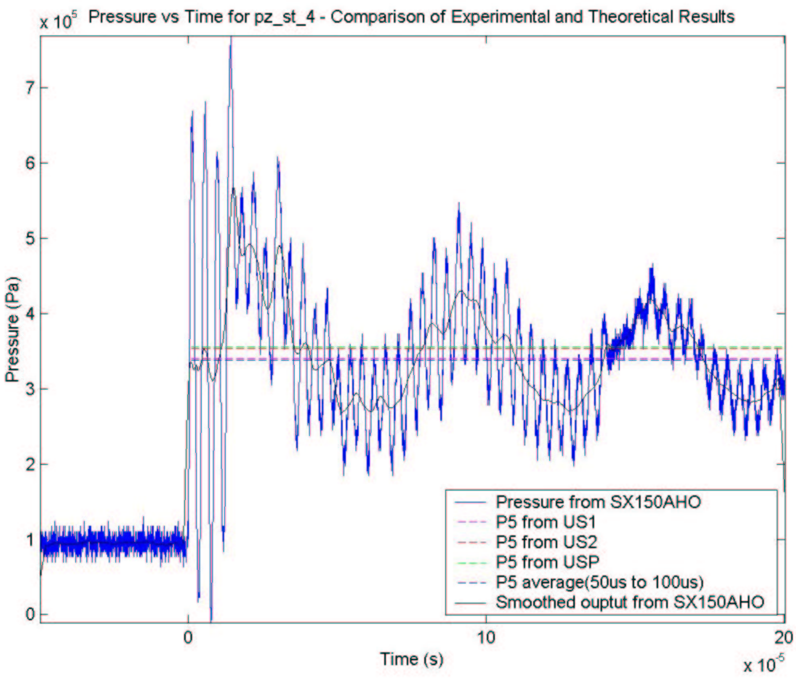

Figure 5.9: Sensor output from Shock Tube test 4, demonstrating multiple modes of vibration

cillation of the silicon diaphragm. The lower frequency oscillations are likely to be caused by the acoustic resonance of air in front of the sensor. Various sensor configurations with a bare silicon chip (no added grease or silastomer) demonstrated similar high frequency oscillations but different lower frequency modes, verifying that the high frequency vibration mode was not related to the configuration of the sensor. This high frequency resonance must therefore be due to the resonance of the silicon diaphragm.

The resonant frequencies of air in front of the pressure transducers can be estimated. For the unmodified pressure transducer, a model of air resonating in a cavity with a small opening can be applied with equation 5.1 ('v' is the speed of sound, 'A' is the area of the inlet, 'L' is the length of the inlet, and 'V' is the volume of the cavity) (HyperPhysics 2003),

$$f = \frac{v}{2\Pi}\sqrt{\frac{A}{VL}} \tag{5.1}$$

Applying this equation to the reflected shock conditions and the geometry of the unmodified sensor, the resonant frequency equated to approximately 8 kHz (period of

1.25e-4 s). Oscillations close to this frequency are partially visible in the Shock Tube data from the unmodified sensors (Shock Tube tests 1 and 2).

For the sensors with the top of the transducer case removed, a model of air resonating as a column can be applied. The model simulates the resonance of air in a cylinder with one closed end. The resonant frequency can be determined with equation 5.2 ('n' is the mode of vibration (n = 1,3,5 etc), 'v' is the speed of sound, 'L' is the length of the cylinder of air) (HyperPhysics 2003),

$$f = \frac{nv}{4L} \tag{5.2}$$

After applying this equation, the resonant frequency equated to approximately 25 kHz (period of 4e-5 s). Oscillations of similar frequency may be noted in the Shock Tube data from the sensors where the top of the case has been removed and little material (grease etc.) was added (Shock Tube tests 3,4,5,6,7,8,11,12 and 13).

A MATLAB script was developed to analyse the power spectrum density of the sensor responses (this script, 'psd_display.m', is displayed in Appendix C). The power spectrum density analysis calculates the magnitude of a range of frequencies, that when added together, produce the sensor output signal. This analysis can be used to identify the resonant frequencies of the response, since these frequencies will be represented by a peak on the power spectrum density plot.

An analysis of the power spectrum density for the various sensor outputs reveals the high frequency resonance of the diaphragm (the lower frequency oscillations related to the resonance of other bodies have very few oscillations, therefore these frequencies are not obvious on the power spectrum density analysis). A very high frequency resonance (several MHz) was identified in most sensor responses however this was found to be signal noise and was not included in the resonant frequency analysis. The power spectrum density of Shock Tube test 4 (shown in figure 5.9) is displayed in figure 5.10.

The power spectrum density in figure 5.10 shows a clear peak about the resonant frequency of the silicon diaphragm at 246.7 kHz (the high frequency oscillations visible in the sensor output). The diaphragm resonant frequencies were recorded for each

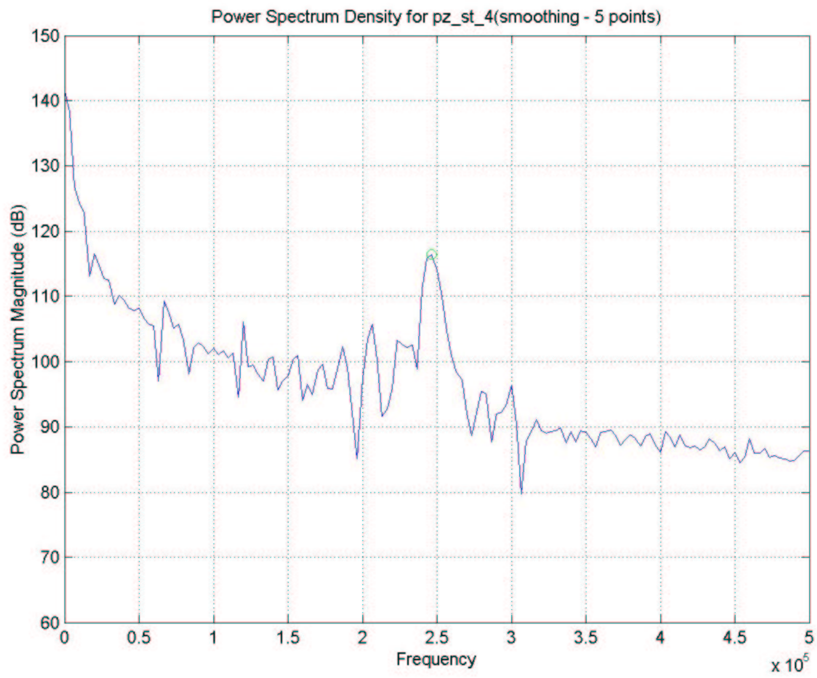

Figure 5.10: The power spectrum density of Shock Tube test 4, showing the resonant frequency of the silicon diaphragm

Shock Tube test (displayed in table 5.4). In the cases where the frequency is 0 Hz, no clear resonant frequency was identifiable.

These results demonstrate how the resonant frequency of the sensor can be affected by adding different substances (such grease epoxy or latex) to the sensor. The first four Shock Tube tests have identical resonant frequencies, since each of these sensor configurations added no substances to the sensor diaphragm. This suggests the resonant frequency of the unmodified silicon diaphragm is 246.7 kHz. Sensors with added layers of grease or latex demonstrated lower resonant frequencies (due to the addition of mass attached to the diaphragm).

The sensor used in Shock Tube test 7 recorded a higher than normal resonant frequency. This is due to the epoxy resin that was added to the sensor, since some epoxy was placed around the edges of the chip, effectively decreasing the size of the flexible diaphragm and therefore increasing the resonant frequency. Unfortunately the value of Offset for the sensors with the epoxy resin was very sensitive the clamping force used to hold the sensors in place. This occurred since the epoxy provided a ridged connection between the silicon chip and the body of the sensor. The drawback of mounting sensitivity made

Shock Test Number	**Resonant Frequency (kHz)**	**Sensor Configuration**
1	246.7	Unmodified
2	246.7	Unmodified
3	246.7	Top of Case Removed
4	246.7	Top of Case Removed
5	240.0	Epoxy Added, Wires Exposed
6	240.0	Epoxy Added, Wires Exposed
7	263.3	Epoxy Added, Wires Covered
8	133.3	Epoxy Added, 1mm Grease
9	106.7	Epoxy Added, 2mm Grease
10	20 (1)	Epoxy Added, 3mm Grease
11	183.3	Latex Added <1mm
12	0	Latex Added, 1mm Grease
13	0	Latex Added, 1mm Grease
14	0	Latex Added, 3mm Grease
15	0	Latex Added, 3mm Grease
16	0	3mm Margarine
17	136.7	3mm Margarine

Table 5.4: Diaphragm resonant frequencies determined from power spectrum density analysis (a resonant frequency of 0Hz indicates that no clear frequency was identified)

note 1: On observation of the sensor response of Shock Tube test 10, a resonance of approximately 20 kHz is present (this does not appear on the power spectrum density analysis due to the small number of oscillations). Since the resonance of this particular sensor with no grease is 263.3 kHz (test 7), with a 1 mm layer of grease is 133.3 kHz (test 8) and a 2 mm layer of grease is 106.7 kHz (test 9), it is possible that the resonant frequency of the sensor diaphragm in test 10 (with a 3 mm layer of grease) is approximately 20 kHz (due to the trend of a decreasing resonant frequency with an increasing vibrating mass).

the used of these sensors less attractive.

The sensors with Margarine (tests 16 and 17) delivered inconsistent results. While the twin peaks evident in the sensor responses in tests 16 and 17 may be due to some form of resonance (refer to plots shown in Appendix E), the true cause of the secondary peak in the sensor response remains unknown. Since the results of sensors with Margarine are inconsistent and difficult to predict, the future use of Margarine in sensors will be avoided.

Fast response piezoelectric sensors exhibit similar resonant frequencies to the values determined for the piezoresistive transducers. The PCB 112B11 piezoelectric sensor, used for the engine and Gun Tunnel pressure measurements (specifications in Appendix B), has a resonant frequency of $\geq$ 200 kHz. This suggests that the transient pressure measurement performance from the low cost piezoresistive devices may be similar to expensive piezoelectric sensors.

5.3.3 Errors Related to Frequency of Measured Pressures

Errors in the output of the piezoresistive pressure transducers occur as the frequency of pressure fluctuations in the test fluid begins to approach the resonant frequency of the diaphragm within the sensor. A second order system can be used to simulate the dynamic characteristics of the silicon diaphragm of a piezoresistive pressure transducer (Ainsworth et al. 2000). The transfer function of such a system can be displayed by equation 5.3 (Ainsworth et al. 2000).

$$F(j\omega) = \frac{1 - \left(\frac{\omega}{\omega_0}\right)^2 - j2h\left(\frac{\omega}{\omega_0}\right)}{\left[\left(1 - \left(\frac{\omega}{\omega_0}\right)^2\right)\right]^2 + 4h^2\left(\frac{\omega}{\omega_0}\right)^2} \tag{5.3}$$

In equation 5.3 ω_0=(k/m)$^{1/2}$ was the undamped natural frequency and h=(c/2mk)$^{1/2}$ was the damping ratio.

For typical step response signals it is possible to determine the damping ratio, however the outputs from many of the Shock Tube tests do not allow the damping ratio to be accurately calculated. From examining the sensor responses, it is possible to deduce that the addition of grease or latex to the sensor typically increased the damping ratio (due to the fewer high frequency oscillations present in the sensor response).

The relative amplitude ratio and phase shift for the transfer function in equation 5.3 are shown in figure 5.11.

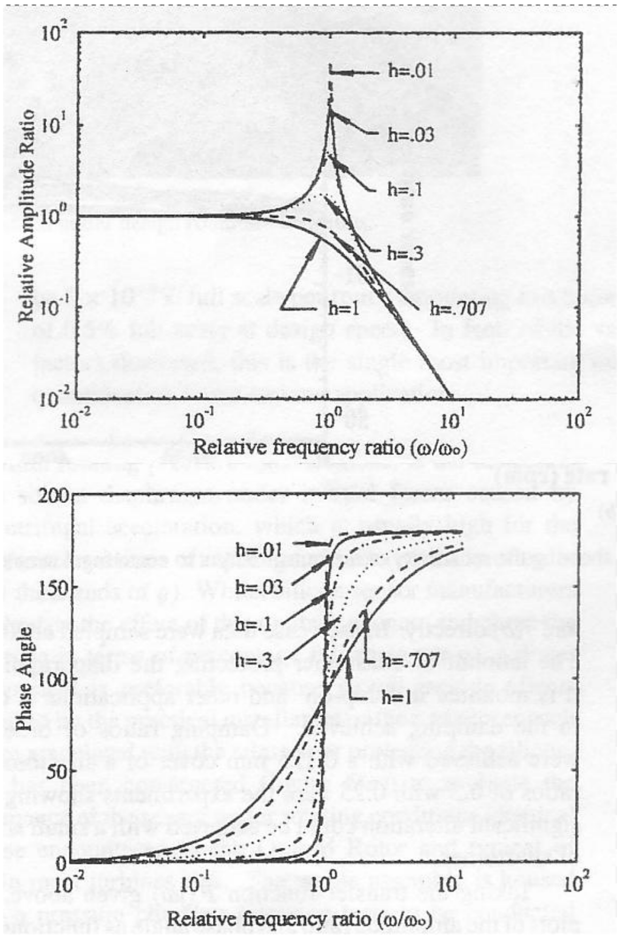

Figure 5.11: The amplitude ratio and phase shift for relative frequency ratios (Ainsworth et al. 2000)

Since the sensors tested in Shock Tube mostly exhibit a very low damping ratio (possibly around 0.01), the error related to the relative amplitude ratio (figure 5.11) increases rapidly as the testing frequency approaches the resonant frequency of the sensor diaphragm. The phase angle of the sensor response also changes dramatically as the testing frequency nears the undamped natural frequency of the sensor (in cases where the damping ratio is small, the undamped natural frequency and the resonant frequency of the sensor diaphragm are very similar). Therefore, to ensure high accuracy for any results obtained from these piezoresistive pressure sensors, the frequency of pressure fluctuations should not exceed a value that is approximately an order of 10 below the resonant frequency of the transducer (1/10 of the diaphragm resonant frequency).

To estimate the error related to a particular test frequency, equation 5.4 can be used (Balachandran & Magrab 2004, eq. 5.99). This equation approximates the amplitude error of a system with a small damping ratio.

$$\frac{f_a}{f_n} = \sqrt{1 - \frac{1}{1+d}} \tag{5.4}$$

In equation 5.4, 'f_a' is applied frequency of pressure fluctuation, 'f_n' is the natural frequency of the diaphragm (since the damping ratio is typically very small, the natural frequency is approximately the resonant frequency of the sensor) and 'd' is the error in the sensor response. If the experimental pressure fluctuations are at 1/10 of the sensor natural frequency ($\frac{f_a}{f_n} = 0.1$), the approximate error is 1.01%.

The various sensor configurations tested typically demonstrated relatively high resonant frequencies. This suggests that piezoresistive pressure transducers may be able to accurately record high frequency pressure fluctuations.

5.3.4 Sensor Response Time

The sensor response time (or rise-time) was identified as the time taken for the sensor output to rise from 10 to 90% of its full scale response after a step input. The response times for each of the sensor configurations were analysed to test the suitability of these sensors to fast-response measurement situations.

As shown in figure 5.12, the 10 and 90% levels were based on the average reflected shock pressure (the average pressure taken from a window of time after the response of the sensor had sufficiently settled).

Initially a smoothed sensor response line was used to indicate the points where the response crossed 10 and 90%. This was later found to introduce errors in situations

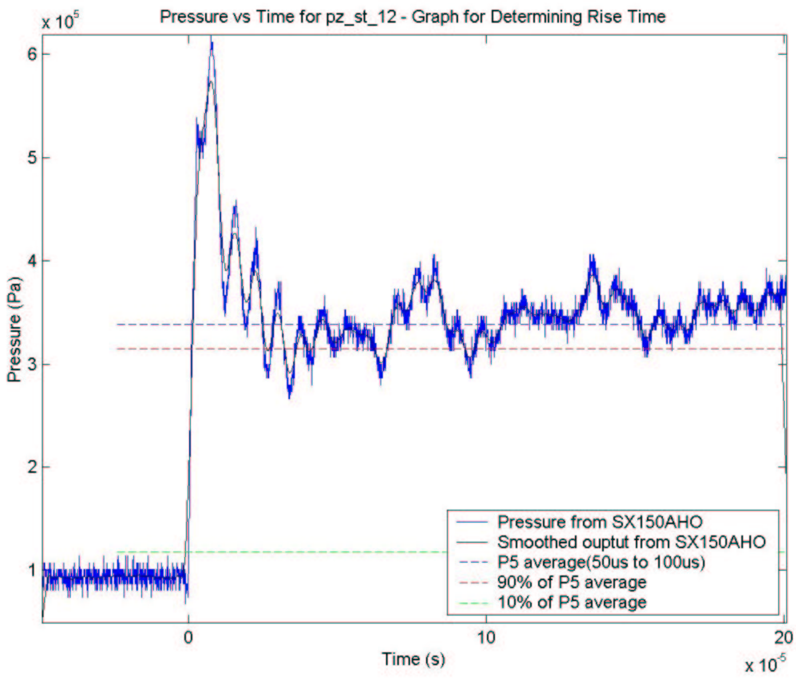

Figure 5.12: The 10 and 90% lines used to measure the response time of the sensor

where particular sensors had very fast response times (the smoothing of the data effectively increased the measured response time). The response times for each of the Shock Tube test results were measured by recording the time that the sensor response (not smoothed) first crossed the 10% line, to the time that the sensor response first crossed the 90% line. In some situations the 10% line was beneath the amplitude of the noise generated before the step input (meaning that the sensor output appeared to cross the 10% line several times before the actual response of the sensor). To obtain useful results from these cases, the output associated with the actual step response of the sensor was identified (the signal which is clearly not associated with noise), and the time at which this line crossed the 10% line was recorded. A summary of the response times for each of the sensors tested can be seen in table 5.5.

The sensor response times displayed in table 5.5 can be explained by examining each sensor configuration. The relatively slow response times of tests 1 and 2 are due to the small opening in the unmodified sensors and the resulting filling time (explained previously in the subsection 5.3.1). The sensors with the top of the case removed and none/or little material covering the sensor recorded the fastest response times. The sensor response times typically decreased as more material (grease etc.) was added

Shock Test Number	**Response Time (μs)**	**Sensor Configuration**
1	12.96	Unmodified
2	12.52	Unmodified
3	0.38	Top of Case Removed
4	0.38	Top of Case Removed
5	0.57	Epoxy Added, Wires Exposed
6	0.67	Epoxy Added, Wires Exposed
7	0.35	Epoxy Added, Wires Covered
8	1.51	Epoxy Added, 1mm Grease
9	2.20	Epoxy Added, 2mm Grease
10	9.69	Epoxy Added, 3mm Grease
11	0.61	Latex Added <1mm
12	0.90	Latex Added, 1mm Grease
13	1.12	Latex Added, 1mm Grease
14	55.46	Latex Added, 3mm Grease
15	40.51	Latex Added, 3mm Grease
16	3.36	3mm Margarine
17	21.45	3mm Margarine

Table 5.5: Response times for sensor outputs for each of the Shock Tube tests

to the sensor diaphragm (since this added more mass to the diaphragm). This can be observed when comparing the response times of tests 7,8,9 and 10 (no grease, thin layer of grease (1 mm), medium layer of grease (2 mm) and thick layer of grease (3 mm) respectively). The combination of grease and latex within the sensor gave the slowest response times (tests 14 and 15) while the sensors containing margarine demonstrated further inconsistency in their results.

The manufacturer's specifications for the unmodified sensors (tests 1 and 2) quote a response time of 0.1 ms, significantly longer than the response times determined experimentally (12.98 μs for test 1 and 12.52 μs for test 2). This difference may be due to the manufacturer stating a response time associated with a worst-case scenario, to avoid litigation if the sensors did not perform to their specifications under some circumstances.

Overall, the experimental results demonstrate that the response time of the transducers can be significantly improved through some simple modifications to the pressure sensors. The response times for several of the modified sensors are also relatively fast, proving that these piezoresistive sensors are capable of providing accurate readings under rapidly changing pressures.

The response times of fast-response piezoelectric sensors are similar to the response times of the piezoresistive sensors used in the Shock Tube experimentation. The PCB 112B11 piezoelectric sensor, used for the engine and Gun Tunnel pressure measurements (specifications in Appendix B), has a response time of ≤ 3 μs. The similarity of the piezoelectric and piezoresistive sensor response times indicates that the piezoresistive sensors are well suited to the measurement of transient pressures.

5.4 Chapter Summary

Overall, a sensor configuration can be selected which best matches the requirements for the pressure measurement situation.

If slower pressure changes are expected, the stock SX150AHO sensor could be used. This transducer would be most effective if the pressure fluctuations were below the resonant frequency of the air inside the pressure sensor - approximately 8 kHz.

The measurement of higher frequency pressure oscillations is best suited to sensors where the top of the transducer case has been removed. These sensors, where only a thin layer of latex or grease has been added, offer high resonant frequencies and fast response times. The addition of a thin layer of grease or latex on the silicon diaphragm can also significantly increase the damping ratio of the sensor if required. Thicker layers of grease may be used if dynamic performance becomes less critical and the sensor must be protected from high speed foreign particles in the test gas or high fluid temperatures.

The sensor with the epoxy resin covering the connecting leads did offered the highest resonant frequency and the fastest response time, however the issues related to the mounting sensitivity of these sensors (where the clamping force influences the sensor Offset) make the choice of using this configuration of sensor less viable.

The modification of the SX150AHO pressure transducer can dramatically alter the dynamic performance of the transducers. This may ultimately enable these low cost piezoresistive pressure transducers (approximately $150) to replace the high cost fast response sensors (such as piezoelectric sensors - approximately $2000) in the measurement of pressures in fast-response thermofluids experiments.

Chapter 6

Pressure Measurement in the USQ Gun Tunnel

6.1 Chapter Overview

This chapter investigates the application of piezoresistive pressure transducers on dynamic pressure measurement within the USQ Gun Tunnel. The pressures produced during a Gun Tunnel test will be measured with a piezoresistive and a piezoelectric pressure transducer. The piezoelectric sensor used is a high end device with proven accuracy and fast response characteristics. This provided a bench mark by which the performance of the piezoresistive sensor could be compared.

6.2 Gun Tunnel Testing

The Operation of the Gun Tunnel produces a short duration test gas flow. A schematic diagram of the Gun Tunnel can be view in figure 6.1

As can be seen in the schematic diagram of the Gun Tunnel (figure 6.1), the apparatus consists of a driver tank, barrel, nozzle and dump tank. In the format used for this project, the end of the barrel was sealed off (not allowing the test gas to enter the

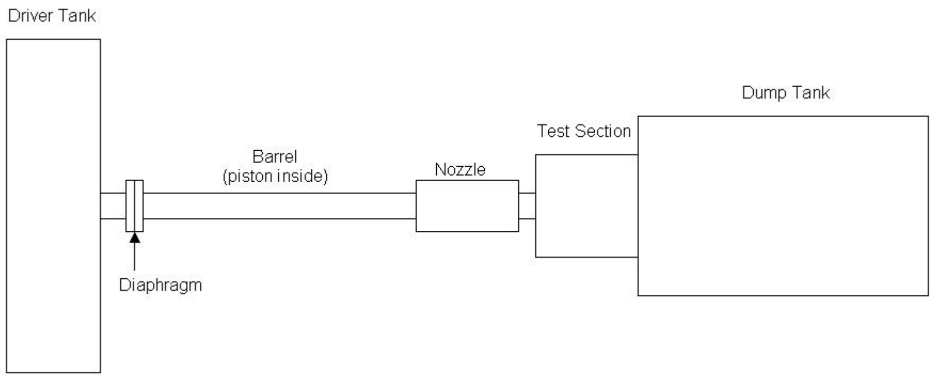

Figure 6.1: A schematic diagram of the USQ Gun Tunnel in the format used for this project (Top View)

converging diverging nozzle, testing section and the dump tank).

The particular sensor used for the Gun Tunnel testing was the Sensym 13U3000 (capable of withstanding a maximum pressure of 3000 psi). This sensor had a layer of silastomer (approximately 2mm thick) covering the pressure sensitive diaphragm to protect the sensor. Due to time constraints, this particular sensor was not analysed for its dynamic response characteristics. While a dynamic response analysis of this particular sensor would be ideal, the previous dynamic testing (using the shock tube) with the SX150AHO senors represents the characteristics of typical piezoresistive pressure transducers. The results from the dynamic response testing suggested that a piezoresistive pressure transducer could provide acceptable results under transient pressure conditions (due to fast response times and high resonant frequencies), therefore this chapter aims to test this theory in a practical application.

The piezoelectric sensor used as the benchmark for the piezoresistive pressure transducer is a PCB 112B11. The specifications for this transducer are shown in Appendix B.

6.2.1 Detailed Experimental Design

The piezoresistive and the piezoelectric sensors were placed at opposite sides of the barrel a short distance before the cap at the end of the barrel. Both sensors were at the same length along the barrel section, and since the flow produced from the Gun Tunnel within the barrel should be radially symmetric (about the axis of the barrel), the same fluid pressure should be simultaneously placed on both sensors during testing.

A photograph of the two pressure sensors mounted in the Gun Tunnel barrel is shown in figure 6.2. Detailed drawings of the mounting screw and barrel are shown in Appendix D.

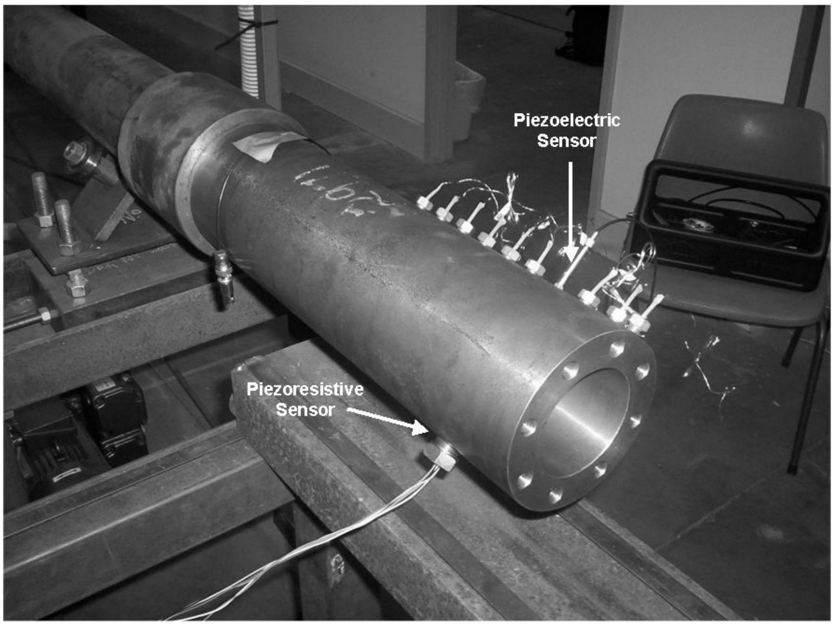

Figure 6.2: Mountings of piezoresistive and piezoelectric sensors in the Gun Tunnel barrel (note: the end of the barrel is unsealed at this stage)

Pressure was built up in the driver tank until the aluminium diaphragm ruptured. The gas from the driver tank then forced a piston along the barrel at high speed. The air in front of the piston was the measured test gas.

While in some Gun Tunnel experiments, the test section (in front of the piston) may be evacuated to a near vacuum prior to the test, this experiment initially had air in the barrel at room temperature and pressure.

A block diagram can be used to represent the method of data capture for this experimentation (figure 6.3)

While this experiment involved high gas temperatures, during the testing period where data was recorded from the piezoresistive sensor, the sensor did not have sufficient time to undergo a significant increase in temperature (pressures were recorded over

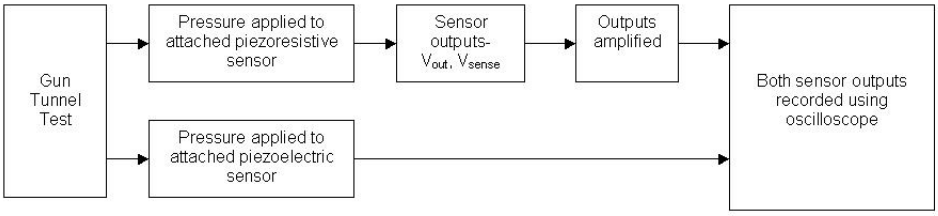

Figure 6.3: A block diagram, showing the method of pressure measurement for the USQ Gun Tunnel

a time window of only 45 ms). Heat transfer calculations were performed to insure that the sensor could not significantly increase in temperature over this time (the 2mm silastomer layer over the sensor effectively insulates the transducer from any significant change in temperature during testing).

6.3 Analysis of Gun Tunnel Results

It was determined that a single Gun Tunnel test was sufficient to test the characteristics of the piezoresistive pressure transducer against the piezoelectric pressure transducer. The results obtained from the Gun Tunnel tests were analysed using a MATLAB script 'gt28_analysis2' (shown in Appendix C).

6.3.1 Comparison with Piezoelectric Sensor

The results obtained from the piezoresistive sensor compared well with the pressure readings taken with the piezoelectric sensor. A graph showing the piezoresistive and piezoelectric outputs is shown in figure 6.4.

The signal from the piezoelectric sensor was clipped at its peak pressure due to the settings of the oscilloscope (see figure 6.4). While this prevents a direct comparison between the recorded peak pressures of both sensors, the dynamic response of the piezoresistive sensor can still be compared to the pressure readings taken from the piezoelectric transducer at different points of the overall sensor response. Figure 6.5 displays the readings after the peak Gun Tunnel pressure. This offers a more detailed

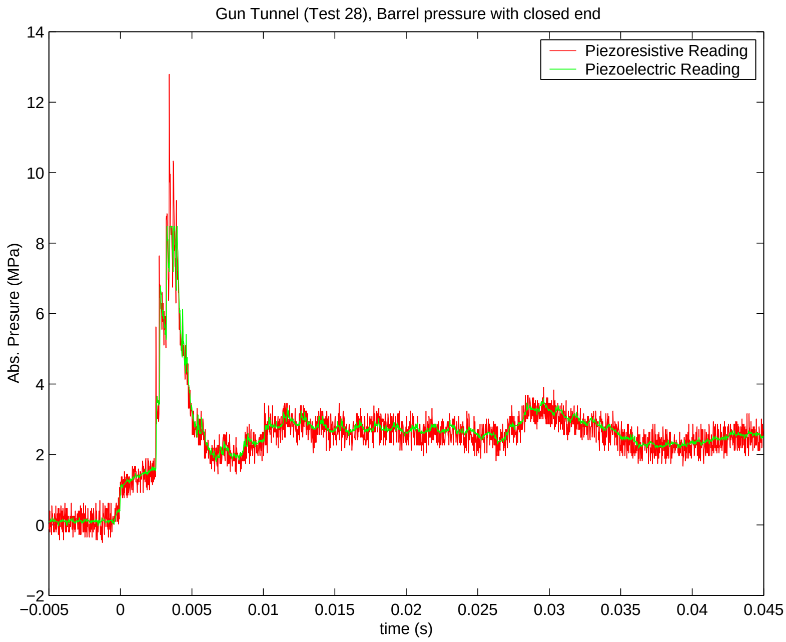

Figure 6.4: A comparison between the piezoresistive and piezoelectric pressure sensors

comparison between the sensor outputs.

Some noise was present in the signal from the piezoresistive sensor, so a smoothing routine was applied to the data. The smoothed output from the piezoresistive sensor is compared with the piezoelectric signal in figure 6.6. If the piezoresistive sensors were to be applied in future thermofluids experiments, it may be possible to further reduce the signal noise to gain clearer results.

The plot in figure 6.6 demonstrates that the piezoresistive sensor is well suited to applications requiring the measurement of transient pressures. There are no obvious signs of phase lag in the piezoresistive sensor in comparison to the piezoelectric signal or diaphragm resonance due to high frequency pressure fluctuations. Figure 6.7 displays the readings after the peak Gun Tunnel pressure, offering a more detailed comparison between the sensor outputs.

On close inspection of the results, it may appear that the piezoresistive sensor has a faster response time than the piezoelectric. While it is possible that the piezoresistive sensor has a faster response time, the slower response of the piezoelectric transducer may be due to the geometry of the sensor mounting in the barrel. The hole exposing the piezoresistive sensor to the test gas was significantly larger than the hole for the

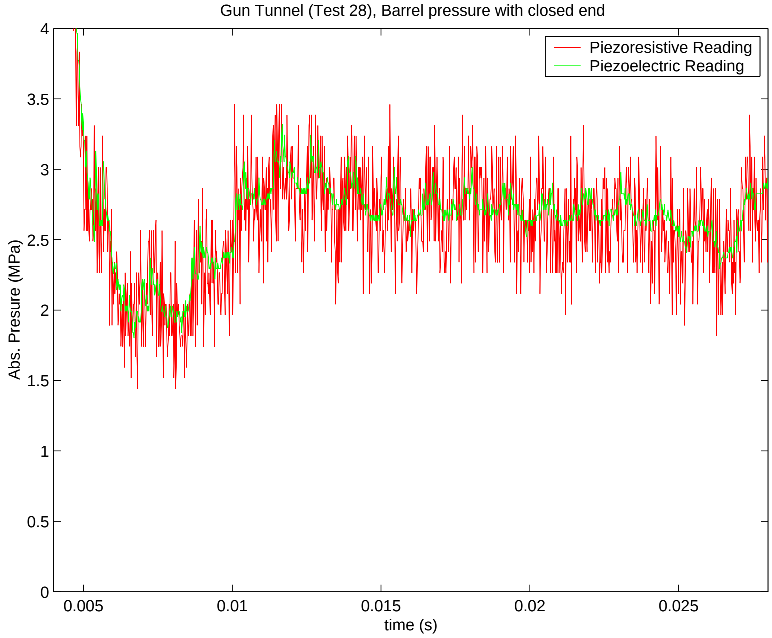

Figure 6.5: A comparison between the piezoresistive and piezoelectric pressure sensors after the peak Gun Tunnel pressure

piezoelectric sensor (8.5mm in comparison to approximately 2mm). This size difference may have allowed the air cavity in front of the piezoresistive sensor change pressure at a slightly faster rate. The true response time of the piezoresistive and piezoelectric transducers could be determined by conducting shock tube tests for each of the sensors, however time constraints did not allow this testing.

6.3.2 Theoretical Analysis

Unfortunately, while a theoretical analysis of the Gun Tunnel test was planned using a Lagrangian quasi one dimensional computational model, essential program files required for these calculations could not be acquired. A theoretical analysis of this experimentation is fortunately not critical, since the output of the piezoresistive pressure transducer has already undergone a comparison with the results obtain from a reliable piezoelectric pressure sensor. The theoretical results would not have been expected to exactly match the pressure readings from the sensors (due to certain assumptions made for the theoretical model), therefore a more valuable analysis was available by simply comparing the outputs of the two types of pressure sensors.

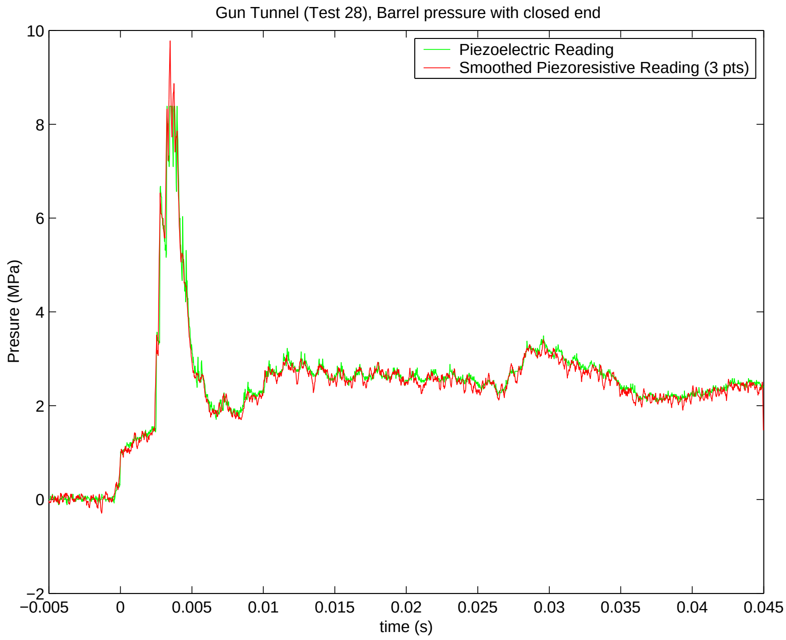

Figure 6.6: A comparison between the smoothed piezoresistive data and the piezoelectric sensor output

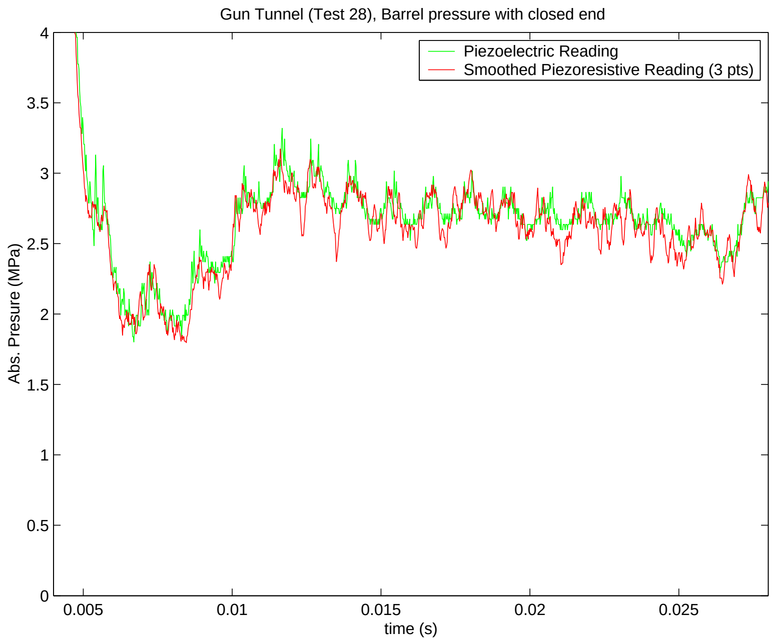

Figure 6.7: A comparison between the smoothed piezoresistive and piezoelectric pressure sensors after the peak Gun Tunnel pressure

6.4 Chapter Summary

Testing with the USQ Gun Tunnel has demonstrated the capabilities of the piezoresistive pressure transducers under transient pressure measurement conditions. The results obtained from the piezoresistive sensor closely match the pressure readings produced by the piezoelectric pressure transducer. The piezoelectric sensor is a high end device, known for its accuracy and fast response characteristics, therefore the similarity of the results obtained using the piezoresistive sensor indicates that the piezoresistive technology may provide a cost-effective solution for pressure measurement in fast-response thermofluids experiments.

Chapter 7

Pressure Measurement of Internal Combustion Engine

7.1 Chapter Overview

This chapter investigates the use of piezoresistive pressure sensors for the measurement of in-cylinder pressures of an internal combustion engine. This explores the dynamic response characteristics of the pressure sensors under high frequency pressure fluctuations with the added complication of temperature compensation. The results obtained from piezoresistive pressure measurements within the cylinder of the internal combustion engine will be compared to the pressure readings from a piezoelectric sensor. This gives an indication of the accuracy obtained from the piezoresistive device. A theoretical engine model will also simulate the cylinder pressures, giving further material to asses the operation of the piezoresistive sensor.

The piezoelectric sensor used as the benchmark for the piezoresistive pressure transducer is a PCB 112B11 (the same sensor used for the Gun Tunnel experimentation).

7.2 Cylinder Pressure Testing

The particular engine used for this experiment was detailed in Chapter 3. The piezoresistive sensor used for the engine testing was originally the Sensym 13U3000 sensor. Since the cylinder pressures recorded in previous experiments did not exceed 500 psi, the Sensym 13U0500 sensor was used (maximum pressure 500 psi). This sensor delivered a better signal to noise ratio when compare to the 13U3000 (maximum pressure 3000 psi) since the testing pressures extended over a greater portion of the total sensor pressure range. A silastomer coating was applied to the pressure sensitive diaphragm of the transducer to protect the diaphragm against high gas temperatures and foreign particles.

7.2.1 Experimental Design

A piezoresistive and a piezoelectric pressure transducer were inserted into the head of the engine in similar locations (this can be seen in figure 7.1)

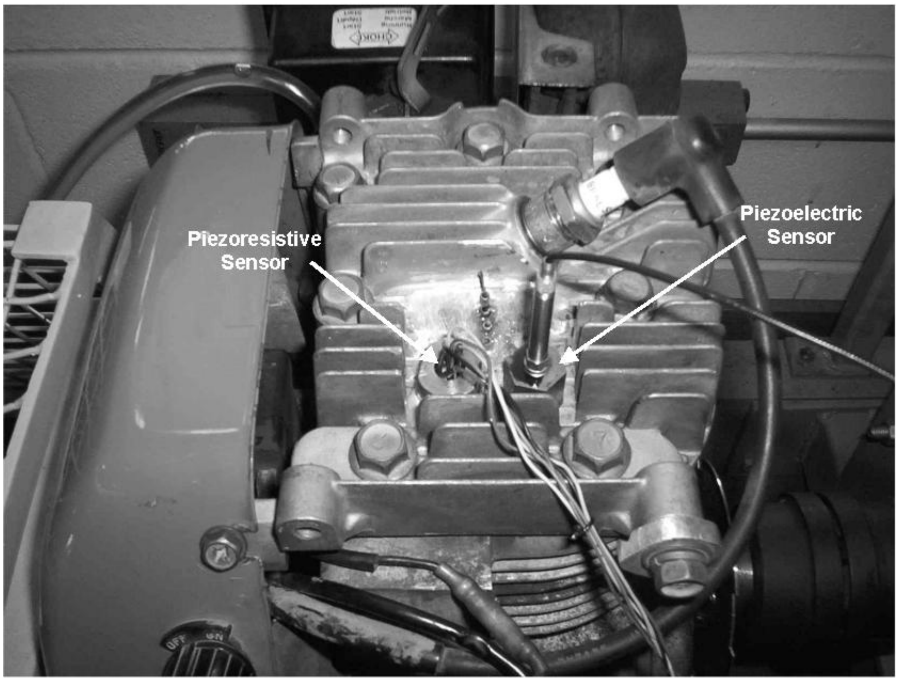

Figure 7.1: A photograph showing the mounting of the piezoelectric (right) and piezoresistive (left) sensors on the engine

Since the engine would normally operate at high temperatures, it was only tested over short periods of time to avoid overheating the pressure transducers.

A shaft encoder (figure 7.2) was used for this experiment to determine the cylinder position in comparison to the pressure readings and for determining the speed of the engine. This allowed the theoretical engine pressures to be applied to the experimental results. Details of the shaft encoder are included in Appendix D. Specifications for the optical sensor used on the encoder are displayed in Appendix B.

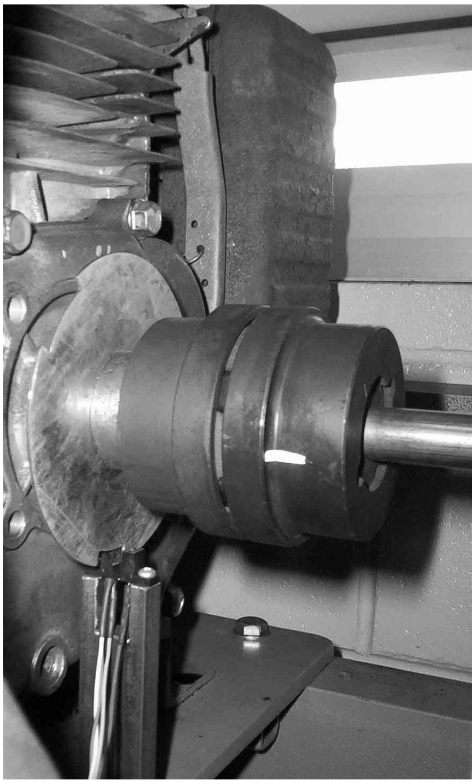

Figure 7.2: The Shaft Encoder attached to the engine

A block diagram representing the method of data capture and pressure measurement is shown in figure 7.3.

During the engine testing process, four different tests were conducted,

1. Engine motored (by external electric motor), throttle closed
2. Engine fired, no load, throttle closed
3. Engine fired, loaded, throttle closed
4. Engine fired, loaded, throttle open

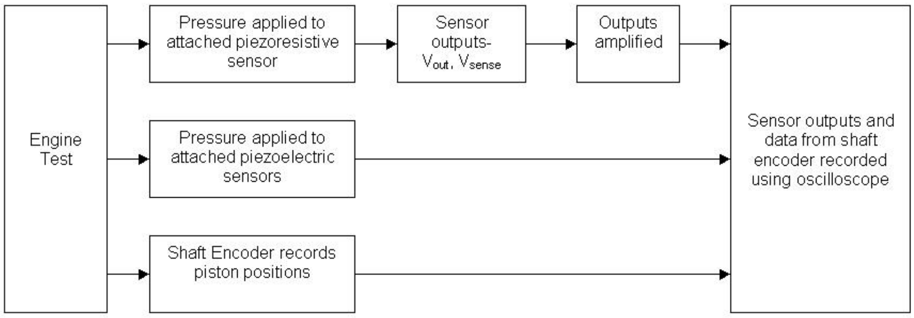

Figure 7.3: A block diagram, showing the method of pressure measurement for the internal combustion engine

To load the engine, a hydraulic pump was used. This pump shifted a known volume of hydraulic oil (3.8e-6 m^3) for each revolution at a known pressure (recorded from pressure gauges). To determine the power output of the engine, equation 7.1 was used.

$$P = \Delta p Q \tag{7.1}$$

In equation 7.1, 'P' is the engine output power, 'Δp' is the hydraulic oil pressure and 'Q' is the oil flow rate.

The layout of the engine testing apparatus can be seen in figure 7.4.

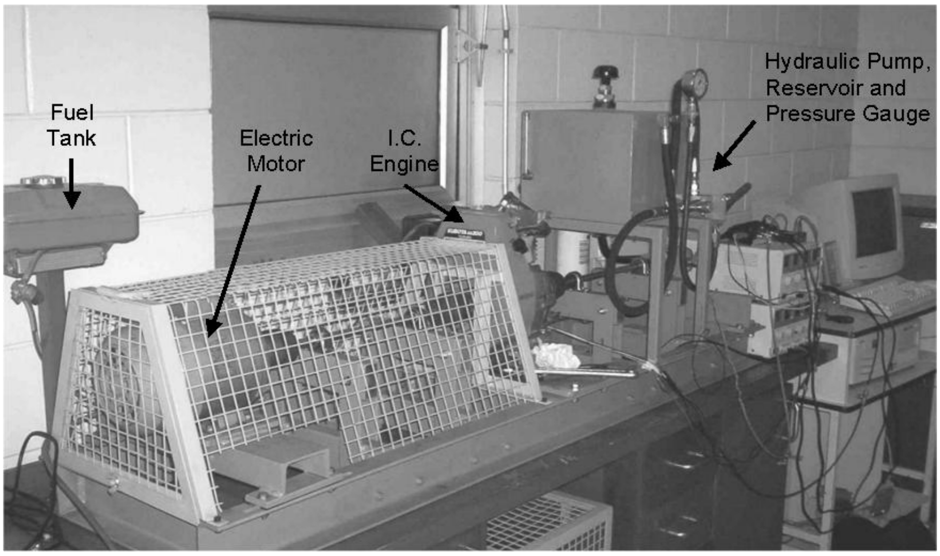

Figure 7.4: The layout of the engine testing apparatus

Due to the operational temperatures of the piezoresistive sensors, the temperature compensation routine (developed in Chapter 4) was used to increase the accuracy of the pressure measurements.

7.3 Analysis of Results

7.3.1 Comparison with Piezoelectric Sensor

Graphs were produced to compare the pressure recorded by the piezoresistive and piezoelectric sensors (figure 7.5 for engine test 1, figure 7.6 for engine test 2, figure 7.7 for engine test 3 and figure 7.8 for engine test 4). Due to high levels of signal noise from the piezoresistive sensor, some data smoothing was utilized. The effects of data smoothing unfortunately reduced the peak pressures displayed in the results for the piezoresistive sensors. To reduce the adverse affects of smoothing, a routine was developed to smooth the low pressure data to a higher extent then the high pressure data (the peak cylinder pressures). It may be possible to reduce the signal noise if the piezoresistive sensors were required for future applications. A MATLAB script, 'engine_1' (see Appendix C) was used to analyse the data collected from each of the engine tests.

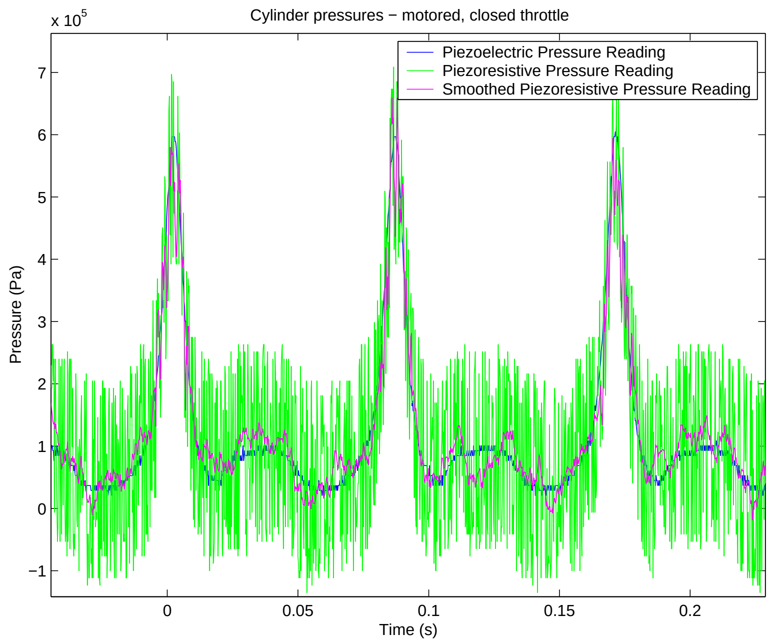

Figure 7.5: Engine pressures determined from the piezoresistive and piezoelectric pressure transducers - motored, closed throttle

The readings obtained with the piezoelectric sensors drifted during the engine testing process (the offset of the piezoelectric measurements changed over time). To correct for this error, the pressures measured with the piezoelectric sensor were altered to match

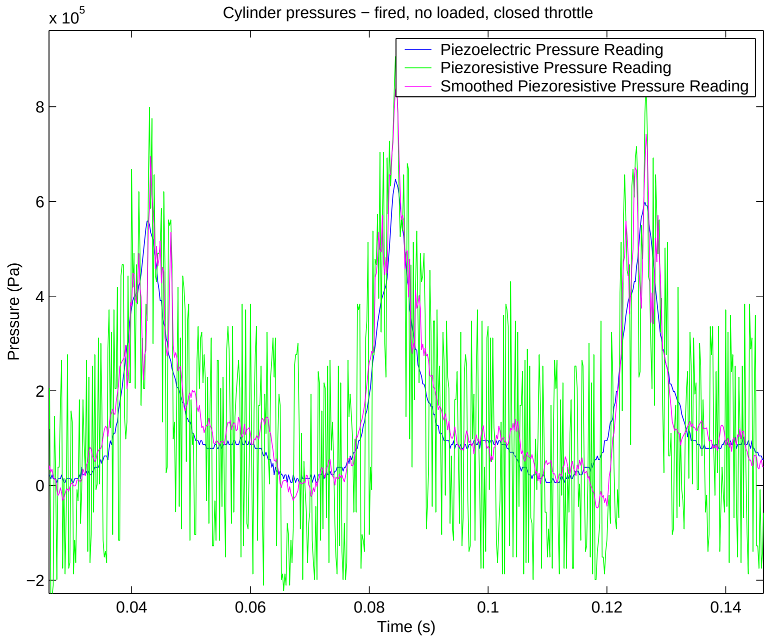

Figure 7.6: Engine pressures determined from the piezoresistive and piezoelectric pressure transducers - fired, closed throttle, no load

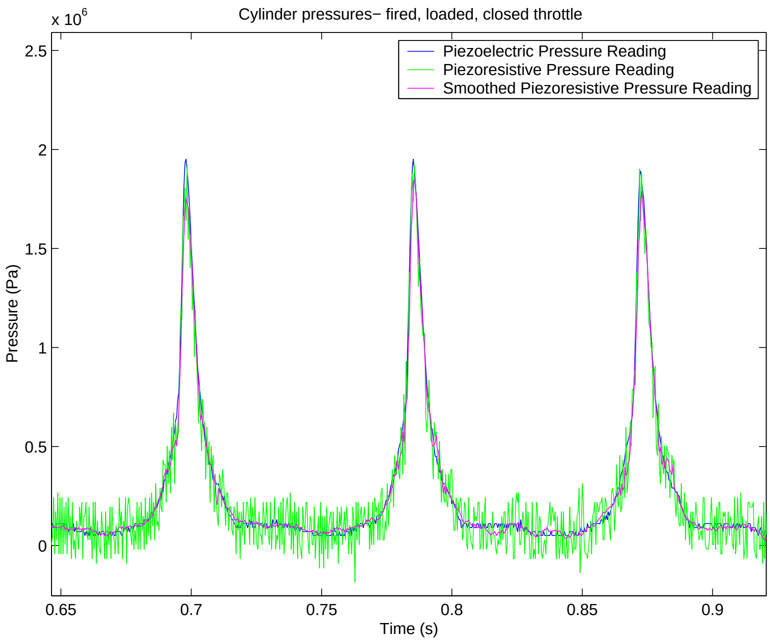

Figure 7.7: Engine pressures determined from the piezoresistive and piezoelectric pressure transducers - fired, closed throttle, loaded

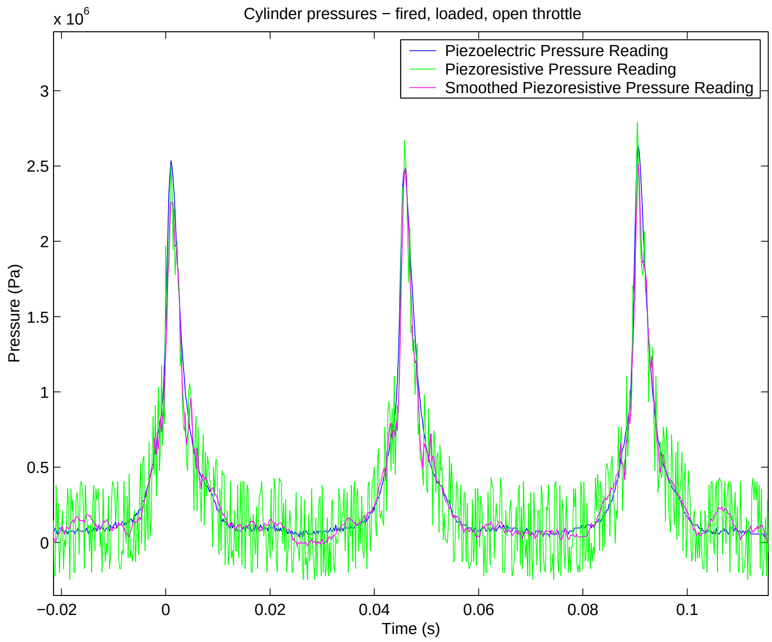

Figure 7.8: Engine pressures determined from the piezoresistive and piezoelectric pressure transducers - fired, open throttle, loaded

the readings from the piezoresistive sensor over a short period of time (20 ms) midway through the exhaust stroke of the engine (relatively low pressure). Since the pressures during the exhaust stroke of the engine were very small compared to the peak engine pressures, any errors introduced to the piezoelectric readings were minimal.

For the loaded engine tests (3 and 4), the output power of the motor is shown in table 7.1.

Engine Test	**Hydraulic Oil Pressure (pa)**	**Output Power (W)**
1	-	-
2	-	-
3	7.584e6	659.8
4	11.721e6	1984.9

Table 7.1: Hydraulic pressures and equivalent engine output power for engine tests

The cylinder pressures recorded with the piezoelectric pressure transducer compared reasonable well with the results from the piezoresistive pressure sensor. The plots of in-cylinder pressure demonstrate that the piezoresistive sensors are capable of providing results similar to those recorded by the piezoelectric sensor. The plots also demonstrate that the results obtained from the piezoresistive sensors are more reliable at higher pressures, or situations where the signal amplitudes are much greater than the noise amplitude. While the peaks of the smoothed piezoresistive data reveal some error (due to the data being averaged over a certain number of data points), the peaks of the raw data (not smoothed) still compare well with the magnitude of the piezoelectric readings. Other differences in pressure readings may also be related to the positioning of the sensors within the head of the cylinder (the cylinder pressures may not be uniformly distributed).

Since the piezoelectric sensor is known for high accuracy and fast response times, the data indicates that the piezoresistive pressure transducer is capable of providing reasonably accurate measurements. The similarity of the results also suggests that the temperature compensation routines are effective. The piezoresistive signal shows no evidence of significant phase lag or amplitude errors associated with high frequencies of pressure fluctuation.

7.3.2 Theoretical Analysis

The theoretical analysis is based upon estimating the internal cylinder pressures using a thermodynamic engine simulation. This simulation was compiled into a series of MATLAB scripts by Dr. David Buttsworth. The engine simulation script allows a comparison of the theoretical pressures developed during motored and fired engine tests with the results obtained from the piezoelectric and piezoresistive pressure transducers. A MATLAB script for comparing the theoretical and measured engine pressures, 'engine_2', is displayed in Appendix C.

While four engine tests were conducted using various conditions, the motored engine test (engine test 1) and the loaded, open throttle test (engine test 4) give the greatest similarity to the theoretical model.

For the motored engine tests, a comparison between the measured and theoretical pressures is shown in figure 7.9.

For the fired engine tests, a comparison between the measured and theoretical pressures is shown in figure 7.10.

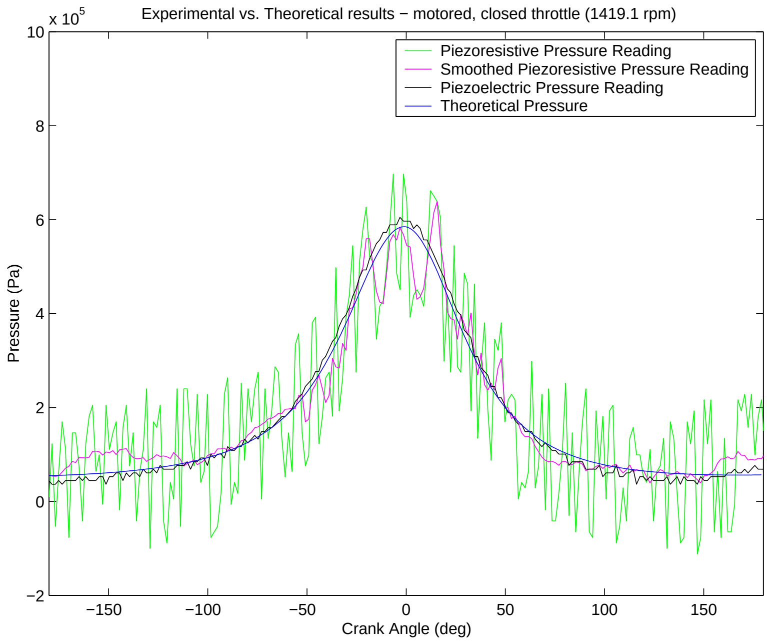

Figure 7.9: A comparison between the theoretical and measured cylinder pressures - motored

The precise values for engine parameters (such as the spark ignition angle, burn duration angle and initial pressure) were unknown, therefore these values were modified until the theoretical results closely matched the recorded values. Ideally these parameters could be determined to give a better indication of the sensor accuracy, however due to time constraints this was not possible.

The results obtained from the theoretical simulations closely match the pressure measurements from the piezoresistive and piezoelectric sensors (figure 7.9 and figure 7.10). While this does not give an accurate indication of sensor accuracy (due to the unknown engine parameters), the close match between the predicted and measured results indicates that pressure readings are close to the pressures expected from the engine.

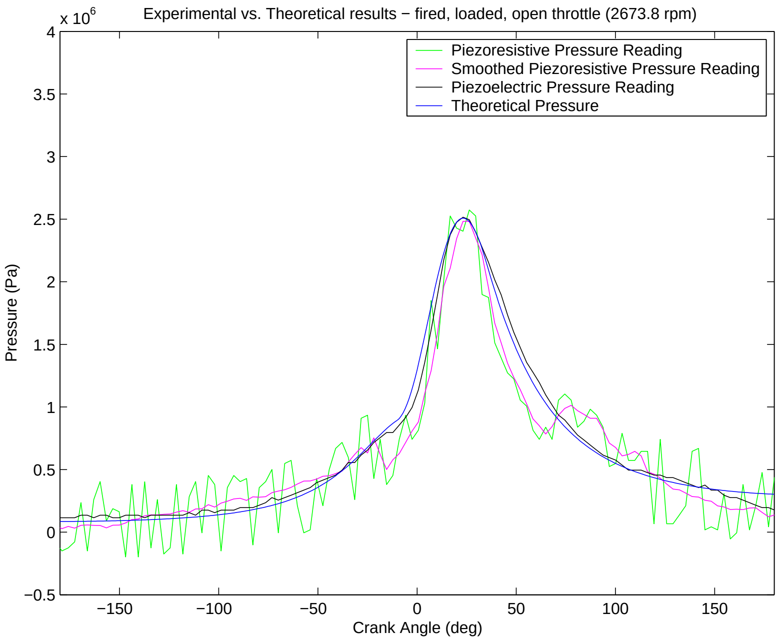

Figure 7.10: A comparison between the theoretical and measured cylinder pressures - fired, open throttle, loaded

7.4 Chapter Summary

The pressure testing within the cylinder of an IC engine has provided a means for testing the dynamic response and temperature calibrations for the piezoresistive pressure transducers.

A comparison between the results of the piezoresistive and piezoelectric transducers demonstrated that the piezoresistive device is capable of reasonably accurate results. There were no obvious indications of phase lag or amplitude errors in the piezoresistive sensor output as a result of the high frequencies of pressure fluctuation. The accuracy of the readings obtained from the piezoresistive pressure sensors also indicates that the temperature compensation routine was effective.

A thermodynamic engine simulation provided a comparison between the practical and theoretical results. This demonstrated that the results obtained from the piezoresistive pressure sensor are approximately at the magnitude predicted by the model. The similarity between these results further reinforces the high performance from the piezoresistive sensors.

Chapter 8

Conclusions and Further Work

8.1 Achievement of Project Objectives

This dissertation has provided a detailed analysis of fast-response piezoresistive pressure transducers for thermofluids experiments. Objectives, set out in the initial pages of this report, have been met, providing an in-depth investigation into the operation and implementation of piezoresistive sensors.

The following objectives have been addressed:

1. **Review existing techniques for temperature measurement and compensation in piezoresistive pressure measurement devices**.

   A review of techniques previously used for temperature compensation was covered during the literature review (Chapter 2). This included past research conducted by Ainsworth et al. (2000), Denos (2002) and Clark (1992).

2. **Devise appropriate electrical circuits to implement such techniques**.

   Electrical circuits were successfully developed to provide pressure measurement and allow for accurate temperature compensation (Chapter 3, Figure 3.2). This circuit was used for the remaining pressure measurement experiments.

3. **Devise suitable apparatus for quasi-static calibration of pressure trans-**

ducers for both pressure and temperature sensitivity.

To perform the room temperature quasi-static calibrations, each of the piezoresistive pressure transducers were connected directly to the Dead Weight Tester. A small oven was modified to allow for a temperature calibration of the piezoresistive sensors, testing the temperature sensitivity of the transducers (Chapter 4). The temperature calibration apparatus allowed the sensor to be held at a particular temperature while a range of pressure were applied.

4. **Perform calibrations on selected transducers**.

   Chapter 4 describes the experimental process of the quasi-static and temperature calibrations. This chapter also displayed the results of the calibrations and compared the experimental results with the manufacturer's specifications.

5. **Investigate the dynamic response of sensors of various configurations (added grease, modified cases etc.) using a shock tube calibration**.

   Using the shock tube facility, the dynamic response of the SX150AHO sensors were tested (Chapter 5). This included tests of sensors with various modifications, including additions of latex and grease and modified sensor cases.

6. **Obtain pressure measurements in a Gun Tunnel**.

   A single test was conducted with the USQ Gun Tunnel (Chapter 6). This test recorded the pressures measured with a piezoresistive sensor piezoelectric sensor.

7. **Analyse the measurements from the Gun Tunnel and compare with data obtained from a piezoelectric sensor**.

   Chapter 6 compared the pressure values recorded from the piezoelectric and piezoresistive sensors. This revealed that piezoresistive sensor was capable of producing similar results to the piezoelectric transducer (a more expensive sensor well suited to this pressure measurement application).

8. **Obtain pressure measurements in an IC engine**.

   Pressure measurements were taken from an internal combustion engine under various conditions (motored, fired, loaded, unloaded etc.)(Chapter 7).

9. **Analyse the measurements from the IC engine and compare with data obtained from a piezoelectric sensor**.

Chapter 7 investigated the comparison between the measurements obtained from the piezoresistive and piezoelectric transducers. The piezoresistive sensor compared relatively well with the output obtained from the piezoelectric sensor.

as time has permitted -

10. **Compare the measurements from the Gun Tunnel with predictions based on a computational model (Lagrangian quasi one dimensional)**

    Due to time constraints and the unavailability of certain program files, a computational model for the analysis of the Gun Tunnel was not investigated.

11. **Compare the measurements from the IC engine with predictions based on a computational model(thermodynamic engine simulation)**.

    A thermodynamic engine simulation was used to provide theoretical results for the cylinder pressures of the IC engine. The actual pressure measurements from both the piezoelectric and piezoresistive sensors compared well with the predicted values.

8.2 Further Work

Future work on piezoresistive pressure sensing technology may be conducted in several areas. The areas of possible further research include an investigation into improving temperature calibration techniques, a more detailed analysis of dynamic response characteristics and the utilization of piezoresistive sensors with other fast-response thermofluid applications.

The temperature calibrations conducted with the modified oven apparatus were effective however they proved to be very slow, as discussed in Chapter 4. Further work could be conducted to develop a pressure testing apparatus that automatically sets the temperature of the sensor and applies a range of pressures while recording the sensor outputs (allowing the calibration process to be completely automated). The creation of such a device would greatly reduce the time and effort required to complete quasi-static pressure and temperature calibrations.

The investigations into sensor dynamic response in this project compared the characteristics of various configurations of pressure sensors. Further work could be conducted with specific configurations to identify quantitative variables related to the dynamic behavior of the sensors (such as damping ratios and settling times). If such variables could be determined, the errors associated with high frequencies of pressure fluctuation could be calculated and tested with further experimentation. Research could also be conducted to compare the dynamic response characteristics of piezoresistive and piezoelectric sensors.

Piezoresistive pressure transducers have possible applications in a wide range of thermofluids experiments. An analysis of the piezoresistive pressure transducers under further pressure measurement applications (such as pressure measurement within the UQ T4 shock tunnel), would give another opportunity to test the suitability of these sensors and provide a better indication of the overall transducer versatility. It may be possible, with further research, for piezoresistive sensors to provide a cost effective replacement for more expensive pressure sensing technologies in a large variety of situations.

References

Ainsworth, R. W., Dietz, A. J. & Nunn, T. A. (1991), 'The use of semi-conductor sensors for blade surface pressure measurement in a model turbine stage', *Journal of Engineering for Gas Turbines and Power* **113**, 261–268.

Ainsworth, R. W., Miller, R. J., Moss, R. W. & Thorpe, S. J. (2000), 'Unsteady pressure measurement', *Measurement Science and Technology* **11**, 1055–1076.

A Two-Stage Free-Piston Driver for Hypervelocity Expansion Tubes (1997), PhD thesis, University of Queensland.

Balachandran, B. & Magrab, E. B. (2004), *Vibrations*, Brooks/Cole-Thomson Learning, 20 Davis Drive, Belmont, CA 94002, USA.

Boerrigter, H. L. & Charbonnier, J. M. (1997), 'Design and calibration of an unsteady pressure measurement system', *International Congress on Instrumentation in Aerospace Simulation Facilities* .

Buttsworth, D. (n.d.), *USQ Gun Tunnel*, `http://www.usq.edu.au/users/buttswod/guntunnel/guntunnelindex.html` Accessed 14/5/04.

Buttsworth, D. R. & Jacobs, P. A. (2000), 'Measurement of fluctuations in a mach 4 shock tunnel nozzle flow', *7th Australiansian Conference on Heat and Mass Transfer* **7**, 53–59.

Clark, D. L. (1992), 'Temperature compensation for piezoresistive pressure transducers at cryogenic temperatures', *Advances in Cryogenic Engineering* **37**, 1447–1452.

Denos, R. (2002), 'Influence of temperature transients and centrifugal force on fast-response pressure transducers', *Experiments in Fluids* **33**, 256–264.

Honeywell (n.d.), *Pressure and Force Sensors*,
`http://content.honeywell.com/sensing/prodinfo/pressure/technical/c15_101.pdf`
Accessed 14/5/04.

Honeywell/Sensym (n.d.), *Low Cost, Stainless Steel Isolated Pressure Sensors*,
`http://content.honeywell.com/sensing/prodinfo/stainsteel/pdf/13%20mm%20series.pdf`
Accessed 15/5/04.

HyperPhysics (2003), *Resonance*,
`http://hyperphysics.phy-astr.gsu.edu/hbase/sound/reson.html#resdef`
Accessed 17/10/04.

MAXIM (2001), *Demystifying Piezoresistive Pressure Sensors*,
`http://www.maxim-ic.com/appnotes.cfm/appnote_number/871`
Accessed 14/5/04.

Microsystems (n.d.), *Piezoresistive Pressure and Temperature Sensor Cluster*,
`http://www.microsystems.metu.edu.tr/piezops/piezops.html`
Accessed 14/5/04.

Appendix A

Project Specification

University of Southern Queensland
Faculty of Engineering and Surveying

ENG 4111/2 Research Project
PROJECT SPECIFICATION

FOR:	**Peter Colin Mckenzie HOCKINGS**
TOPIC:	Fast-Response Piezoresistive Pressure Transducers for Thermofluids Experiments
SUPERVISORS:	Dr. David Buttsworth Dr. Ahmad Sharifian
ENROLMENT:	ENG 4111 – S1, D, 2004; ENG 4112 – S2, D, 2004
PROJECT AIM:	This project aims to identify the frequency and temperature response characteristics of low cost piezoresistive pressure transducers and provide accurate calibration to allow these pressure sensors to be used in fast-response thermofluids experiments.

PROGRAMME: Issue B, 18 October 2004

1. Review existing techniques for temperature measurement and compensation in piezoresistive pressure measurement devices.

2. Devise appropriate electrical circuits to implement such techniques.

3. Devise suitable apparatus for quasi-static calibration of pressure transducers for both pressure and temperature sensitivity.

4. Perform calibrations on selected transducers.

5. Investigate the dynamic response of sensors of various configurations (added grease, modified cases etc.) using a shock tube calibration.

6. Obtain pressure measurements in a Gun Tunnel.

7. Analyse the measurements from the Gun Tunnel and compare with data obtained from a piezoelectric sensor.

8. Obtain pressure measurements in an IC engine.

9. Analyse the measurements from the IC engine and compare with data obtained from a piezoelectric sensor.

As time permits:

10. Compare the measurements from the Gun Tunnel with predictions based on a computational model (Lagrangian quasi one dimensional).

11. Compare the measurements from the IC engine with predictions based on a computational model (thermodynamic engine simulation).

AGREED:______________________(Student) ______________________(Supervisor)

(dated) ___ / ___ / ___

Appendix B

Specification and Data Sheets

Appendix B Contents

B.1 Specifications for 13U0500 and 13U3000 Piezoresistive Sensors

LOW COST, STAINLESS STEEL ISOLATED PRESSURE SENSORS
SenSym ICT

13mm Series

Low Cost, Stainless Steel Isolated Pressure Sensors

0 to 500, 1,000, 2,000 3,000 and 5,000 psi Pressure Sensors

These SenSym ICT 13mm stainless steel devices are designed for high pressure applications that involve measurement of hostile media in harsh environments. This series uses SenSym ICT's proven piezoresistive semiconductor sensor chip in an oil isolated housing with or without an integral ceramic for temperature compensation and calibration. This design has proven to be highly reliable, stable, and accurate.

These sensors feature a weld ring collar and special back support ring for high cycle life capability as they are designed for further package integration in OEM applications. Parts are available with pressure ranges from 500 through 5,000 psi and can be used with voltage or current supplies.

Contact your local SenSym ICT representative, the factory, or go to Sensym ICT's Web site at www.sensym-ict.com for additional details.

APPLICATIONS

13C and 13U

- Industrial Controls
- Hydraulic Controls
- Tank Pressure Transmitter

FEATURES

13C and 13U

- Rugged - Isolated Stainless Steel Package
- Reliable Semiconductor Technology

13C Compensated Series

- Calibrated and Temperature Compensated
- Voltage or Current Supply Options
- Absolute & Sealed Gauge Pressures

13U Uncompensated Series

- Low Cost Cell Package
- Absolute Pressure

EQUIVALENT BASIC CIRCUIT

13mm COMPENSATED SERIES

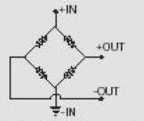

13mm UNCOMPENSATED SERIES

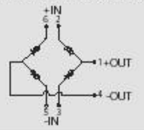

invensys
Sensor Systems

LOW COST, STAINLESS STEEL ISOLATED PRESSURE SENSORS
SenSym ICT

13mm Compensated Series

PRESSURE SENSOR CHARACTERISTICS (all devices)

Environmental Specifications (all devices)

Temperature Ranges

Compensated:	0°C to +82°C	Vibration:	10G at 20-2000 Hz
Operating:	-40°C to +125°C	Shock:	100G for 11 msec
Storage:	-40°C to +125°C	Life:	1 Million cycles minimum
		Insulation Resistance:	100MΩ at 50 Vdc

Maximum Ratings (all devices)

Voltage Version "K" : Supply Voltage V_S = +15 Vdc
Current Version "L" : Supply Current I_S = +2.0 mA

PRESSURE RANGE SPECIFICATIONS

SenSym ICT Part No.	Pressure Range	Full Scale Span(2)	Proof Pressure(7)	Burst Pressure(8)
13C 0500P (A,S) (1,4,5,6) (K,L)	0-500 psi	98mV to 102mV	1500 psi	2500 psi
13C 1000P (A,S) (1,4,5,6) (K,L)	0-1000 psi	98mV to 102mV	3000 psi	5000 psi
13C 2000P (A,S) (1,4,5,6) (K,L)	0-2000 psi	98mV to 102mV	6000 psi	10,000 psi
13C 3000P (A,S) (1,4,5,6) (K,L)	0-3000 psi	98mV to 102mV	9000 psi	10,000 psi
13C 5000P (A,S) (1,4,5,6) (K,L)	0-5000 psi	148mV to 152mV	10,000 psi	10,000 psi

PERFORMANCE CHARACTERISTICS(1)

Characteristic	Min	Typical	Max	Units
Zero Pressure Offset	-2	0	+2	mV
Pressure Non-Linearity(3)	–	±0.1	±0.25	%FSS
Pressure Hysteresis(3)	–	±0.015	±0.030	%FSS
Repeatability	–	±0.010	±0.030	%FSS
Temp. Effect on Span(4)	–	±0.5	±1.0	%FSS
Temp. Effect on Offset(4)	–	±0.5	±1.0	%FSS
Thermal Hysteresis (0 to 82°C)	–	±0.1	±0.3	%FSS
Long Term Stability of Offset & Span(5)	–	±0.1	±0.3	%FSS
Response Time(6)	–	0.1	–	ms
Common Mode Voltage (Voltage Version "K")(9)	.50	1.25	2.0	Vdc
Input Resistance (Current Version "L")	2.0	4.5	8.0	kΩ
Input Resistance (Voltage Version "K")	8.0	25	50	kΩ
Output Resistance	3.0	4.5	6.0	kΩ

13mm COMPENSATED SERIES SPECIFICATION NOTES

Note 1: Reference Conditions (unless otherwise noted): T_A=25°C Supply V_S=10Vdc±0.01Vdc or I_S=1.5mA±0.0015mA.

Note 2: Full-Scale Span is the algebraic difference between the output voltage at full-scale pressure and the output at zero pressure. Full-Scale Span (FSS) is ratiometric to the supply voltage.

Note 3: Pressure Non-Linearity is based on best-fit straight line from the zero to the full-scale pressure. Pressure Hysteresis is the maximum output difference at any point within the operating pressure range for increasing and decreasing pressure.

Note 4: Maximum error band of the offset voltage or span over the compensated temperature range, relative to the 25°C reading.

Note 5: Long term stability over a six month period.

Note 6: Response time for a 0 psi to Full-Scale Span pressure step change, 10% to 90% rise time.

Note 7: The maximum pressure that can be applied without changing the transducer's performance or accuracy.

Note 8: The maximum pressure that can be applied to a transducer without rupture of either the sensing element or transducer case.

Note 9: Common Mode Voltage as measured from output to ground.

13mm Series

PHYSICAL DIMENSIONS

Dimensions in inches (mm)

PACKAGE 1 (See Note)
RING WITH BACK SUPPORT

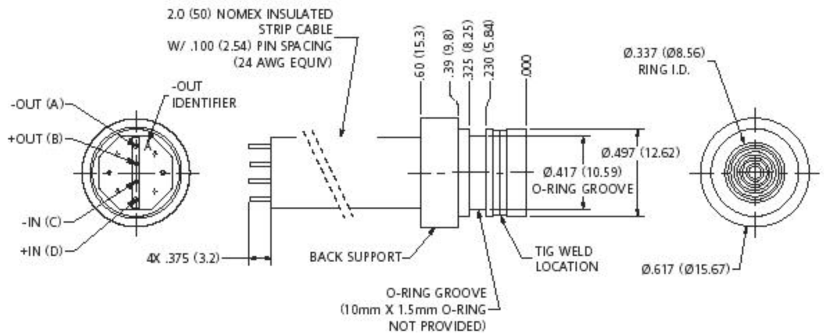

Note: Non-concentricity effects at the diaphragm weld area may cause runout of up to ±0.006" between the upper and lower portions of the sensor body. (It is recommended to use a counter bore to mate with this device to allow for this non-concentricity.)

PACKAGE 4
1/8-27 NPT

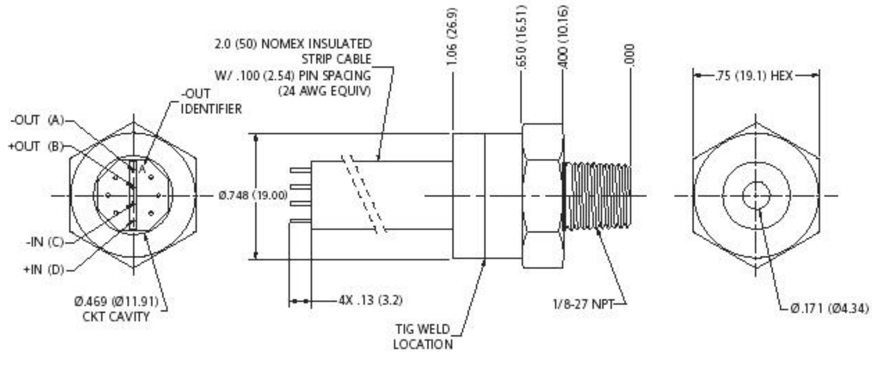

13mm Series

LOW COST, STAINLESS STEEL ISOLATED PRESSURE SENSORS
SenSym ICT

PHYSICAL DIMENSIONS (con't)

Dimensions in inches (mm)

PACKAGE 5
1/4-18 NPT

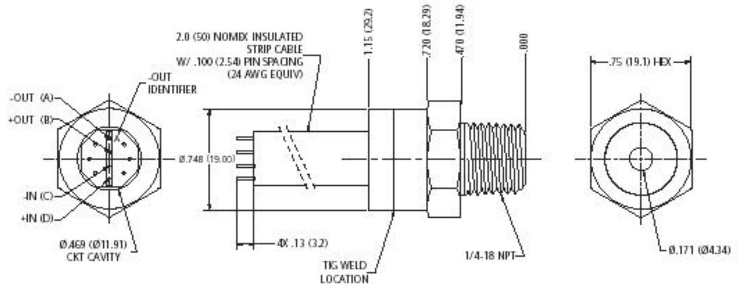

PACKAGE 6
7/16-20 UNF

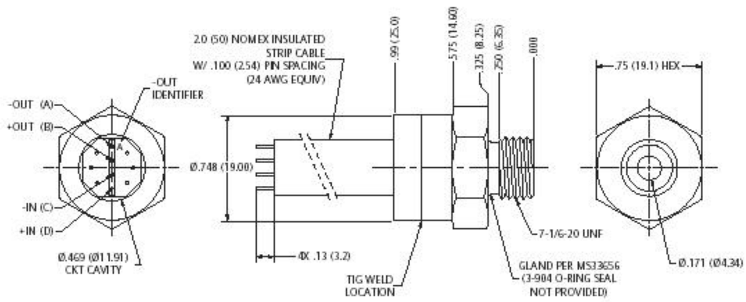

13mm Uncompensated Series

PRESSURE RANGE SPECIFICATIONS

SenSym ICT Part No.	Pressure Range	Full-Scale Span[2]	Proof Pressure[7]	Burst Pressure[8]
13U 0500P A 0 K	0-500 psi	175mV to 300mV	1200 psi	2400 psi
13U 1000P A 0 K	0-1000 psi	175mV to 300mV	3000 psi	5000 psi
13U 2000P A 0 K	0-2000 psi	175mV to 300mV	6000 psi	10,000 psi
13U 3000P A 0 K	0-3000 psi	175mV to 300mV	9000 psi	10,000 psi
13U 5000P A 0 K	0-5000 psi	290mV to 500mV	10,000 psi	10,000 psi

PERFORMANCE CHARACTERISTICS[1]

Characteristic	Min	Typical	Max	Units
Zero Pressure Offset	-7.5	0	+7.5	mV/V
Pressure Non-Linearity[3]	–	±0.1	±0.25	%FSS
Pressure Hysteresis[3]	–	±0.015	±0.030	%FSS
Repeatability	–	±0.010	±0.030	%FSS
Temp. Coefficient of Span[4] (0 to 82°C)	360	720	1260	ppm/°C
Temp. Coefficient of Resistance[4] (0 to 82°C)	2700	3420	4500	ppm/°C
Temp. Coefficient of Offset[4] (0 to 82°C)	–	30	–	μV/V/°C
Thermal Hysteresis (0 to 82°C)	–	±0.1	±0.3	%FSS
Long Term Stability of Offset & Span[5]	–	±0.1	±0.3	%FSS
Response Time[6]	–	0.1	–	ms
Input Resistance	4.0	4.75	6.0	kΩ
Output Resistance	4.0	4.75	6.0	kΩ

PHYSICAL DIMENSIONS

Dimensions in inches (mm)

PACKAGE 0 (See Note) RING AND CELL

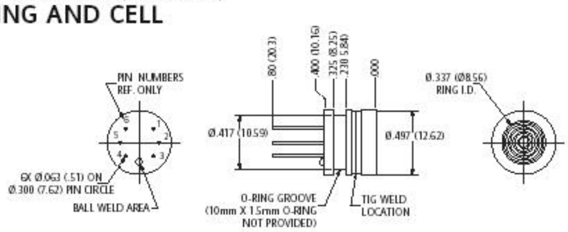

Note : Non-concentricity effects at the diaphragm weld area may cause runout of up to ±0.006" between the upper and lower portions of the sensor body. (It is recommended to use a counter bore to mate with this device to allow for this non-concentricity.)

13mm UNCOMPENSATED SERIES SPECIFICATION NOTES

Note 1: Reference Conditions (unless otherwise noted): T_A=25°C Supply V_S=5Vdc±0.01Vdc or I_S=1.0 mA±0.0015mA

Note 2: Full-Scale Span is the algebraic difference between the output voltage at full-scale pressure and the output at zero pressure. Full-Scale Span (FSS) is ratiometric to the supply voltage.

Note 3: Pressure Non-Linearity is based on best-fit straight line from the zero to the full-scale pressure. Pressure Hysteresis is the maximum output difference at any point within the operating pressure range for increasing and decreasing pressure.

Note 4: The error band resulting from maximum deviation of a transducers output parameter (offset, span, or resistance) as temperature is varied from 25°C to any other temperature within the specified range (0 to 82°C). This parameter is not 100% tested and is guaranteed by process design and tested on a sample basis only. Temperature coefficient of span is evaluated using a constant current source.

Note 5: Long term stability over a six month period.

Note 6: Response time for a 0 psi to Full-Scale Span pressure step change, 10% to 90% rise time.

Note 7: The maximum pressure that can be applied without changing the transducer's performance or accuracy.

Note 8: The maximum pressure that can be applied to a transducer without rupture of either the sensing element or transducer case.

LOW COST, STAINLESS STEEL ISOLATED PRESSURE SENSORS
SenSym ICT

13mm Series

Low Cost, Stainless Steel Isolated Pressure Sensors

ORDERING INFORMATION - PART # DESCRIPTION

13mm Compensated Series

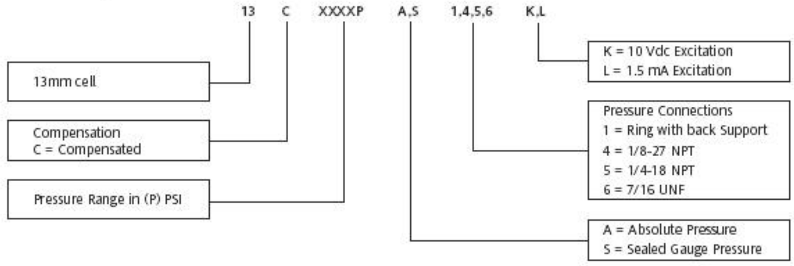

For example: Part **#13C3000PS4K** = 13 mm Cell, Compensated, 3000 psi, Sealed Gauge, 1/8NPT Port with 10 Vdc excitation.

13mm Uncompensated Series

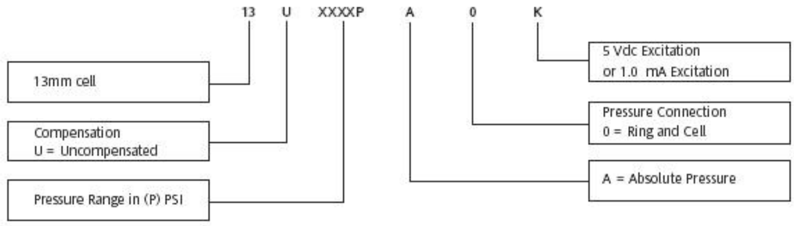

For example: **Part #13U 3000PA0K** = 13 mm Cell, Uncompensated, 3000 psi, Absolute, Ring pressure connection with 5 Vdc excitation.

invensys
Sensor Systems

1 408 954 6700
FAX: 408 954 9458
SenSym ICT
1804 McCarthy Boulevard
Milpitas, CA 95035
www.sensym-ict.com

SEN0106_3000_4/02

B.2 Specifications for SX150AHO Piezoresistive Sensor

SX PRESSURE SERIES
SenSym ICT

SX Series

Low Cost Pressure Sensors

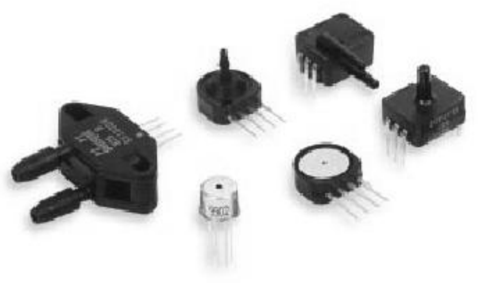

The SX Series of pressure sensors provide the lowest cost components for measuring pressures up to 150 psi. These sensors were specifically designed for use with non-corrosive, non-ionic media, such as air, dry gases, and the like. Convenient pressure ranges are available to measure differential, gauge, and absolute pressures from 0 to 1 psi (SX01) up to 0 to 150 psi (SX150).

The Absolute (A) devices have an internal vacuum reference and an output voltage proportional to absolute pressure. The Differential (D) devices allow application of pressure to either side of the diaphragm and can be used for gauge or differential pressure measurements.

This product is packaged either in SenSym ICT's standard low cost chip carrier "button" package, a plastic ported "N" package, or a metal TO5 Package with or without gel. All packages are designed for applications where the sensing element is to be integral to the OEM equipment. These packages can be o-ring sealed, epoxied, and/or clamped onto a pressure fitting. A closed-bridge four-pin SIP configuration is provided for electrical connection to the "Button" or "N" Package. The TO5 Package offers a 5-pin open-bridge configuration. A DIP Package is also available, which mounts on a PC board like a standard IC with through-hole pins. This extremely small size package enables the use of multiple sensors in a limited available space application.

Because of its high-impedance bridge, the SX Series is ideal for portable and low power or battery operated systems. Due to its low noise, the SX is an excellent choice for medical and other low pressure applications.

Contact your local SenSym ICT representative, the factory, or go to Sensym ICT's Web site at www.sensym-ict.com for additional details.

APPLICATIONS

- Medical Instrumentation
- Barometric Measurement
- Pneumatic Controls
- Battery Powered Equipment

FEATURES

- Low Cost
- High-Impedance Bridge
- Absolute and Differential (Gauge)
- Low Noise
- Low Power Consumption for Battery Power

EQUIVALENT CIRCUITS

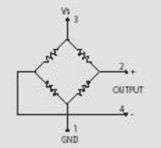

BUTTON, NIPPLE AND "N" PACKAGE

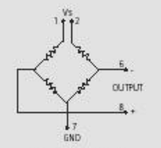

TO AND DIP PACKAGE

invensys
Sensor Systems

SX PRESSURE SERIES
SenSym ICT

SX Series

PRESSURE SENSOR CHARACTERISTICS

Maximum Ratings (For All Devices)

Supply Voltage, V_S	+12 Vdc
Temperature Ranges:	
Operating	-40°C to +85°C
Storage	-55°C to +125°C
Common-Mode Pressure	150 psig
Lead Soldering Temperature (2-4 Seconds)	250°C

PERFORMANCE CHARACTERISTICS[1]

Characteristics	Min	Typ	Max	Unit
Zero Pressure Offset[5]	-35	-20	0	mV
Temperature Coefficient of Offset[6,9]	–	+4	–	µV/V/°C
Combined Pressure Non-Linearity and Pressure Hysteresis[3]	–	0.2	±0.5	%FSS
Long Term Stability of Offset & Span[8]	–	0.1	–	%FSS
Response Time[7]	–	100	–	µsec
Input Resistance	–	4.1	–	kΩ
Temperature Coefficient of Resistance[6,9]	+690	+750	+810	ppm/°C
Temperature Coefficient of Span[6,9]	-2550	-2150	-1900	ppm/°C
Output Resistance	–	4.1	–	kΩ
Repeatability[4]	–	0.5	–	%FSS

SX PERFORMANCE CHARACTERISTICS[1]

Part Number	Operating Pressure (psi)	Sensitivity (mV/V/psi)	Full-Scale Span[2] (mV)			Burst Pressure (psi)
		Typ	Min	Typ	Max	
SX01	0-1	4.0	15	20	25	20
SX05	0-5	3.0	50	75	100	20
SX15	0-15	1.5	75	110	150	45
SX30	0-30	0.75	75	110	150	90
SX100	0-100	0.3	100	150	200	150
SX150	0-150	0.15	75	110	150	200

*Maximum Pressure above which can cause permanent sensor failure

ORDERING INFORMATION

To order, use the following part number(s):

Pressure Range	Order Part Number				
	Button Package	Nipple Package	"N" Package	TO Package	DIP Package
0 to 1 psid or psig	SX01D	SX01DP1	SX01DN	SX01GSO	SX01GD2, SX01DD4
0 to 5 psid or psig	SX05D	SX05DP1	SX05DN	SX05GSO	SX05GD2, SX05DD4
0 to 15 psia	SX15A	SX15AP1	SX15AN	SX15AHO	SX15AD2, SX15AD4
0 to 30 psia	SX30A	SX30AP1	SX30AN	SX30AHO	SX30AD2, SX30AD4
0 to 100 psia	SX100A	–	SX100AN	SX100AHO	SX100AD2, SX100AD4
0 to 150 psia	SX150A	–	SX150AN	SX150AHO	–
0 to 15 psid or psig	SX15D	SX15DP1	SX15DN	SX15GSO	SX15GD2, SX15DD4
0 to 30 psid or psig	SX30D	SX30DP1	SX30DN	SX30GSO	SX30GD2, SX30DD4
0 to 100 psid or psig	SX100D	–	SX100DN	SX100GSO	SX100GD2, SX100DD4
0 to 150 psid or psig	SX150D	–	–	SX150GSO	–

SPECIFICATION NOTES (for all devices)

Note 1: Reference Conditions: T_A = 25°C Supply V_S = 5 Vdc Common Line Pressure = 0 psig Pressure Applied to P1

Note 2: Full-Scale Span is the algebraic difference between the output voltage at full-scale pressure and the output at zero pressure. Full-Scale Span is ratiometric to the supply voltage.

Note 3: Pressure Hysteresis - the maximum output difference at any point within the operating pressure range for increasing and decreasing pressure.
Pressure Non-Linearity – the maximum deviation of measure output, at constant temperature (25°), from "best straight line" through three points (offset pressure, full-scale pressure, one-half full-scale pressure).

Note 4: Maximum difference in output at any pressure within the operating pressure range and the temperature range within 0°C to +70°C after:
a) 100 temperature cycles, 0°C to +70°C
b) 1 million pressure cycles, 0 psi to Full-Scale Span

Note 5: The zero pressure offset is 0 mV Min, 20 mV Typ and 35 mV Max for part numbers SXxxxGD2 and SXxxxDD4.

Note 6: Slope of best straight line fit from 0°C to 70°C. For operation outside this temperature range, contact factory for more information.

Note 7: Response time for a 0 psi to Full-Scale Span pressure step change, 10% to 90% rise time.

Note 8: Long term stability over a one year period.

Note 9: This parameter is not 100% tested. It is guaranteed by process design.

SX Series

SX PRESSURE SERIES
SenSym ICT

ELECTRICAL CONNECTIONS

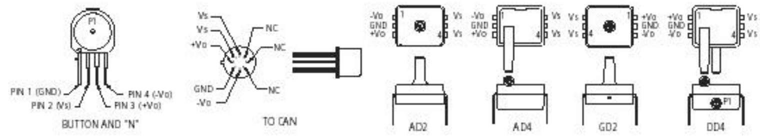

PACKAGE OUTLINES

Button Package

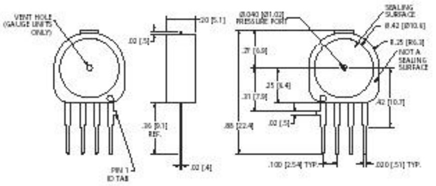

Nipple Package

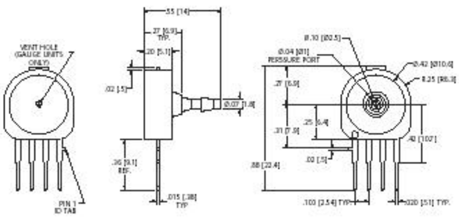

N Housing Package

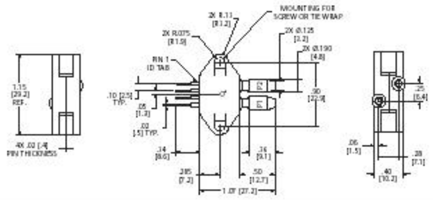

D2 Dip Package

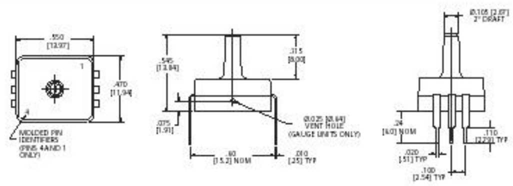

SX PRESSURE SERIES
SenSym ICT

SX Series

Low Cost Pressure Sensors

PACKAGE OUTLINES (con't)

DD4 Dip Package

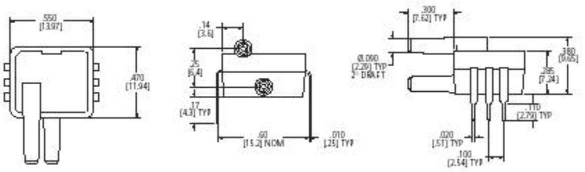

AD4 Dip Package

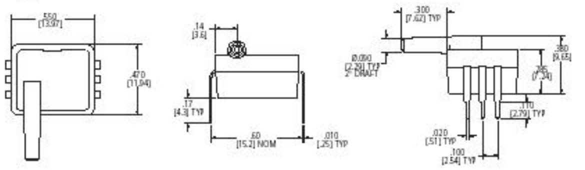

TO5 Package

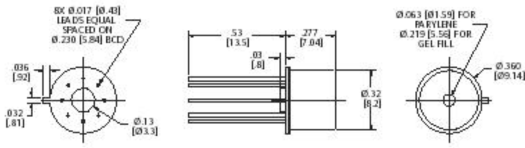

TO39 Package

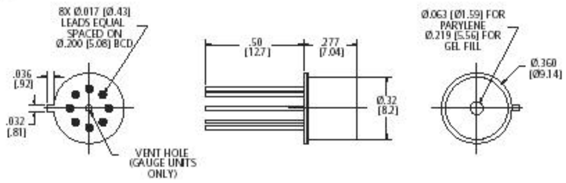

invensys
Sensor Systems

1 408 954 6700
FAX: 408 954 9458
SenSym ICT
1804 McCarthy Boulevard
Milpitas, CA 95035
www.sensym-ict.com

B.3 Specifications for INA114 Instrumental Amplifier

BURR-BROWN®

INA114

Precision INSTRUMENTATION AMPLIFIER

FEATURES

- LOW OFFSET VOLTAGE: 50μV max
- LOW DRIFT: 0.25μV/°C max
- LOW INPUT BIAS CURRENT: 2nA max
- HIGH COMMON-MODE REJECTION: 115dB min
- INPUT OVER-VOLTAGE PROTECTION: ±40V
- WIDE SUPPLY RANGE: ±2.25 to ±18V
- LOW QUIESCENT CURRENT: 3mA max
- 8-PIN PLASTIC AND SOL-16

APPLICATIONS

- BRIDGE AMPLIFIER
- THERMOCOUPLE AMPLIFIER
- RTD SENSOR AMPLIFIER
- MEDICAL INSTRUMENTATION
- DATA ACQUISITION

DESCRIPTION

The INA114 is a low cost, general purpose instrumentation amplifier offering excellent accuracy. Its versatile 3-op amp design and small size make it ideal for a wide range of applications.

A single external resistor sets any gain from 1 to 10,000. Internal input protection can withstand up to ±40V without damage.

The INA114 is laser trimmed for very low offset voltage (50μV), drift (0.25μV/°C) and high common-mode rejection (115dB at G = 1000). It operates with power supplies as low as ±2.25V, allowing use in battery operated and single 5V supply systems. Quiescent current is 3mA maximum.

The INA114 is available in 8-pin plastic and SOL-16 surface-mount packages. Both are specified for the –40°C to +85°C temperature range.

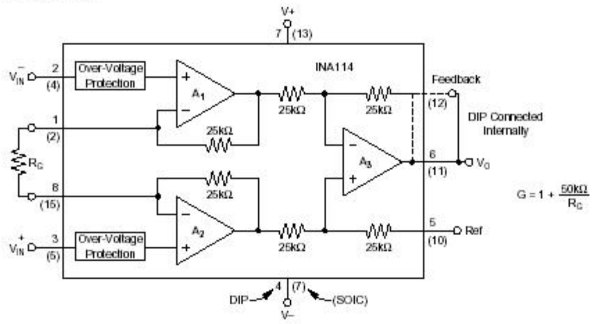

International Airport Industrial Park • Mailing Address: PO Box 11400, Tucson, AZ 85734 • Street Address: 6730 S. Tucson Blvd., Tucson, AZ 85706 • Tel: (520) 746-1111 • Twx: 910-952-1111
Internet: http://www.burr-brown.com/ • FAXLine: (800) 548-6133 (US/Canada Only) • Cable: BBRCORP • Telex: 066-6491 • FAX: (520) 889-1510 • Immediate Product Info: (800) 548-6132

 PDS-1142D Printed in U.S.A. March, 1998

SPECIFICATIONS

ELECTRICAL

At $T_A = +25°C$, $V_S = \pm15V$, $R_L = 2k\Omega$, unless otherwise noted.

PARAMETER	CONDITIONS	INA114BP, BU MIN	INA114BP, BU TYP	INA114BP, BU MAX	INA114AP, AU MIN	INA114AP, AU TYP	INA114AP, AU MAX	UNITS
INPUT								
Offset Voltage, RTI								
Initial	$T_A = +25°C$		±10 + 20/G	±50 + 100/G		±25 + 30/G	±125 + 500/G	μV
vs Temperature	$T_A = T_{MIN}$ to T_{MAX}		±0.1 + 0.5/G	±0.25 + 5/G		±0.25 + 5/G	±1 + 10/G	μV/°C
vs Power Supply	$V_S = \pm2.25V$ to $\pm18V$		0.5 + 2/G	3 + 10/G		*	*	μV/V
Long-Term Stability			±0.2 + 0.5/G			*		μV/mo
Impedance, Differential			$10^{10} \parallel 6$			*		Ω ‖ pF
Common-Mode			$10^{10} \parallel 6$			*		Ω ‖ pF
Input Common-Mode Range		±11	±13.5		*	*		V
Safe Input Voltage				±40			*	V
Common-Mode Rejection	$V_{CM} = \pm10V$, $\Delta R_S = 1k\Omega$							
	G = 1	80	96		75	90		dB
	G = 10	96	115		90	106		dB
	G = 100	110	120		106	110		dB
	G = 1000	115	120		106	110		dB
BIAS CURRENT			±0.5	±2		*	±5	nA
vs Temperature			±8			*		pA/°C
OFFSET CURRENT			±0.5	±2		*	±5	nA
vs Temperature			±8			*		pA/°C
NOISE VOLTAGE, RTI	$G = 1000$, $R_S = 0\Omega$							
f = 10Hz			15			*		$nV/\sqrt{Hz}$
f = 100Hz			11			*		$nV/\sqrt{Hz}$
f = 1kHz			11			*		$nV/\sqrt{Hz}$
f_B = 0.1Hz to 10Hz			0.4			*		μVp-p
Noise Current								
f=10Hz			0.4			*		$pA/\sqrt{Hz}$
f=1kHz			0.2			*		$pA/\sqrt{Hz}$
f_B = 0.1Hz to 10Hz			18			*		pAp-p
GAIN								
Gain Equation			$1 + (50k\Omega/R_G)$			*		V/V
Range of Gain		1		10000	*		*	V/V
Gain Error	G = 1		±0.01	±0.05		*	*	%
	G = 10		±0.02	±0.4		*	±0.5	%
	G = 100		±0.05	±0.5		*	±0.7	%
	G = 1000		±0.5	±1		*	±2	%
Gain vs Temperature	G = 1		±2	±10		*	±10	ppm/°C
50kΩ Resistance[1]			±25	±100		*	*	ppm/°C
Nonlinearity	G = 1		±0.0001	±0.001		*	±0.002	% of FSR
	G = 10		±0.0005	±0.002		*	±0.004	% of FSR
	G = 100		±0.0005	±0.002		*	±0.004	% of FSR
	G = 1000		±0.002	±0.01		*	±0.02	% of FSR
OUTPUT								
Voltage	$I_O = 5mA$, T_{MIN} to T_{MAX}	±13.5	±13.7		*	*		V
	$V_S = \pm11.4V$, $R_L = 2k\Omega$	±10	±10.5		*	*		V
	$V_S = \pm2.25V$, $R_L = 2k\Omega$	±1	±1.5		*	*		V
Load Capacitance Stability			1000			*		pF
Short Circuit Current			+20/–15			*		mA
FREQUENCY RESPONSE								
Bandwidth, –3dB	G = 1		1			*		MHz
	G = 10		100			*		kHz
	G = 100		10			*		kHz
	G = 1000		1			*		kHz
Slew Rate	$V_O = \pm10V$, G = 10	0.3	0.6		*	*		V/μs
Settling Time, 0.01%	G = 1		18			*		μs
	G = 10		20			*		μs
	G = 100		120			*		μs
	G = 1000		1100			*		μs
Overload Recovery	50% Overdrive		20			*		μs
POWER SUPPLY								
Voltage Range		±2.25	±15	±18	*	*	*	V
Current	$V_{IN} = 0V$		±2.2	±3		*	*	mA
TEMPERATURE RANGE								
Specification		–40		85	*		*	°C
Operating		–40		125	*		*	°C
θ_{JA}			80			*		°C/W

* Specification same as INA114BP/BU.

NOTE: (1) Temperature coefficient of the "50kΩ" term in the gain equation.

PIN CONFIGURATIONS

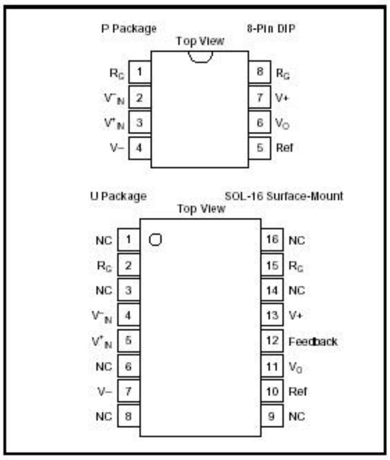

ABSOLUTE MAXIMUM RATINGS(1)

Supply Voltage	±18V
Input Voltage Range	±40V
Output Short-Circuit (to ground)	Continuous
Operating Temperature	–40°C to +125°C
Storage Temperature	–40°C to +125°C
Junction Temperature	+150°C
Lead Temperature (soldering, 10s)	+300°C

NOTE: (1) Stresses above these ratings may cause permanent damage.

ELECTROSTATIC DISCHARGE SENSITIVITY

This integrated circuit can be damaged by ESD. Burr-Brown recommends that all integrated circuits be handled with appropriate precautions. Failure to observe proper handling and installation procedures can cause damage.

ESD damage can range from subtle performance degradation to complete device failure. Precision integrated circuits may be more susceptible to damage because very small parametric changes could cause the device not to meet its published specifications.

PACKAGE/ORDERING INFORMATION

PRODUCT	PACKAGE	PACKAGE DRAWING NUMBER(1)	TEMPERATURE RANGE
INA114AP	8-Pin Plastic DIP	006	–40°C to +85°C
INA114BP	8-Pin Plastic DIP	006	–40°C to +85°C
INA114AU	SOL-16 Surface-Mount	211	–40°C to +85°C
INA114BU	SOL-16 Surface-Mount	211	–40°C to +85°C

NOTE: (1) For detailed drawing and dimension table, please see end of data sheet, or Appendix C of Burr-Brown IC Data Book.

TYPICAL PERFORMANCE CURVES

At T_A = +25°C, V_S = ±15V, unless otherwise noted.

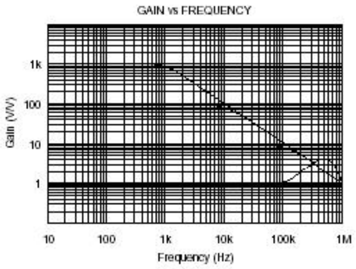

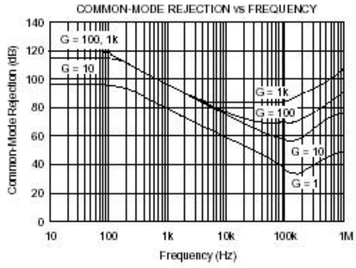

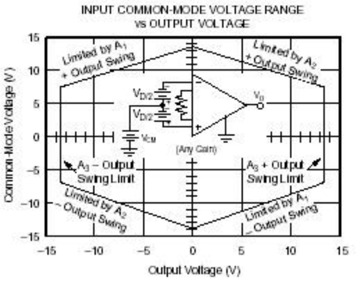

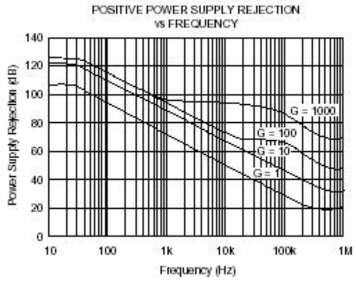

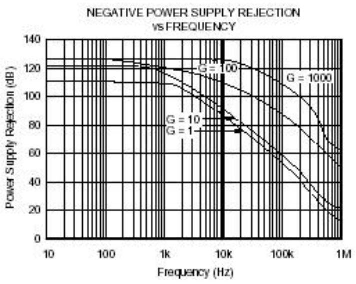

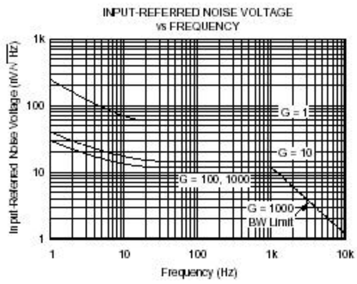

TYPICAL PERFORMANCE CURVES (CONT)

At $T_A = +25°C$, $V_S = ±15V$, unless otherwise noted.

SETTLING TIME vs GAIN

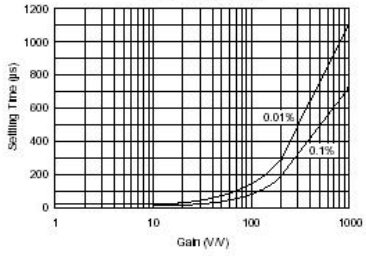

OFFSET VOLTAGE WARM-UP vs TIME

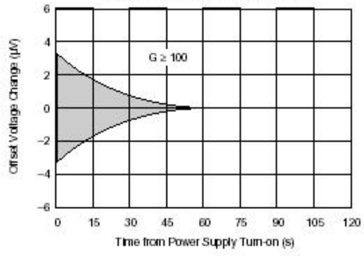

INPUT BIAS AND INPUT OFFSET CURRENT vs TEMPERATURE

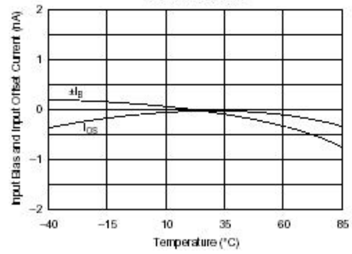

INPUT BIAS CURRENT vs DIFFERENTIAL INPUT VOLTAGE

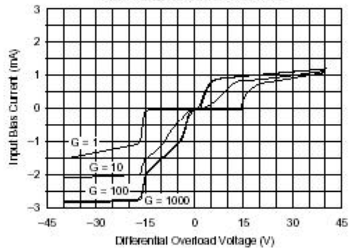

INPUT BIAS CURRENT vs COMMON-MODE INPUT VOLTAGE

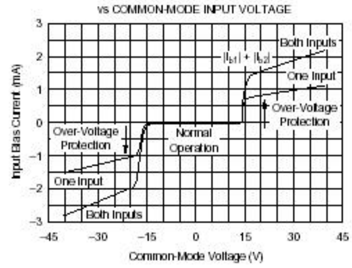

MAXIMUM OUTPUT SWING vs FREQUENCY

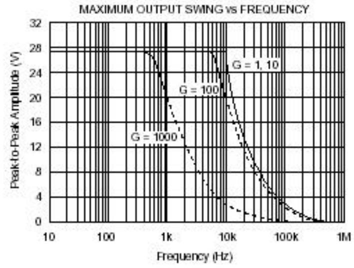

TYPICAL PERFORMANCE CURVES (CONT)

At T_A = +25°C, V_S = ±15V, unless otherwise noted.

SLEW RATE vs TEMPERATURE

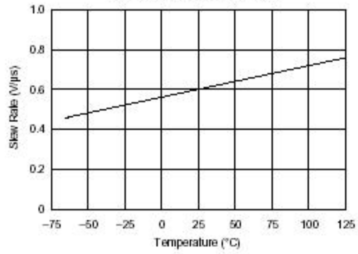

OUTPUT CURRENT LIMIT vs TEMPERATURE

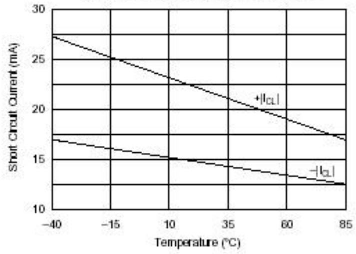

QUIESCENT CURRENT vs TEMPERATURE

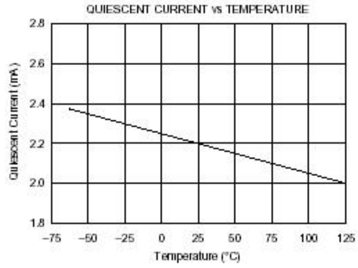

QUIESCENT CURRENT AND POWER DISSIPATION vs POWER SUPPLY VOLTAGE

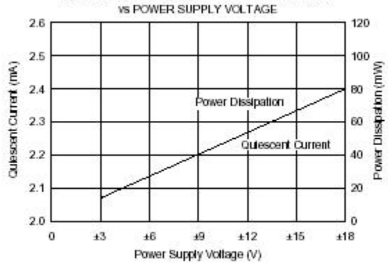

POSITIVE SIGNAL SWING vs TEMPERATUE (R_L = 2kΩ)

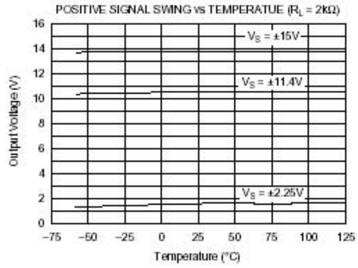

NEGATIVE SIGNAL SWING vs TEMPERATUE (R_L = 2kΩ)

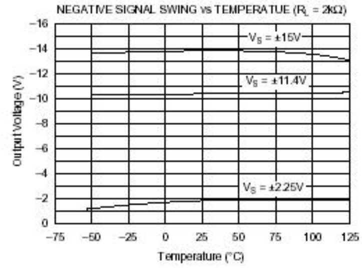

TYPICAL PERFORMANCE CURVES (CONT)

At T_A = +25°C, V_S = ±15V, unless otherwise noted.

LARGE SIGNAL RESPONSE, G = 1

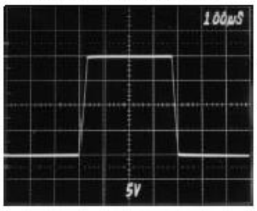

SMALL SIGNAL RESPONSE, G = 1

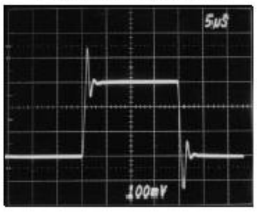

LARGE SIGNAL RESPONSE, G = 1000

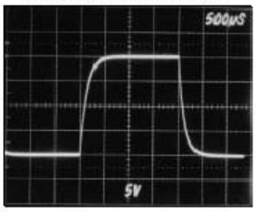

SMALL SIGNAL RESPONSE, G = 1000

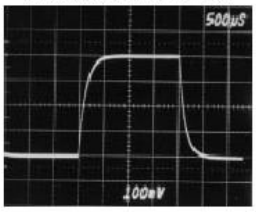

INPUT-REFERRED NOISE, 0.1 to 10Hz

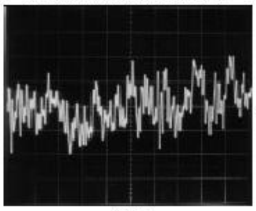

APPLICATION INFORMATION

Figure 1 shows the basic connections required for operation of the INA114. Applications with noisy or high impedance power supplies may require decoupling capacitors close to the device pins as shown.

The output is referred to the output reference (Ref) terminal which is normally grounded. This must be a low-impedance connection to assure good common-mode rejection. A resistance of 5Ω in series with the Ref pin will cause a typical device to degrade to approximately 80dB CMR (G = 1).

SETTING THE GAIN

Gain of the INA114 is set by connecting a single external resistor, R_G:

$$G = 1 + \frac{50\text{ k}\Omega}{R_G} \qquad (1)$$

Commonly used gains and resistor values are shown in Figure 1.

The 50kΩ term in equation (1) comes from the sum of the two internal feedback resistors. These are on-chip metal film resistors which are laser trimmed to accurate absolute values. The accuracy and temperature coefficient of these resistors are included in the gain accuracy and drift specifications of the INA114.

The stability and temperature drift of the external gain setting resistor, R_G, also affects gain. R_G's contribution to gain accuracy and drift can be directly inferred from the gain equation (1). Low resistor values required for high gain can make wiring resistance important. Sockets add to the wiring resistance which will contribute additional gain error (possibly an unstable gain error) in gains of approximately 100 or greater.

NOISE PERFORMANCE

The INA114 provides very low noise in most applications. For differential source impedances less than 1kΩ, the INA103 may provide lower noise. For source impedances greater than 50kΩ, the INA111 FET-input instrumentation amplifier may provide lower noise.

Low frequency noise of the INA114 is approximately 0.4μVp-p measured from 0.1 to 10Hz. This is approximately one-tenth the noise of "low noise" chopper-stabilized amplifiers.

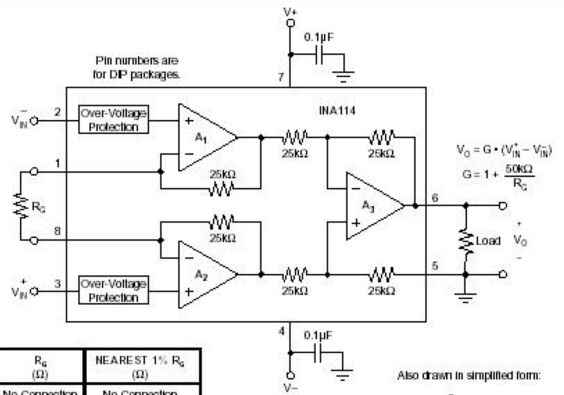

DESIRED GAIN	R_G (Ω)	NEAREST 1% R_G (Ω)
1	No Connection	No Connection
2	50.00k	49.9k
5	12.50k	12.4k
10	5.556k	5.62k
20	2.632k	2.61k
50	1.02k	1.02k
100	505.1	511
200	251.3	249
500	100.2	100
1000	50.05	49.9
2000	25.01	24.9
5000	10.00	10
10000	5.001	4.99

Also drawn in simplified form:

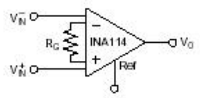

FIGURE 1. Basic Connections.

OFFSET TRIMMING

The INA114 is laser trimmed for very low offset voltage and drift. Most applications require no external offset adjustment. Figure 2 shows an optional circuit for trimming the output offset voltage. The voltage applied to Ref terminal is summed at the output. Low impedance must be maintained at this node to assure good common-mode rejection. This is achieved by buffering trim voltage with an op amp as shown.

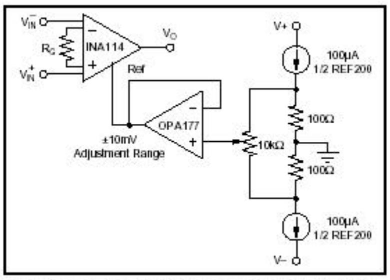

FIGURE 2. Optional Trimming of Output Offset Voltage.

INPUT BIAS CURRENT RETURN PATH

The input impedance of the INA114 is extremely high—approximately $10^{10}\Omega$. However, a path must be provided for the input bias current of both inputs. This input bias current is typically less than ±1nA (it can be either polarity due to cancellation circuitry). High input impedance means that this input bias current changes very little with varying input voltage.

Input circuitry must provide a path for this input bias current if the INA114 is to operate properly. Figure 3 shows various provisions for an input bias current path. Without a bias current return path, the inputs will float to a potential which exceeds the common-mode range of the INA114 and the input amplifiers will saturate. If the differential source resistance is low, bias current return path can be connected to one input (see thermocouple example in Figure 3). With higher source impedance, using two resistors provides a balanced input with possible advantages of lower input offset voltage due to bias current and better common-mode rejection.

INPUT COMMON-MODE RANGE

The linear common-mode range of the input op amps of the INA114 is approximately ±13.75V (or 1.25V from the power supplies). As the output voltage increases, however, the linear input range will be limited by the output voltage swing of the input amplifiers, A_1 and A_2. The common-mode range is related to the output voltage of the complete amplifier—see performance curve "Input Common-Mode Range vs Output Voltage."

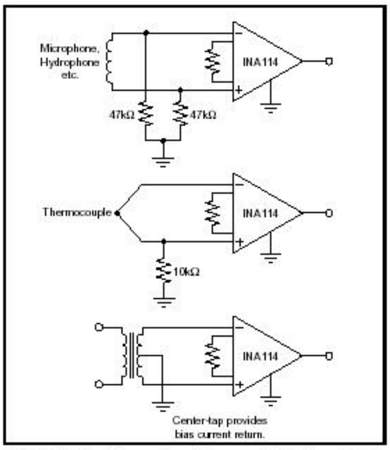

FIGURE 3. Providing an Input Common-Mode Current Path.

A combination of common-mode and differential input signals can cause the output of A_1 or A_2 to saturate. Figure 4 shows the output voltage swing of A_1 and A_2 expressed in terms of a common-mode and differential input voltages. Output swing capability of these internal amplifiers is the same as the output amplifier, A_3. For applications where input common-mode range must be maximized, limit the output voltage swing by connecting the INA114 in a lower gain (see performance curve "Input Common-Mode Voltage Range vs Output Voltage"). If necessary, add gain after the INA114 to increase the voltage swing.

Input-overload often produces an output voltage that appears normal. For example, an input voltage of +20V on one input and +40V on the other input will obviously exceed the linear common-mode range of both input amplifiers. Since both input amplifiers are saturated to nearly the same output voltage limit, the difference voltage measured by the output amplifier will be near zero. The output of the INA114 will be near 0V even though both inputs are overloaded.

INPUT PROTECTION

The inputs of the INA114 are individually protected for voltages up to ±40V. For example, a condition of –40V on one input and +40V on the other input will not cause damage. Internal circuitry on each input provides low series impedance under normal signal conditions. To provide equivalent protection, series input resistors would contribute excessive noise. If the input is overloaded, the protection circuitry limits the input current to a safe value (approximately 1.5mA). The typical performance curve "Input Bias Current vs Common-Mode Input Voltage" shows this input current limit behavior. The inputs are protected even if no power supply voltage is present.

OUTPUT VOLTAGE SENSE (SOL-16 package only)

The surface-mount version of the INA114 has a separate output sense feedback connection (pin 12). Pin 12 must be connected to the output terminal (pin 11) for proper operation. (This connection is made internally on the DIP version of the INA114.)

The output sense connection can be used to sense the output voltage directly at the load for best accuracy. Figure 5 shows how to drive a load through series interconnection resistance. Remotely located feedback paths may cause instability. This can be generally be eliminated with a high frequency feedback path through C_1. Heavy loads or long lines can be driven by connecting a buffer inside the feedback path (Figure 6).

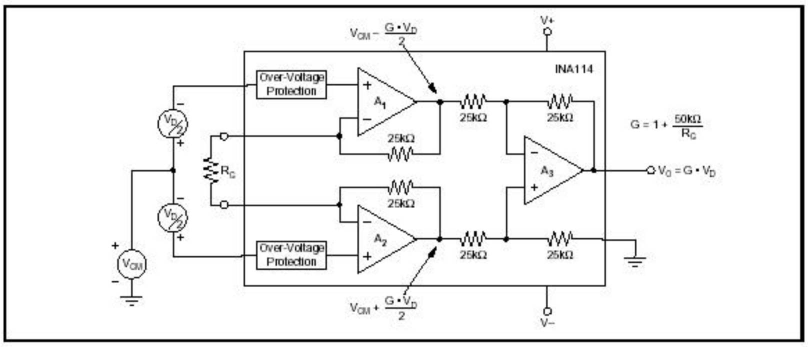

FIGURE 4. Voltage Swing of A_1 and A_2.

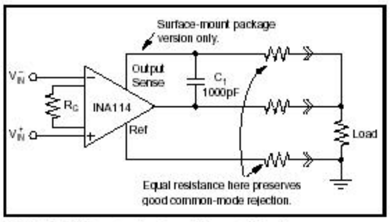

FIGURE 5. Remote Load and Ground Sensing.

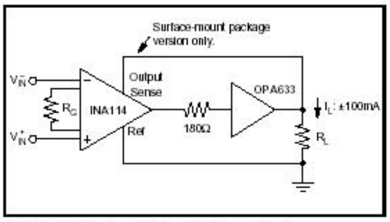

FIGURE 6. Buffered Output for Heavy Loads.

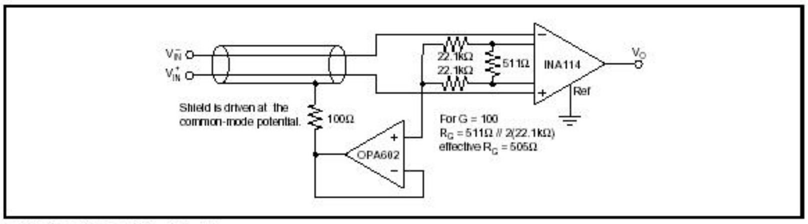

FIGURE 7. Shield Driver Circuit.

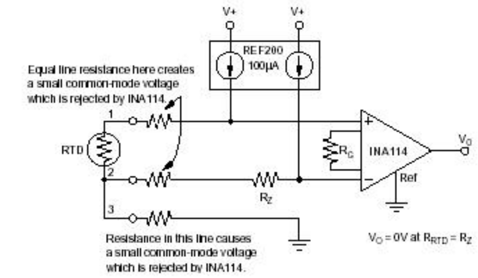

FIGURE 8. RTD Temperature Measurement Circuit.

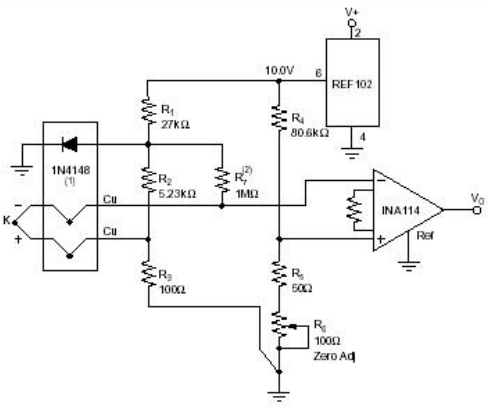

ISA TYPE	MATERIAL	SEEBECK COEFFICIENT (µV/°C)	R_2 (R_3 = 100Ω)	R_4 (R_5 + R_6 = 100Ω)
E	Chromel Constantan	58.5	3.48kΩ	56.2kΩ
J	Iron Constantan	50.2	4.12kΩ	64.9kΩ
K	Chromel Alumel	39.4	5.23kΩ	80.6kΩ
T	Copper Constantan	38.0	5.49kΩ	84.5kΩ

NOTES: (1) –2.1mV/°C at 200µA. (2) R_7 provides down-scale burn-out indication.

FIGURE 9. Thermocouple Amplifier With Cold Junction Compensation.

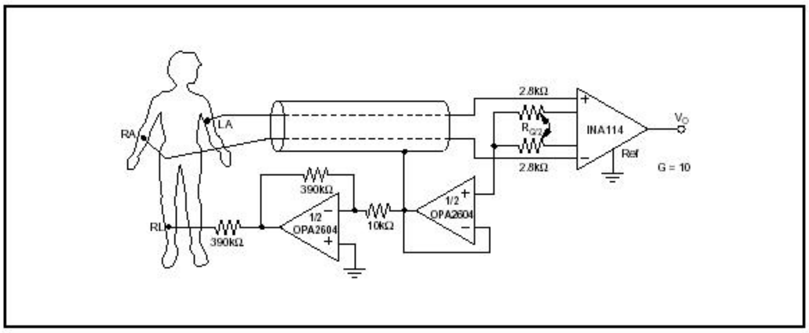

FIGURE 10. ECG Amplifier With Right-Leg Drive.

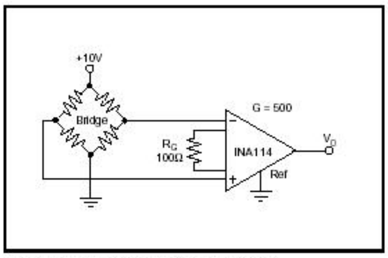

FIGURE 11. Bridge Transducer Amplifier.

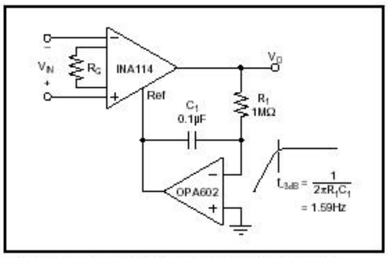

FIGURE 12. AC-Coupled Instrumentation Amplifier.

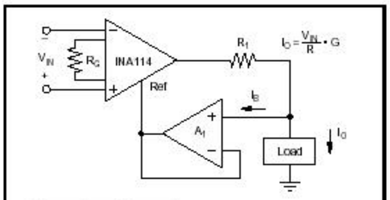

A_1	I_B Error
OPA177	±1.5nA
OPA602	1pA
OPA128	75fA

FIGURE 13. Differential Voltage-to-Current Converter.

B.4 Specifications for PCB 112B11 Piezoelectric Sensor

PCB PIEZOTRONICS INC.

Model 112B11

Product Type: Pressure Transducer, Pressure Sensor

Engine combustion pressure sensor, 3000 psi, 1 pC/psi, cylinder head, flush mount

PERFORMANCE	**ENGLISH**	**SI**
Sensitivity (+25%-10%)	1.0 pC/psi	0.145 pC/kPa
Measurement Range	3 kpsi	20,685 kPa
Maximum Pressure (static)	5 kpsi	34,475 kPa
Resolution	10 mpsi	0.069 kPa [1]
Resonant Frequency	≥ 200 kHz	≥ 200 kHz
Rise Time (Reflected)	≤ 3.0 μ sec	≤ 3.0 μ sec
Non-Linearity	≤ 2.0 % FS	≤ 2.0 % FS [2]
ENVIRONMENTAL		
Acceleration Sensitivity	0.002 psi/g	0.0014 kPa/(m/s^2)
Temperature Range (Operating)	-100 to +600 °F	-73 to +316 °C
Temperature Coefficient of Sensitivity	≤ 0.03 %/°F	≤ 0.054 %/°C
Maximum Flash Temperature	4500 °F	2482 °C
Maximum Shock	10,000 g pk	98,100 m/s^2 pk
ELECTRICAL		
Output Polarity (Positive Pressure)	Negative	Negative
Capacitance	20 pF	20 pF
Insulation Resistance (at room temp)	10^{12} ohm	10^{12} ohm
(600°F(316°C))	10^9 ohm	10^9 ohm
PHYSICAL		
Sensing Element	Quartz	Quartz
Housing Material	Invar	Invar
Diaphragm	Invar	Invar
Sealing	Welded Hermetic	Welded Hermetic
Electrical Connector	10-32 Coaxial Jack	10-32 Coaxial Jack
Weight (with clamp nut)	0.2 oz	6.0 gm
SUPPLIED ACCESSORIES:		
Model 060A03 Clamp nut, 5/16-24-2A thd, 1/4" hex, stainless steel (1)		
Model 065A05 Seal sleeve sensor recess mount 0.248" OD x 0.221" ID x 0.240" thk 17-7 (1)		
Model 065A29 Seal, .250" OD x .218" ID x .015", 316L (3)		
Model 069A83 Sleeve Spacer, .248" OD x .221" ID x .25 thk, 17-4PH (1)		
Model 069A93 Sleeve Spacer, .248" OD x .221" ID, 17-4PH (1)		
Model 069A94 Sleeve Spacer, .248" OD x .221" ID, ST STL (1)		
OPTIONAL VERSIONS		
M - Metric Mount		
Supplied Accessory : Model 060A05 Clamp nut M7 x 0.75-6G thd (1) replaces Model 060A03		
P - Positive Output Polarity		

All specifications are at room temperature unless otherwise specified.

NOTES:
[1] Resolution dependent on range setting and cable length used in charge system.
[2] Zero-based, least-squares, straight line method.

B.5 Specifications for Encoder Optical Sensor

Slotted, Through Scan

with Logic

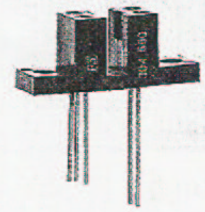

L. 25
W. 6
H. 10
F.C. 19
Dia. 3

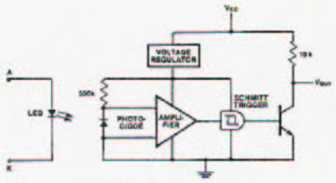

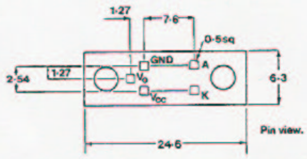

A slotted opto-switch comprising an infra-red source and integrated photodetector. The i.c. photodetector consists of a photodiode, amplifier, voltage regulator, Schmitt trigger and output stage. An important feature is its wide supply voltage range, +4·5 V to 16 V, which allows the output to interface directly to TTL, LS/TTL and C-MOS. The detector can sink 10 TTL loads when the infra-red beam is interrupted. The output rise and fall times are independent of object speed and the integrated voltage regulator ensures high noise immunity. Applications include position detection, paper sensing, counting, optical encoding and level sensing. Operating temperature range: -40°C to +100°C.

technical specification	
diode	
V_F max. (at I_F=29mA)	1.5V
V_R max.	3V
I_F max. (cont.)	50mA
photodetector	
Operating supply voltage range	+4.5 to +12VDC
Max. dissipation	250mW at +25°C
Output sink current	15mA max
Operating current	15mA max.
coupled	
Propagation delay times	
(high to low, ot low to high)	5µs
Output rise times	180ns max. 150ns typ.
Output fall time	50ns max. 23ns typ.
Max. operating frequency	100kHz

RS Data Sheet No. **232-2447, Mar 97** is available.

	stock no.	price each A$ 1-24	25-99
opto-switch	**304-560**	**18·10**	**13·60**

Appendix C

MATLAB Scripts and Functions

Appendix C Contents

C.1 MATLAB Scripts and Functions

The following MATLAB (version 6) programs are scripts and functions that were used to analyse the experimental data.

Listing C.1: Load_cal2.m

```
function [span,offset]=load_cal2(file_name,nrows,ncolumns,Vs,p1,doplots)....
    ;

% load_cal2.m
%
% Function for determining the Span and Offset
% from a set of calibration data (from the Dead
% Weight tester)
%
% INPUTS -
% file_name - file name of calibration data (eg cal.txt)
% nrow - numbers of rows of calibration (number of pressures tested)
% ncolumn - number of columns of data (usually 2 or 3)
% Vs - supply voltage to calibration
% p1 - atmospheric pressure during calibration
% doplots - 1 if plots required, 0 if not
%
% OUTPUTS
% span - matrix of span values
% offest - matrix of offset values

%==================================================================
% Data layout in calibration file as follows -
% column 1, pressure in PSI
% column 2, Vout
% column 3 (optional), Vout (decreasing pressure)

N = 1; %linear fit

% Remove text from data file (data column headings)
fid=fopen(file_name);
fscanf(fid,'%s',ncolumns);
for i=1:nrows,
    i;
    for j=1:ncolumns,
        num(i,j)=fscanf(fid,'%f',1);
    end
end

% Convert calibration pressures from psi to Pa
x = num(:,1).*6894.8 + p1;  %convert pressure to Pa (absolute)

% Linear regression for 1st set of data (increasing pressure)
y1 = num(:,2);
[P1] = POLYFIT(x,y1,N);
offset1 = P1(2)/Vs; %mv/V
span1 = P1(1)/Vs;  %mV/V-pa
span(1,1)=span1;  %span of fisrt set of data (up)
offset(1,1)=offset1;   %offset of first set of data (up)

% Linear regression if 2nd set of data (decreasing pressure)
if ncolumns>2,
    y2 = num(:,3);
    [P2] = POLYFIT(x,y2,N);
    offset2 = P2(2)/Vs; %mv/V
    span2 = P2(1)/Vs;  %mV/V-pa
    span(1,2)=span2;   %span of second set of data (down)
    offset(1,2)=offset2;   %offset of second set of data (down)

    % Average Span and Offset
```

```
    y3 = [y1; y2];
    x3 = [x; x];
    [P3] = POLYFIT(x3,y3,N);
    offset3 = P3(2)/Vs; %mv/V
    span3 = P3(1)/Vs;  %mV/V-pa
    span(1,3)=span3;    %average span (up and down)
    offset(1,3)=offset3;    %average offset (up and down)
end
% Give calibration plots if required
if doplots
    figure(1)
    plot(x,y1,'o',x,polyval(P1,x))
    title('Calibration with increasing pressure')
    xlabel('Pressure (Pa)')
    ylabel('Sensor Output (mV)')
    %text(1e5,-150,[num2str(P1(1)),' mV/Pa']);
    if ncolumns>2
        figure(2)
        plot(x,y2,'o',x,polyval(P2,x))
        title('Calibration with decreasing pressure')
        xlabel('Pressure (Pa)')
        ylabel('Sensor Output (mV)')
        %text(1e5,-150,[num2str(P2(1)),' mV/Pa']);
        figure(5)
        plot(x3,y3,'o',x3,polyval(P3,x3),'m');
        hold on
    end
end
```

Listing C.2: Temp_cal2.m

```
% temp_cal2.m
%
% Script to determine the temperature effects
% on the 13U0500 piezoresistive pressure sensor

%==========================================================
% Data on previous sensor calibrations:
% 13U0500_1.txt @ approx 22.0 deg C   av. Vsense = 91.8mv
% 13U0500_2.txt @ approx 53.0 deg C   av. Vsense = 856mv
% 13U0500_3.txt @ approx 100.5 deg C   av. Vsense = 1957mv
% 13U0500_4.txt @ approx 138.5 deg C   av. Vsense = 2885mv

% Allocate test temperatures
temp1 = 273 + 22;
temp2 = 273 + 53;
temp3 = 273 + 100.5;
temp4 = 273 + 138.5;
TEMP = [temp1 temp2 temp3 temp4];   % K

% Allocate average values for Vsense for each test
Vsense_temp = [91.8 856 1957 2885];  %mv

% Average atm pressure
p1 = 9.38e4;   %Pa

% Determine the actual sensor supply voltage
% for each test
Vs1 = 15 - Vsense_temp(1)/1000;
Vs2 = 15 - Vsense_temp(2)/1000;
Vs3 = 15 - Vsense_temp(3)/1000;
Vs4 = 15 - Vsense_temp(4)/1000;

% Correct Vsense for circuit supply voltage (total 30V)
Vsense_temp_new = [Vsense_temp(1)/30 Vsense_temp(2)/30 Vsense_temp(3)/30....
     Vsense_temp(4)/30] ;

% Load Span and Offset for each calibration
[span1,offset1]=load_cal2('13U0500_1.txt',8,3,Vs1,p1,0);
[span2,offset2]=load_cal2('13U0500_2.txt',8,3,Vs2,p1,0);
[span3,offset3]=load_cal2('13U0500_3.txt',8,3,Vs3,p1,0);
[span4,offset4]=load_cal2('13U0500_4.txt',8,3,Vs4,p1,0);

% Plot Span against temperature
temp_span = [span1(3) span2(3) span3(3) span4(3)];
figure(1);
plot(TEMP,temp_span,'b',TEMP,temp_span,'r*');
hold on

% Plot Offset against temperature
temp_offset = [offset1(3) offset2(3) offset3(3) offset4(3)];
figure(2);
plot(TEMP,temp_offset,'b',TEMP,temp_offset,'r*');
hold on

figure(4)
plot(TEMP,temp_offset,'b',TEMP,temp_offset,'r*');
hold on

% Determine Span temperature sensitivity (linear)
N = 1;
[Pspan] = POLYFIT(TEMP,temp_span,N);
dspandt = Pspan(1);   %(mV/V.Pa)/C
% Plot linear regression of Span against data points
figure(1);
%plot(TEMP,Pspan(2)+Pspan(1)*TEMP,'r')
title('Relationship between Span and Temperature')
ylabel('Span (mV/V.Pa)')
xlabel('Temperature (K)')
hold off

% Determine Offset temperature sensitivity
```

```
[Poffset] = POLYFIT(TEMP, temp_offset ,2);
doffsetdt = Poffset(1);  %(mV/V)/C
figure(2);
%plot(TEMP, Poffset(3)+Poffset(2)*TEMP+Poffset(1)*TEMP.^2, 'r')
title('Relationship between Offset and Temperature')
ylabel('Offset (mV/V)')
xlabel('Temperature (K)')
hold off

% Determine Offset temperature sensitivity (linear) - upto approx 370K
[Poffset2] = POLYFIT(TEMP(1:3), temp_offset(1:3),1);
doffsetdt2 = Poffset2(1);
% Plot linear regression of Offset against data points
figure(4);
plot(TEMP(1:3),Poffset2(2)+Poffset2(1)*TEMP(1:3),'r')
hold off

% Plot Vsense and temperature
figure(3)
plot(TEMP, Vsense_temp_new, 'b',TEMP, Vsense_temp_new, 'r*')
hold on

% Determine Vsense temperature sensitivity (linear)
[PVsense] = POLYFIT(TEMP, Vsense_temp_new,N);
% Plot linear regressoin of Vsense against data points
%plot(TEMP, PVsense(2)+PVsense(1)*TEMP, 'r')
title('Relationship between V_{sense} and Temperature')
ylabel('V_{sense} (mV/V)')
xlabel('Temperature (K)')
hold off
dVsensedt = PVsense(1); %mV/V

%=================================================================
% Calculate the errors associated with
% temperature compensation

% Initalize the Vout matrix
Vout = zeros(8,1);

% Step through the calibration data for each temperature
for i=1:4

    % Load calibration data
    eval(['file_name=''13U0500_',int2str(i),'.txt'';']);

    fid=fopen(file_name);
    fscanf(fid, '%s',3);
    for i=1:8,
        i;
        for j=1:3,
            num(i,j)=fscanf(fid, '%f',1);
        end
    end

    % Convert calibration pressures from psi to Pa
    num(:,1) = num(:,1).*6894.8 + p1; % Pa

    % Define pressures and related Vout
    % Test Pressures
    x = num(:,1); % Pa
    % Vout - increasing pressure
    y1 = num(:,2);
    % Vout - decreasing pressure
    y2 = num(:,3);
    % Vout - average
    y3 = (y1+y2)/2;

    % Record values of Vout
    Vout = [Vout y3];
end

% Trim zeros from Vout matrix
Vout = Vout(:,(2:5));
```

```
% Calculate uncompensated pressure values (Pa abs)
% use approximate Span and Offest from 25 deg C

span_25 = span1(3) + Pspan(1)*3    %mV/V.Pa
offset_25 = interp1([273 TEMP],[1.56807 temp_offset],(273+25),'linear')

% Supply voltage for each test is different (due to Vsense)
pressures_uncomp(:,1) = (Vout(:,1)-offset_25*Vs1)/(span_25 * Vs1); %Pa
pressures_uncomp(:,2) = (Vout(:,2)-offset_25*Vs2)/(span_25 * Vs2); %Pa
pressures_uncomp(:,3) = (Vout(:,3)-offset_25*Vs3)/(span_25 * Vs3); %Pa
pressures_uncomp(:,4) = (Vout(:,4)-offset_25*Vs4)/(span_25 * Vs4); %Pa

Vsense_25 = PVsense(2)+PVsense(1)*298
%Vsense_temp = [91.8 856 1957 2885]
temp1 = ((91.8/30) - Vsense_25) / dVsensedt + 25
temp2 = ((856/30) - Vsense_25) / dVsensedt + 25
temp3 = ((1957/30) - Vsense_25) / dVsensedt + 25
temp4 = ((2885/30) - Vsense_25) / dVsensedt + 25

span1 = span_25 + Pspan(1)*(temp1-25)
span2 = span_25 + Pspan(1)*(temp2-25)
span3 = span_25 + Pspan(1)*(temp3-25)
span4 = span_25 + Pspan(1)*(temp4-25)

offset1 = interp1([273 TEMP],[0.5155 temp_offset],(temp1+273),'linear')
offset2 = interp1([273 TEMP],[0.5155 temp_offset],(temp2+273),'linear')
offset3 = interp1([273 TEMP],[0.5155 temp_offset],(temp3+273),'linear')
% Upper Offset value extrapolated from last 2 data points
offset4 = interp1([273 TEMP 420],[0.5155 temp_offset 1.0875],(temp4+273)....
    ,'linear')

% Calculate compenstated pressure values (Pa abs)
pressures_comp(:,1) = (Vout(:,1)-offset1*Vs1)/(span1*Vs1); %Pa
pressures_comp(:,2) = (Vout(:,2)-offset2*Vs2)/(span2*Vs2); %Pa
pressures_comp(:,3) = (Vout(:,3)-offset3*Vs3)/(span3*Vs3); %Pa
pressures_comp(:,4) = (Vout(:,4)-offset4*Vs4)/(span4*Vs4); %Pa

% Determine difference between predicted and actual pressure
% (uncompensated) - percentage FS
error_uncomp1 = ((x)-pressures_uncomp(:,1))/(500*6894.8+p1)*100;
error_uncomp2 = ((x)-pressures_uncomp(:,2))/(500*6894.8+p1)*100;
error_uncomp3 = ((x)-pressures_uncomp(:,3))/(500*6894.8+p1)*100;
error_uncomp4 = ((x)-pressures_uncomp(:,4))/(500*6894.8+p1)*100;

% Determine difference between predicted and actual pressure
% (compensated) - percentage FS
error_comp1 = ((x)-pressures_comp(:,1))/(500*6894.8+p1)*100;
error_comp2 = ((x)-pressures_comp(:,2))/(500*6894.8+p1)*100;
error_comp3 = ((x)-pressures_comp(:,3))/(500*6894.8+p1)*100;
error_comp4 = ((x)-pressures_comp(:,4))/(500*6894.8+p1)*100;

% Convert pressures to percentage FS
pressures = (x)/(500*6894.8+p1)*100;

% Plot uncompensated errors
figure(5)
plot(pressures,error_uncomp1,'*',pressures,error_uncomp2,'s',pressures,....
    error_uncomp3,'^',pressures,error_uncomp4,'d')
AXIS([0 100 -15 5]);
GRID on
Legend('22.0 C','53.0 C','100.5 C','138.5 C',3);
Title('Errors Before Temperature Compensation');
ylabel('Pressure Error (%FS)');
xlabel('Pressure (%FS)');

% Plot compensated errors
figure(6)
plot(pressures,error_comp1,'*',pressures,error_comp2,'s',pressures,....
    error_comp3,'^',pressures,error_comp4,'d')
AXIS([0 100 -5 5]);
```

```
GRID on
Legend('22.0 C','53.0 C','100.5 C','138.5 C',3);
Title('Errors After Temperature Compensation');
ylabel('Pressure Error (%FS)');
xlabel('Pressure (%FS)');
```

Listing C.3: Shock_analysis2.m

```
% shock_analysis2.m
%
% Script for analysis of Shock Tube data using the
% piezoresistive SX150AHO pressure sensor

%===========================================================
% Summary of Shock Tube Tests -
%           1        2        3        4        5        6        7        8 ....
        9        10       11       12       13       14       15       16 ....
       17
Pburst=[    430      570      565      395      555      505      568      545 ....
       485      460      560      440      460      430      475      595     ....
    420]; % gauge kPa
Patm=[      700.30   700.30   709.45   709.45   705.45   705.45   705.45   ....
    706.10   706.10   706.10   701.05   701.05   701.05   701.05   701.05   ....
    701.05   701.05]*133.322368 % atm. pressure in Pa
Tamb=[      21.2     21.2     22.8     22.8     22.8     18.5     18.5     18.5     18.3....
       18.3     18.3     20.0     20.0     20.0     20.0     20.0     20.0     ....
    20.0]; % degC best estimate of st lab temperature
Cal= [      1        1        2        2        3        3        4        5 ....
        5        6        7        7        7        8        8        9 ....
        9  ];    % number corresponding to calibration number (eg 1 = ....
    calibratoin sx150_1)
%pz_st_9 tested with medium grease - calibration for thin grease used
%pz_st_12 tested with thin grease - calibration for no grease used (cal ....
    7)
%pz_st_13 tested with thin grease - calibration for no grease used (cal ....
    7)
%Temp and Pressure(atm) for 16 and 17 were assumed from previous tests -....
     no data taken during testing

% 1 = unmodified pressure transducer
% 2 = stock sensor with top cut off (physically a different sensor to ....
    case 1 ???)
% 3 = top off, epoxy added, but wires still exposed (physically ....
    different to 1 and 2)
% 4 = top off, epoxy added, wires covered (physically different sensor ....
    to 1, 2, and 3)
% 5 = sensor 4 with thin layer grease (about 1mm thick)
% 6 = sensor 5 with thickest layer of grease (filling up to sensor lip)
% 7 = sensor from 2 with thin layer of latex added
% 8 = sensor 7 with grease filling up to sensor lip
% 9 = sensor with margarine (made thinner with additional canola oil) ....
    filled to top

% Voltage drop across bridge
Vexcite=ones(1,17)*12; Vexcite(1)=12.4; % V

% No. cellophane diaphragms
Ndiaphragms=ones(1,17)*4; Ndiaphragms(1)=3;

% Arrangement of data in text files from wavestar
nrows=2500;
ncolumns=12;

% Distances between pressure sensors
dx1_2=0.6935; % m
dx2_3=0.1735+0.003; % m (taking into account the distance from the front....
     of the plate to the silicon chip)

% If shock speeds need to be redetermined let findshockspeeds = 1
findshockspeeds=1;


% All data in files pz_st_x where x=1:15 consists of 12 columns of the ....
    follwing variables
% columns 1 to 8 long time base
% columns 9 to 12 short time base
% 1 = time (long)
% 2 = piezoelectric 1
```

```
% 3 = time (long)
% 4 = piezoelectric 2
% 5 = time (long)
% 6 = vout
% 7 = time (long)
% 8 = vsense
% 9 = time (short)
% 10 = vout
% 11 = time (short)
% 12 = vsense

if findshockspeeds
    % Step through each shock tube test (1 to 17)
    for i=1:17,
        i;
        % Load shock tube test data
        eval(['file_name=''pz_st_',int2str(i),'.txt'';']);
        data=load_wavestar_2(file_name,nrows,ncolumns);

        % Locate shock arrival times at each pressure sensor
        % Piezoelectric 1
        figure(1);
        plot(data(:,2))
        eval(['heading=''pz\_st\_',int2str(i),' A'';']);
        Title(heading)
        zoom on;
        pause
        % Shock time at piezoelectric 1
        [nt1,dummy]=ginput(1); nt1=round(nt1);

        % Piezoelectric 2
        plot(data(:,4))
        eval(['heading=''pz\_st\_',int2str(i),' B'';']);
        Title(heading)
        zoom on;
        pause
        % Shock time at piezoelectric 2
        [nt2,dummy]=ginput(1); nt2=round(nt2);

        % Piezoresistive (long time scale)
        plot(data(:,6))
        eval(['heading=''pz\_st\_',int2str(i),' C'';']);
        Title(heading)
        zoom on;
        pause
        % Shock time at piezoresistive long time scale
        [nt3,dummy]=ginput(1); nt3=round(nt3);

        % Piezoresistive (short time scale)
        plot(data(:,10))
        eval(['heading=''pz\_st\_',int2str(i),' D'';']);
        Title(heading)
        zoom on;
        pause
        % Shock time at piezoresistive short time base
        [nt3s,dummy]=ginput(1); nt3s=round(nt3s);

        % Time of flight for shock
        dt1=data(nt2,1)-data(nt1,1);
        dt2=data(nt3,1)-data(nt2,1);
        % Find velocities
        us1=dx1_2/dt1;
        us2=dx2_3/dt2;

        % Determine approximate shock speed at piezoresistive sensor
        us_coeff=polyfit([data(nt1,1) data(nt2,1) data(nt3,1)],[-(dx1_2+...
            dx2_3) -dx2_3 0],2);
        usp=2*us_coeff(1)*data(nt3,1)+us_coeff(2); %m/s

        % Ambient temperature
        T1 = Tamb(i)+273;  % K
        % Determine shock pressures, temperatures and mach numbers
        % for each possible shock speed
```

```
[p5_us1,T5_us1,Ms_us1,Mr_us1]=p_T_reflected(Patm(i),T1,us1);
[p5_us2,T5_us2,Ms_us2,Mr_us2]=p_T_reflected(Patm(i),T1,us2);
[p5_usp,T5_usp,Ms_usp,Mr_usp]=p_T_reflected(Patm(i),T1,usp);

% Load calibration data for related pressure sensor
eval(['file_name2=''sx150_',int2str(Cal(i)),'.txt'';']);
[Span(Cal(i),:),Offset(Cal(i),:)] = load_cal2(file_name2,15,3,....
    Vexcite(i),Patm(i),0);

% Find zero level and apply sensitivity to piezoresistive sensor
sensitivity=(Span(Cal(i),3)*Vexcite(i)*1e-3); % V/Pa
pz_long=(data(:,6)-mean(data(1:nt3,6)))/sensitivity+Patm(i); %Pa
pz_short=(data(:,10)-mean(data(1:nt3s,10)))/sensitivity+Patm(i);....
    %Pa

% Create time variables
t_long=data(:,1);
t_short=data(:,9);

% Smooth piezoresistive data (short time scale)
pz_short_smo = smo(pz_short,20);

% Graph 1 - short time, compare exp. with theo. results
% for P5 (reflected shock pressure)
figure(3);
plot(t_short-t_short(nt3s),pz_short,'b');
hold on;
% Determine average shock pressure according to shock test ....
    number
if i<3
    p5_av_short = mean(pz_long((nt3+75):(nt3+100))) % 4 us steps....
        (300us to 400 us)
end
if i>2 & i<14
    p5_av_short = mean(pz_short((nt3s+500):(nt3s+1000))) %0.1 us....
        data steps (50us to 100us)
end
if i>=14
    p5_av_short = mean(pz_short((nt3s+1600):(nt3s+2000))) %0.1 ....
        us data steps (pz_st_14 & pz_st_15 have a much slower ....
        response) (160us to 210us)
end
% Compare actual and estimated reflected shock pressures
plot([0 t_short(nrows)],[p5_us1 p5_us1],'m--',[0 t_short(nrows)....
    ],[p5_us2 p5_us2],'r--',[0 t_short(nrows)],[p5_usp p5_usp],'....
    g--',[0 t_short(nrows)],[p5_av_short p5_av_short],'b--');
plot(t_short-t_short(nt3s),pz_short_smo,'k');
AXIS tight
if i<3
    Legend('Pressure from SX150AHO','P5 from US1','P5 from US2',....
        'P5 from USP','P5 average(300us to 400us)','Smoothed ....
        ouptut from SX150AHO',4);
end
if i>2&i<14
    Legend('Pressure from SX150AHO','P5 from US1','P5 from US2',....
        'P5 from USP','P5 average(50us to 100us)','Smoothed ....
        ouptut from SX150AHO',4);
end
if i>=14
    Legend('Pressure from SX150AHO','P5 from US1','P5 from US2',....
        'P5 from USP','P5 average(160us to 200us)','Smoothed ....
        ouptut from SX150AHO',4);
end
eval(['heading=''Pressure vs Time for pz\_st\_',int2str(i),' - ....
    Comparison of Experimental and Theoretical Results'';']);
Title(heading)
ylabel('Pressure (Pa)')
xlabel('Time (s)')
eval(['graphname=''pz_st_',int2str(i),'_1'';']);
AXIS tight
```

```
cd Graphs;
% Save plot image
saveas(3,graphname,'jpg');
saveas(3,graphname,'eps');
cd('..');
hold off;
pause

% Graph 2 - short time, find rise time from
% 10% (green) to 90% (red) of average pressure (blue)
figure(4);
plot(t_short-t_short(nt3s),pz_short,'b',t_short-t_short(nt3s),....
    pz_short_smo,'k');
AXIS tight
Legend('Pressure from SX150AHO','Smoothed ouptut from SX150AHO'....
    ,4)
eval(['heading=''Pressure vs Time for pz\_st\_',int2str(i),' - ....
    Graph for Determining Rise Time'';']);
Title(heading)
ylabel('Pressure (Pa)')
xlabel('Time (s)')
pause
hold on;
plot([-2.5e-5 t_short(nrows)],[p5_av_short p5_av_short],'b--'....
    ,[-2.5e-5 t_short(nrows)],[0.9*(p5_av_short-Patm(i))+Patm(i)....
    0.9*(p5_av_short-Patm(i))+Patm(i)],'r--');
if i<3
    Legend('Pressure from SX150AHO','Smoothed ouptut from ....
        SX150AHO','P5 average(300us to 400us)','90% of P5 ....
        average',4);
end
if i>2 & i<14
    Legend('Pressure from SX150AHO','Smoothed ouptut from ....
        SX150AHO','P5 average(50us to 100us)','90% of P5 average....
        ',4);
end
if i>=14
    Legend('Pressure from SX150AHO','Smoothed ouptut from ....
        SX150AHO','P5 average(160us to 200us)','90% of P5 ....
        average',4);
end
zoom on;
pause
% Select point where Blue line first crosses Red
[rise_upper,dummy]=ginput(1);
plot([-2.5e-5 t_short(nrows)],[0.1*(p5_av_short-Patm(i))+Patm(i)....
    0.1*(p5_av_short-Patm(i))+Patm(i)],'g--');
if i<3
    Legend('Pressure from SX150AHO','Smoothed ouptut from ....
        SX150AHO','P5 average(300us to 400us)','90% of P5 ....
        average','10% of P5 average',4);
end
if i>2 & i<14
    Legend('Pressure from SX150AHO','Smoothed ouptut from ....
        SX150AHO','P5 average(50us to 100us)','90% of P5 average....
        ','10% of P5 average',4);
end
if i>=14
    Legend('Pressure from SX150AHO','Smoothed ouptut from ....
        SX150AHO','P5 average(160us to 200us)','90% of P5 ....
        average','10% of P5 average',4);
end
zoom on;
pause
% Select point where Blue line first crosses Green
[rise_lower,dummy]=ginput(1);
rise_time=rise_upper-rise_lower;
eval(['graphname=''pz_st_',int2str(i),'_2'';']);
AXIS tight
cd Graphs;
% Save plot image
```

```
        saveas(4,graphname,'jpg');
        saveas(4,graphname,'eps');
        cd('..');
        hold off;

        % Graph 3 - long time, compare exp. with theo results
        % for P5 (p5 average from 0.5 to 1.5ms)
        figure (5);
        plot(t_long-t_long(nt3),pz_long,'b');
        p5_av_long = mean(pz_long((nt3+125):(nt3+375))); %4 us data ....
            steps
        hold on;
        plot([0 t_long(nrows)],[p5_us1 p5_us1],'y--',[0 t_long(nrows)],[....
            p5_us2 p5_us2],'r--',[0 t_long(nrows)],[p5_usp p5_usp],'g--'....
            ,[0 t_long(nrows)],[p5_av_long p5_av_long],'b--');
        AXIS tight
        Legend('Pressure from SX150AHO','P5 from US1','P5 from US2','P5 ....
            from USP','P5 average (0.5 ms to 1.5 ms)',4);
        eval(['heading=''Pressure vs Time for pz\_st\_',int2str(i),' - ....
            Comparison of Experimental and Theoretical Results'';']);
        Title(heading);
        ylabel('Pressure (Pa)');
        xlabel('Time (s)');
        eval(['graphname=''pz_st_',int2str(i),'_3'';']);
        AXIS tight
        cd Graphs;
        % Save plot image
        saveas(5,graphname,'jpg');
        saveas(5,graphname,'eps');
        cd('..');
        hold off;

        % Save data for shock tube test
        eval(['save pz_st_',int2str(i),';']);
        pause

        % Save specific variable in 'test_data' matrix
        test_data(i,1) = p5_us1; %Pa
        test_data(i,2) = p5_us2; %Pa
        test_data(i,3) = p5_usp; %Pa
        test_data(i,4) = p5_av_short; %Pa
        test_data(i,5) = p5_av_long; %Pa
        test_data(i,6) = rise_time; %s
    end

% save 'test_data' matrix
save test_data test_data -ascii -tabs;
save test_data test_data;

end

% in saved files (pz_st_x where x=1:15) the following values are ....
    included -
% us1 - shock speed from piezoelectric 1 to piezoelectric 2
% us2 - shock speed from piezoelectric 2 to piezoresistive sensor
% usp - Polynomial fit (second order) to displacement and time - speed =....
     slope at time of shock impact
% p5_us1 - pressure after reflected shock wave (based on us1)
% p5_us2 - pressure after reflected shock wave (based on us2)
% p5_usp - pressure after reflected shock wave (based on usp)
% T5_us1 - temperature after reflected shock wave (based on us1)
% T5_us2 - temperature after reflected shock wave (based on us2)
% T5_usp - temperature after reflected shock wave (based on usp)
% Ms_us1 - Mach number of incident shock wave (based on us1)
% Ms_us2 - Mach number of incident shock wave (based on us2)
% Ms_usp - Mach number of incident shock wave (based on usp)
% Mr_us1 - Mach number of reflected shock wave (based on us1)
% Mr_us2 - Mach number of reflected shock wave (based on us2)
% Mr_usp - Mach number of reflected shock wave (based on usp)
% p5_av_short - average pressure from sensor from Z50 - 100us
% p5_av_long - average pressure from sensor from 0.5 to 1.5 ms
```

```
% rise_time - time for signal (short) to rise from 10% to 90% of ....
    p5_av_short
```

Listing C.4: P_T_reflected.m

```
function [p5,T5,Ms,Mr]=p_T_reflected(p1,T1,us)

% p_T_reflected.m
%
% The function is used in conjunction
% with functions developed by Dr. David Buttsworth
%
% INPUTS -
% p1 - atmospheric pressure, Pa
% T1 - testing temperature (air), K
% us - inbound shock speed, m/s
%
% OUTPUTS
% p5 - reflected shock pressure, Pa
% T5 - reflected shock temperature, K
% Ms - inbound shock Mach number
% Mr - reflected shock Mach number

%==================================================================
% Determine gas properties within shock tube

g=1.4;
R=287;
a1=sqrt(g*R*T1);
Ms=us/a1;
p2p1=p2onp1s(Ms,g);
T2T1=T2onT1(p2p1,g);
Mr=mreflect(Ms,g);
p5p2=p2onp1s(Mr,g);
T5T2=T2onT1(p5p2,g)
p5=p5p2.*p2p1*p1
T2=T2T1*T1
T5=T5T2.*T2T1*T1
% u2=vel2(p2p1,a1,g)
```

Listing C.5: Fill_Time.m

```
% Fill_Time.m
%
% Script for calculating and plotting the
% filling time of a stock SX150AHO sensor

%==========================================================
% Determine filling characteristics of unmodified sensors
% (pz_st_1 and pz_st_2)

% Step through shock tube tests 1 and 2
for i=1:2,
    cd('..')
    eval(['load pz_st_',int2str(i),';']);
    cd Filltime

    % Due to the limits of the interpolation tables,
    % T5_usp must not exceed 433 K
    if i==2
        T5_usp = 433
    end

    % Run filling routine 'sx150_fill.m' - originally created by
    % Dr. David Buttsworth. Certain values within this script
    % (eg. inlet area) were changed to match the sensor
    % dimensions

    % To simlutate possible effects of the shock wave, the value of
    % 'ptube0' (initial pressure) in 'sx150_fill.m' was altered

    sx150_fill;
    R = 297;
    Vol = (0.0074^2*pi/4)*0.0041 - 0.0016*0.00317^2;

    % Plot fill time and compare with recorded sensor
    % pressures
    figure(6);
    plot(t_short-t_short(nt3s),pz_short,'b');
    hold on;
    p5_av_short = mean(pz_long((nt3+75):(nt3+100))) %(300us to 400us)
    plot([0 t_short(nrows)],[p5_us1 p5_us1],'m--',[0 t_short(nrows)],[....
        p5_us2 p5_us2],'r--',[0 t_short(nrows)],[p5_usp p5_usp],'g--',[0....
         t_short(nrows)],[p5_av_short p5_av_short],'b--');
    plot(t_short-t_short(nt3s),pz_short_smo,'k');
    AXIS tight
    plot(T,X(:,1)*R.*X(:,2)/Vol,'r');
    xlabel('Time (s)');
    ylabel('Pressure (Pa)');
    eval(['heading=''Pressure vs Time for pz\_st\_',int2str(i),' - ....
        Comparison of Experimental and Theoretical Results'';']);
    Title(heading)
    eval(['graphname=''pz_st_',int2str(i),'_6'';']);
    Legend('Pressure from SX150AHO','P5 from US1','P5 from US2','P5 from....
         USP','P5 average(300us to 400us)','Smoothed ouptut from ....
        SX150AHO','Theoretical Filling Pressure',4);
    cd('..');
    cd Graphs;
    % Save plot images
    saveas(6,graphname,'jpg');
    saveas(6,graphname,'eps');
    cd('..');
    cd Filltime;
    hold off;
    pause

    clear
end
```

Listing C.6: Psd_display.m

```
% psd_display.m
%
% Script for analysis of resonant frequencies of shock tube data
% Performs a power spectrum density analysis of data

%==========================================================================
% Step through each shock tube test (1 to 17)
for i=1:17
    % Load shock tube test data
    eval(['load pz_st_',int2str(i),';']);

    % Smooth piezoresistive sensor response (to elminate high frequency ....
        signal noise)
    smoothed = smo(pz_short(nt3s:(length(pz_short))),5);
    % Swith directry to preform PSD analysis
    cd external;

    % Plot PSD (psd.m is a MATLAB produced script)
    figure(6); psd(smoothed,3000,1e7);
    eval(['heading=''Power Spectrum Density for pz\_st\_',int2str(i),'(....
        smoothing - 5 points)'';']);
    Title(heading);
    zoom on;
    pause;
    hold on;
    % Select obvious peak of PSD
    % If no obvious frequency present - input 0 Hz
    [freq1,dummy]=ginput(1); freq1=round(freq1);
    plot(freq1,dummy,'go')
    zoom out;
    hold off;

    % Save PSD Plot
    eval(['graphname=''pz_st_',int2str(i),'_4'';']);
    cd('..');
    cd Graphs;
    saveas(6,graphname,'jpg');
    saveas(6,graphname,'eps');

    % Save PSD plot with more appropriate axes
    axis([0 5e5 60 150]);
    eval(['graphname=''pz_st_',int2str(i),'_5'';']);
    saveas(6,graphname,'jpg');
    saveas(6,graphname,'eps');
    cd('..');

    % Record resonant frequency
    frequencies(i)=freq1
end

% save set of resonant frequencies
save frequencies frequencies -ascii -tabs;
save frequencies frequencies;
```

Listing C.7: Gt28_analysis2.m

```
% gt28_analysis2.m
%
% Script for comparing the Gun Tunnel pressures
% recorded with the piezoelectric (112B11) and
% piezoresisitve (13U3000) sensors

%==========================================================
% Load Gun Tunnel Data
data=load_wavestar_2('gt28.txt',2500,10);

% Piezoelectric recorded as column 2, column 10
% Piezoresistive recorded as column 4 (pressure) column 6 (temperature) ....
    column 8

% Average atmospheric pressure:
p1 = 9.38e4;

% Assign times from experimental data
tim1=data(:,1);
tim2=data(:,7);

pze1=data(:,2)*10;
pze2=data(:,10)*10; % factor of 10 because:
% Kistler charge amp set up with 149.7pC/MPa (deadweight tested 29/4/04)....
     and 10MPa/V output
% But note that manufacturer's calibration data for this transducer is:
% 1.088pC/psi (for 0-300psi) = 157.8 pC/MPa and
% 1.107pC/psi (for 0-3000psi) = 160.6 pC/MPa
% For a given pressure, the transducer produces a given charge (in pC),
% but if we have specified a sensitivity in pC/MPa that is less than the....
     real value,
% we will overestimate the pressure proportionately.

% If the manufacturer's value is actually correct, we should make this ....
    adjustment:
pze1=pze1*149.7/157.8 + p1/1e6;
pze2=pze2*149.7/157.8 + p1/1e6;

% caluculate pressure from piezoresisitve sensor
pzr=-(data(:,8)-mean(data(1:200,8)))/(1.786e-3*15)+p1/1e6; % Pa (abs)

% Smooth data for Vsense
pzrT=smo((data(:,6).*1000),100);

% Plot piezoelectric and raw piezoresistive pressure data
figure(1)
plot(tim2,pzr,'r',tim1,pze1,'g')
xlabel('time (s)')
ylabel('Abs. Presure (MPa)')
title('Gun Tunnel (Test 28), Barrel pressure with closed end')
legend('Piezoresistive Reading','Piezoelectric Reading')

% Plot piezoelectric and smoothed piezoresistive data
figure(2)
plot(tim1,pze1,'g',tim2,smo(pzr,3),'r')
xlabel('time (s)')
ylabel('Abs. Presure (MPa)')
title('Gun Tunnel (Test 28), Barrel pressure with closed end')
legend('Piezoelectric Reading','Smoothed Piezoresistive Reading (3 pts)'....
    )

% Plot close-up on raw data to show differences between results
figure(3)
plot(tim2,pzr,'r',tim1,pze1,'g')
xlabel('time (s)')
ylabel('Abs. Presure (MPa)')
title('Gun Tunnel (Test 28), Barrel pressure with closed end')
legend('Piezoresistive Reading','Piezoelectric Reading')
AXIS([4e-3 28e-3 0 4])
```

```
% Plot close-up on smoothed data to show differences between results
figure(5)
plot(tim1,pze1,'g',tim2,smo(pzr,3),'r')
xlabel('time (s)')
ylabel('Abs. Presure (MPa)')
title('Gun Tunnel (Test 28), Barrel pressure with closed end')
legend('Piezoelectric Reading','Smoothed Piezoresistive Reading (3 pts)'....
    )
AXIS([4e-3 28e-3 0 4])
```

Listing C.8: Engine_1.m

```
% engine_1.m
%
% Script for analysis of engine data.
% This script provides an analysis of engine pressures
% recorded by a piezoelectric (13U0500) and a
% piezoresisitve (112B11) sensor

%========================================================================
% 4 different engine data sets collected,
% step through each data set -
for k=5

    % Run temperature calibration to load values
    % for dspan/dt, doffset/dt etc.
    temp_cal2

    %======================================================================
    % Load relavent engine data
    eval(['file_name=''pz_en_',int2str(k),'.txt'';']);
        data=load_wavestar_2(file_name,2500,8);

    % Layout of information in engine data files -
        % column 1 - time for piezoelectric
        % column 2 - readings for piezoelectric
        % column 3 - time for piezoresitive
        % column 4 - Vout
        % column 5 - time for piezoresistive
        % column 6 - Vsense
        % column 7 - time for encoder
        % column 8 - Output for encoder

        %....  ==================================================================....

    % Determine the position of the piston relative to the pressure data
    % Plot encoder data
        figure(1)
        plot(data(:,8),'g');
        zoom on;
        pause
        [enc1,dummy]=ginput(1);  % input value anywhere between end of ....
            long slot and start or short slot
        enc1 = round(enc1);

    % Determine points of encoder signals
    % (these points are the edges of the encoder slots)
    enc_new = [0];
        enc_new2 = [0];
        trigger_A = 0;
        for i=1:1500
        point = enc1 + i;
            if data(point,8)<1
            encdummy = point;
            if trigger_A == 1
                if encdummy ~ enc1+i-1
                    enc_new2 = [enc_new2 encdummy];
                end
            end
            trigger_A = 0;
        end
        if data(point,8)>1
            encdummy = point;
            trigger_B = 0;
            if trigger_A == 0
                if encdummy ~ enc1+i-1
                    enc_new = [enc_new encdummy];
                    trigger_A = 1;
                end
            end
        end
        end
```

```
% Allocate times to encoder signal points
enc_time1 = data(enc_new(2),7);
    enc_time2 = data(enc_new(5),7);
    enc_time3 = data(enc_new(8),7);
    enc_time4 = data(enc_new(11),7);
    enc_time5 = data(enc_new(14),7);
    enc_time6 = data(enc_new(17),7);
    enc2_time1 = data(enc_new2(2),7);
    enc2_time2 = data(enc_new2(5),7);
    enc2_time3 = data(enc_new2(8),7);
    enc2_time4 = data(enc_new2(11),7);
    enc2_time5 = data(enc_new2(14),7);
    enc2_time6 = data(enc_new2(17),7);

% Determine period of engine revolution
    period = ((enc_time2 - enc_time1) + (enc_time3 - enc_time2) + (....
        enc_time4 - enc_time3) + (enc_time5 - enc_time4) + (....
        enc_time6 - enc_time5))/5;

%==================================================================
% Fit encoder data to function for cylinder volume

% Determine the length of time for each slot
    time_slot1_b = ((data(enc_new2(2),7)-data(enc_new(2),7)) + (data....
        (enc_new2(5),7)-data(enc_new(5),7)) + (data(enc_new2(8),7)-....
        data(enc_new(8),7)) + (data(enc_new2(11),7)-data(enc_new(11)....
        ,7)) + (data(enc_new2(14),7)-data(enc_new(14),7)) + (data(....
        enc_new2(17),7)-data(enc_new(17),7)))/6;
    time_slot2_a = ((data(enc_new(3),7)-data(enc_new(2),7)) + (data(....
        enc_new(6),7)-data(enc_new(5),7)) + (data(enc_new(9),7)-data....
        (enc_new(8),7)) + (data(enc_new(12),7)-data(enc_new(11),7)) ....
        + (data(enc_new(15),7)-data(enc_new(14),7)) + (data(enc_new....
        (18),7)-data(enc_new(17),7)))/6;
    time_slot2_b = ((data(enc_new2(3),7)-data(enc_new(2),7)) + (data....
        (enc_new2(6),7)-data(enc_new(5),7)) + (data(enc_new2(9),7)-....
        data(enc_new(8),7)) + (data(enc_new2(12),7)-data(enc_new(11)....
        ,7)) + (data(enc_new2(15),7)-data(enc_new(14),7)) + (data(....
        enc_new2(18),7)-data(enc_new(17),7)))/6;
    time_slot3_a = ((data(enc_new(4),7)-data(enc_new(2),7)) + (data(....
        enc_new(7),7)-data(enc_new(5),7)) + (data(enc_new(10),7)-....
        data(enc_new(8),7)) + (data(enc_new(13),7)-data(enc_new(11)....
        ,7)) + (data(enc_new(16),7)-data(enc_new(14),7)) + (data(....
        enc_new(19),7)-data(enc_new(17),7)))/6;
    time_slot3_b = ((data(enc_new2(4),7)-data(enc_new(2),7)) + (data....
        (enc_new2(7),7)-data(enc_new(5),7)) + (data(enc_new2(10),7)-....
        data(enc_new(8),7)) + (data(enc_new2(13),7)-data(enc_new(11)....
        ,7)) + (data(enc_new2(16),7)-data(enc_new(14),7)) + (data(....
        enc_new2(19),7)-data(enc_new(17),7)))/6;
    slot_time = [0 time_slot1_b time_slot2_a time_slot2_b ....
        time_slot3_a time_slot3_b];

% Determine precise slot angles
    slot_angle = slot_time/period*2*pi;

% Slot_position is the measured cylinder position (from TDC) for ....
    each encoder slot
    slot_position = [48.1 45.3 1.2 0 36.4 47.2]./1000; %m
    %plot(slot_angle,slot_position);

% Engine Data (adapted from enginedata.m created by Dr. David ....
    Buttsworth)
%=========== engine geometry ================================
b=0.069; % engine bore (m)
stroke=0.054; % engine stroke (m)
eps=0.287693; % half stroke to rod ratio, s/2l
r=6.1; % compression ratio
Vtdc=pi/4*b^2*stroke/(r-1); % volume at TDC
```

```
Vbdc=pi/4*b^2*stroke+Vtdc; % volume at BDC
%==========================================================================
% Calculate engine parameters related to encoder slots
    slot_volume = slot_position*(b^2*pi/4)+Vtdc;
    theta = 0:0.01:4*pi;
    V=Vtdc*(1+(r-1)/2*(1-cos(theta)+ 1/eps*(1-(1-eps^2*sin(theta)....
        .^2).^0.5)));
    figure(8);
    plot(theta,V,'b');
    hold on;
    plot(slot_angle,slot_volume,'r*');
    X = ones(1,6);

% Match volume function with encoder slots and piston positions
    for i = 1:6
    angle_solve = slot_angle(i);
    volume_solve = slot_volume(i);
    x = 4; % move function close to expected point
    j = 1;
    while j == 1
        V=Vtdc*(1+(r-1)/2*(1-cos(angle_solve+x)+ 1/eps*(1-(1-eps^2*....
            sin(angle_solve+x).^2).^0.5)));

        if abs(V-volume_solve)>1e-7
            x = x - abs(V-volume_solve)*10;
        end

        if abs(V-volume_solve)<=1e-7
            j = 0;
        end
    end
    X(i) = x;
    V=Vtdc*(1+(r-1)/2*(1-cos(theta+X(i))+ 1/eps*(1-(1-eps^2*sin(....
        theta+X(i)).^2).^0.5)));
    plot(theta,V,'g');
end
 x_avg = mean(X);
    % This value for x_avg can be used in the following volume ....
        calculation -
    % V=Vtdc*(1+(r-1)/2*(1-cos(theta+x_avg)+ 1/eps*(1-(1-eps^2*sin(....
        theta+x_avg).^2).^0.5)))

    %.... ==========================================================================....

    % Plot Data - Compare pressures between Piezoelectric and ....
        Piezoresistive

% determine operational temperature
    Vsense_mean = mean(data(:,6))*1000; %mv
    Vsupply_test = 15 - Vsense_mean/1000; %V
    test_temp = ((Vsense_mean/30) - PVsense(2))/PVsense(1); % K

% Apply temperature compensation
% Determine span & offset for temperature (corrected for Vsupply)
span = span_25 + Pspan(1)*((test_temp-273)-25); %mV/V-pa
    span = span*Vsupply_test;  %mV/pa
    % Linear Extrapolation used to insert lowest data point for ....
        interpolation
offset = interp1([273 TEMP],[0.5155 temp_offset],test_temp,'linear')....
    ; %mV/V
    offset = offset*Vsupply_test; %mV
    % compare pressures
    piezoel = data(:,2)*1e6+9.38e4; %piezoelectric pressure (Pa abs)
    piezores1 = (data(:,4)*1000-offset)/span; % piezoresistive ....
        pressure (Pa abs)
    piezores2 = (data(:,4)*1000-offset)/span;

% Smooth data according to pressure level to preserve peak pressures....
    .
% Low pressure levels - high smoothing
```

```
% High pressure levels (above cutoff) - low smoothing
if k == 2
    cutoff = 2e5;
end
if k == 3
    cutoff = 3e5;
end
if k == 4
    cutoff = 3e5;
end
if k == 5
    cutoff = 5e5;
end

for num = 21:2480
    if (mean((data((num-10:num+10),4)*1000-offset)/span)) <= cutoff
        piezores2(num)=mean((data((num-10:num+10),4)*1000-offset)/....
            span);
    end
    if (mean((data((num-10:num+10),4)*1000-offset)/span)) > cutoff
       piezores2(num)=mean((data((num-2:num+1),4)*1000-offset)/span)....
           ;
    end
end

    % Correct for drift in piezoelectric signal
    figure(11);
    plot(piezoel);
    zoom on;
    pause
    % Select point in middle of exhaust stroke of piezoelectric (....
        time taken 0.01 s either side of point), 400us steps
[time_average,dummy]=ginput(1);
    time_average=round(time_average);
    difference1 = mean((piezoel((time_average-25):(time_average+25))....
        ));
    difference2 = mean((piezores1((time_average-25):(time_average....
        +25))));
    total_diff = difference2 - difference1;
    piezoel = piezoel + total_diff;

    % Compare corrected pressures (time based)
    figure(12)
    plot(data(:,1),piezoel);
    hold on
    plot(data(:,3),piezores1,'g',data(:,3),piezores2,'m');
    %AXIS([0.3 0.6 -0.2e6 2.2e6]);
    xlabel('Time (s)');
    ylabel('Pressure (Pa)');
    if k == 2
    Title('Cylinder pressures - motored, closed throttle (1419.1 rpm....
        )');
end
if k == 3
    Title('Cylinder pressures - fired, no loaded, closed throttle ....
        (2868.1 rpm)');
end
if k == 4
    Title('Cylinder pressures- fired, loaded, closed throttle ....
        (1373.6 rpm)');
end
if k == 5
    Title('Cylinder pressures - fired, loaded, open throttle (2673.8....
         rpm)');
end
    Legend('Piezoelectric Pressure Reading','Piezoresistive Pressure....
         Reading', 'Smoothed Piezoresistive Pressure Reading');
    hold off

% Compare corrected pressures (crank angle based)
    figure(13)
```

```
        plot(((data(:,1)-enc_time1-(period*((2*pi-x_avg)/(2*pi)))))/....
            period)*2*pi,piezoel);
        hold on
        plot(((data(:,3)-enc_time1-(period*((2*pi-x_avg)/(2*pi)))))/....
            period)*2*pi,piezores1,'g',((data(:,3)-enc_time1-(period....
            *((2*pi-x_avg)/(2*pi)))))/period)*2*pi,piezores2,'m');
        %AXIS([0.3 0.6 -0.2e6 2.2e6]);
        xlabel('Crank Angle (Radians)');
        ylabel('Pressure (Pa)');
        if k == 2
        Title('Cylinder pressures - motored, closed throttle (1419.1 rpm....
            )');
    end
    if k == 3
        Title('Cylinder pressures - fired, no loaded, closed throttle ....
            (2868.1 rpm)');
    end
    if k == 4
        Title('Cylinder pressures- fired, loaded, closed throttle ....
            (1373.6 rpm)');
    end
    if k == 5
        Title('Cylinder pressures - fired, loaded, open throttle (2673.8....
             rpm)');
    end
        Legend('Piezoelectric Pressure Reading','Piezoresistive Pressure....
             Reading', 'Smoothed Piezoresistive Pressure Reading');
        hold off
        %.... ==================================================================....

    % Save calculated engine data

    eval(['save pz_en_',int2str(k),';']);

    clear
end
```

Listing C.9: Engine_2.m

```
% engine_2.m
%
% Script for comparing the theoretical and measured cylinder pressures

% This script is run in conjunction with the scripts
% for the thermodynamic engine simulation developed by
% Dr. David Buttsworth

%!!!!!!!!!!!!!!!!! IMPORTANT !!!!!!!!!!!!!!!!!!!!!!!
% The following variables were changed in the script
% 'enginedata.m' to match the specifications of the
% engine used -
% b = 0.069;  engine bore (m)
% stroke = 0.054;   engine stroke (m)
% eps = 0.287693;  half stroke to rod ratio, s/2l
% r = 6.1;  compression ratio

% CHANGE FILE 'enginedata.m' TO MATCH ENGINE TEST NUMBER
% Engine Test        Calculated Engine Speeds    Conditions
% pz_en_2                1419.1 rpm                thetas=179.9*pi/180,    ....
    thetab=0.1*pi/180        p1 = 5.5e4
% pz_en_3                2868.1 rpm                thetas=0*pi/180,        ....
    thetab=70*pi/180         p1 = 4e4
% pz_en_4                1373.6 rpm                thetas=-10*pi/180,      ....
    thetab=55*pi/180         p1 = 8e4
% pz_en_5                2673.8 rpm                thetas=-10*pi/180,      ....
    thetab=45*pi/180         p1 = 8.5e4
%!!!!!!!!!!!!!!!!! IMPORTANT !!!!!!!!!!!!!!!!!!!!!!!

% Experimental Description
% pz_en_2 - motored, closed throttle
% pz_en_3 - fired, closed throttle, no load
% pz_en_3 - fired, closed throttle, loaded
% pz_en_4 - fired, open throttle, loaded

%======================================================================
% Run Ahrind.m
% This script (developed by Dr. David Buttsworth) runs the
% thermodynamic engine simulation
Ahrind
% Load results from engine simulation
load ahrind.mat;

% CHANGE 'data_set' NUMBER TO MATCH ENGINE TEST NUMBER (2 to 5)
data_set = 3;

% Load Experimental Engine Data
cd('..')
eval(['load pz_en_',int2str(data_set),';'])
cd Engine

%======================================================================
% Plot cylinder pressures
figure(1);
plot(thetacomp,pTuWQlHl(:,1)/1e6); hold on;
plot(thetacomb,pTbTuWQlHl(:,1)/1e6);
plot(thetaexp,pTbWQlHl(:,1)/1e6);
xlabel('crank angle (degrees ATC)')
ylabel('pressure (MPa)')
hold off

%======================================================================
% Determine cylinder pressures with respect to time
thetacomp_new = ((thetacomp+pi)/(2*pi))*period;
thetacomb_new = ((thetacomb+pi)/(2*pi))*period;
thetaexp_new = ((thetaexp+pi)/(2*pi))*period;

% the value of 'cycle' will be 1 or 3, according to
% if the theoretical data is 180 deg out of phase
```

```
cycle = 3;
%cycle = 1;

% Plot experimental and theoretical data (time scale)
figure(7)
plot(data(:,3)-enc_time1-(period*((2*pi-x_avg)/(2*pi))),piezores1,'g',....
    data(:,3)-enc_time1-(period*((2*pi-x_avg)/(2*pi))),piezores2,'m',....
    data(:,1)-enc_time1-(period*((2*pi-x_avg)/(2*pi))),piezoel,'k');
hold on;
plot(thetacomp_new+cycle*(period/2),pTuWQlHl(:,1));
plot(thetacomb_new+cycle*(period/2),pTbTuWQlHl(:,1));
plot(thetaexp_new+cycle*(period/2),pTbWQlHl(:,1));
xlabel('Time (s)');
ylabel('Pressure (Pa)');
if data_set == 2
     Title('Experimental vs. Theoretical results - motored, closed ....
         throttle (1419.1 rpm)');
end
if data_set == 3
     Title('Experimental vs. Theoretical results - fired, no load, closed....
          throttle (2868.1 rpm)');
end
if data_set == 4
     Title('Experimental vs. Theoretical results - fired, loaded, closed ....
         throttle (1373.6 rpm)');
end
if data_set == 5
     Title('Experimental vs. Theoretical results - fired, loaded, open ....
         throttle (2673.8 rpm)');
end
Legend('Piezoresistive Pressure Reading', 'Smoothed Piezoresistive ....
    Pressure Reading','Piezoelectric Pressure Reading','Theoretical ....
    Pressure');
hold off

% Plot experimental and theoretical data (crank angle scale)
figure(8)
plot((data(:,3)-enc_time1-(period*((2*pi-x_avg)/(2*pi))))/period....
    *360-(180+180*cycle),piezores1,'g',(data(:,3)-enc_time1-(period*((2*....
    pi-x_avg)/(2*pi))))/period*360-(180+180*cycle),piezores2,'m',(data....
    (:,1)-enc_time1-(period*((2*pi-x_avg)/(2*pi))))/period*360-(180+180*....
    cycle),piezoel,'k');
hold on;
plot((thetacomp_new+cycle*(period/2))/period*360-(180+180*cycle),....
    pTuWQlHl(:,1));
plot((thetacomb_new+cycle*(period/2))/period*360-(180+180*cycle),....
    pTbTuWQlHl(:,1));
plot((thetaexp_new+cycle*(period/2))/period*360-(180+180*cycle),pTbWQlHl....
    (:,1));
%plot((data(:,3)-enc_time1-(period*((2*pi-x_avg)/(2*pi))))/period....
    *360-360,data(:,8)*1e6);
xlabel('Crank Angle (deg)');
ylabel('Pressure (Pa)');
if data_set == 2
     Title('Experimental vs. Theoretical results - motored, closed ....
         throttle (1419.1 rpm)');
    AXIS([-180 180 -0.2e6 1e6]);
end
if data_set == 3
     Title('Experimental vs. Theoretical results - fired, no load, closed....
          throttle (2868.1 rpm)');
    AXIS([-180 180 -0.2e6 1e6]);
end
if data_set == 4
     Title('Experimental vs. Theoretical results - fired, loaded, closed ....
         throttle (1373.6 rpm)');
    AXIS([-180 180 -0.2e6 2.5e6]);
end
if data_set == 5
```

```
    Title('Experimental vs. Theoretical results - fired, loaded, open ....
        throttle (2673.8 rpm)');
    AXIS([-180 180 -0.5e6 4e6]);
end
Legend('Piezoresistive Pressure Reading', 'Smoothed Piezoresistive ....
    Pressure Reading','Piezoelectric Pressure Reading','Theoretical ....
    Pressure');
hold off

%==========================================================================
% Determine the output power of the motor

pump = 3.8e-6; %m^3/rev

if data_set == 4
    dp = 1100; % psi
    dp = dp*6894.8;
    flow_rate = 1373.6/60*pump;
    Power = flow_rate*dp;
end
if data_set == 5
    dp = 1700; %psi
    dp = dp*6894.8; %pa
    flow_rate = 2673.8/60*pump;
    Power = flow_rate*dp;
end

clear
```

Appendix D

Detail and Assembly Drawings

Appendix D Contents

D.1 Detail Drawings for SX150AHO Pressure Attachment

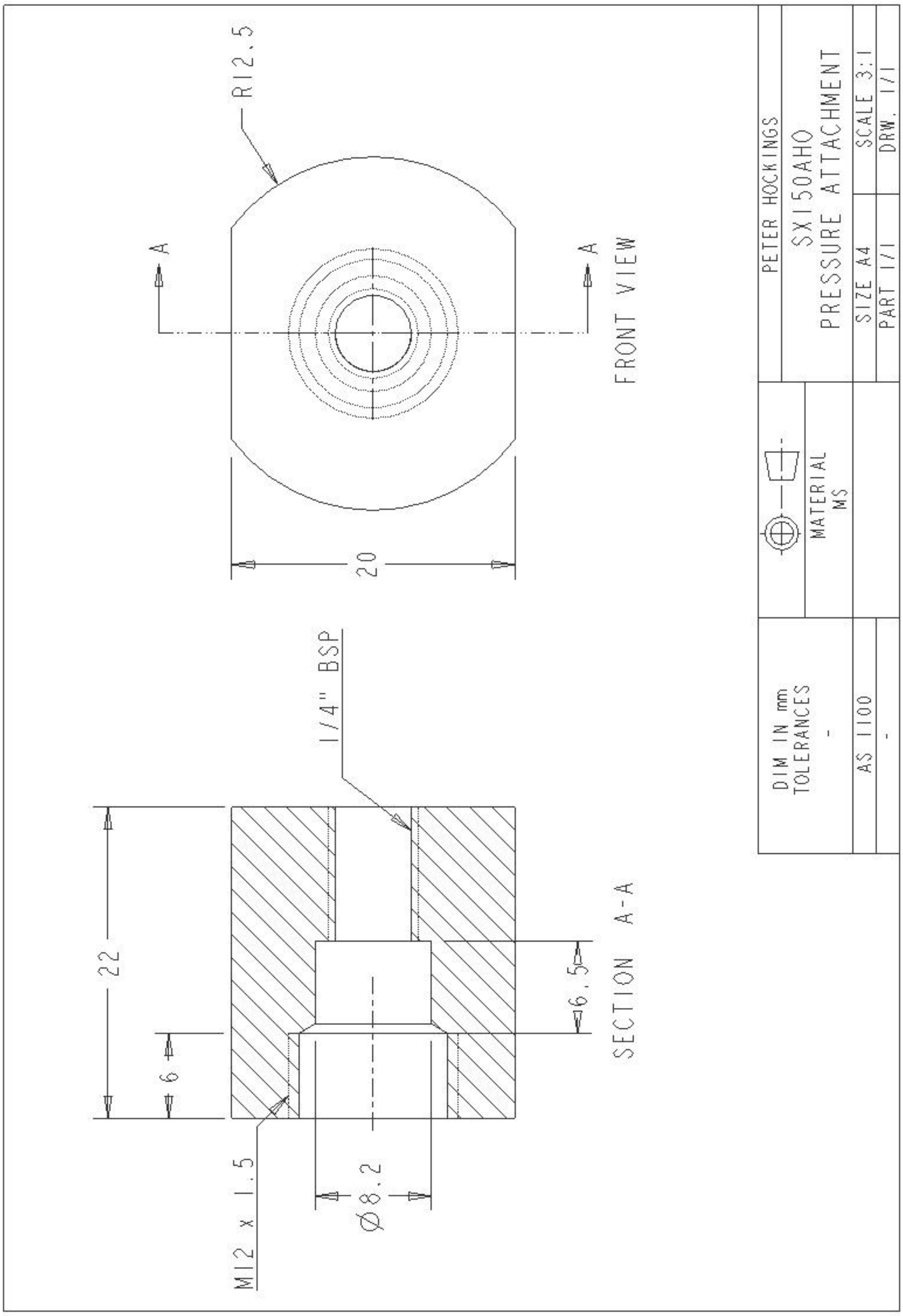

D.2 Detail Drawings for Oven Insulating Tube

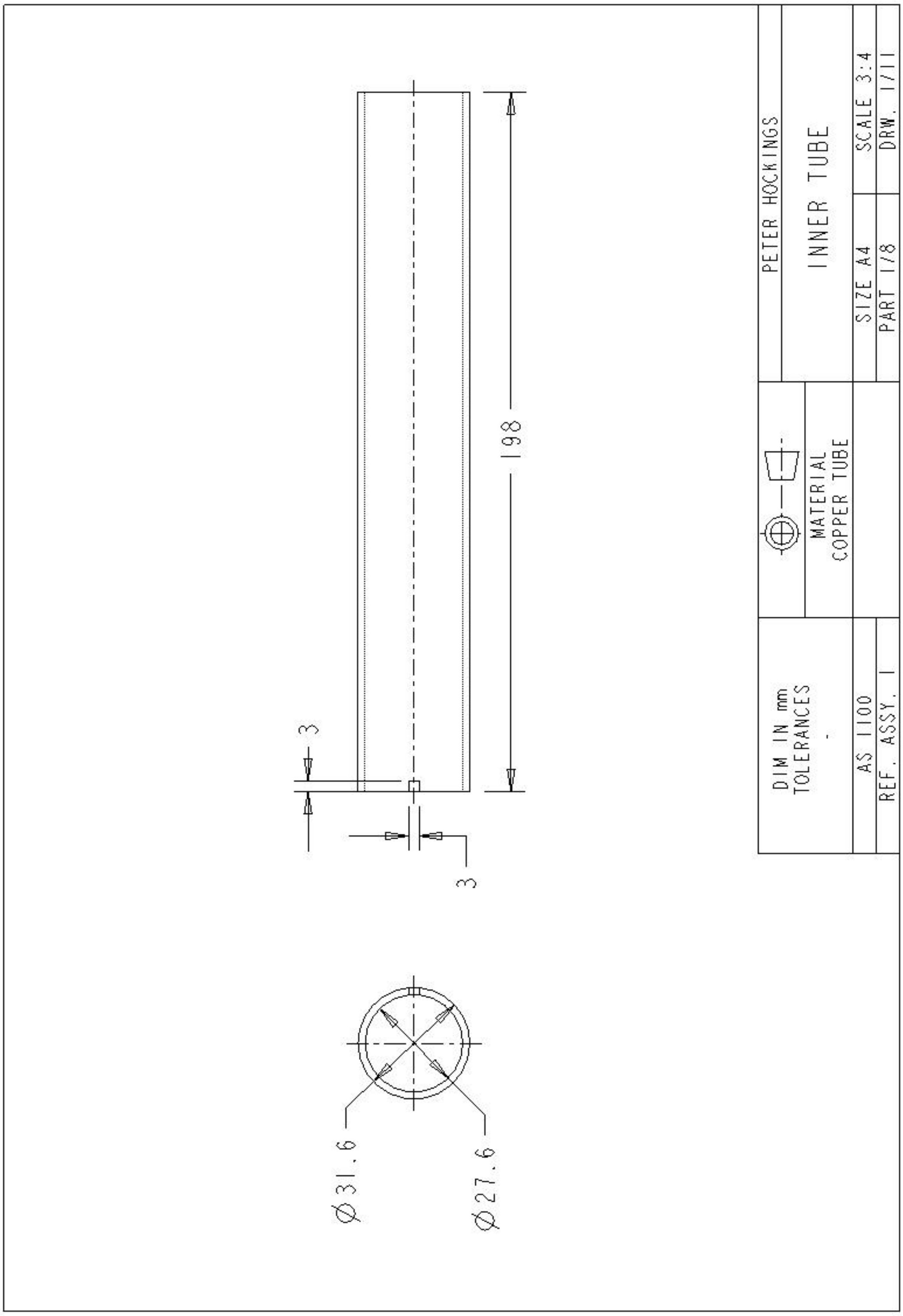

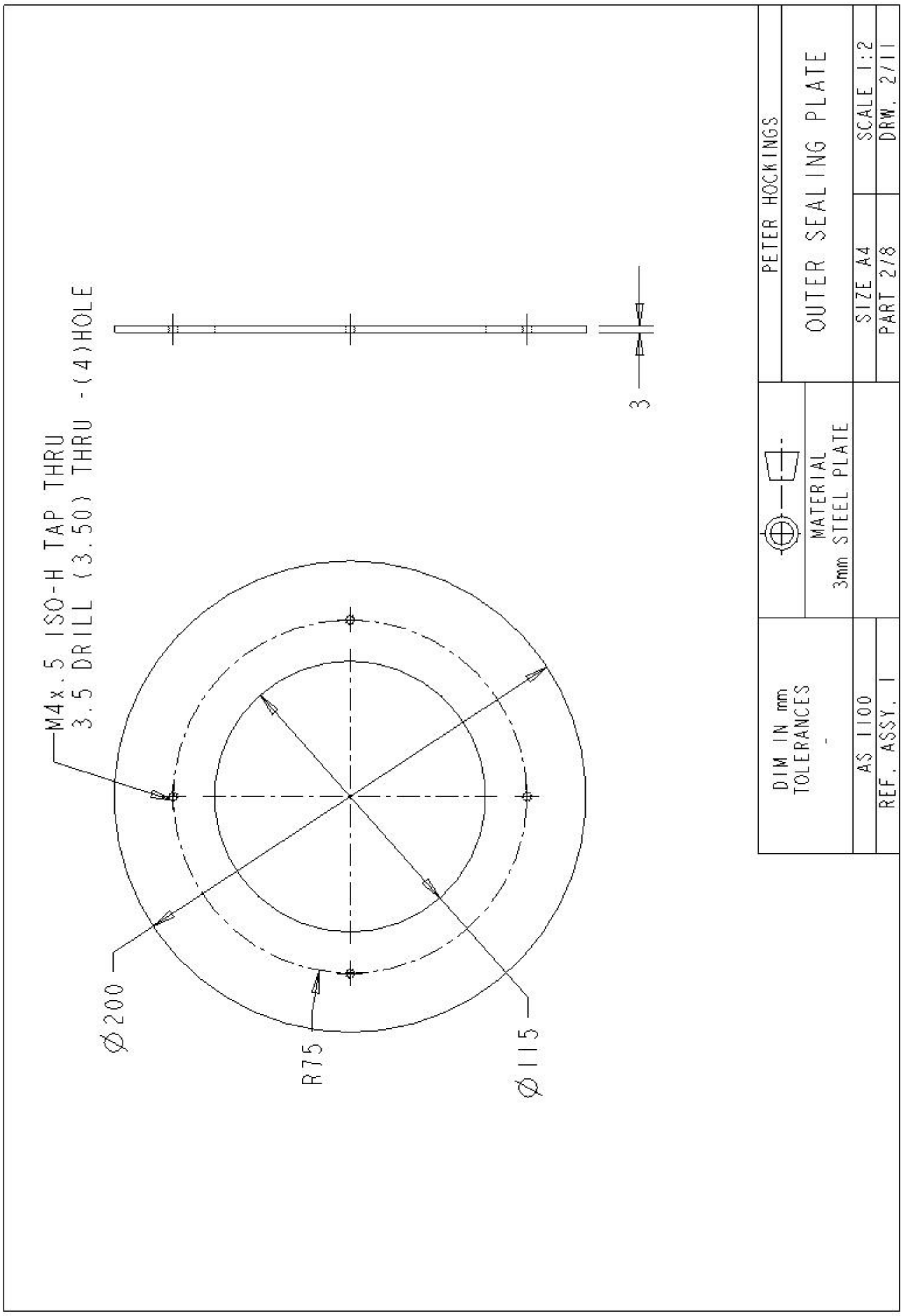
M4x.5 ISO-H TAP THRU
3.5 DRILL (3.50) THRU -(4)HOLE
3
Ø200
R75
Ø115
PETER HOCKINGS
OUTER SEALING PLATE
SIZE A4
PART 2/8
SCALE 1:2
DRW. 2/11
MATERIAL
3mm STEEL PLATE
DIM IN mm
TOLERANCES
-
AS 1100
REF. ASSY. 1

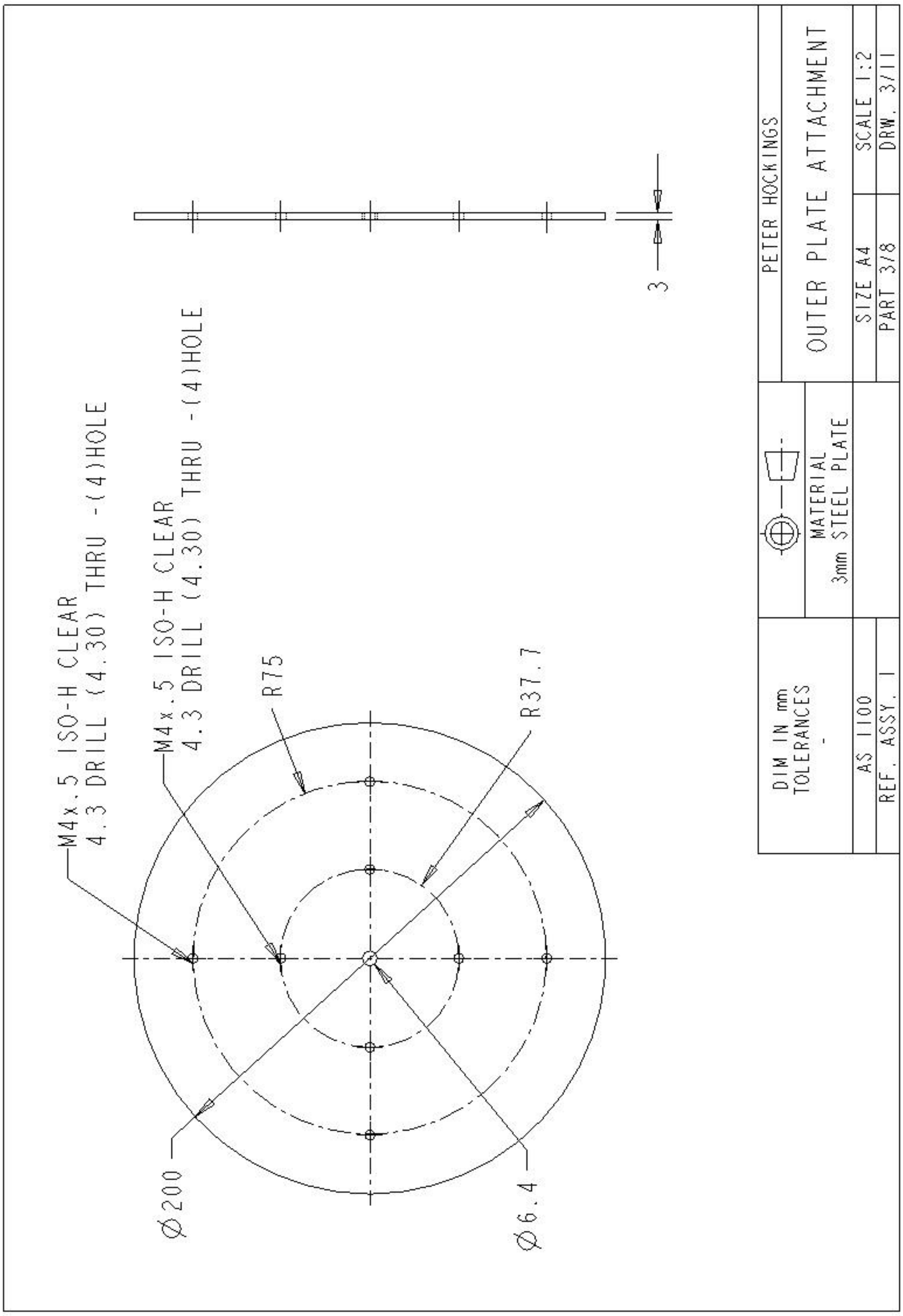
M4x.5 ISO-H CLEAR
4.3 DRILL (4.30) THRU -(4)HOLE
M4x.5 ISO-H CLEAR
4.3 DRILL (4.30) THRU -(4)HOLE
R75
R37.7
Ø200
Ø6.4
3
PETER HOCKINGS
OUTER PLATE ATTACHMENT
SIZE A4
PART 3/8
SCALE 1:2
DRW. 3/11
MATERIAL
3mm STEEL PLATE
DIM IN mm
TOLERANCES
-
AS 1100
REF. ASSY. 1

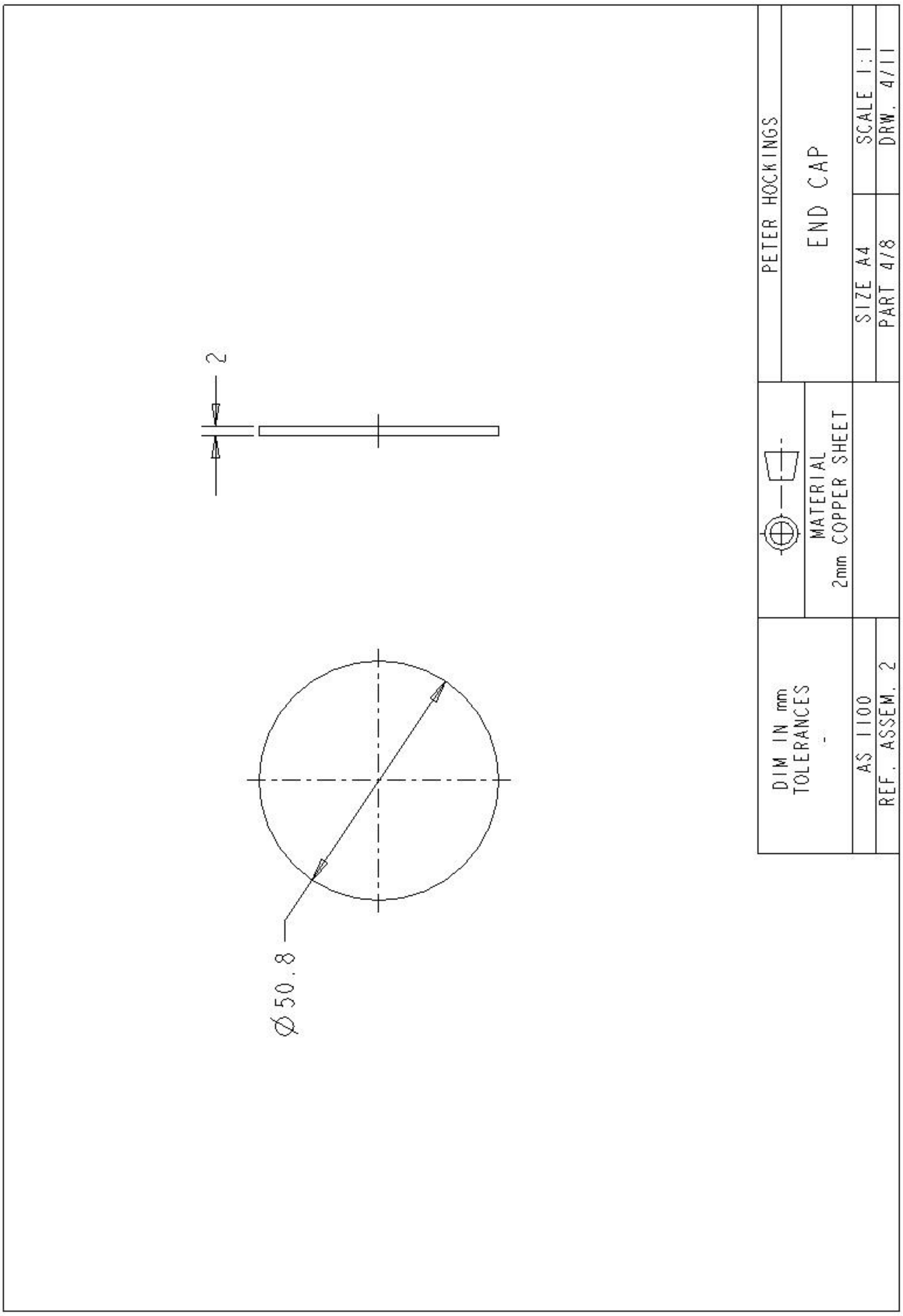

2
Ø50.8
PETER HOCKINGS
END CAP
SIZE A4
PART 4/8
SCALE 1:1
DRW. 4/11
MATERIAL
2mm COPPER SHEET
DIM IN mm
TOLERANCES
-
AS 1100
REF. ASSEM. 2

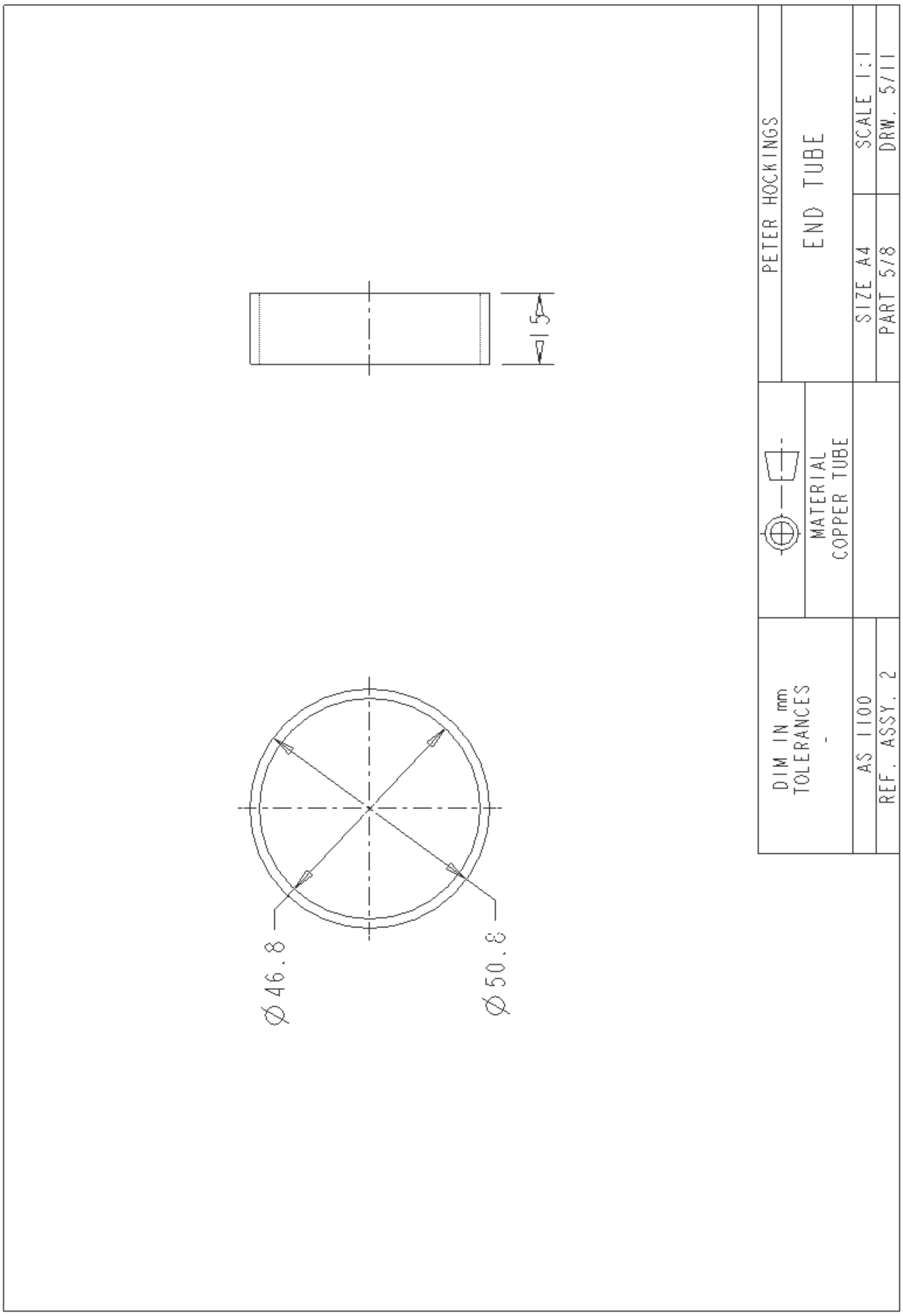
PETER HOCKINGS
END TUBE
SIZE A4
SCALE 1:1
PART 5/8
DRW. 5/11
MATERIAL
COPPER TUBE
DIM IN mm
TOLERANCES
-
AS 1100
REF. ASSY. 2
15
Ø46.8
Ø50.8

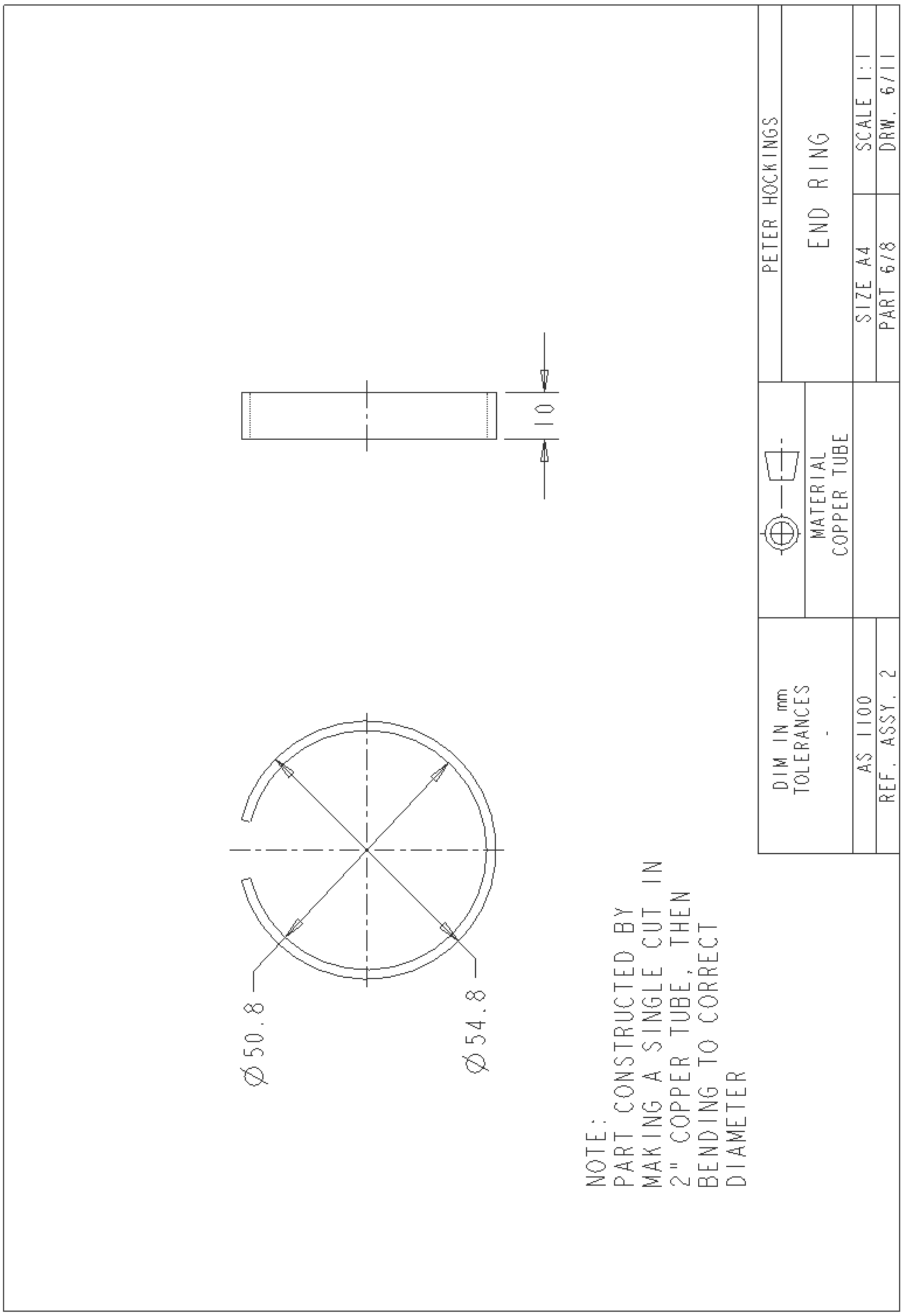
PETER HOCKINGS
END RING
SIZE A4
SCALE 1:1
PART 6/8
DRW. 6/11
MATERIAL
COPPER TUBE
DIM IN mm
TOLERANCES
-
AS 1100
REF. ASSY. 2
10
Ø50.8
Ø54.8
NOTE:
PART CONSTRUCTED BY
MAKING A SINGLE CUT IN
2" COPPER TUBE, THEN
BENDING TO CORRECT
DIAMETER

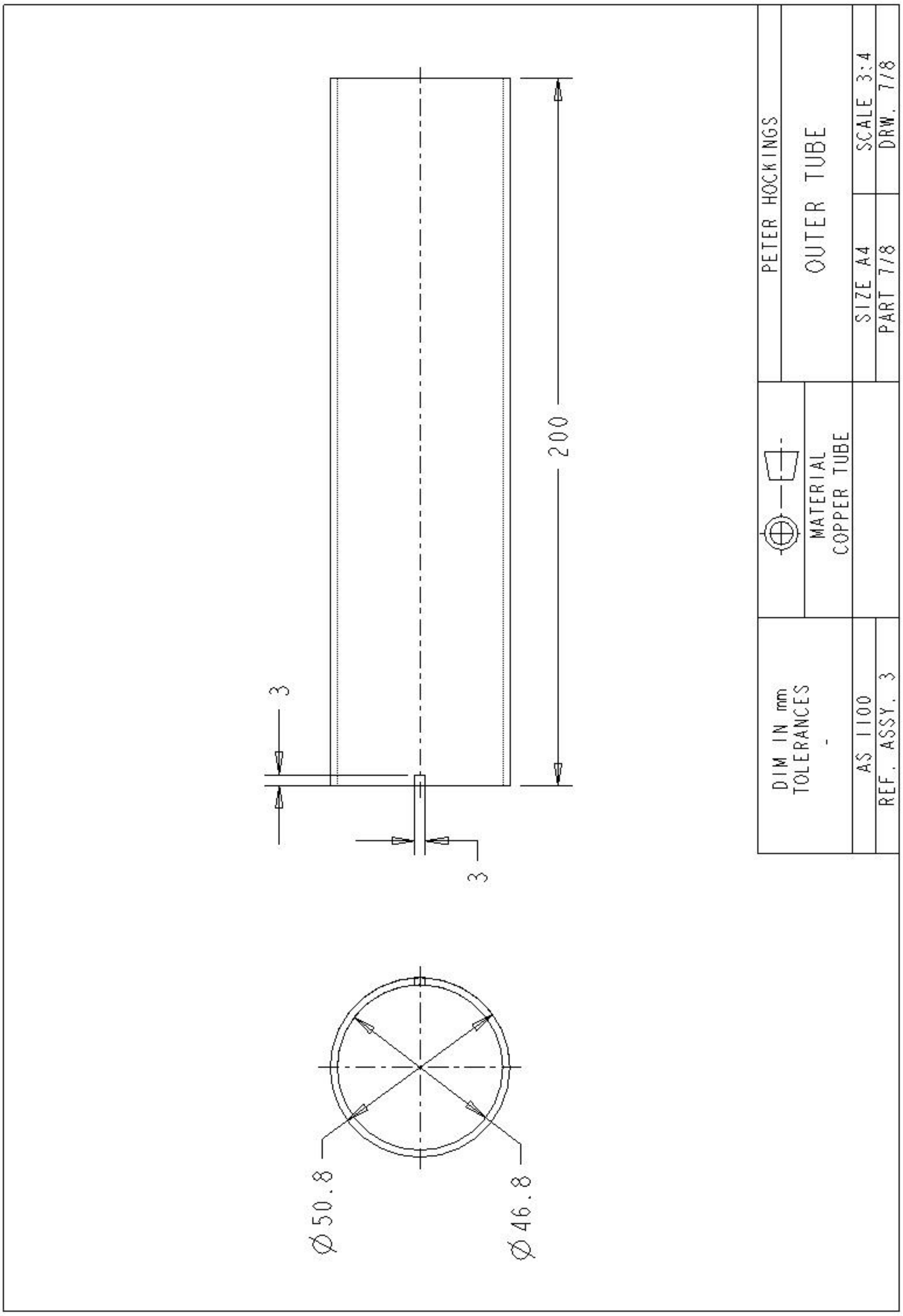
200
3
3
Ø50.8
Ø46.8
PETER HOCKINGS
OUTER TUBE
SIZE A4
SCALE 3:4
PART 7/8
DRW. 7/8
MATERIAL
COPPER TUBE
DIM IN mm
TOLERANCES
-
AS 1100
REF. ASSY. 3

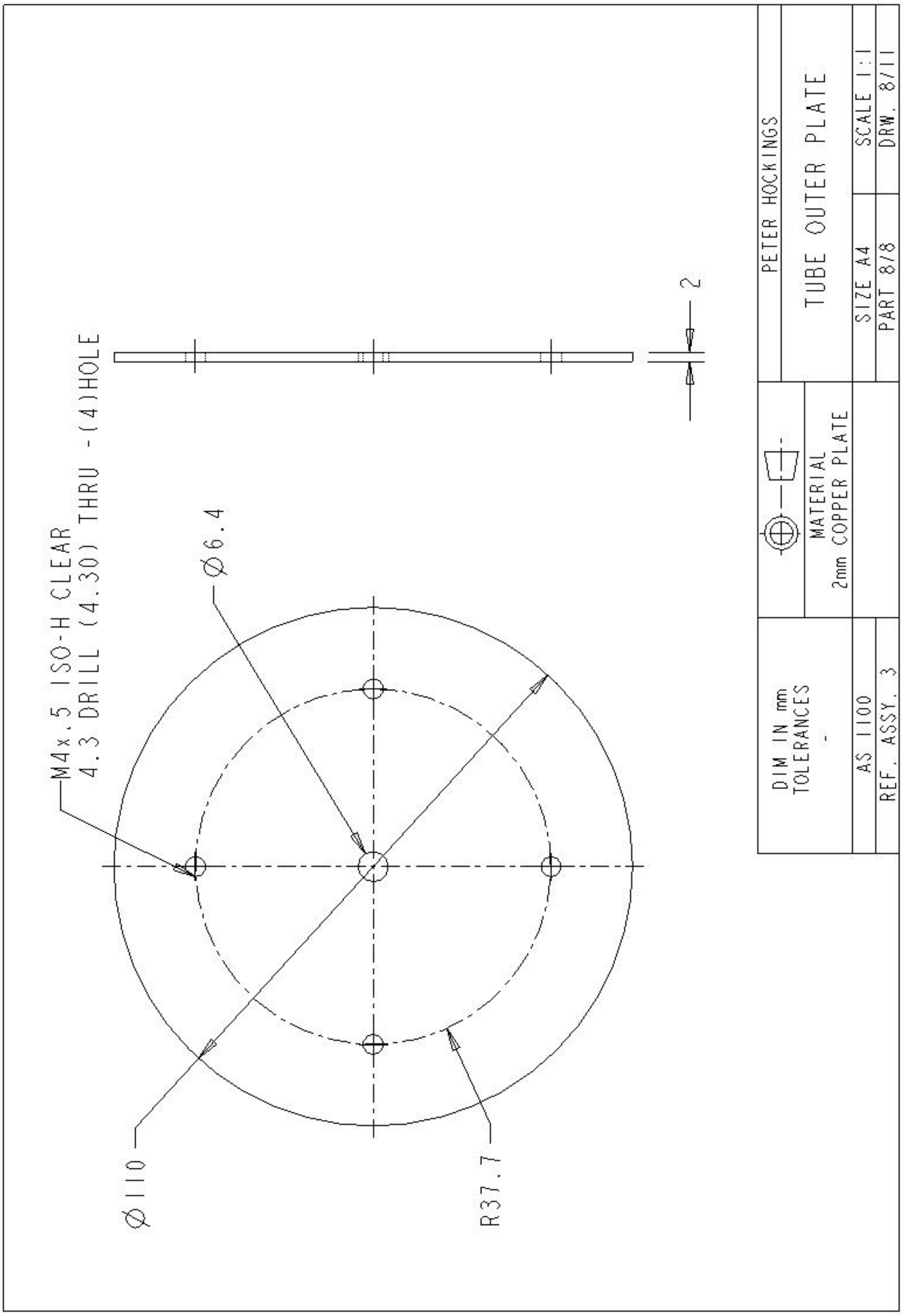
M4x.5 ISO-H CLEAR
4.3 DRILL (4.30) THRU -(4)HOLE
Ø6.4
Ø110
R37.7
2
PETER HOCKINGS
TUBE OUTER PLATE
SIZE A4
PART 8/8
SCALE 1:1
DRW. 8/11
MATERIAL
2mm COPPER PLATE
DIM IN mm
TOLERANCES
-
AS 1100
REF. ASSY. 3

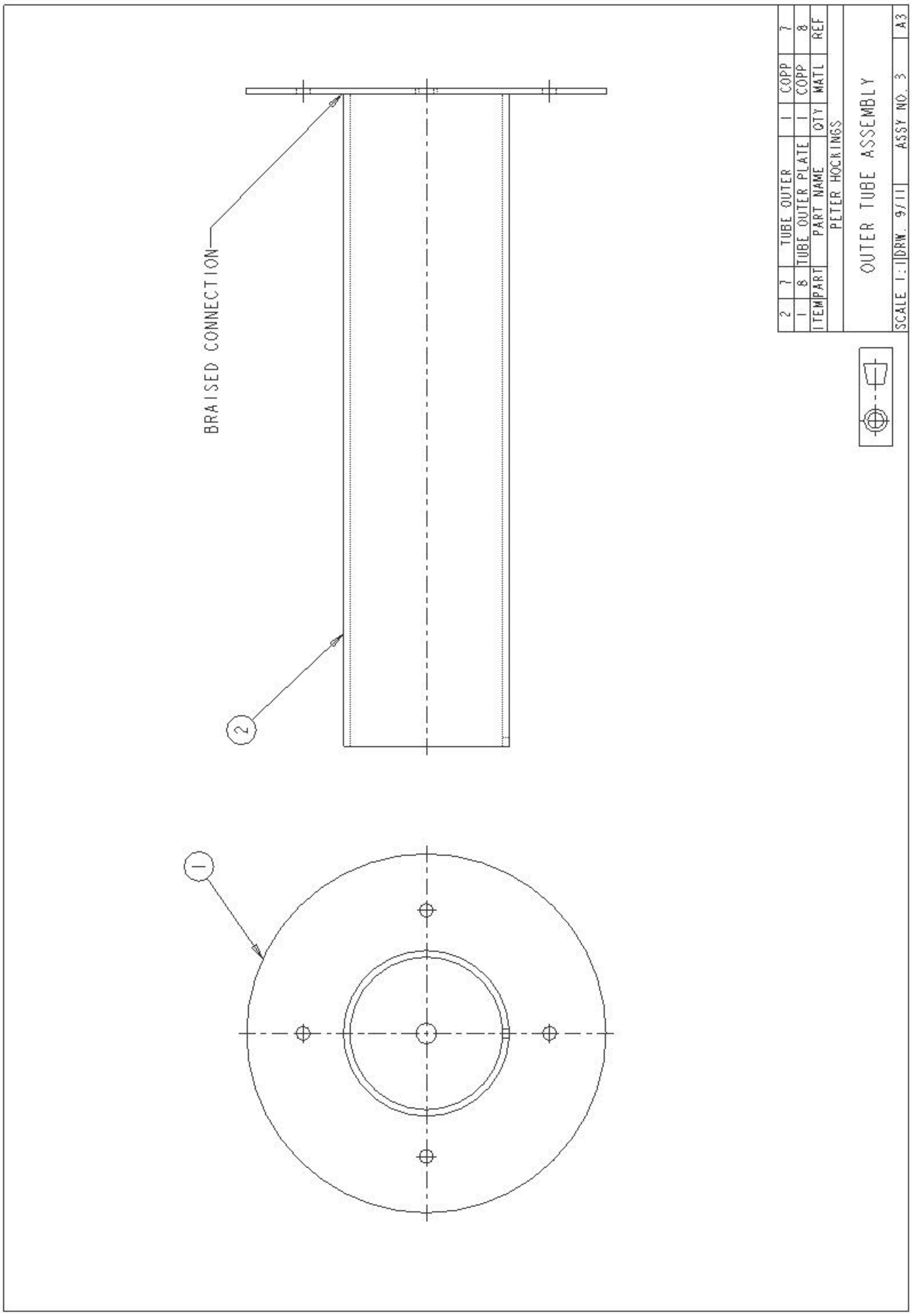
BRAISED CONNECTION
2
1
2 7 TUBE OUTER 1 COPP 7
1 8 TUBE OUTER PLATE 1 COPP 8
ITEM PART PART NAME QTY MATL REF
PETER HOCKINGS
OUTER TUBE ASSEMBLY
SCALE 1:1 DRW. 9/11 ASSY NO. 3 A3

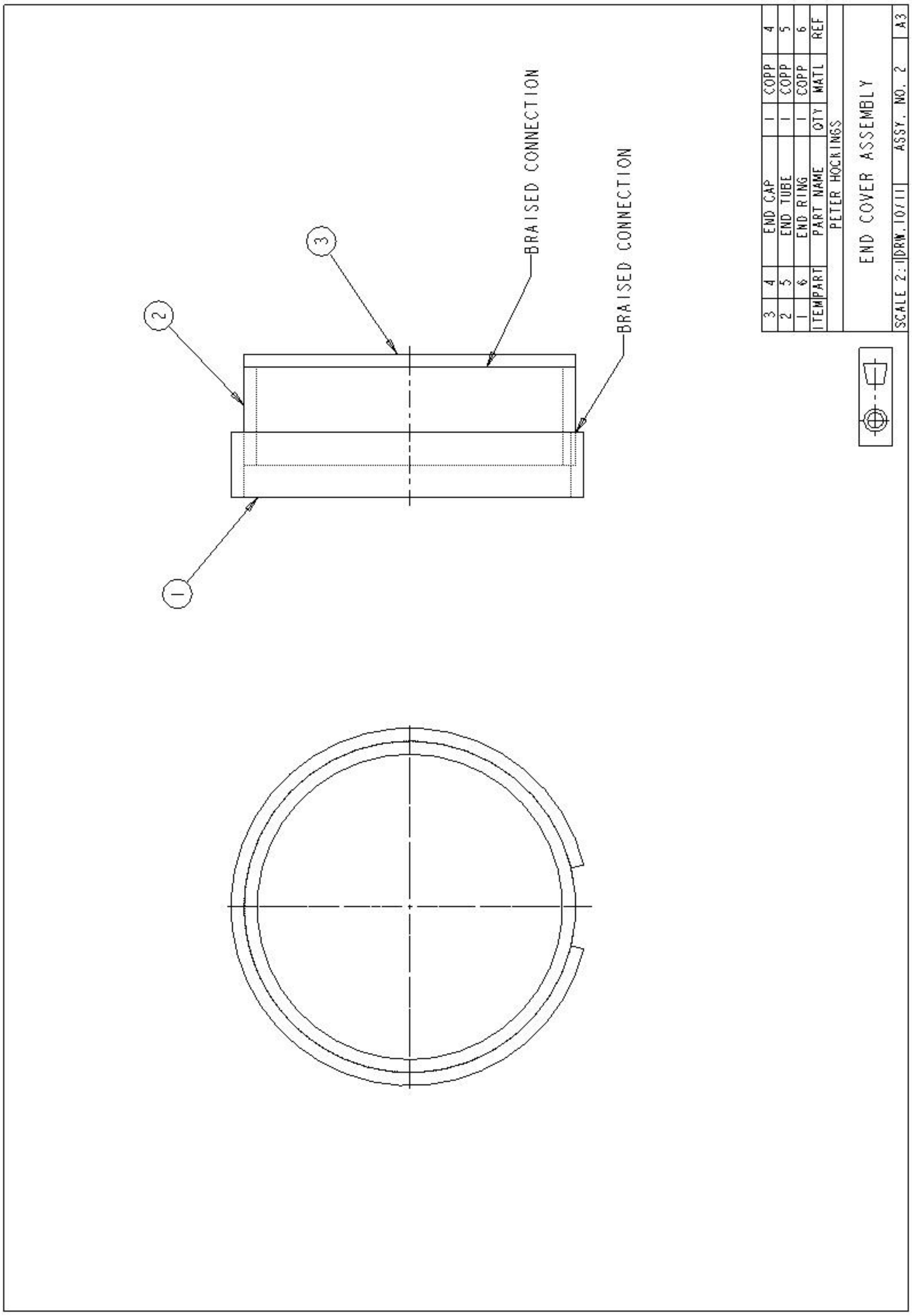
BRAISED CONNECTION
BRAISED CONNECTION
1
2
3
3 4 END CAP 1 COPP 4
2 5 END TUBE 1 COPP 5
1 6 END RING 1 COPP 6
ITEM PART PART NAME QTY MATL REF
PETER HOCKINGS
END COVER ASSEMBLY
SCALE 2:1 DRW. 10/11 ASSY. NO. 2 A3

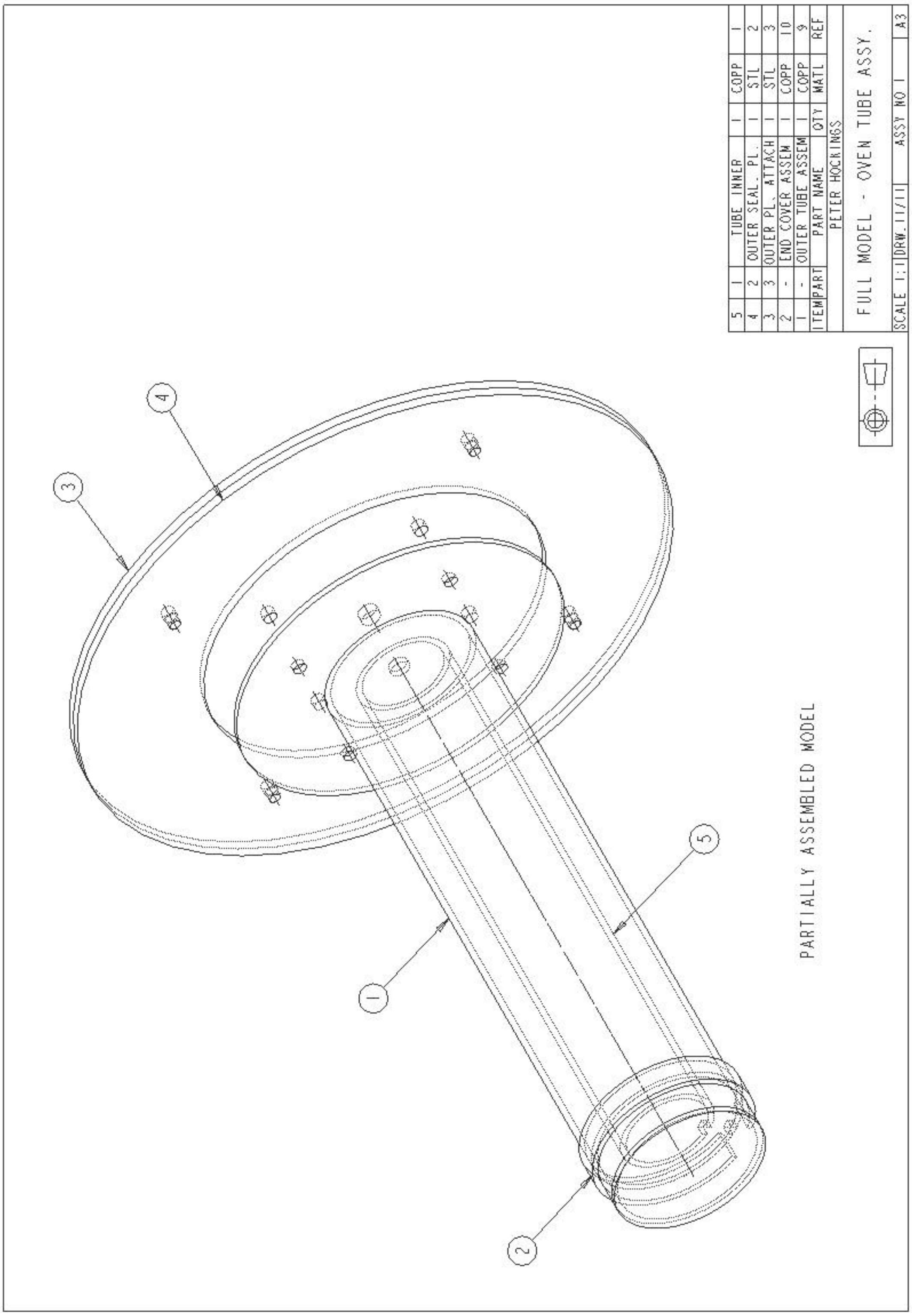

5 | 1 | TUBE INNER | 1 | COPP | 1
4 | 2 | OUTER SEAL. PL. | 1 | STL | 2
3 | 3 | OUTER PL. ATTACH | 1 | STL | 3
2 | - | END COVER ASSEM | 1 | COPP | 10
1 | - | OUTER TUBE ASSEM | 1 | COPP | 9
ITEM | PART | PART NAME | QTY | MATL | REF
PETER HOCKINGS
FULL MODEL - OVEN TUBE ASSY.
SCALE 1:1 | DRW. 11/11 | ASSY NO 1 | A3
PARTIALLY ASSEMBLED MODEL
1
2
3
4
5

D.3 Detail Drawings for Shock Tube Sensor Mountings

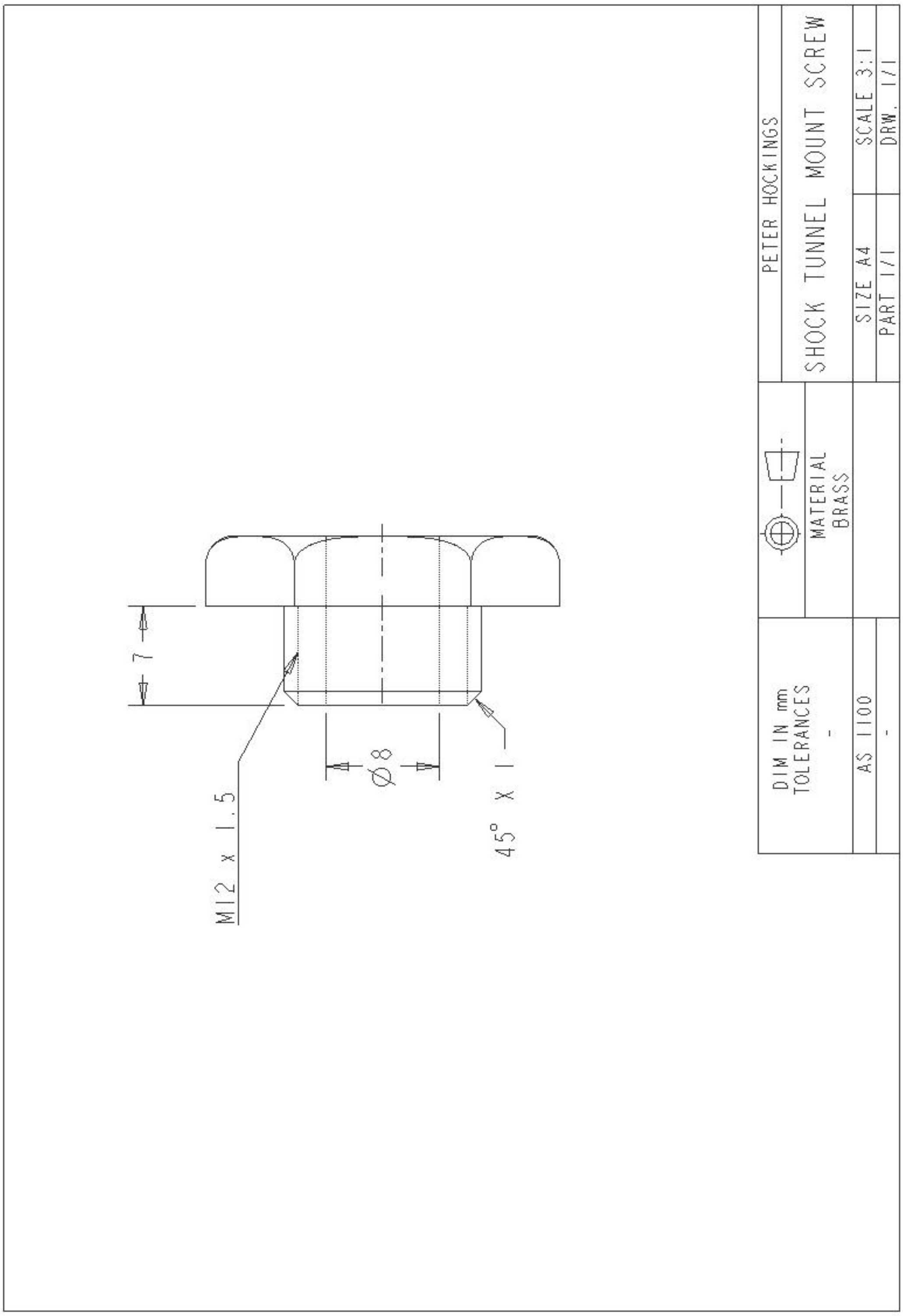

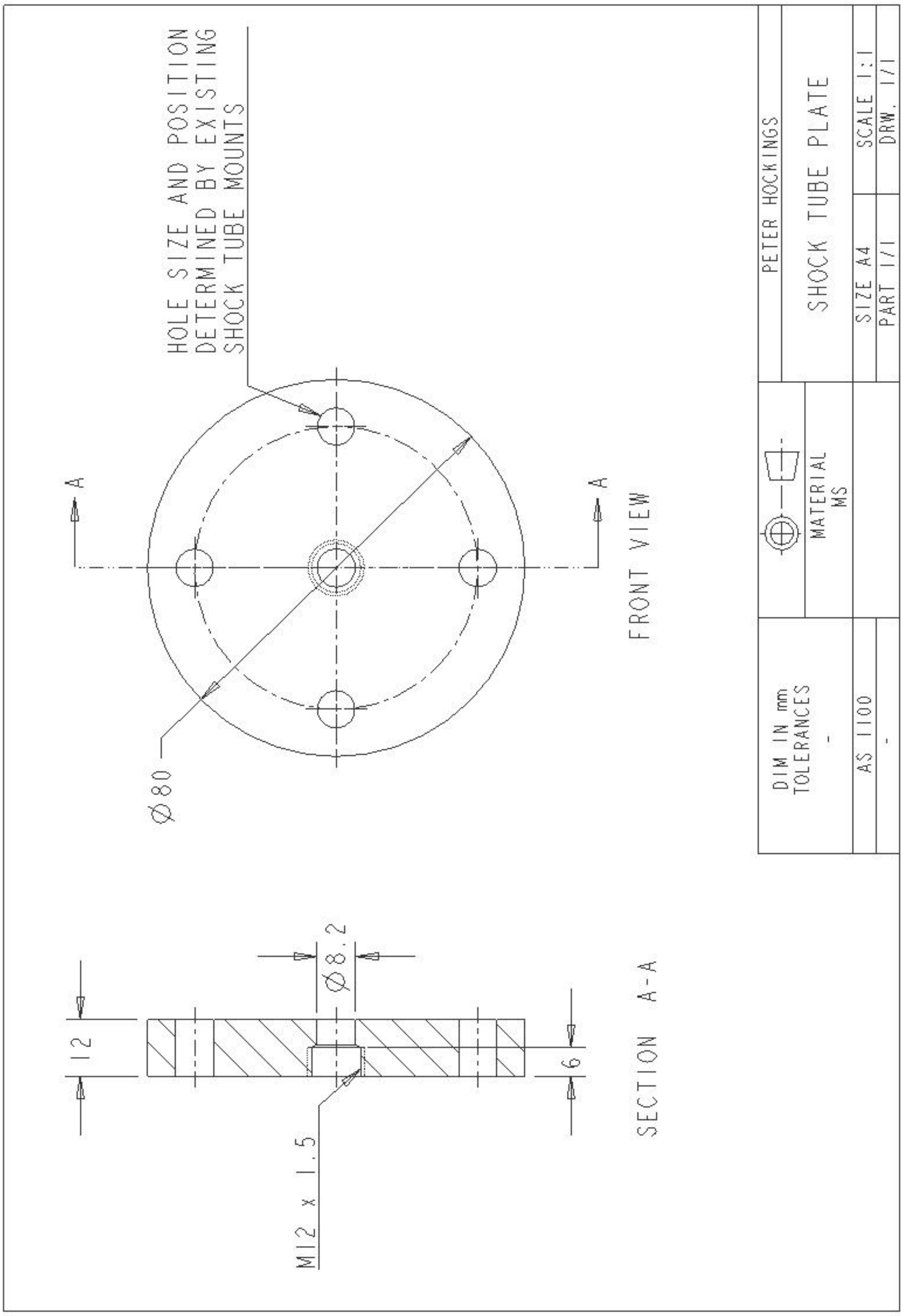
HOLE SIZE AND POSITION
DETERMINED BY EXISTING
SHOCK TUBE MOUNTS
A
A
Ø80
FRONT VIEW
12
Ø8.2
6
M12 x 1.5
SECTION A-A
PETER HOCKINGS
SHOCK TUBE PLATE
SIZE A4
SCALE 1:1
PART 1/1
DRW. 1/1
MATERIAL
MS
DIM IN mm
TOLERANCES
-
AS 1100
-

D.4 Detail Drawings for Gun Tunnel Sensor Mountings

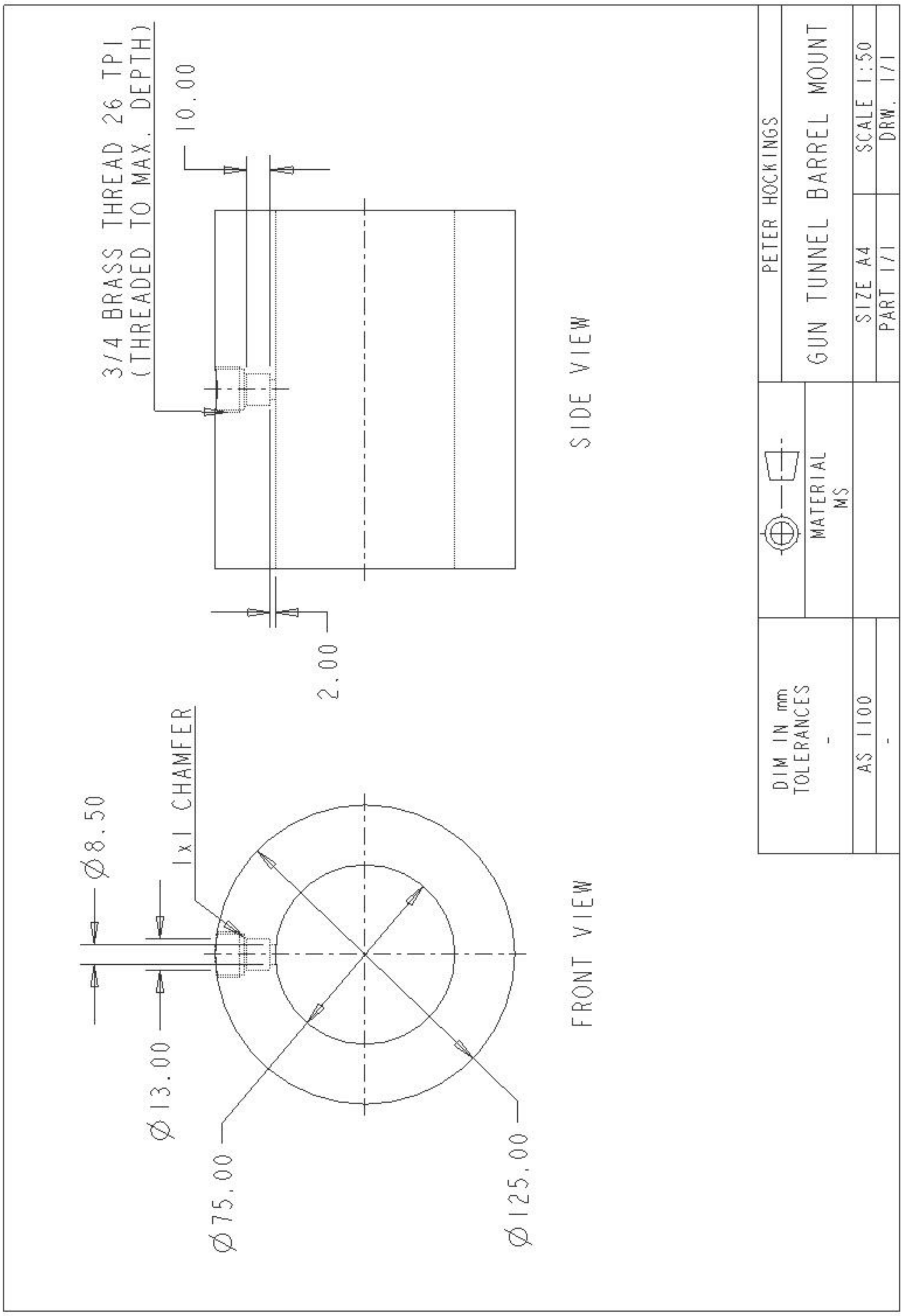

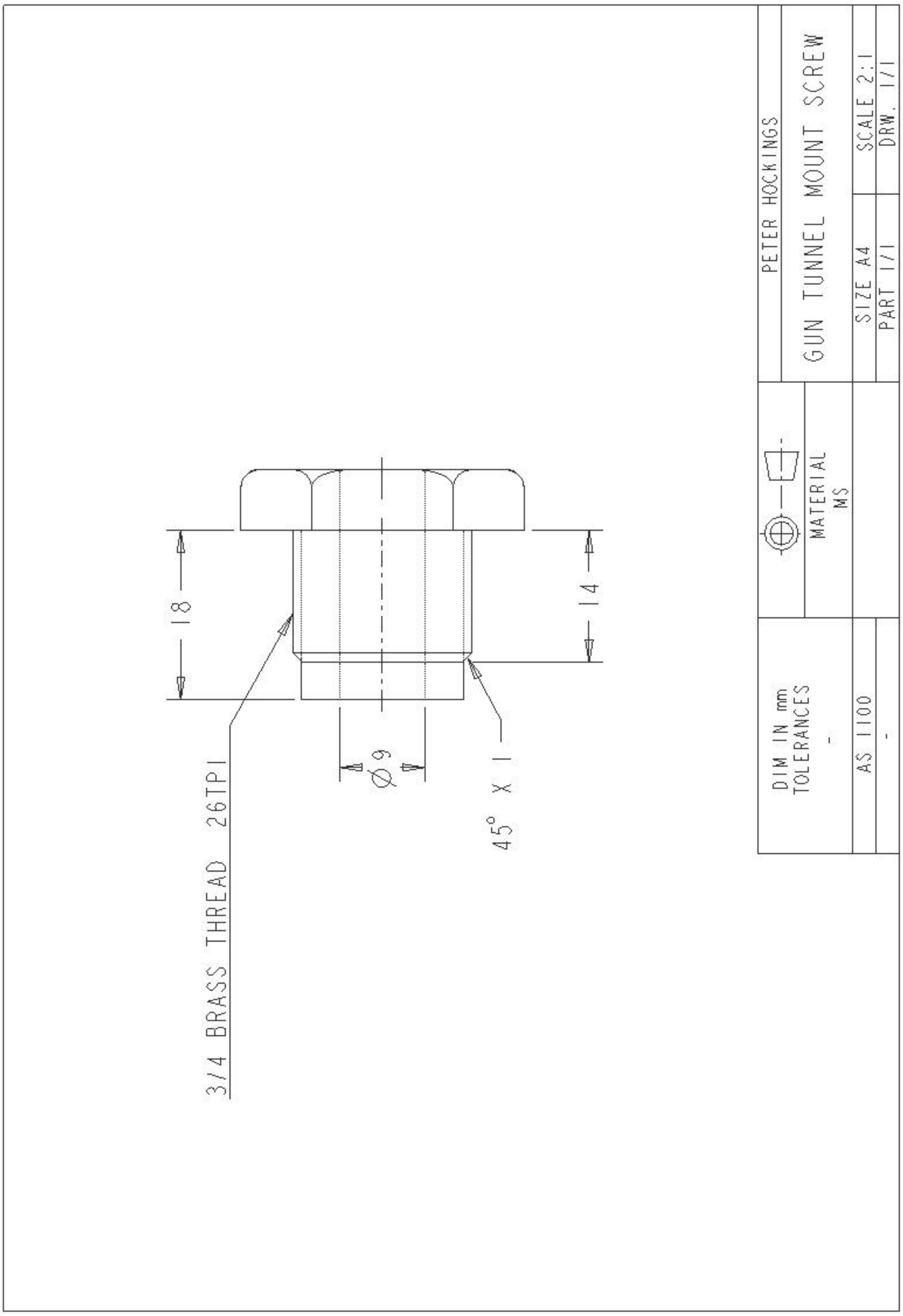
3/4 BRASS THREAD 26TPI
18
14
Ø9
45° X 1
PETER HOCKINGS
GUN TUNNEL MOUNT SCREW
SIZE A4
PART 1/1
SCALE 2:1
DRW. 1/1
MATERIAL
MS
DIM IN mm
TOLERANCES
-
AS 1100
-

D.5 Detail Drawings for Engine Shaft Encoder

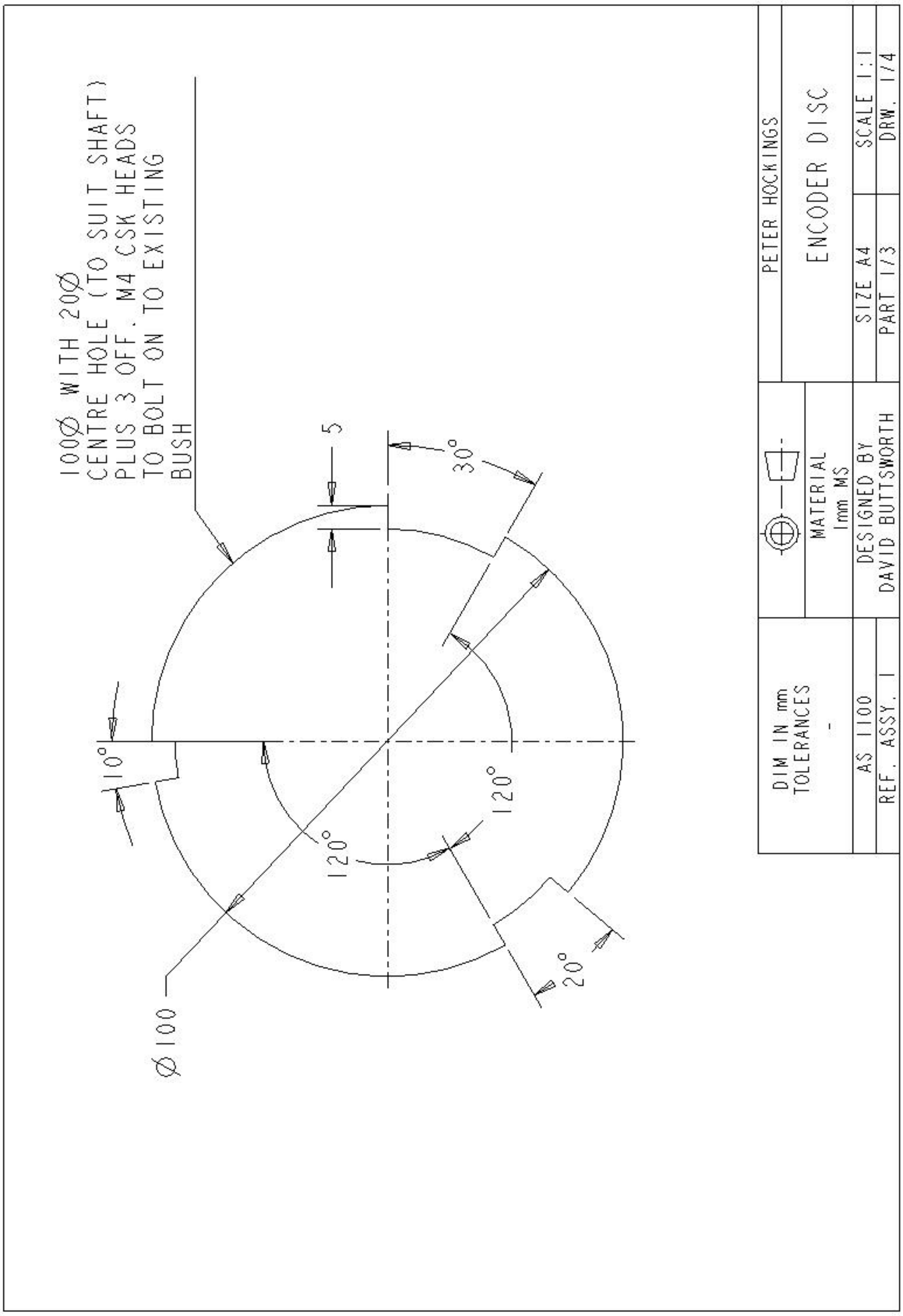

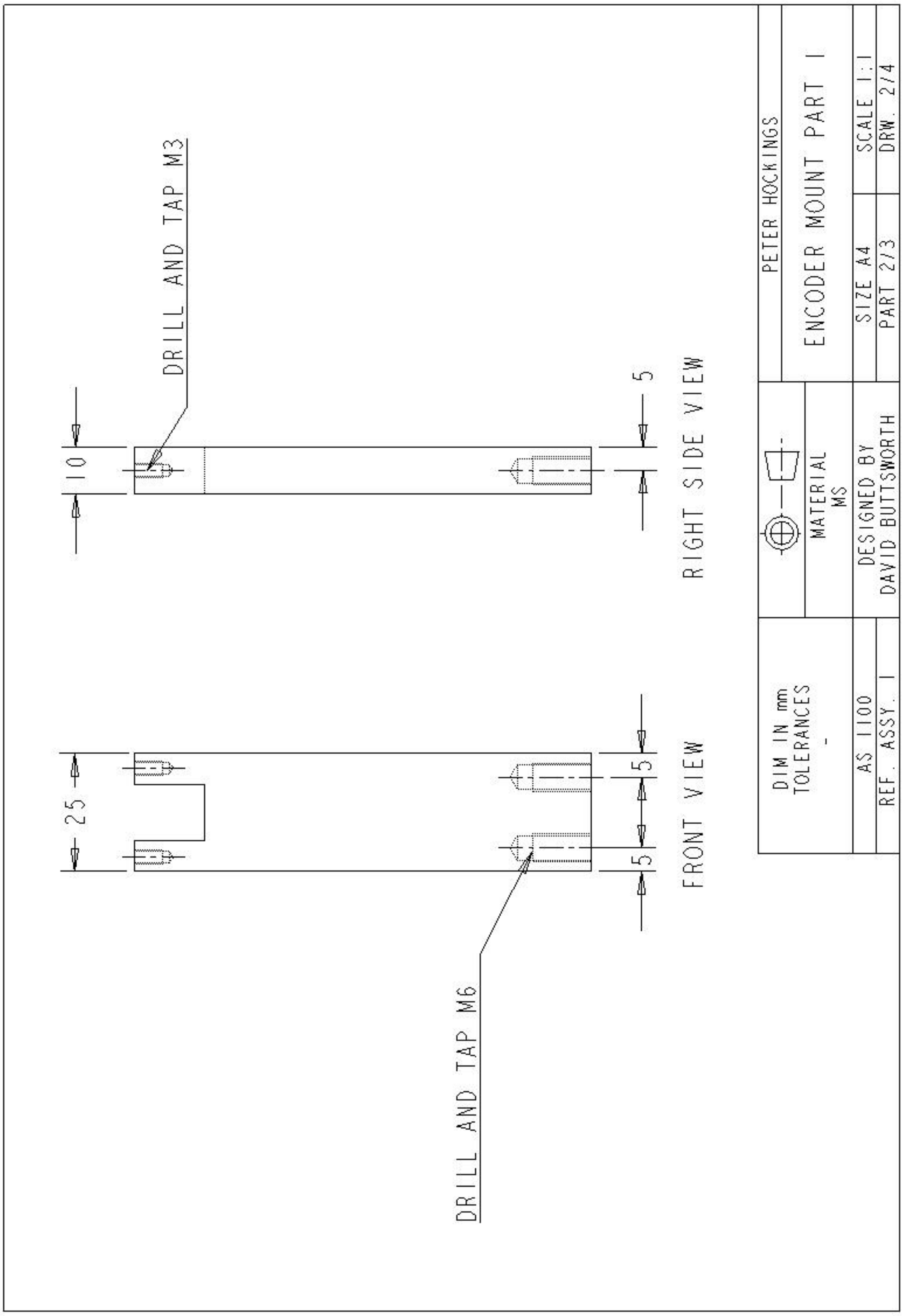
DRILL AND TAP M3
10
5
RIGHT SIDE VIEW
25
5
5
FRONT VIEW
DRILL AND TAP M6
PETER HOCKINGS
ENCODER MOUNT PART 1
SIZE A4
SCALE 1:1
PART 2/3
DRW. 2/4
MATERIAL
MS
DESIGNED BY
DAVID BUTTSWORTH
DIM IN mm
TOLERANCES
-
AS 1100
REF. ASSY. 1

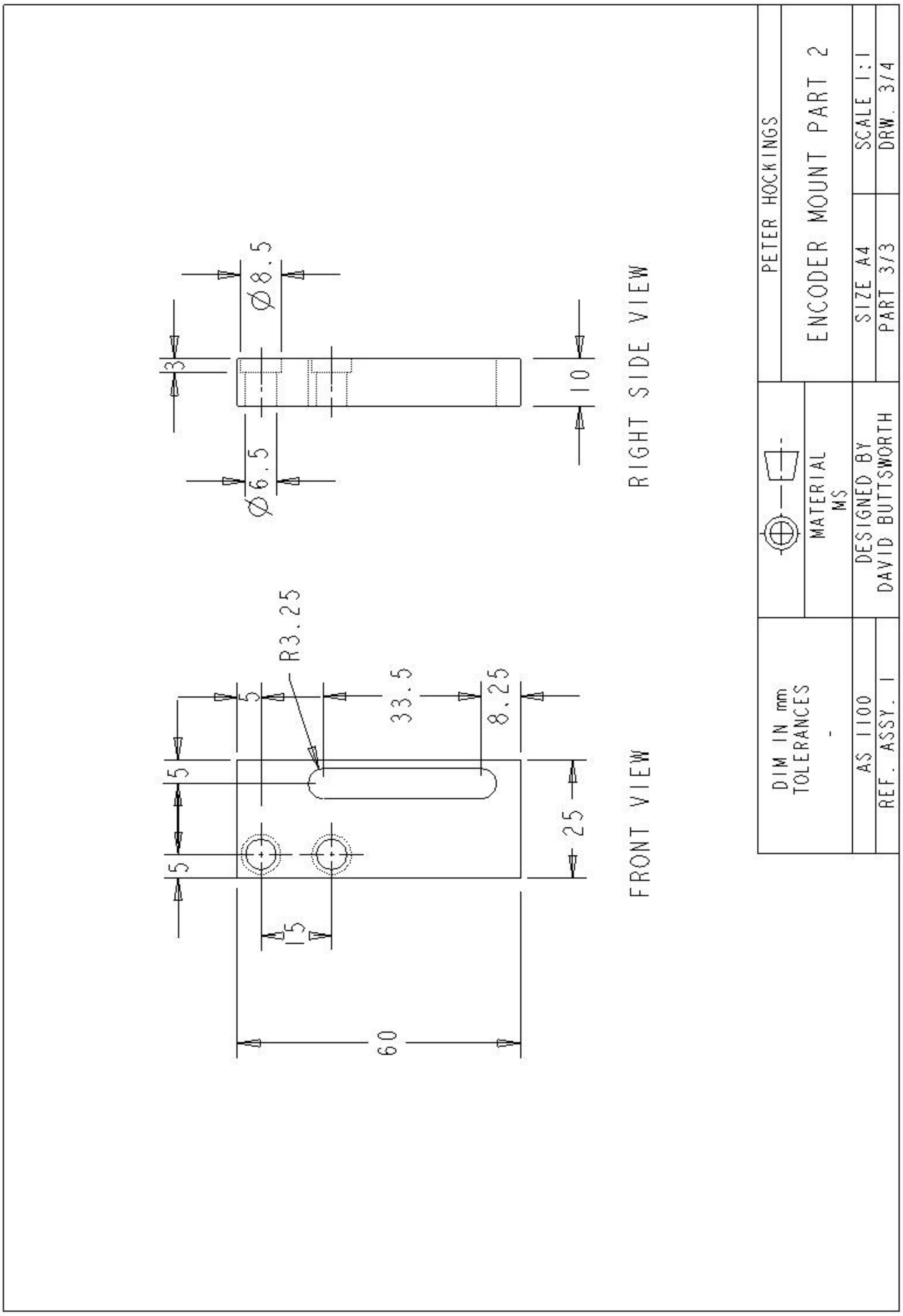
FRONT VIEW
RIGHT SIDE VIEW
R3.25
5
33.5
8.25
5
5
25
15
60
Ø8.5
Ø6.5
3
10
PETER HOCKINGS
ENCODER MOUNT PART 2
SIZE A4
PART 3/3
SCALE 1:1
DRW. 3/4
MATERIAL
MS
DESIGNED BY
DAVID BUTTSWORTH
DIM IN mm
TOLERANCES
-
AS 1100
REF. ASSY. 1

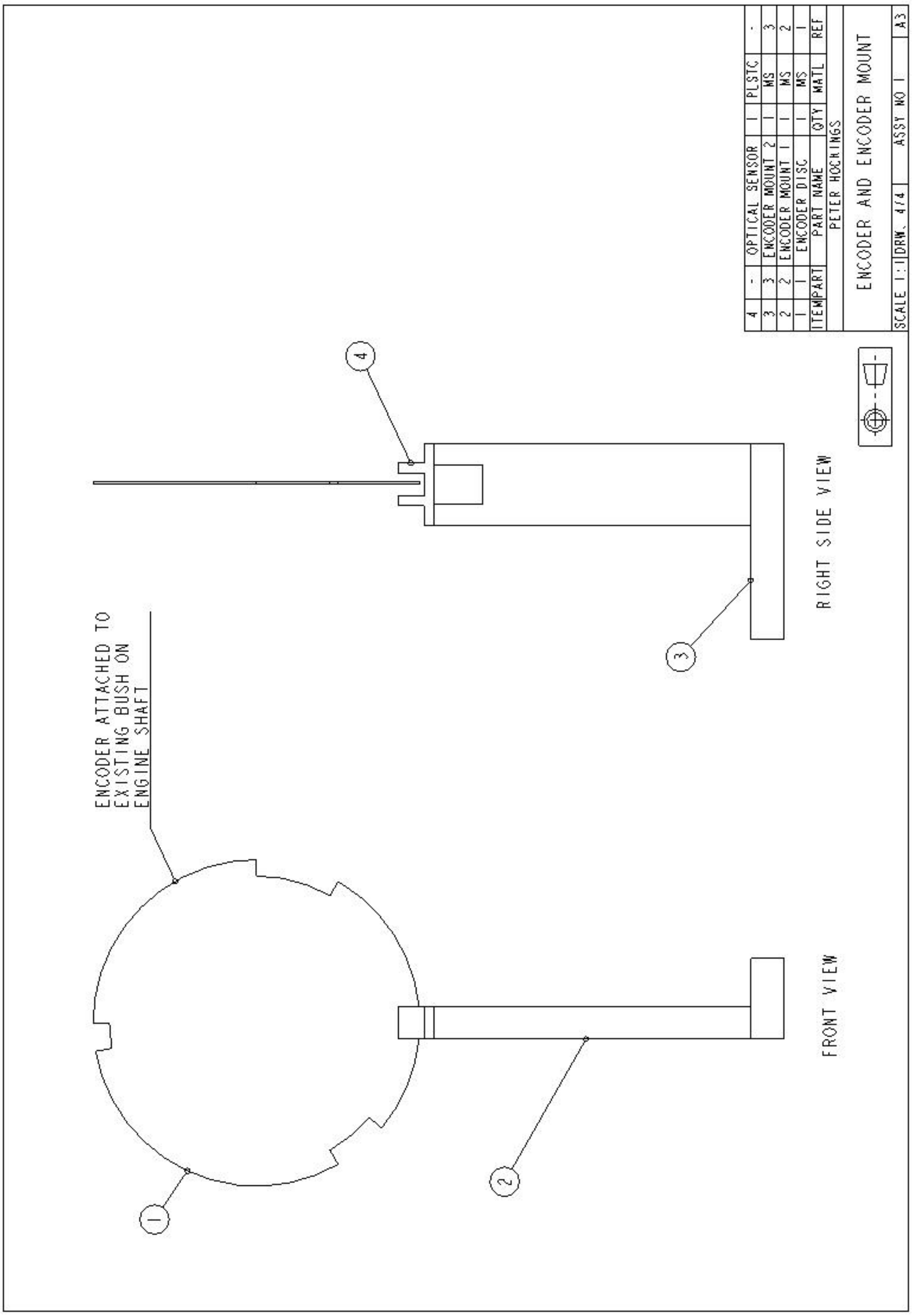
4 - OPTICAL SENSOR 1 PLSTC -
3 3 ENCODER MOUNT 2 1 MS 3
2 2 ENCODER MOUNT 1 1 MS 2
1 1 ENCODER DISC 1 MS 1
ITEM PART PART NAME QTY MATL REF
PETER HOCKINGS
ENCODER AND ENCODER MOUNT
SCALE 1:1 DRW. 4/4 ASSY NO 1 A3
ENCODER ATTACHED TO
EXISTING BUSH ON
ENGINE SHAFT
1
2
3
4
RIGHT SIDE VIEW
FRONT VIEW

Appendix E

Shock Tube Experimental Data

Appendix E Contents

E.1 Shock Tube Experimental Data

The following plots display the experimental results recorded from each shock tube test. 4 plots were generated for each shock tube test. These plots, in order of display, are as follows,

1. The short time scale response to compare measured and theoretical reflected shock pressures.
2. The short time scale response for determining the rise-time.
3. The long time scale response to compare measured and theoretical reflected shock pressures.
4. The power spectrum density of the short time scale response.

The shock tube test number is also displayed in the plot headings with 'pz_st_x' where 'x' is the shock tube test number (1 to 17)

E.1.1 Shock Tube Test 1

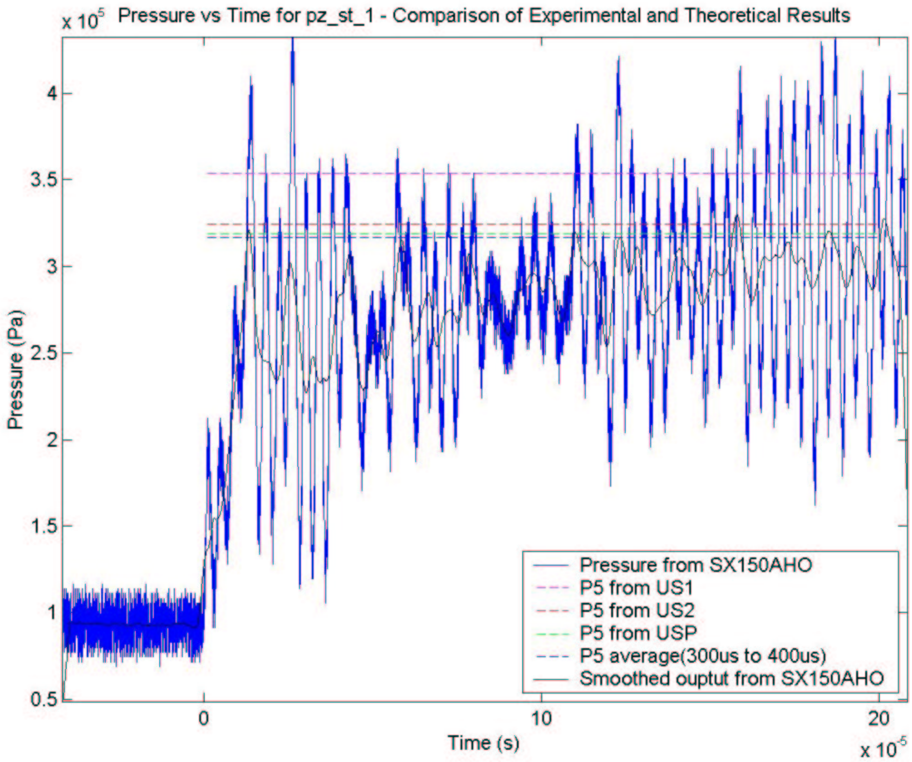

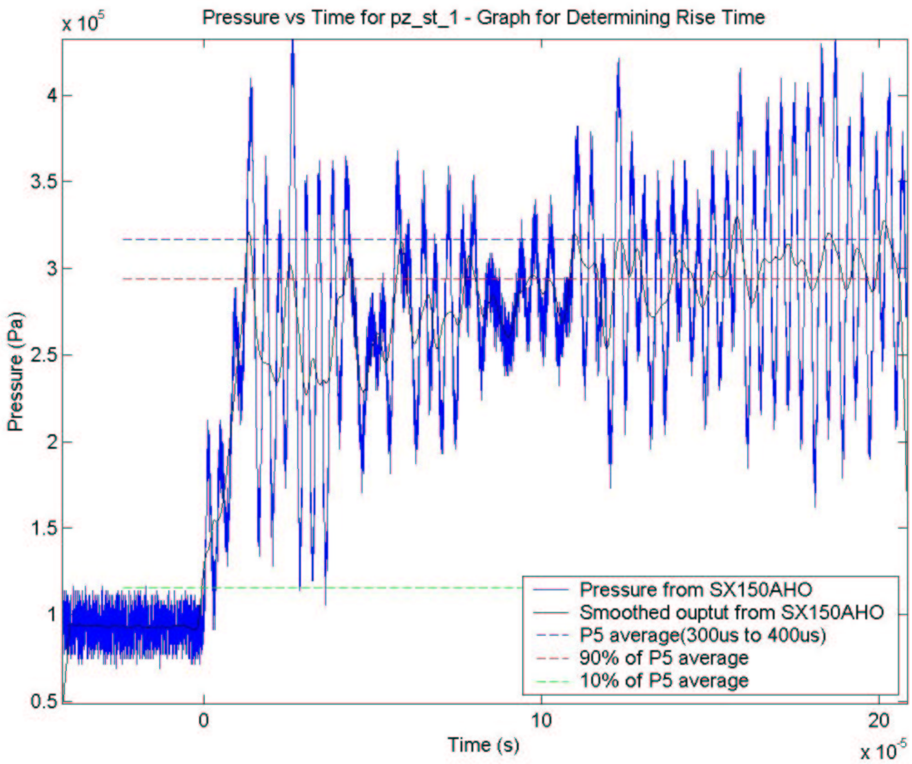

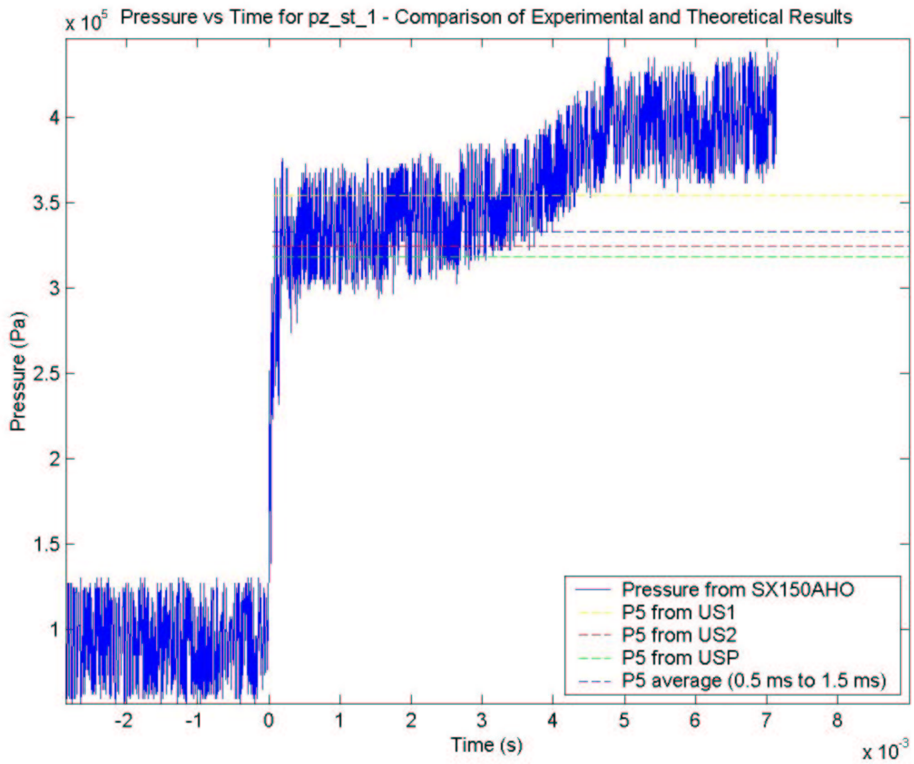

Pressure vs Time for pz_st_1 - Comparison of Experimental and Theoretical Results
x 10^5
Pressure (Pa)
Time (s)
x 10^-3
Pressure from SX150AHO
P5 from US1
P5 from US2
P5 from USP
P5 average (0.5 ms to 1.5 ms)

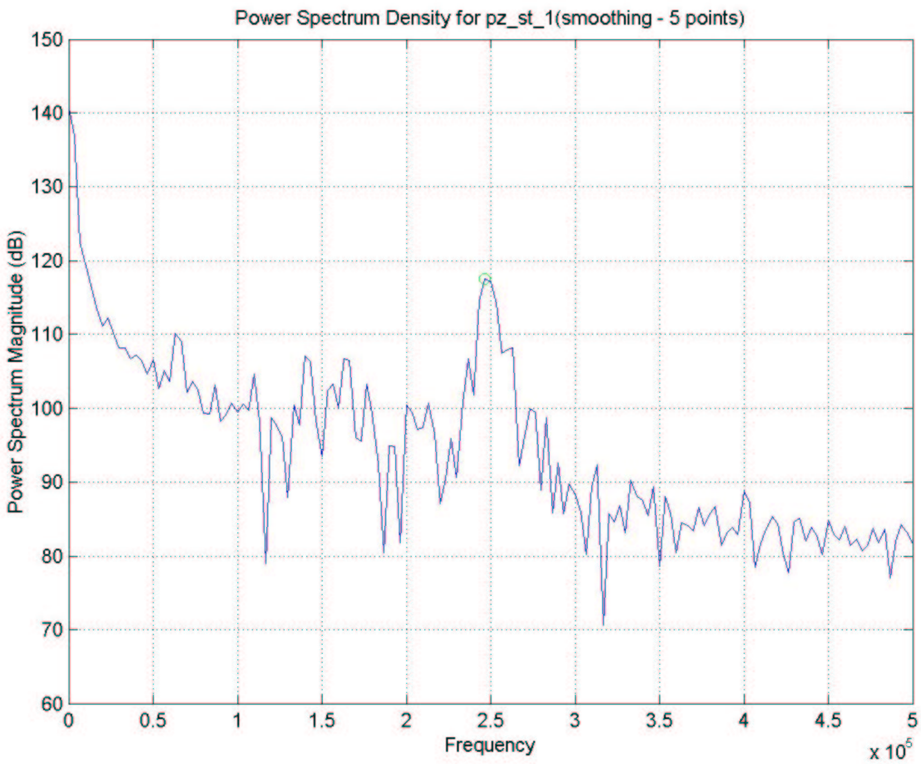

Power Spectrum Density for pz_st_1(smoothing - 5 points)
Power Spectrum Magnitude (dB)
Frequency
x 10^5

E.1.2 Shock Tube Test 2

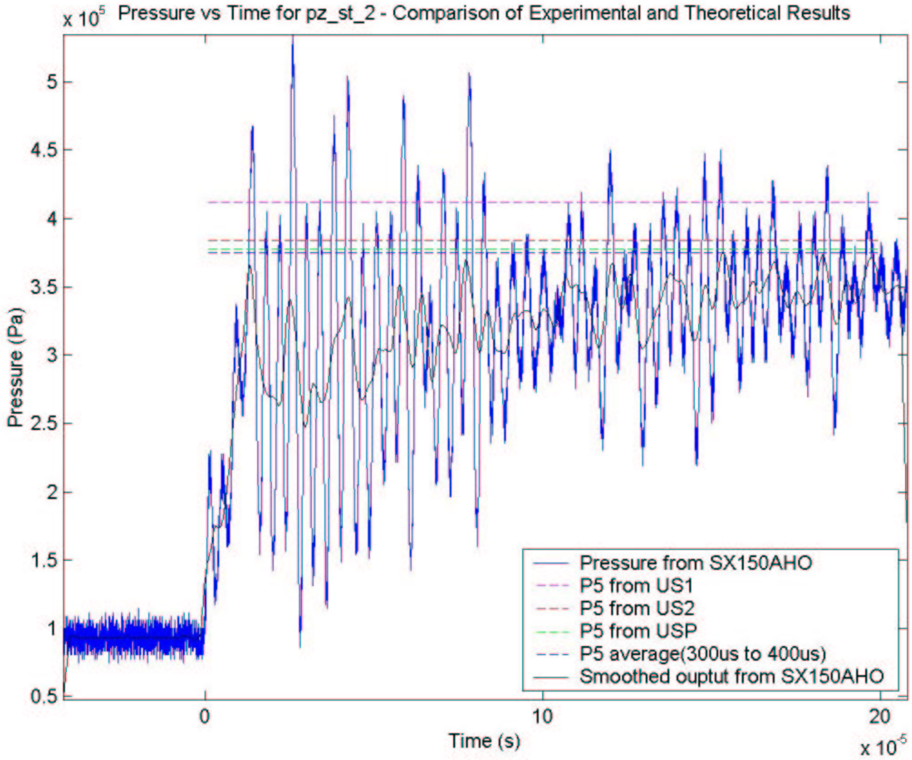

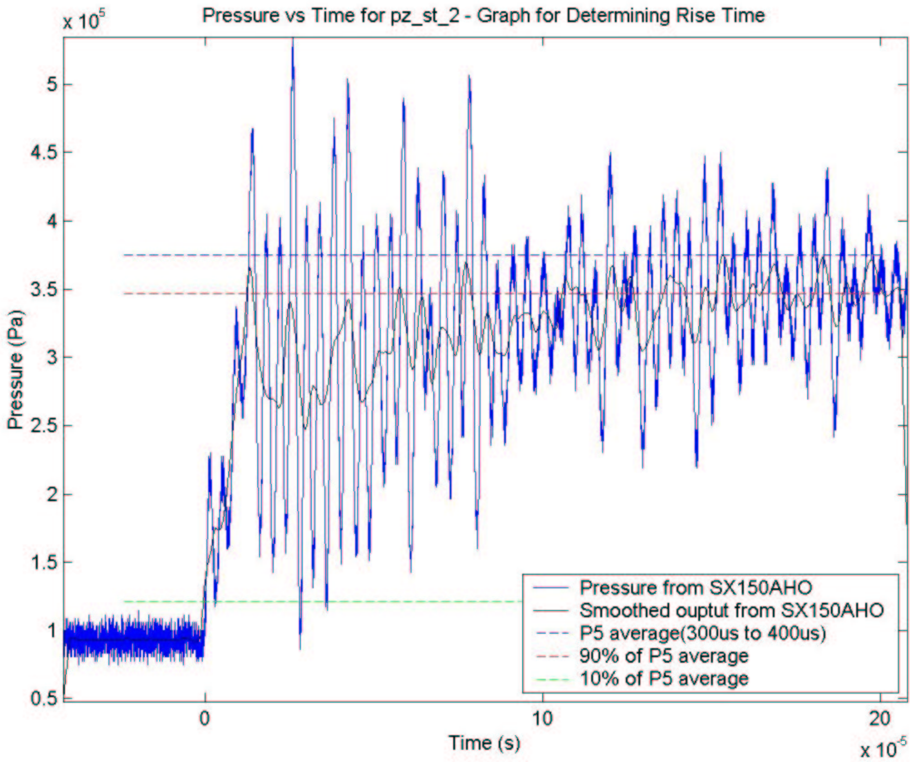

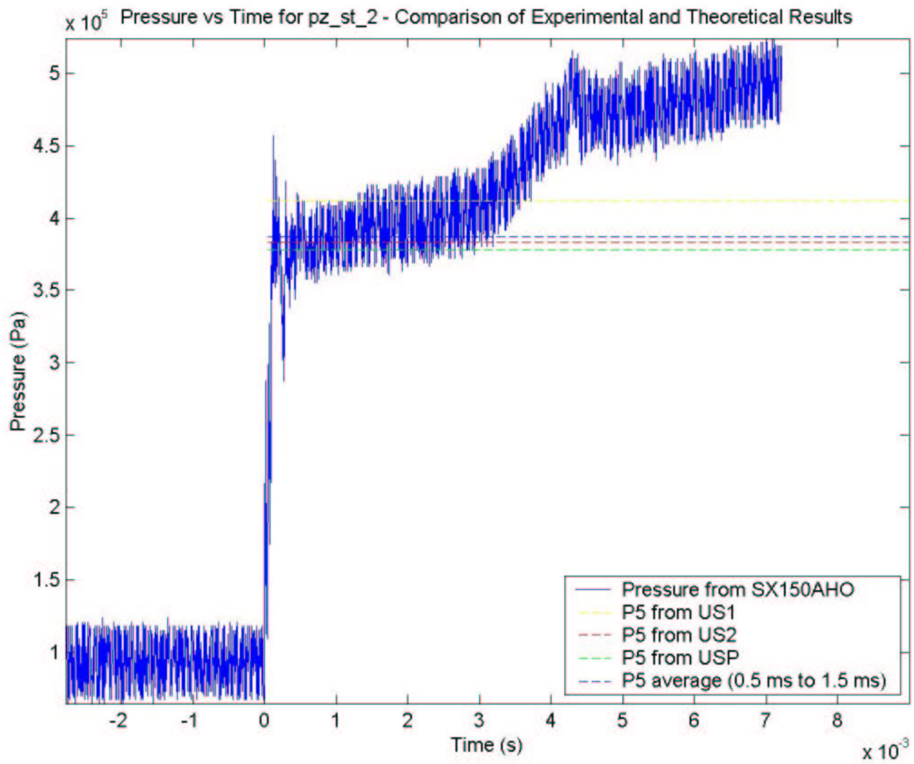
x 10^5 Pressure vs Time for pz_st_2 - Comparison of Experimental and Theoretical Results
Pressure (Pa)
Time (s)
x 10^-3
Pressure from SX150AHO
P5 from US1
P5 from US2
P5 from USP
P5 average (0.5 ms to 1.5 ms)

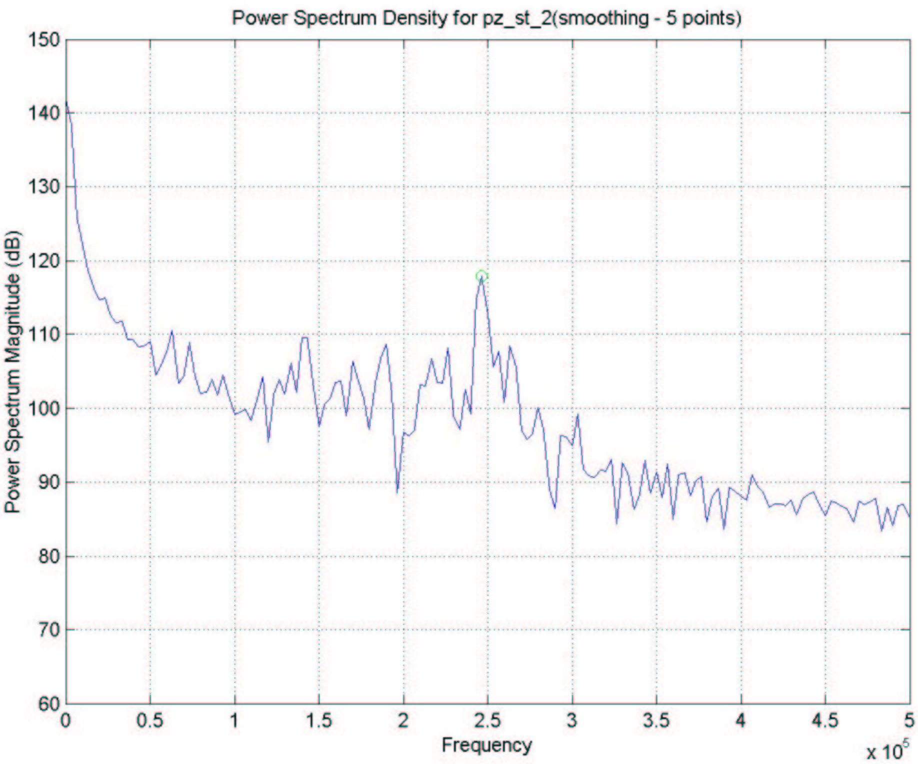
Power Spectrum Density for pz_st_2(smoothing - 5 points)
Power Spectrum Magnitude (dB)
Frequency
x 10^5

E.1.3 Shock Tube Test 3

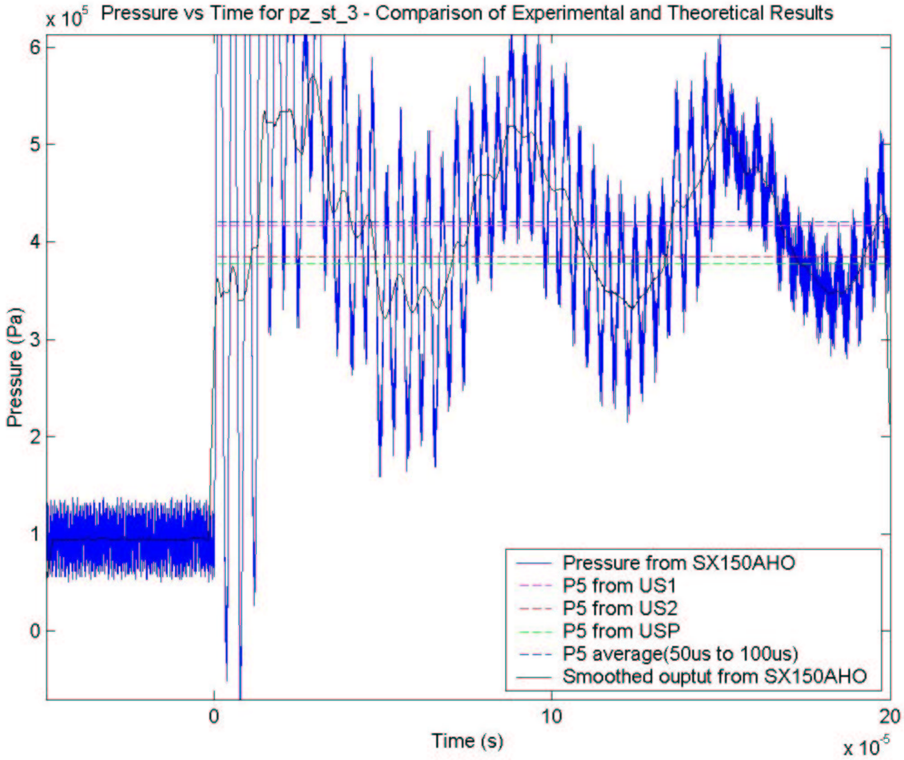

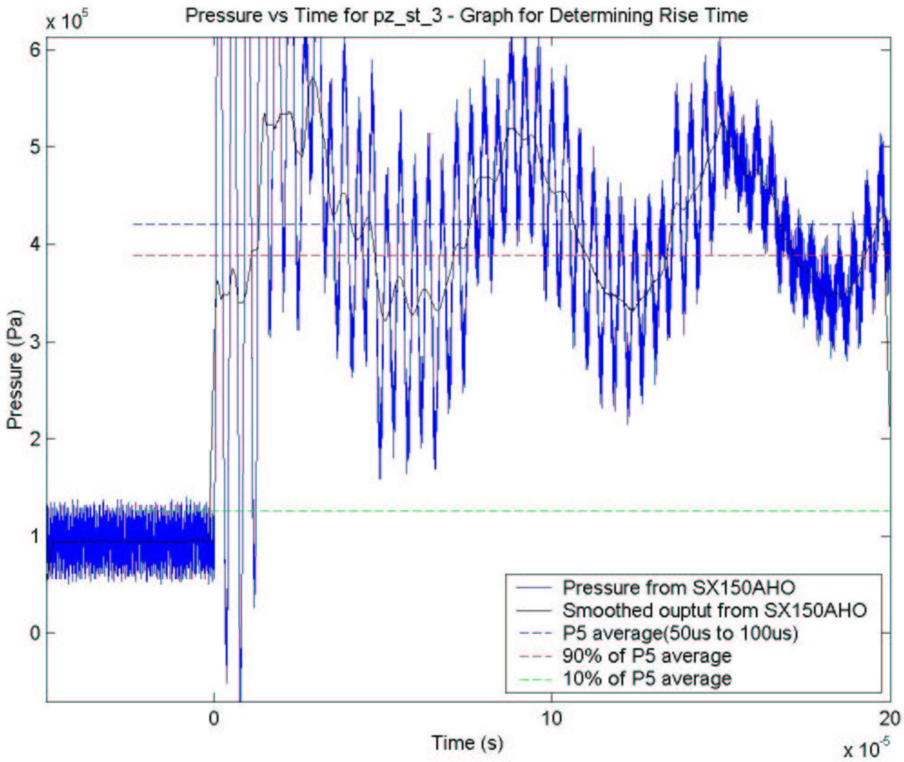

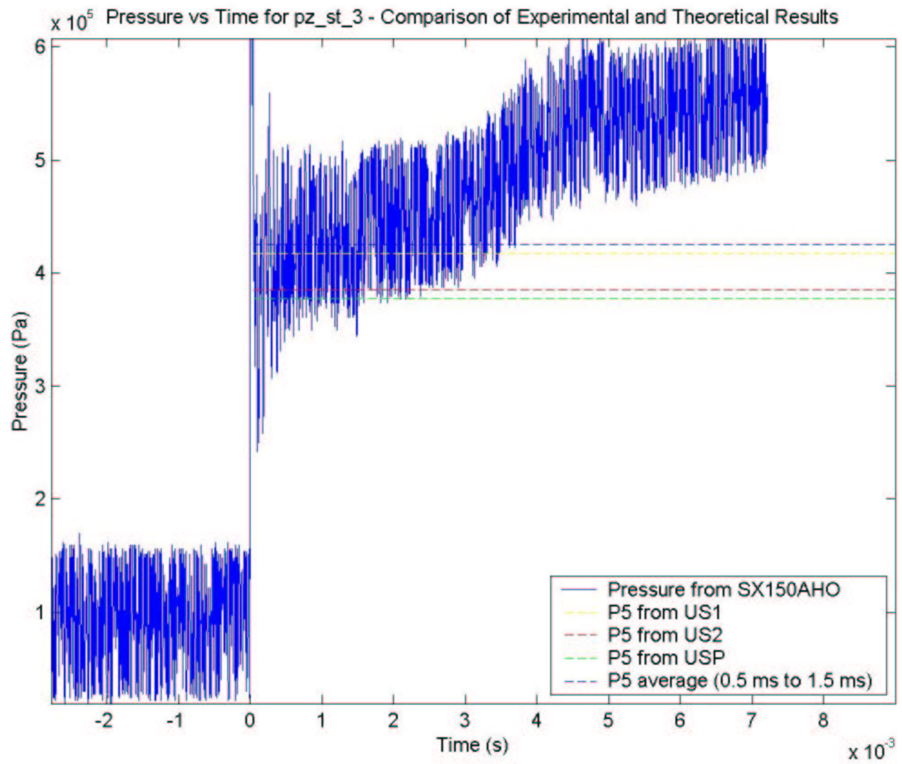
x 10^5 Pressure vs Time for pz_st_3 - Comparison of Experimental and Theoretical Results
Pressure (Pa)
Time (s)
x 10^-3
Pressure from SX150AHO
P5 from US1
P5 from US2
P5 from USP
P5 average (0.5 ms to 1.5 ms)

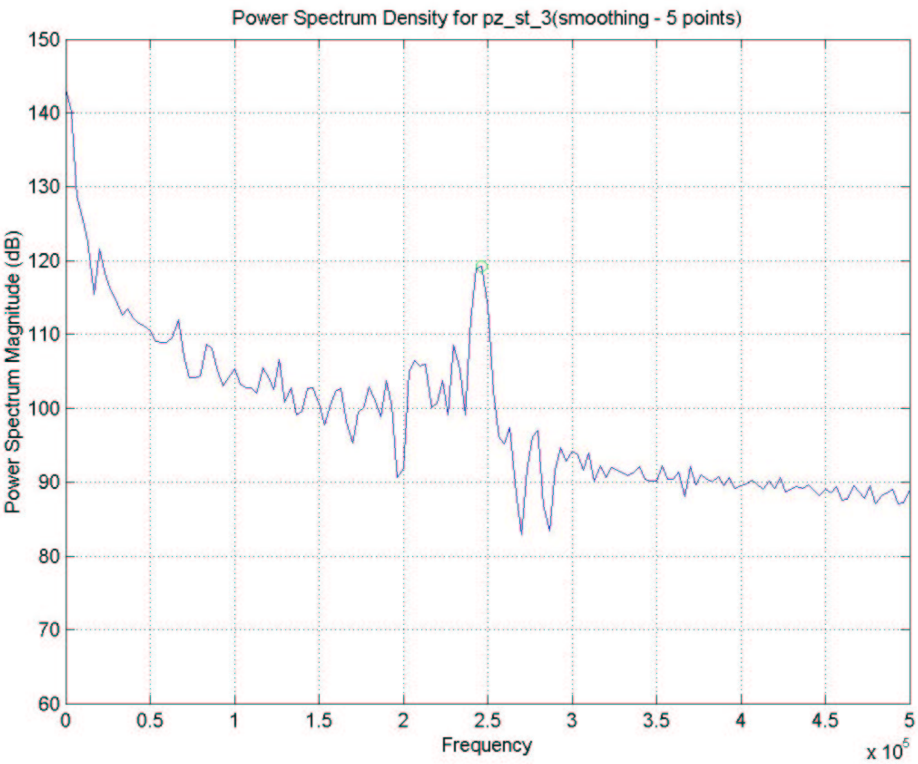
Power Spectrum Density for pz_st_3(smoothing - 5 points)
Power Spectrum Magnitude (dB)
Frequency
x 10^5

E.1.4 Shock Tube Test 4

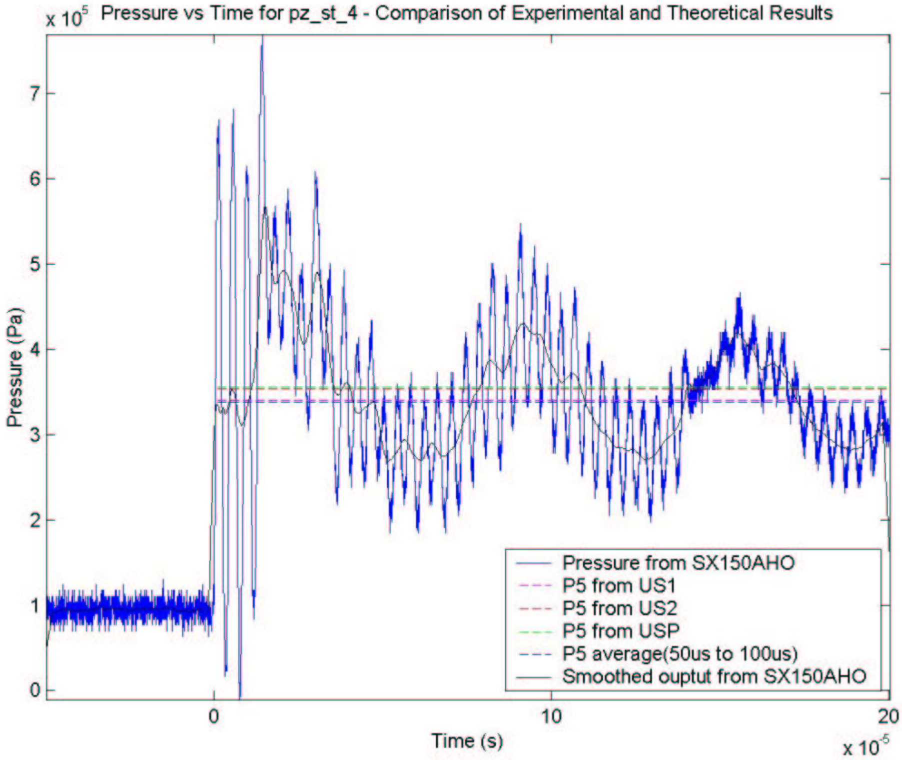

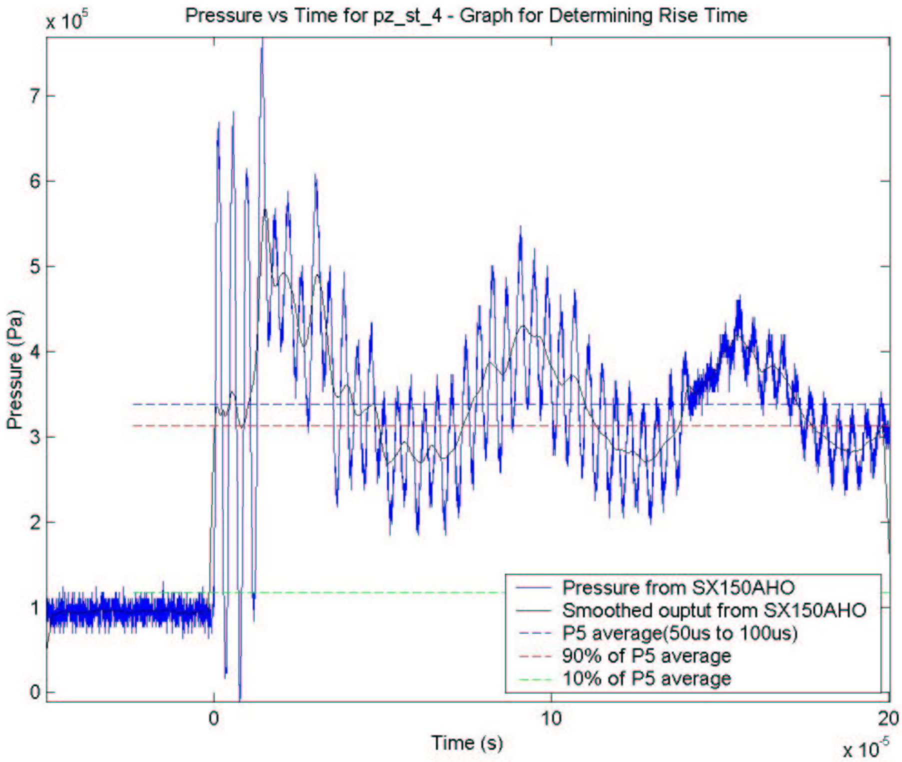

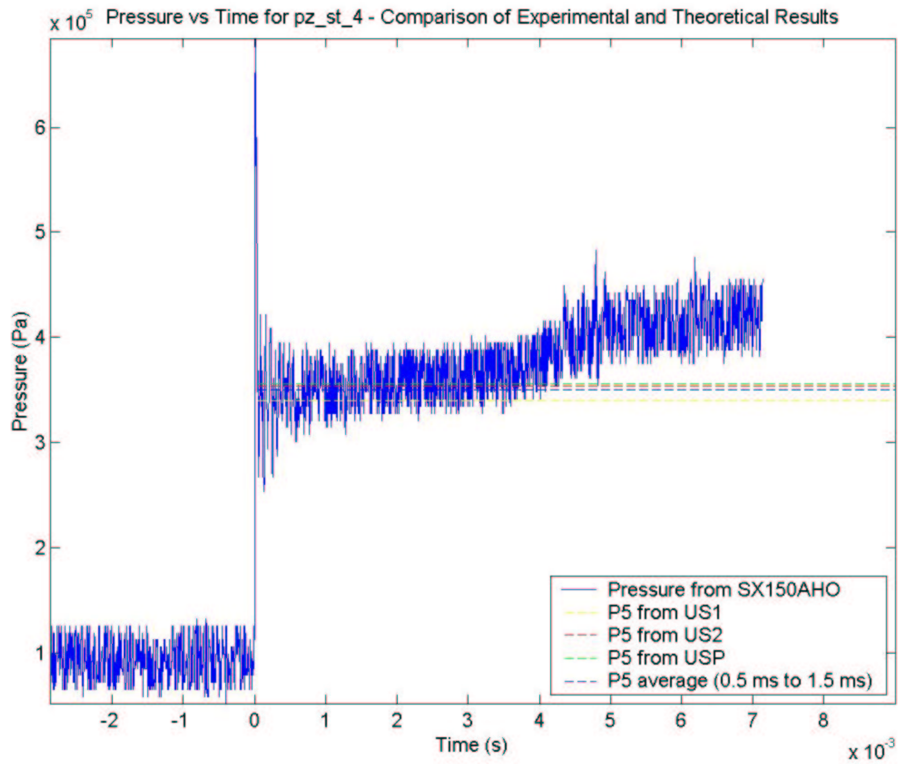

x 10^5 Pressure vs Time for pz_st_4 - Comparison of Experimental and Theoretical Results
Pressure (Pa)
Time (s)
x 10^-3
Pressure from SX150AHO
P5 from US1
P5 from US2
P5 from USP
P5 average (0.5 ms to 1.5 ms)

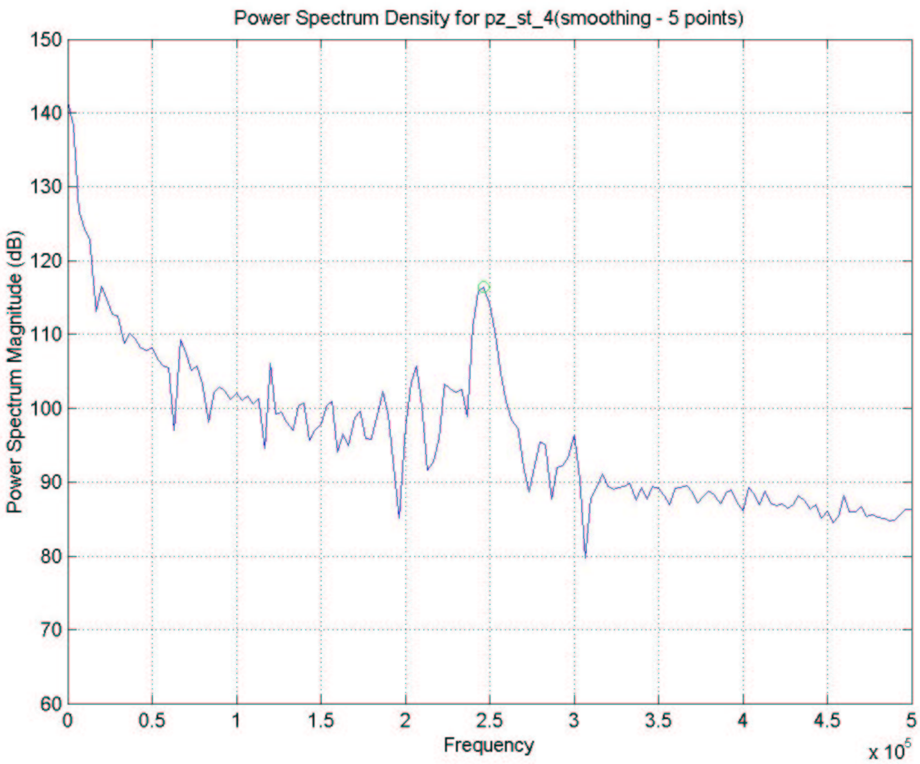

Power Spectrum Density for pz_st_4(smoothing - 5 points)
Power Spectrum Magnitude (dB)
Frequency
x 10^5

E.1.5 Shock Tube Test 5

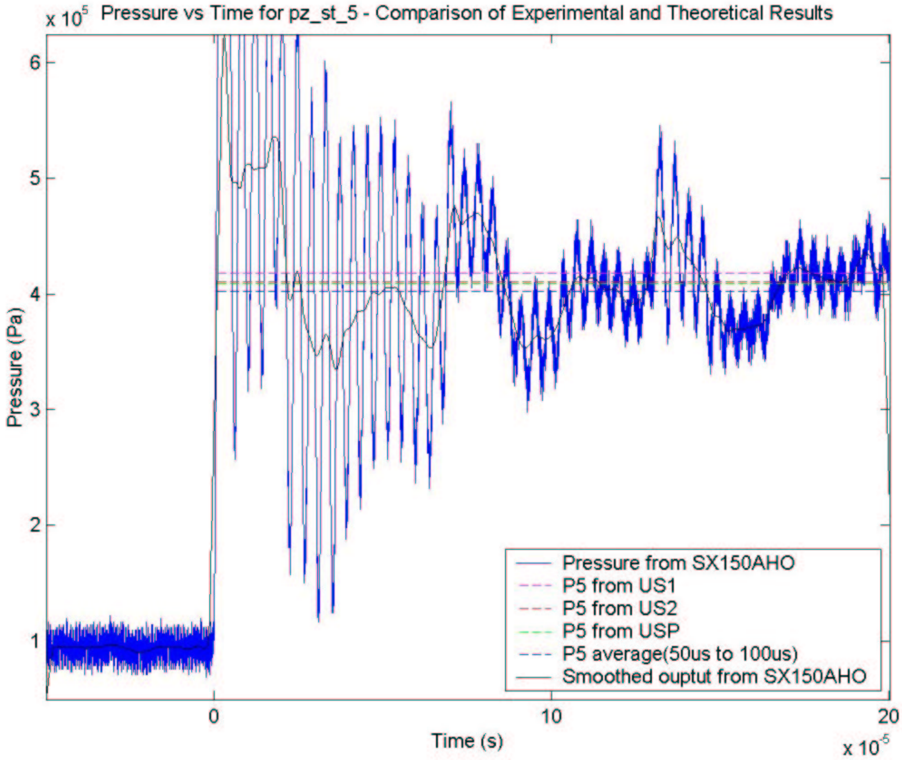

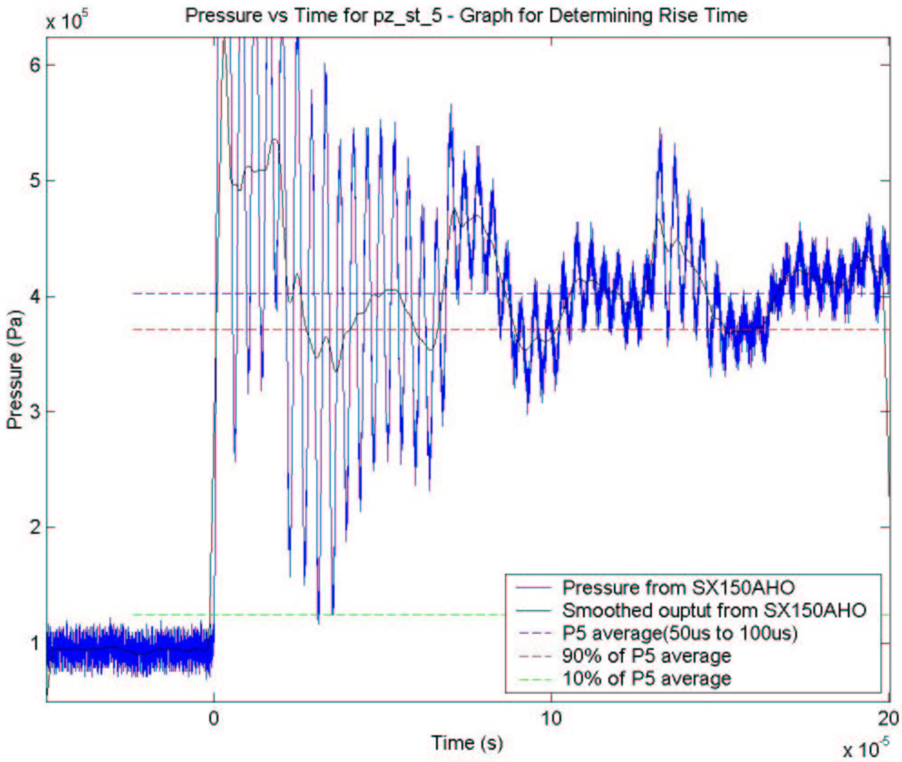

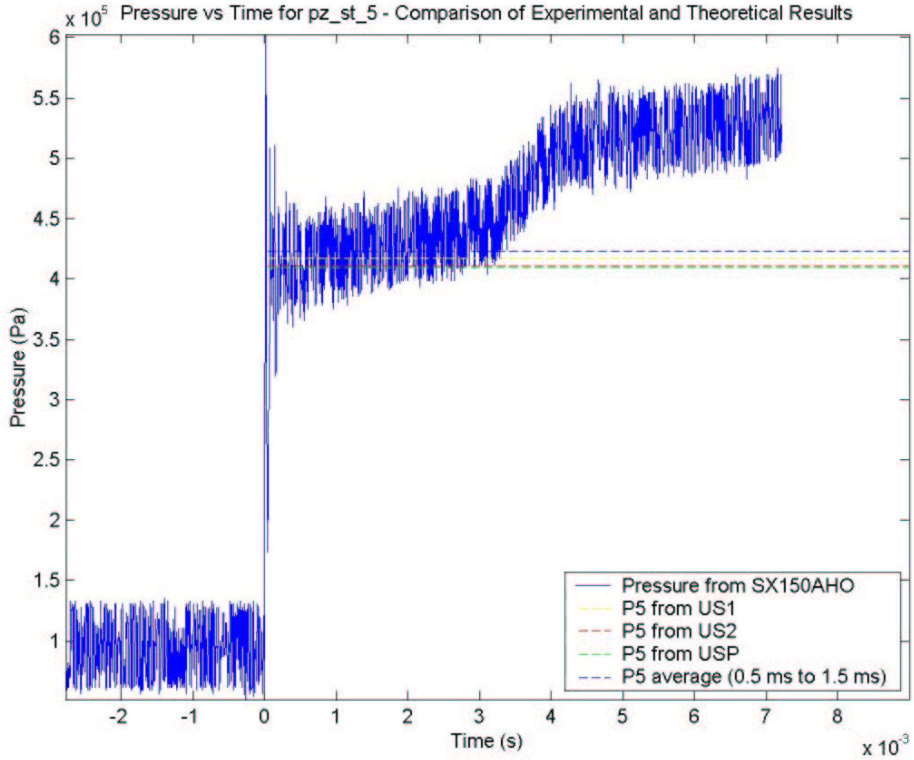

x 10^5 Pressure vs Time for pz_st_5 - Comparison of Experimental and Theoretical Results
Pressure (Pa)
Time (s)
x 10^-3
Pressure from SX150AHO
P5 from US1
P5 from US2
P5 from USP
P5 average (0.5 ms to 1.5 ms)

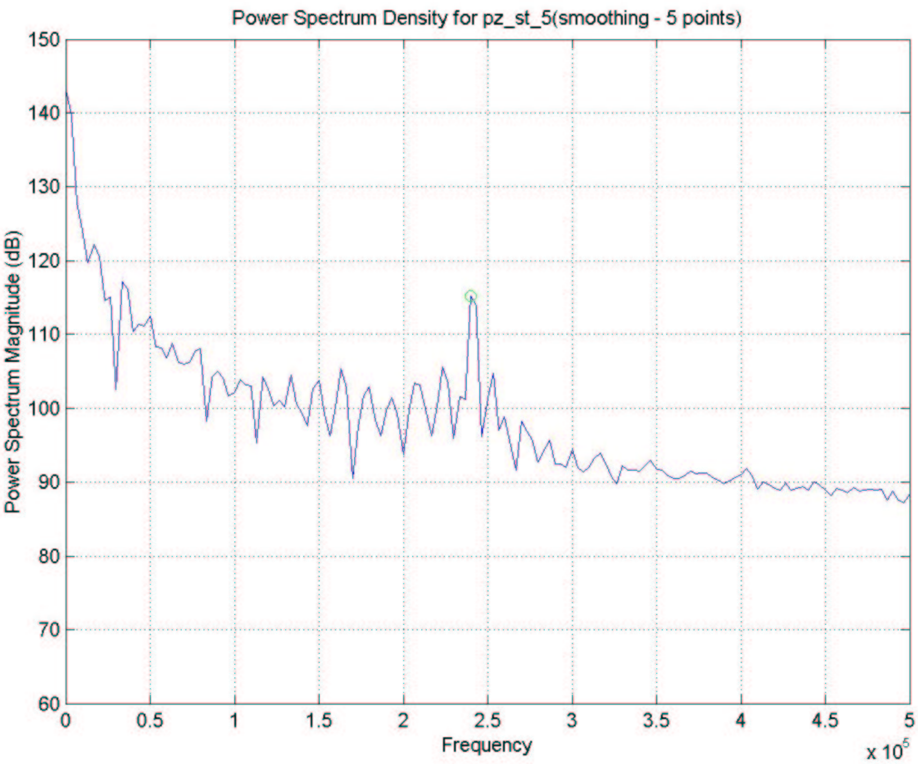

Power Spectrum Density for pz_st_5(smoothing - 5 points)
Power Spectrum Magnitude (dB)
Frequency
x 10^5

E.1.6 Shock Tube Test 6

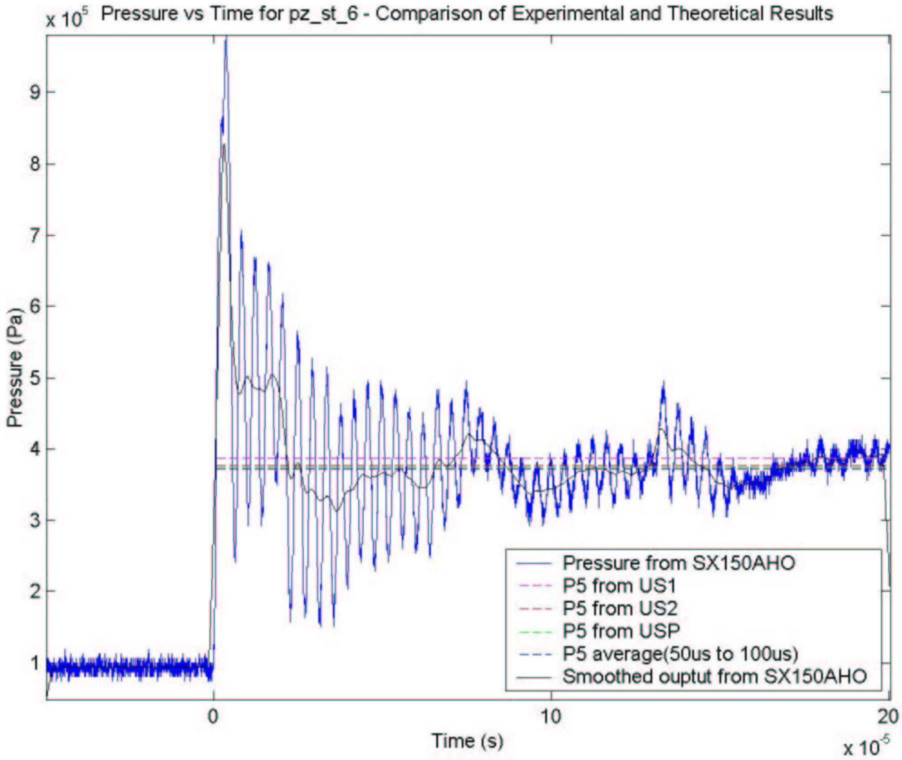

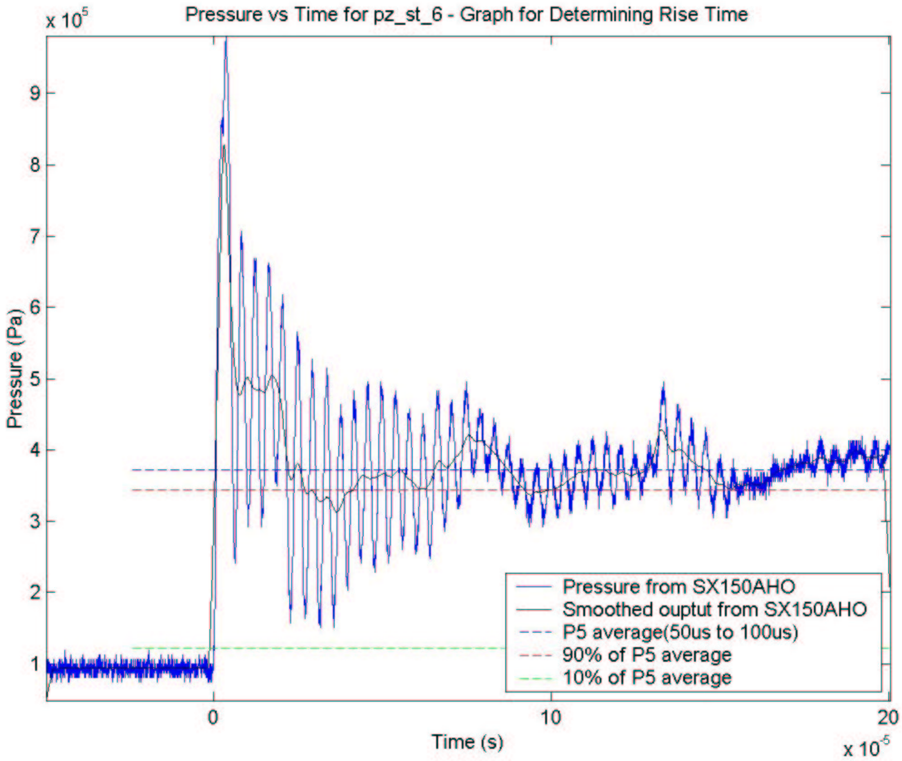

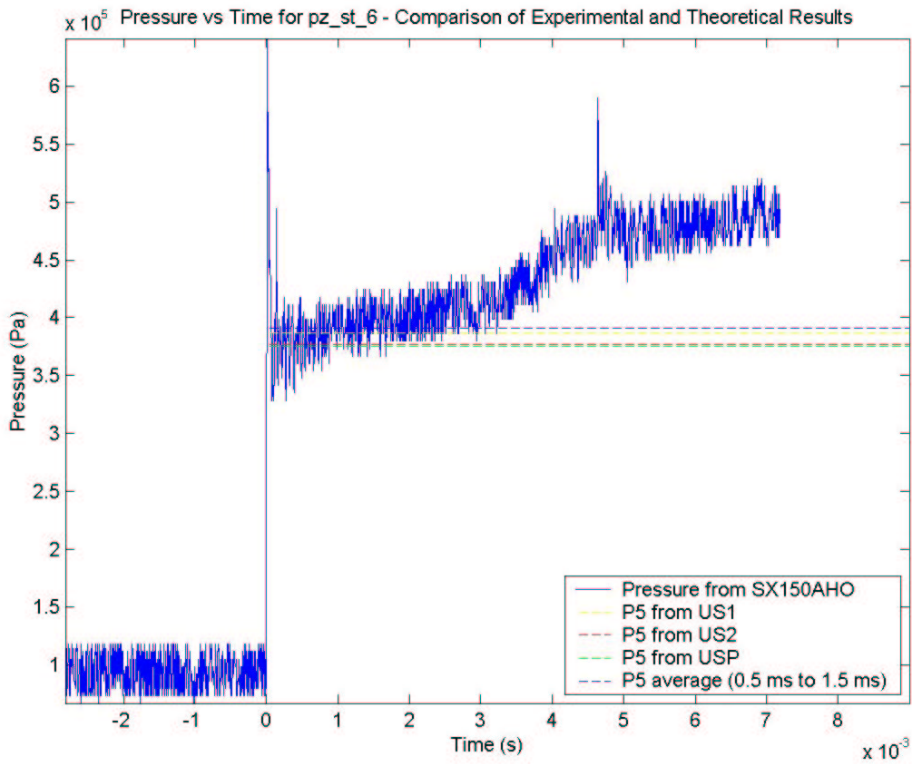
Pressure vs Time for pz_st_6 - Comparison of Experimental and Theoretical Results
x 10^5
Pressure (Pa)
Time (s)
x 10^-3
Pressure from SX150AHO
P5 from US1
P5 from US2
P5 from USP
P5 average (0.5 ms to 1.5 ms)

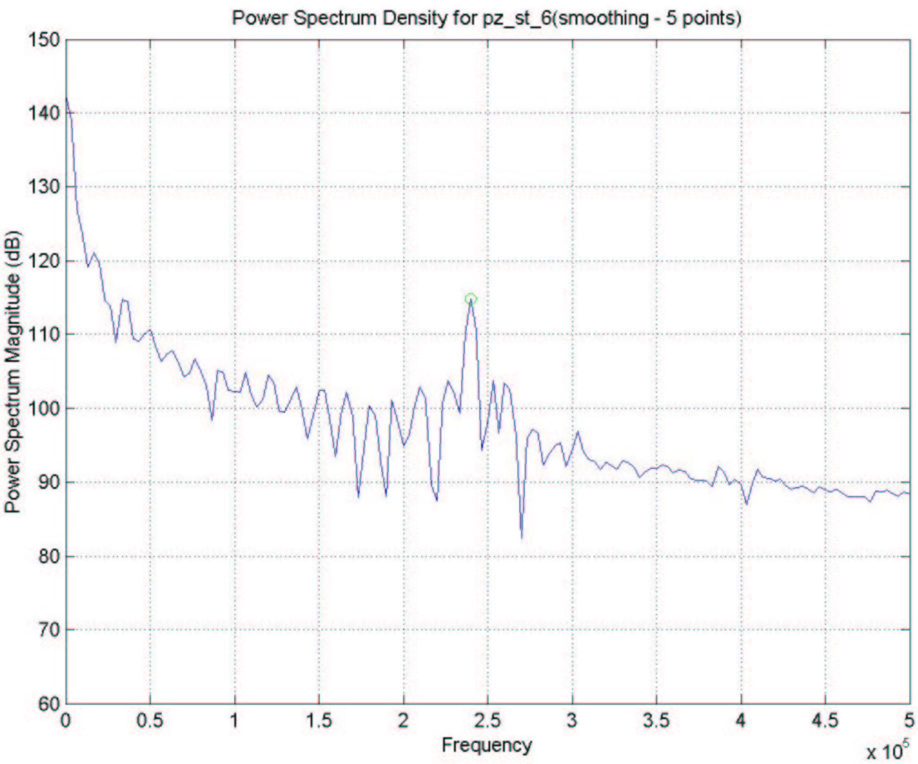
Power Spectrum Density for pz_st_6(smoothing - 5 points)
Power Spectrum Magnitude (dB)
Frequency
x 10^5

E.1.7 Shock Tube Test 7

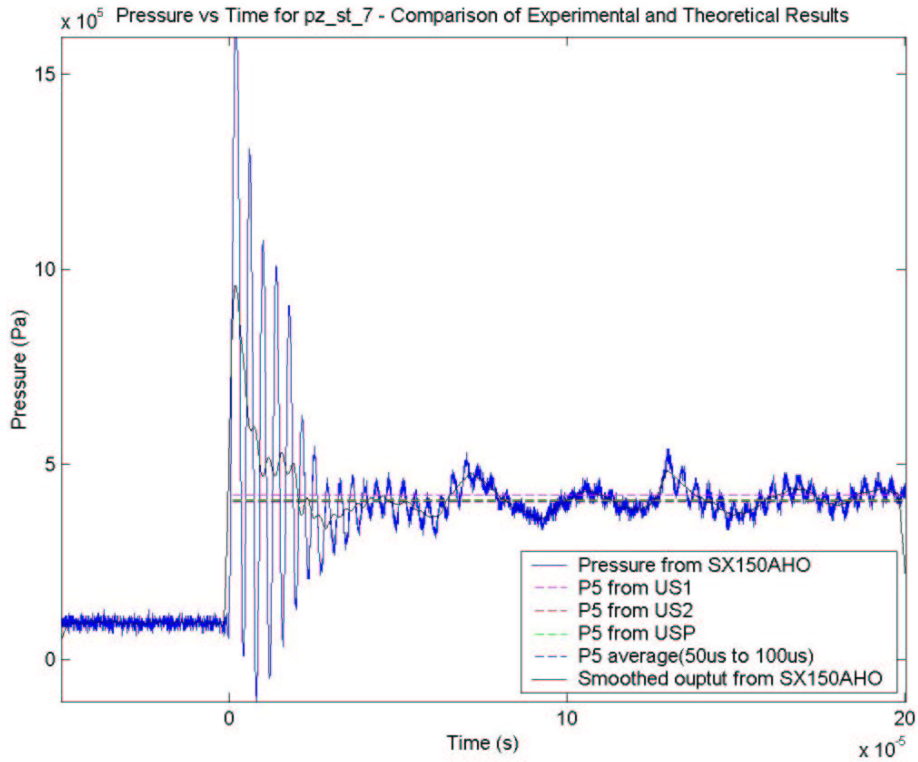

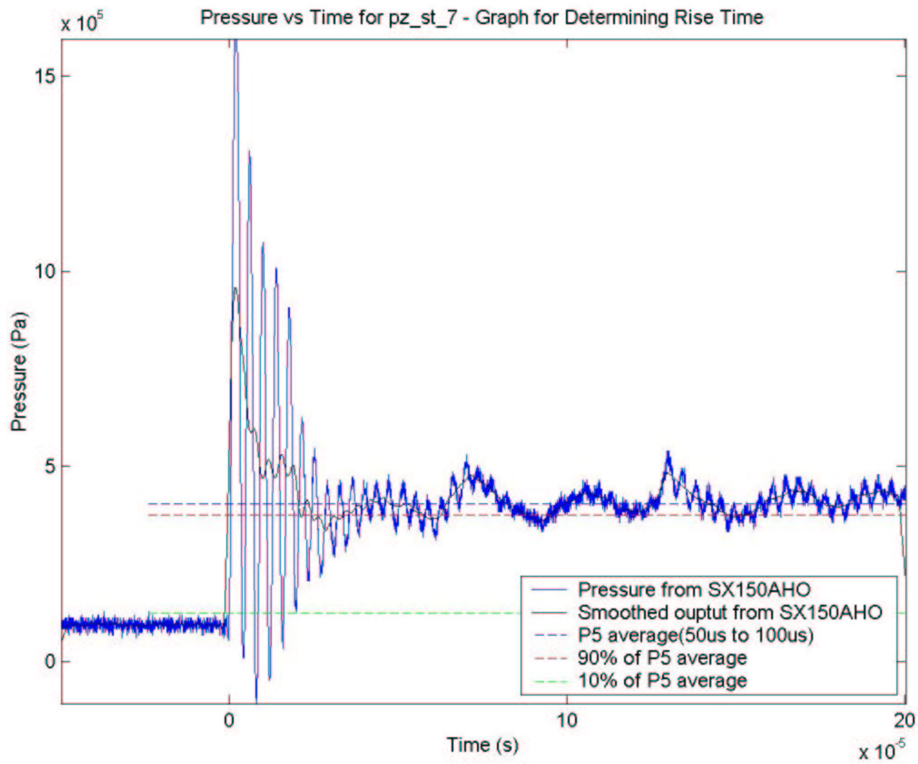

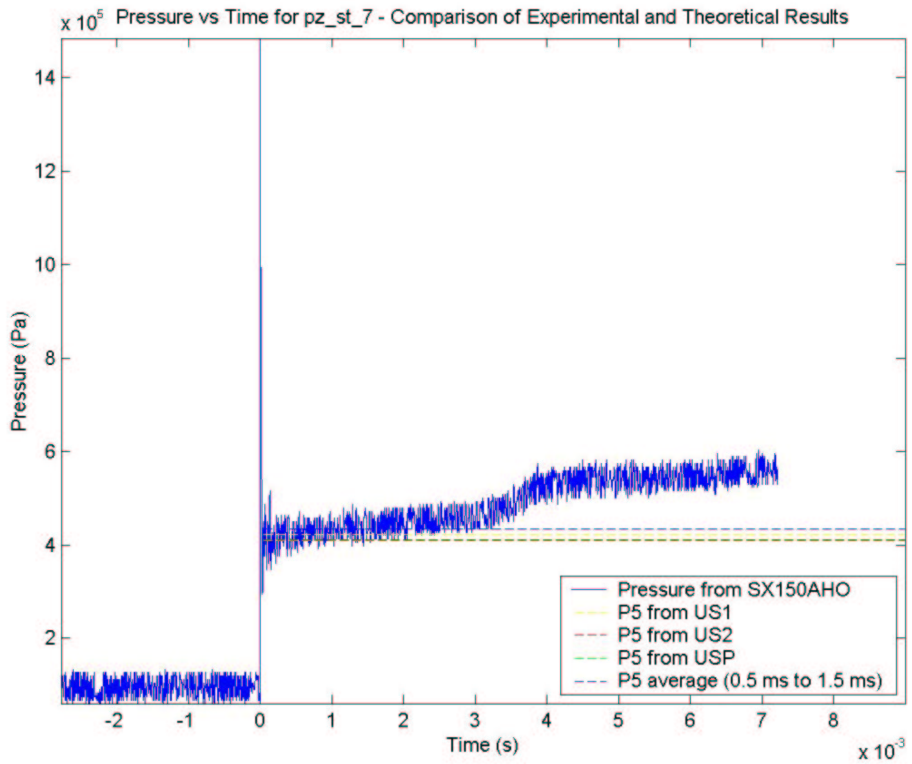

Pressure vs Time for pz_st_7 - Comparison of Experimental and Theoretical Results
x 10^5
Pressure (Pa)
Time (s)
x 10^-3
Pressure from SX150AHO
P5 from US1
P5 from US2
P5 from USP
P5 average (0.5 ms to 1.5 ms)

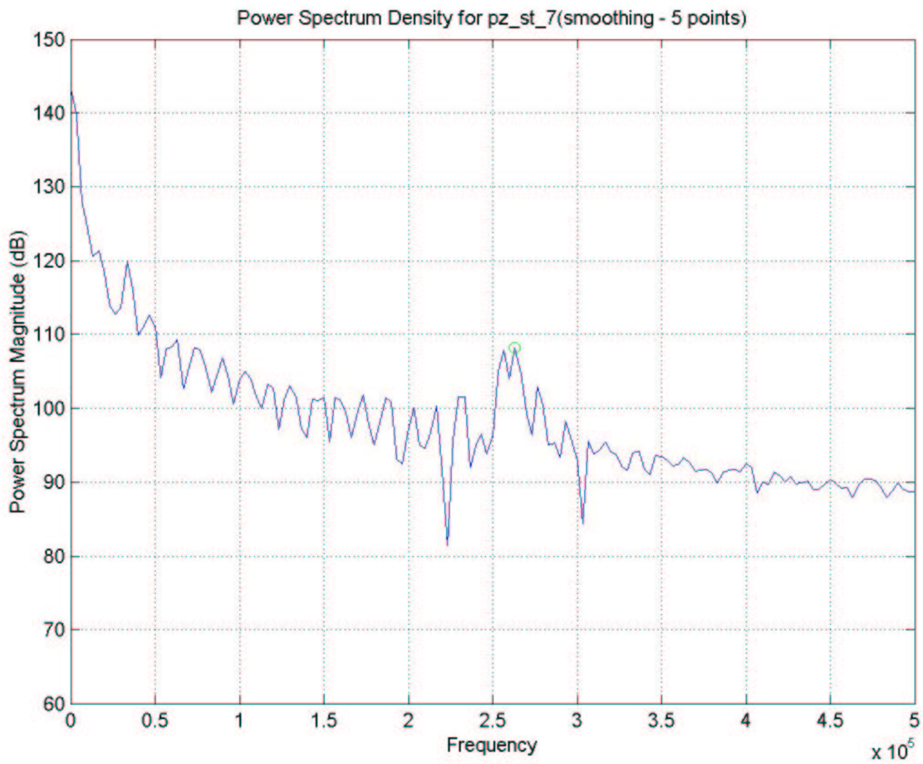

Power Spectrum Density for pz_st_7(smoothing - 5 points)
Power Spectrum Magnitude (dB)
Frequency
x 10^5

E.1.8 Shock Tube Test 8

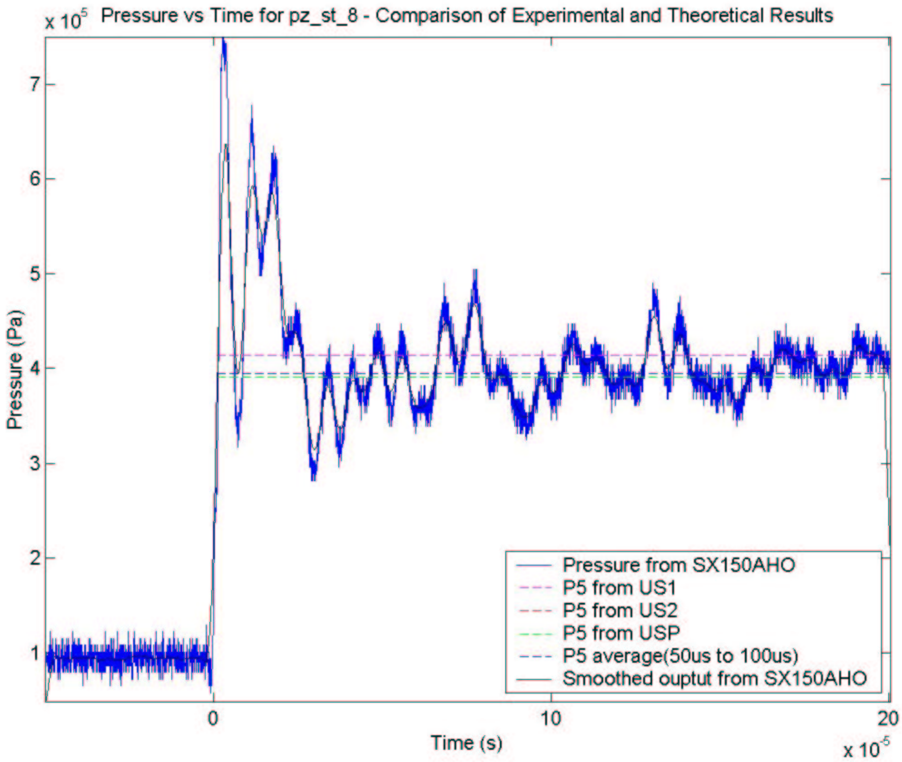

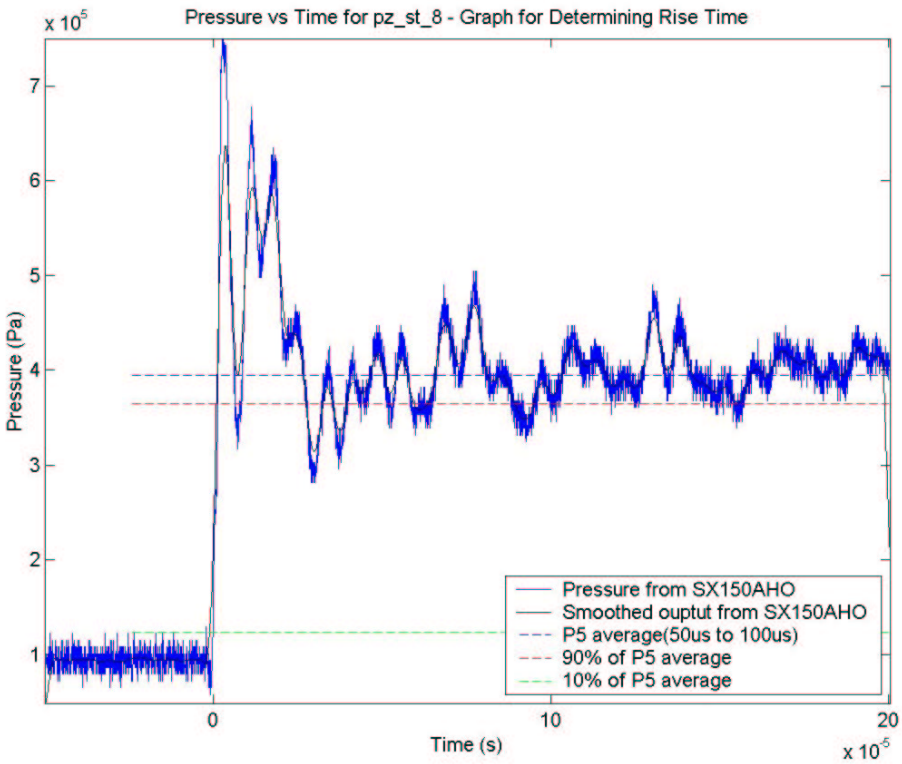

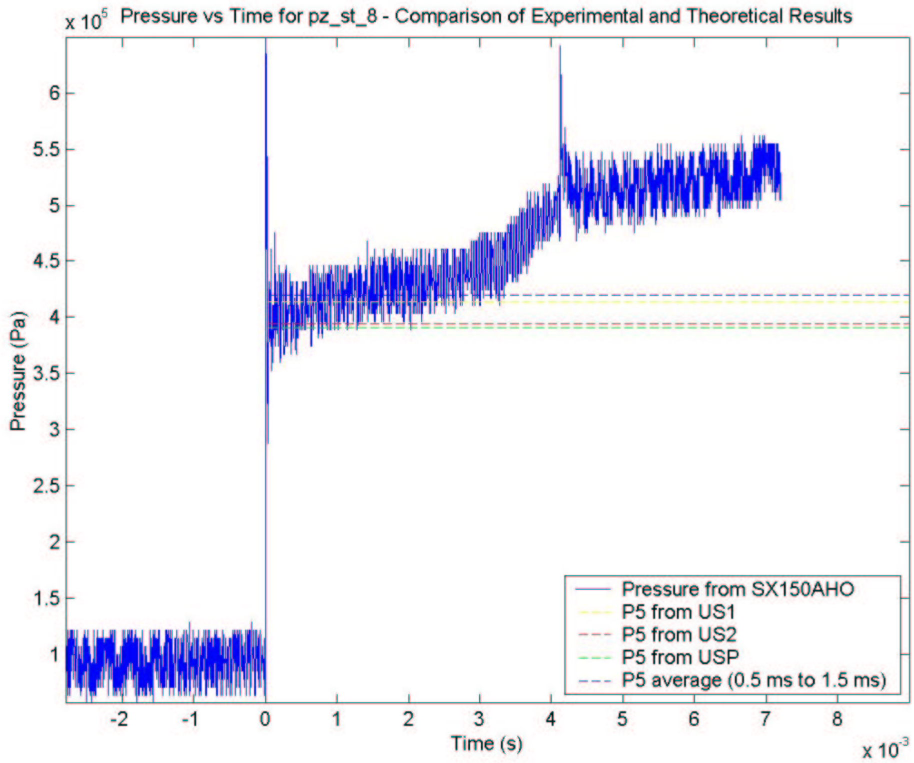
x 10^5 Pressure vs Time for pz_st_8 - Comparison of Experimental and Theoretical Results
Pressure (Pa)
Time (s)
x 10^-3
Pressure from SX150AHO
P5 from US1
P5 from US2
P5 from USP
P5 average (0.5 ms to 1.5 ms)

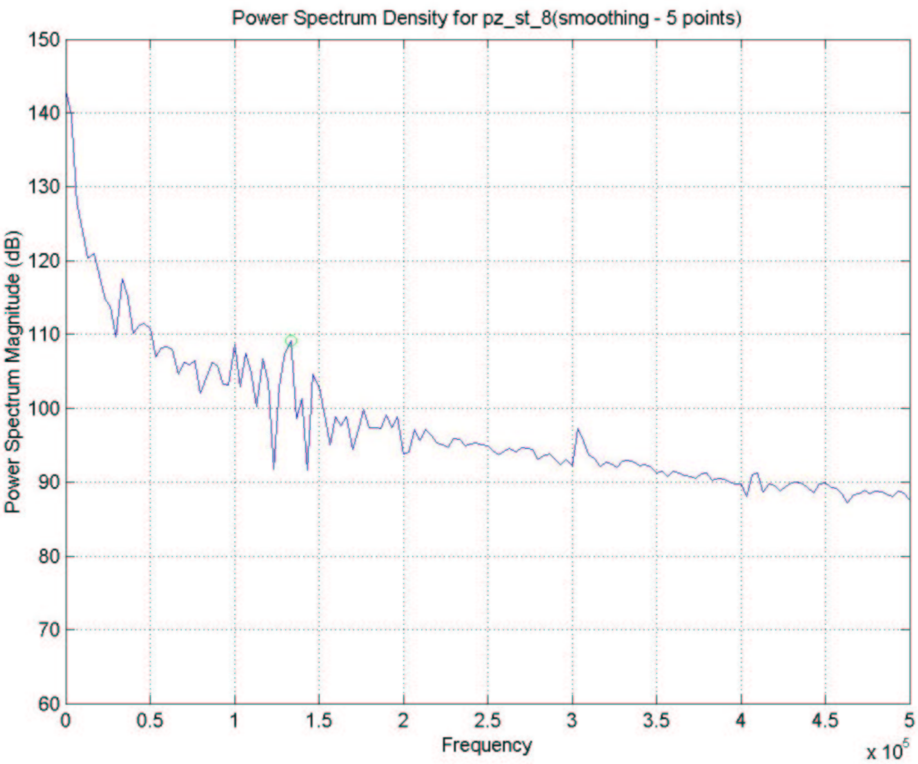
Power Spectrum Density for pz_st_8(smoothing - 5 points)
Power Spectrum Magnitude (dB)
Frequency
x 10^5

E.1.9 Shock Tube Test 9

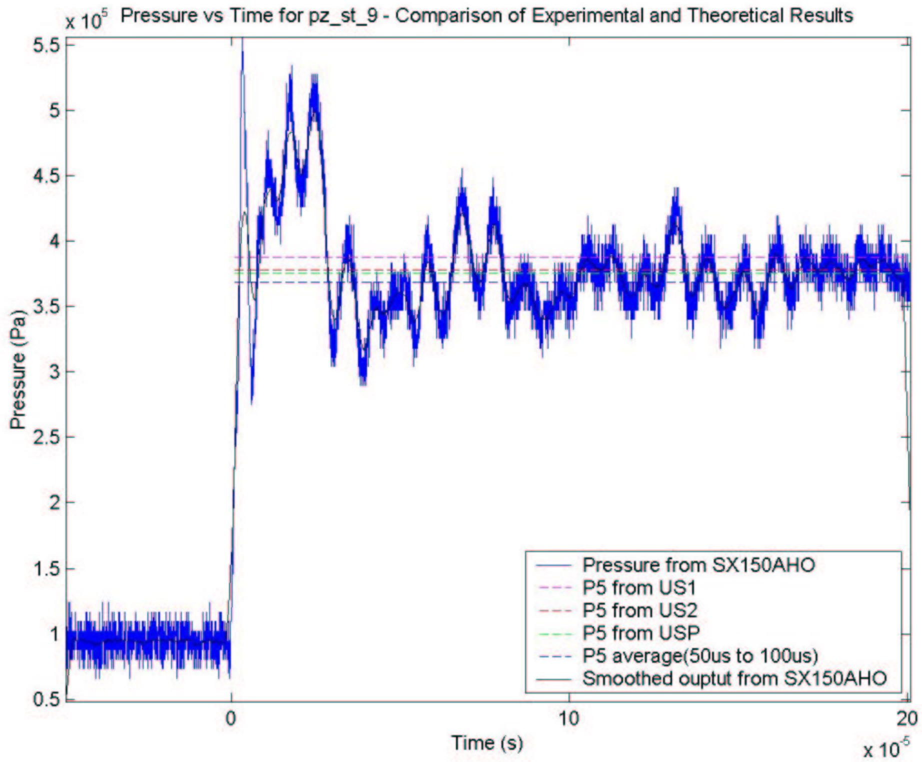

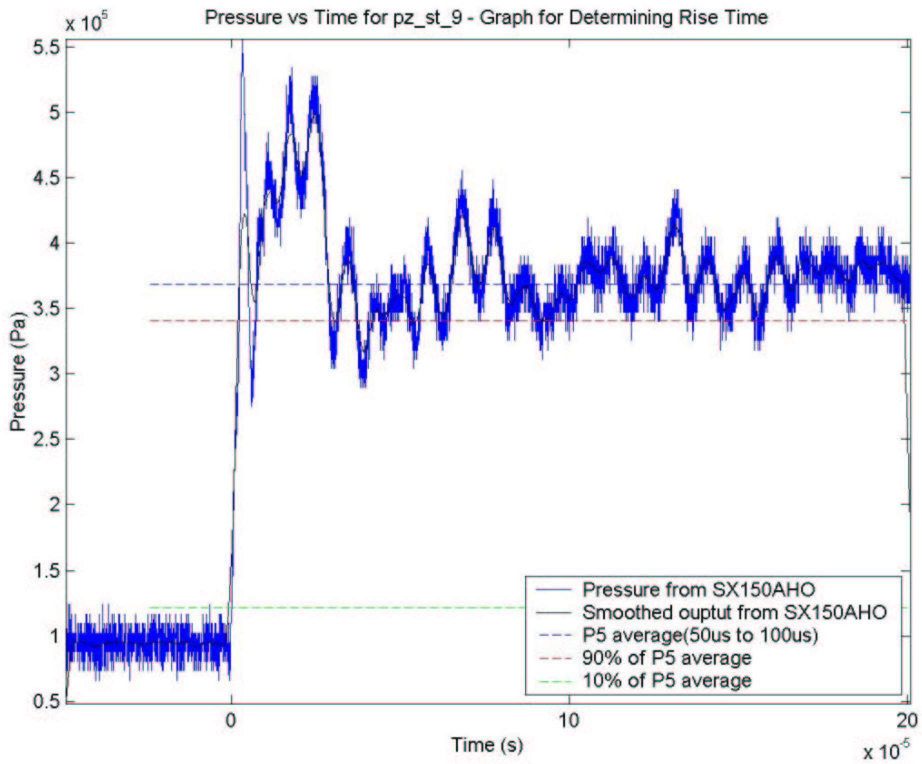

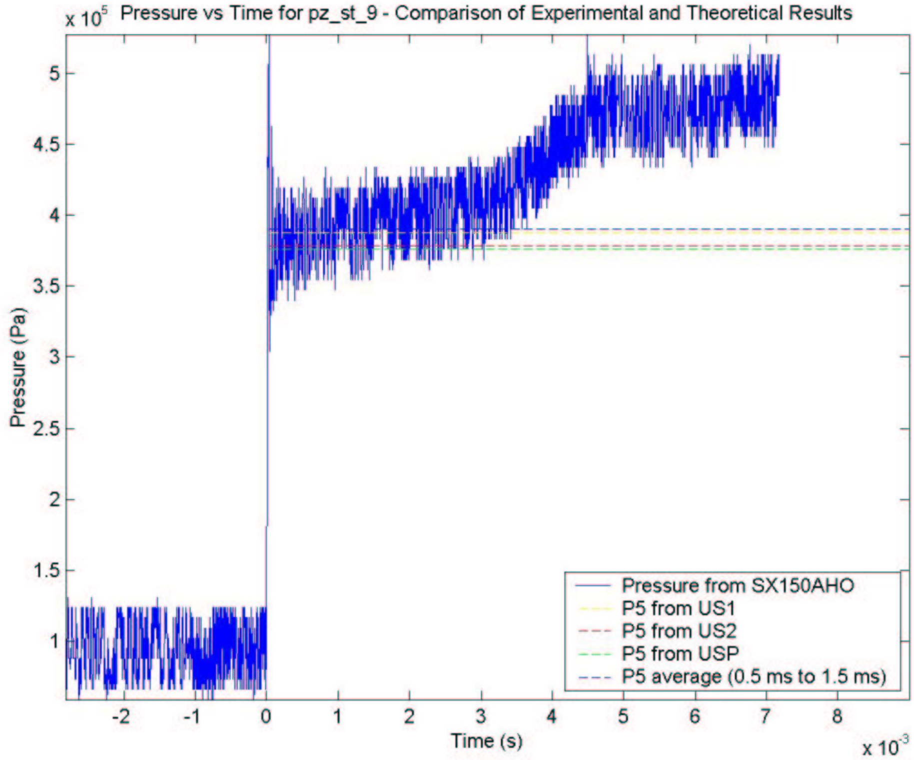

x 10^5 Pressure vs Time for pz_st_9 - Comparison of Experimental and Theoretical Results
Pressure (Pa)
Time (s)
x 10^-3
Pressure from SX150AHO
P5 from US1
P5 from US2
P5 from USP
P5 average (0.5 ms to 1.5 ms)

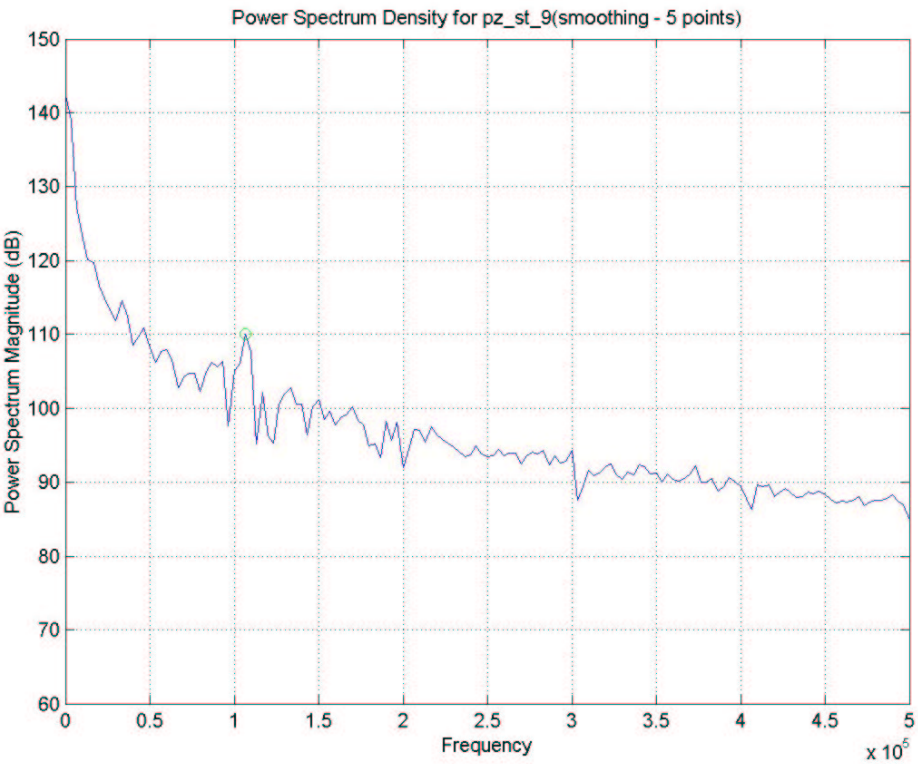

Power Spectrum Density for pz_st_9(smoothing - 5 points)
Power Spectrum Magnitude (dB)
Frequency
x 10^5

E.1.10 Shock Tube Test 10

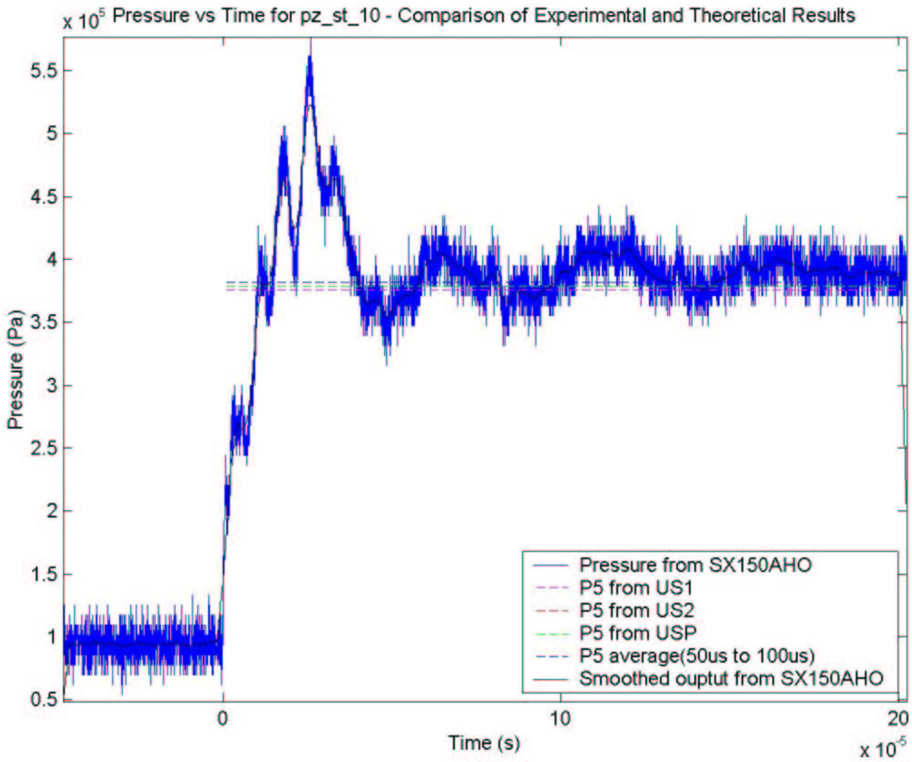

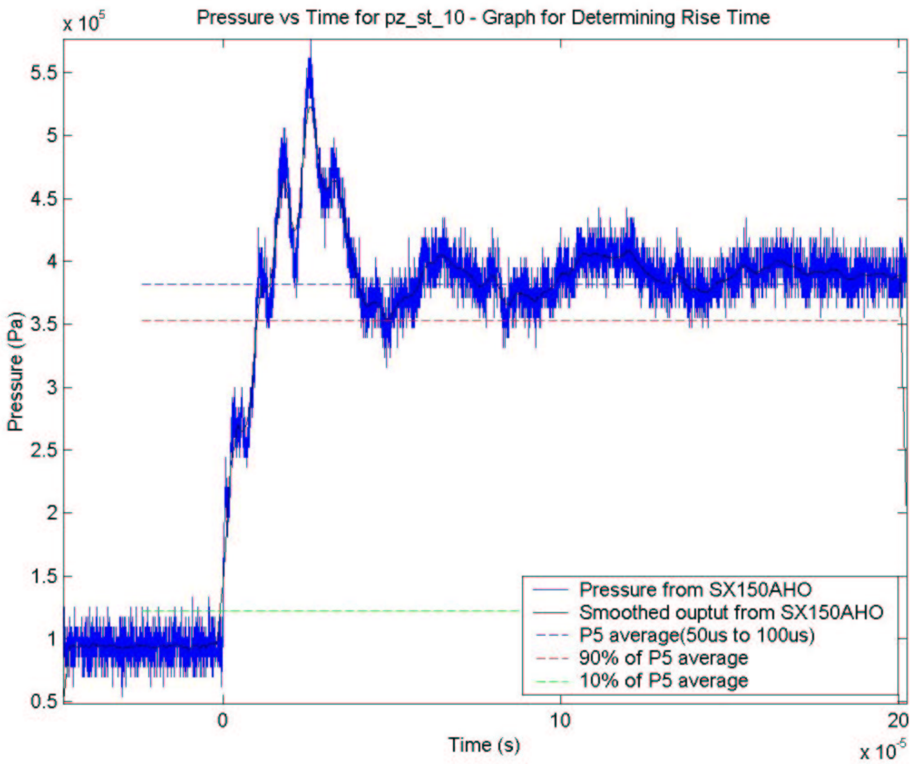

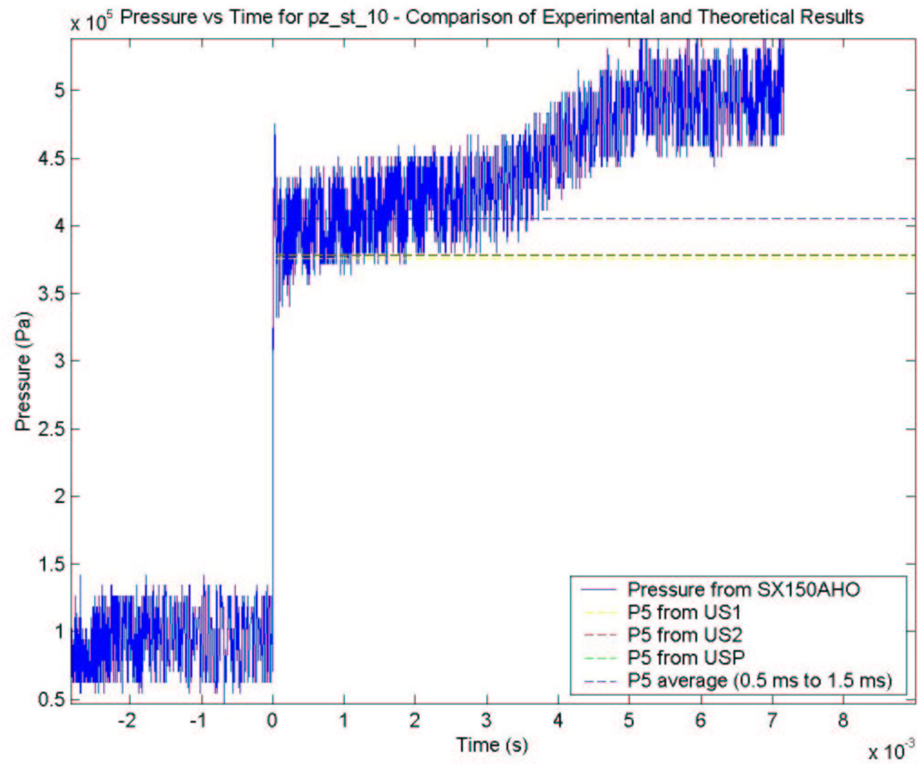
x 10^5 Pressure vs Time for pz_st_10 - Comparison of Experimental and Theoretical Results
Pressure (Pa)
Time (s)
x 10^-3
Pressure from SX150AHO
P5 from US1
P5 from US2
P5 from USP
P5 average (0.5 ms to 1.5 ms)

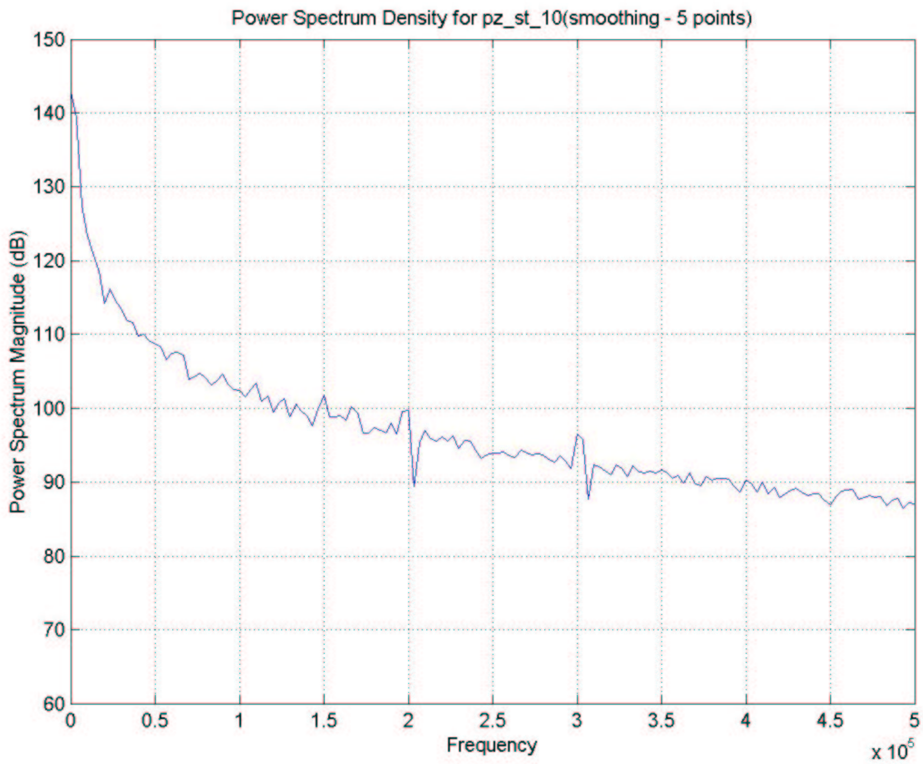
Power Spectrum Density for pz_st_10(smoothing - 5 points)
Power Spectrum Magnitude (dB)
Frequency
x 10^5

E.1.11 Shock Tube Test 11

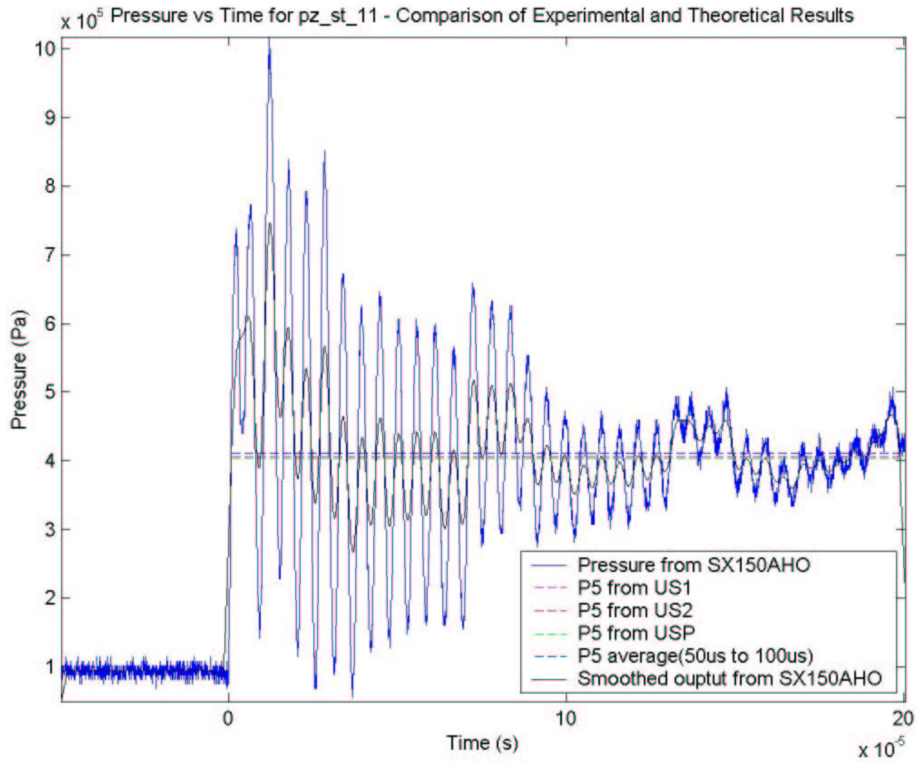

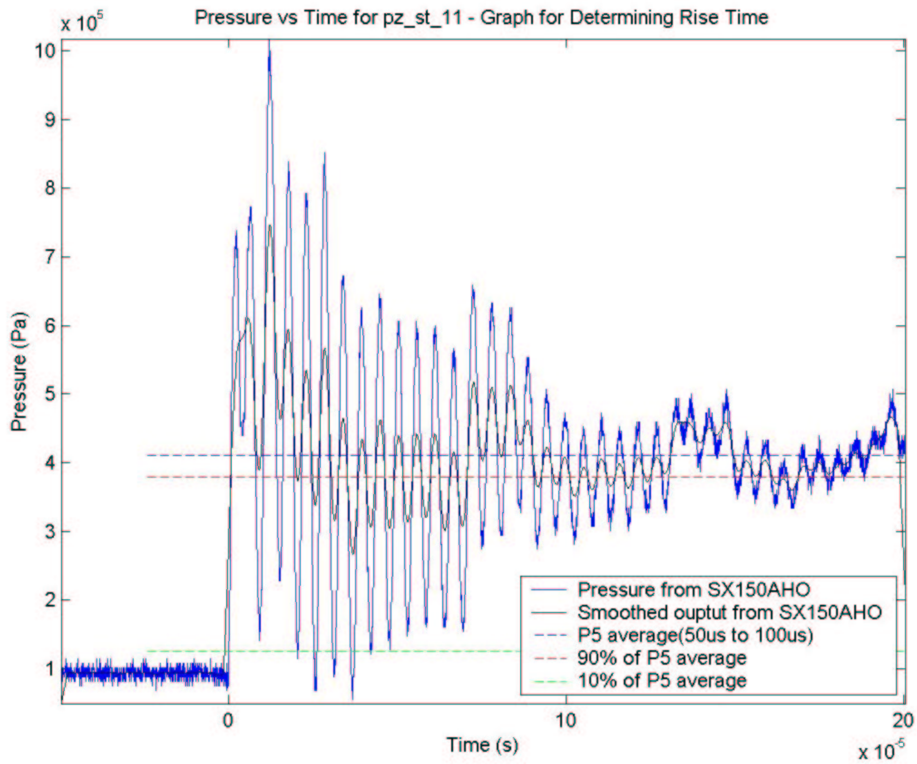

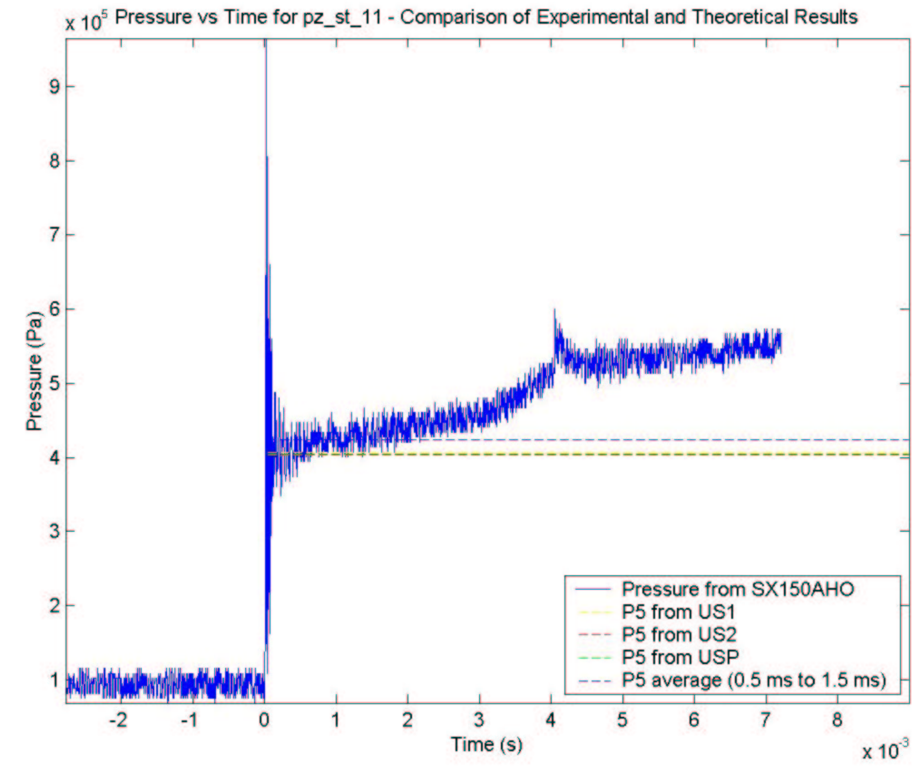
x 10^5 Pressure vs Time for pz_st_11 - Comparison of Experimental and Theoretical Results
Pressure (Pa)
Time (s)
x 10^-3
Pressure from SX150AHO
P5 from US1
P5 from US2
P5 from USP
P5 average (0.5 ms to 1.5 ms)

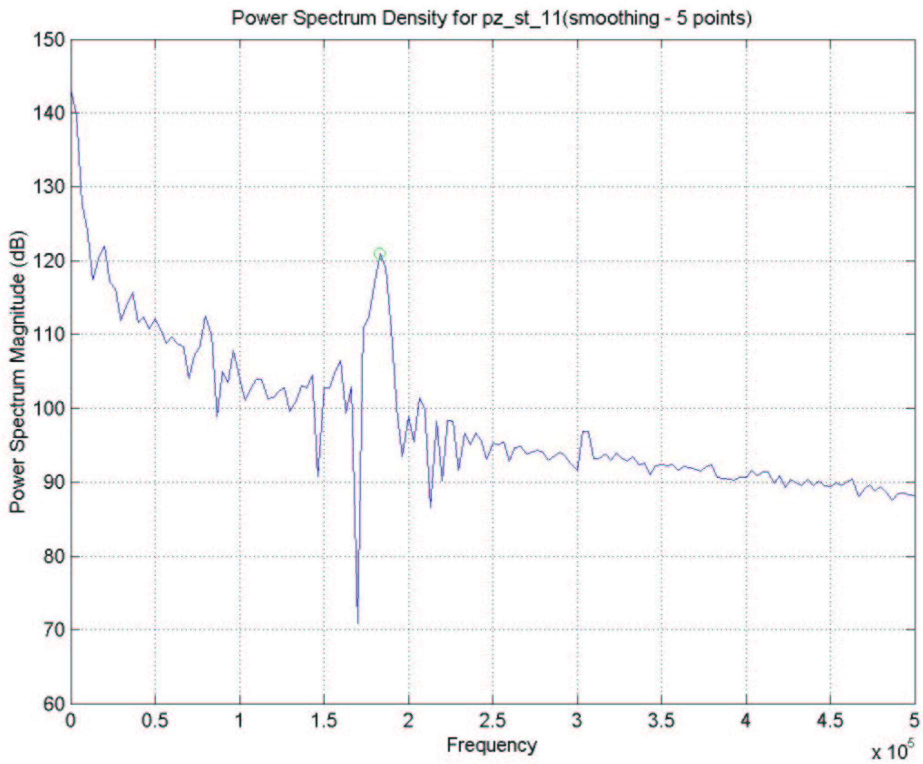
Power Spectrum Density for pz_st_11(smoothing - 5 points)
Power Spectrum Magnitude (dB)
Frequency
x 10^5

E.1.12 Shock Tube Test 12

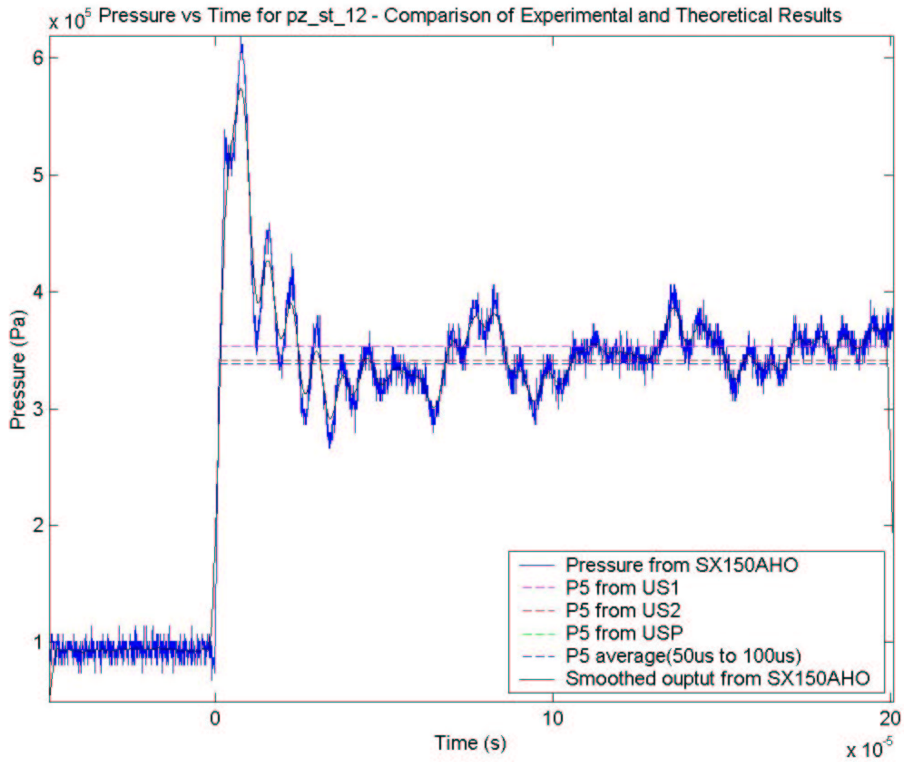

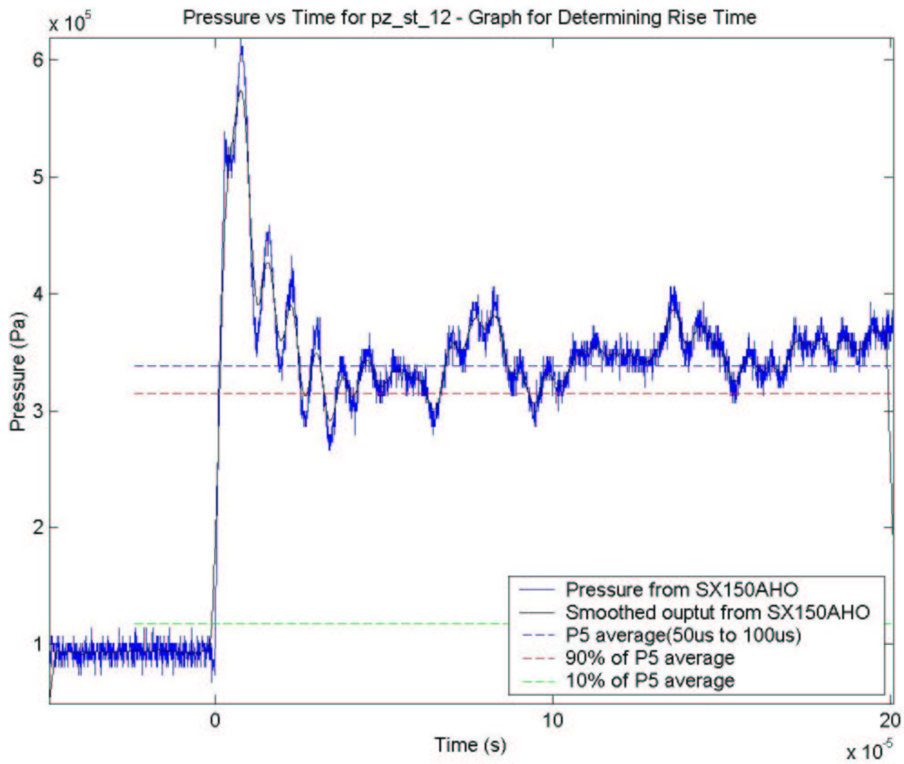

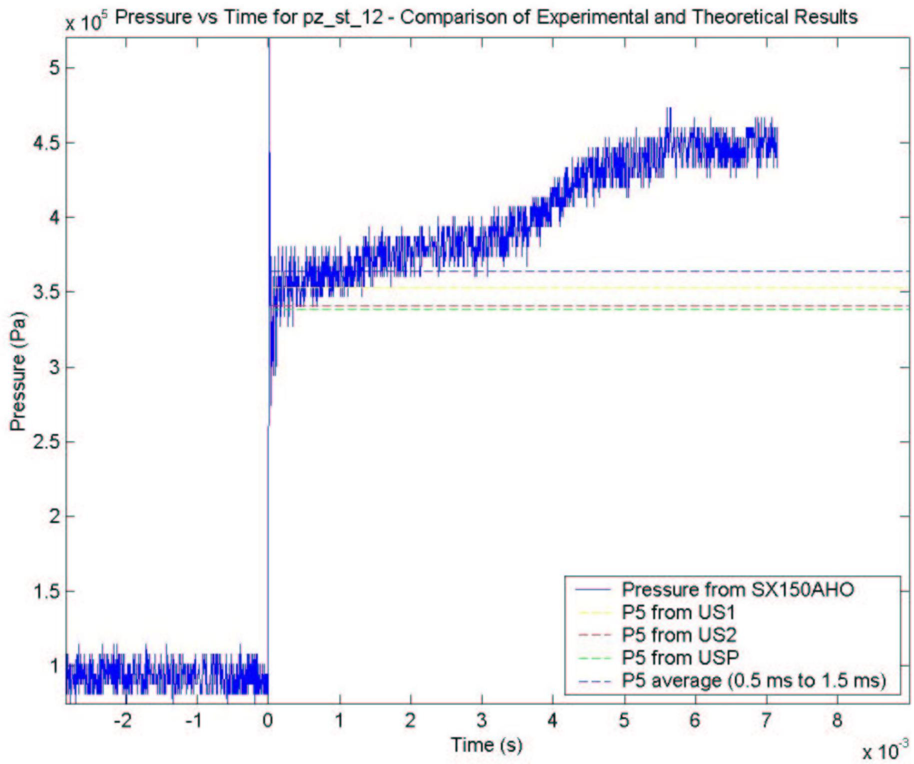
x 10^5 Pressure vs Time for pz_st_12 - Comparison of Experimental and Theoretical Results
Pressure (Pa)
Time (s)
x 10^-3
Pressure from SX150AHO
P5 from US1
P5 from US2
P5 from USP
P5 average (0.5 ms to 1.5 ms)
5
4.5
4
3.5
3
2.5
2
1.5
1
-2
-1
0
1
2
3
4
5
6
7
8

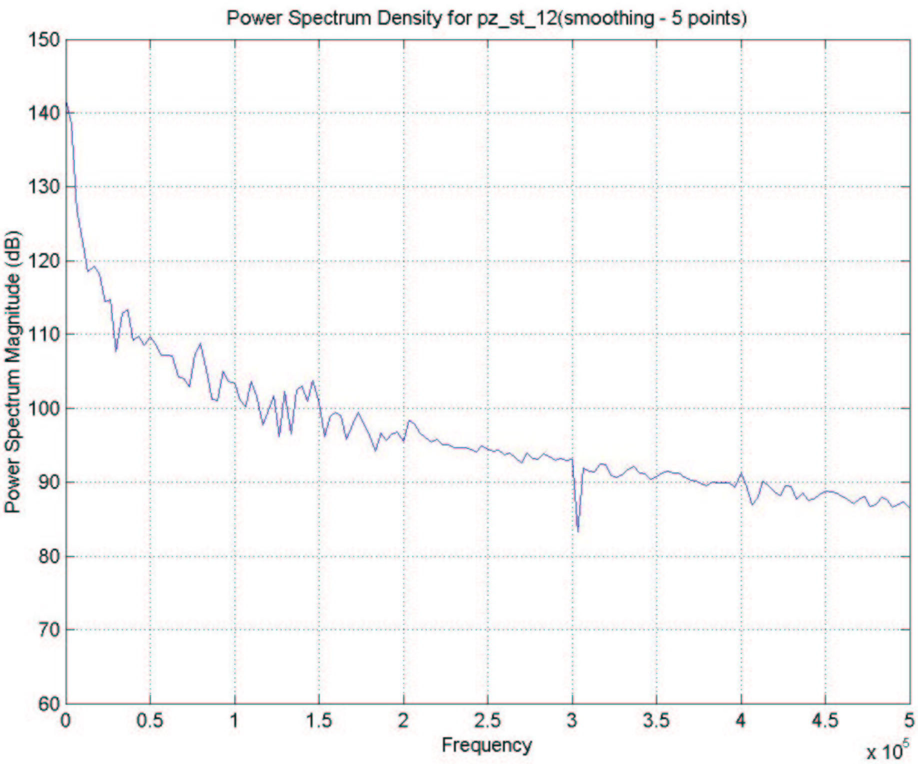
Power Spectrum Density for pz_st_12(smoothing - 5 points)
Power Spectrum Magnitude (dB)
Frequency
x 10^5
150
140
130
120
110
100
90
80
70
60
0
0.5
1
1.5
2
2.5
3
3.5
4
4.5
5

E.1.13 Shock Tube Test 13

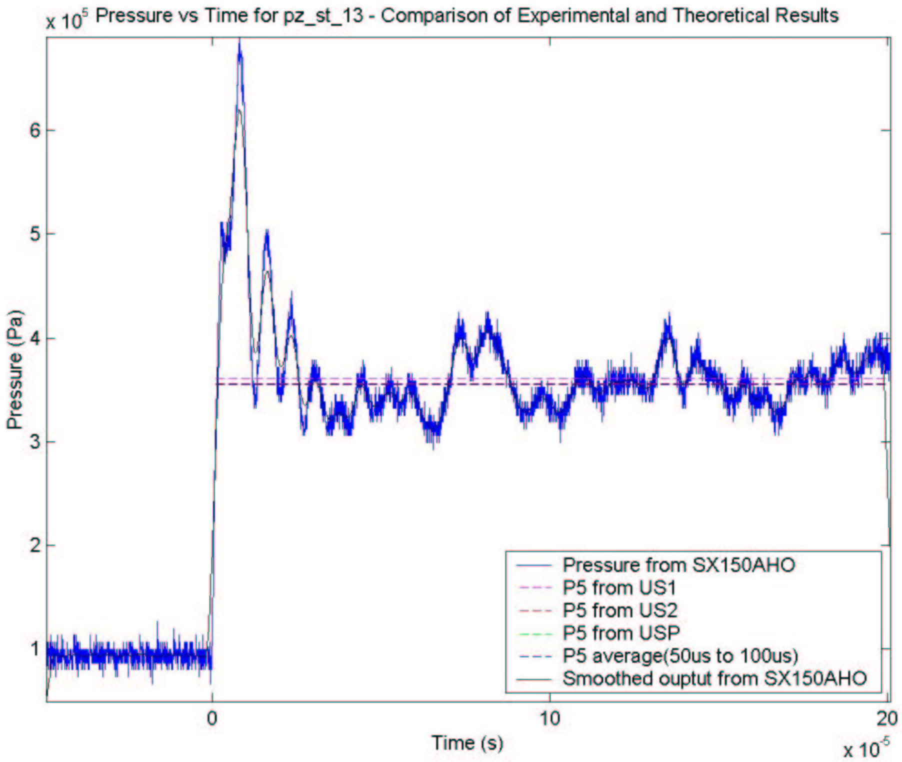

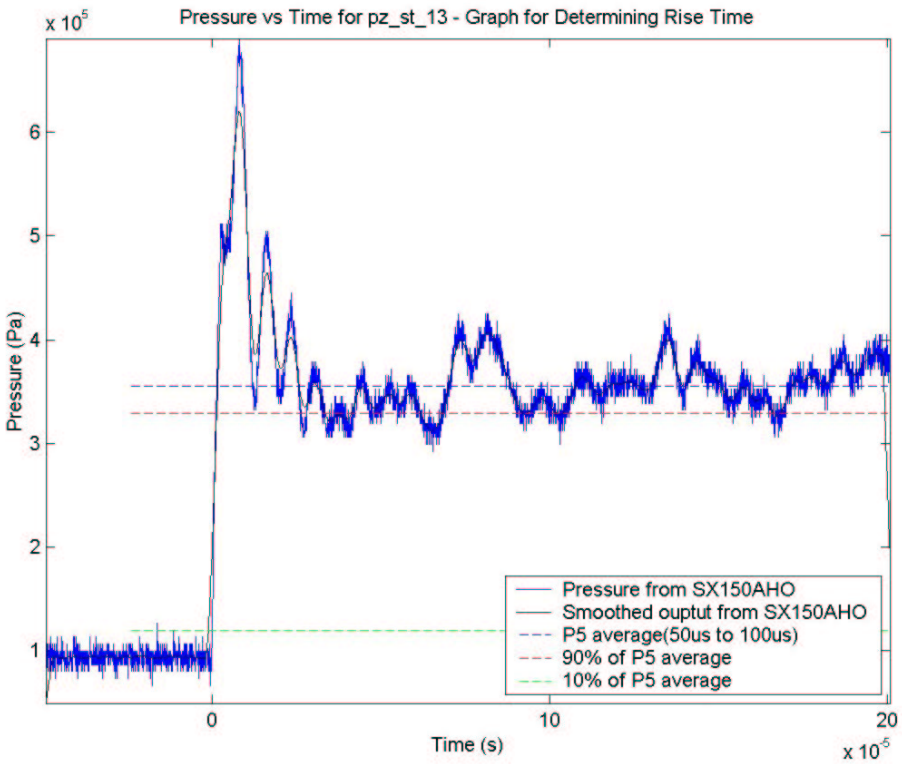

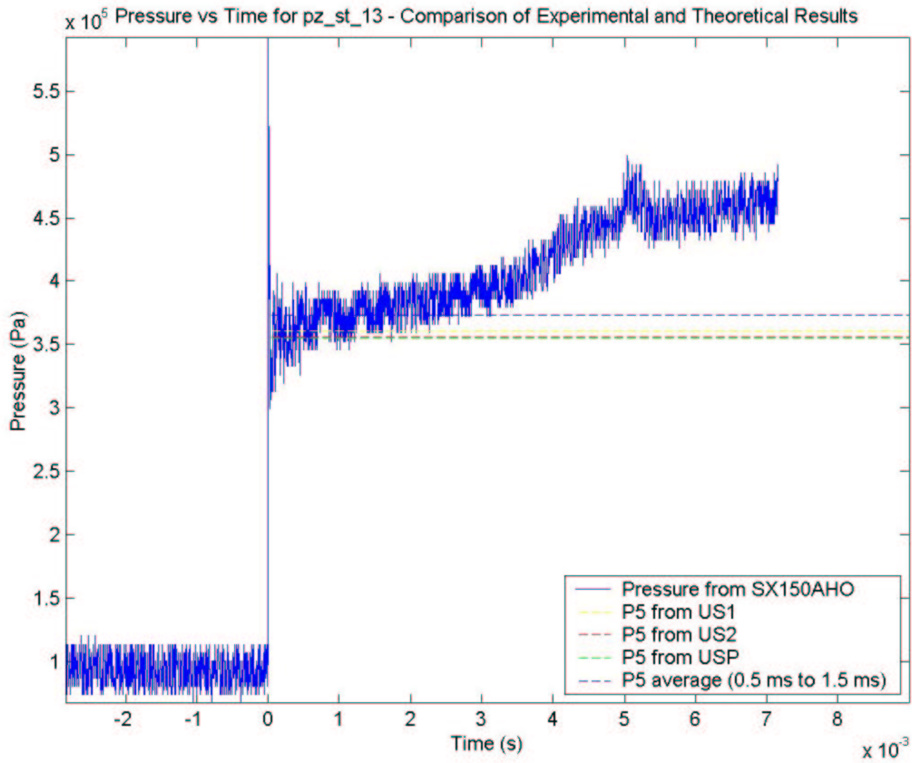
x 10^5 Pressure vs Time for pz_st_13 - Comparison of Experimental and Theoretical Results
Pressure (Pa)
Time (s)
x 10^-3
Pressure from SX150AHO
P5 from US1
P5 from US2
P5 from USP
P5 average (0.5 ms to 1.5 ms)

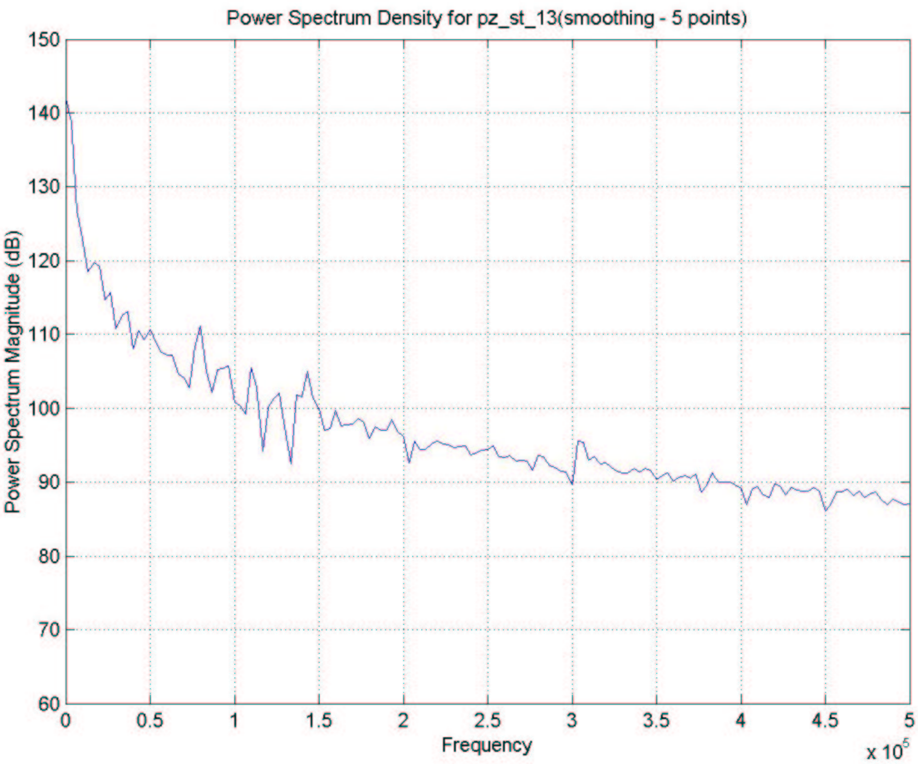
Power Spectrum Density for pz_st_13(smoothing - 5 points)
Power Spectrum Magnitude (dB)
Frequency
x 10^5

E.1.14 Shock Tube Test 14

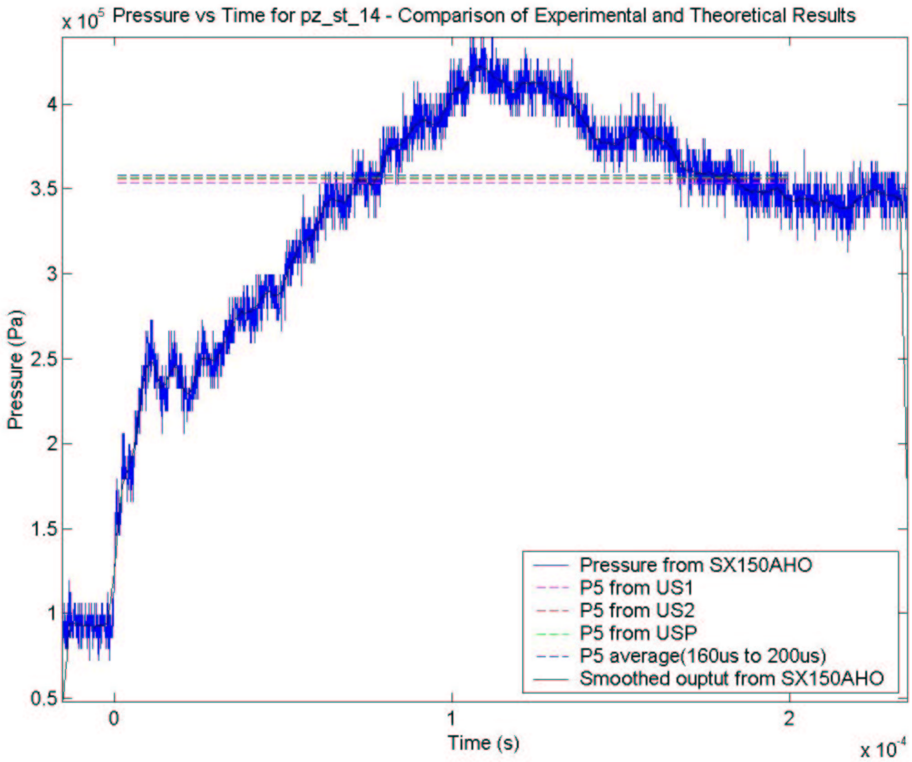

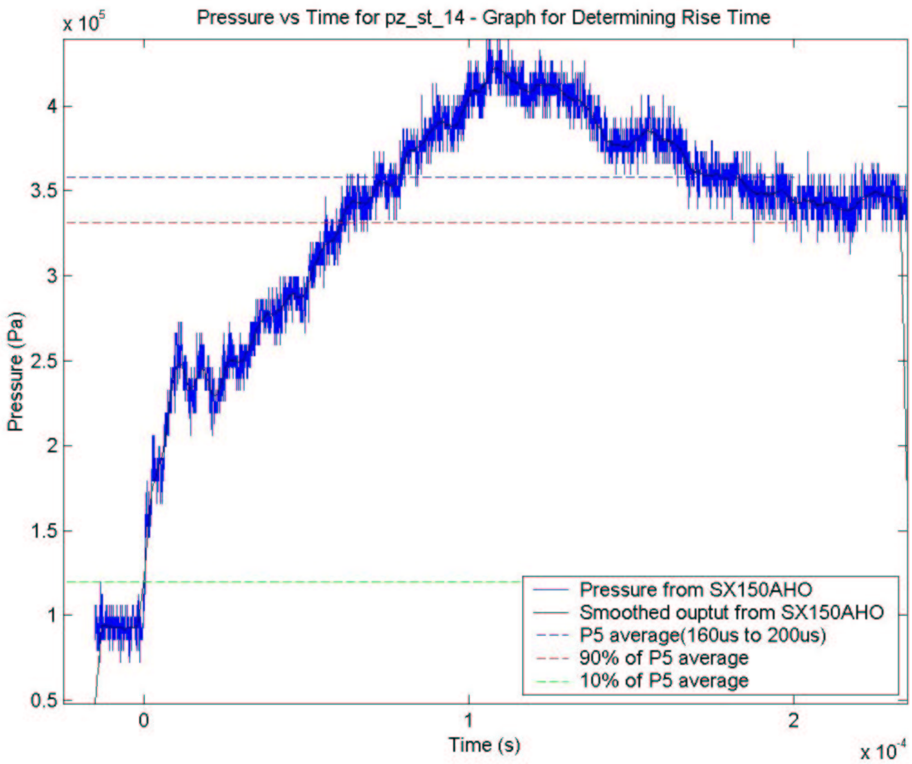

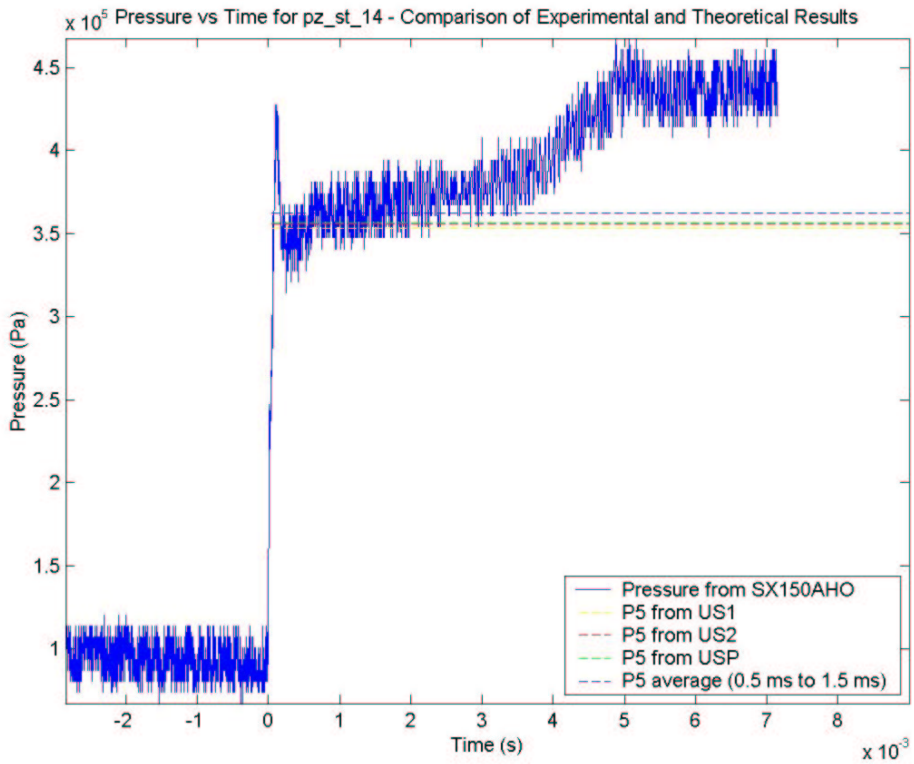
x 10^5 Pressure vs Time for pz_st_14 - Comparison of Experimental and Theoretical Results
Pressure (Pa)
Time (s)
x 10^-3
Pressure from SX150AHO
P5 from US1
P5 from US2
P5 from USP
P5 average (0.5 ms to 1.5 ms)

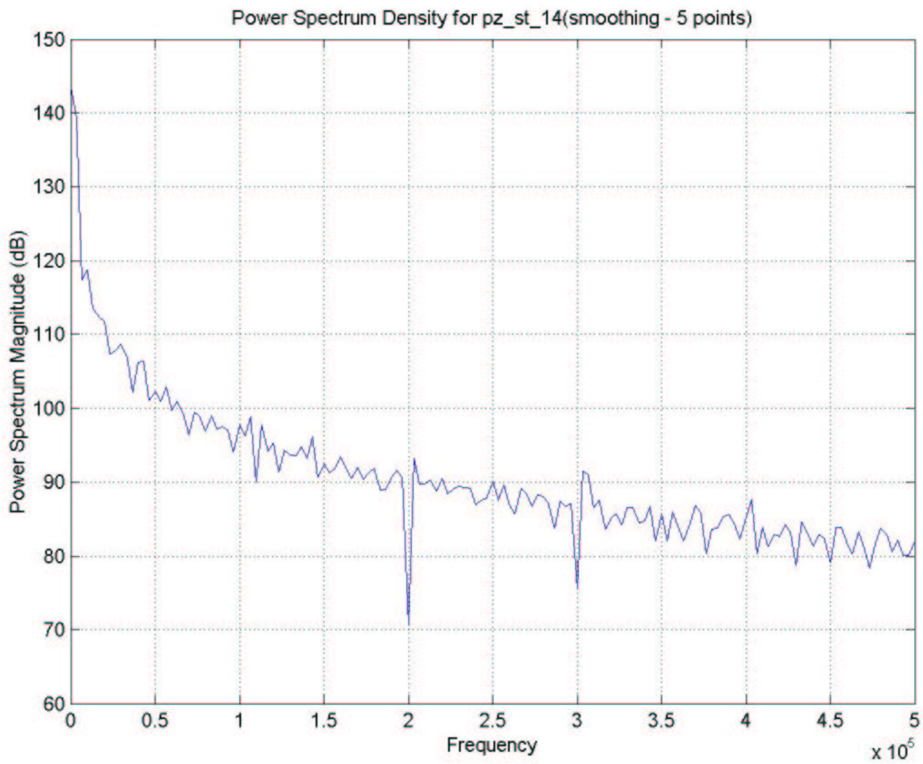
Power Spectrum Density for pz_st_14(smoothing - 5 points)
Power Spectrum Magnitude (dB)
Frequency
x 10^5

E.1.15 Shock Tube Test 15

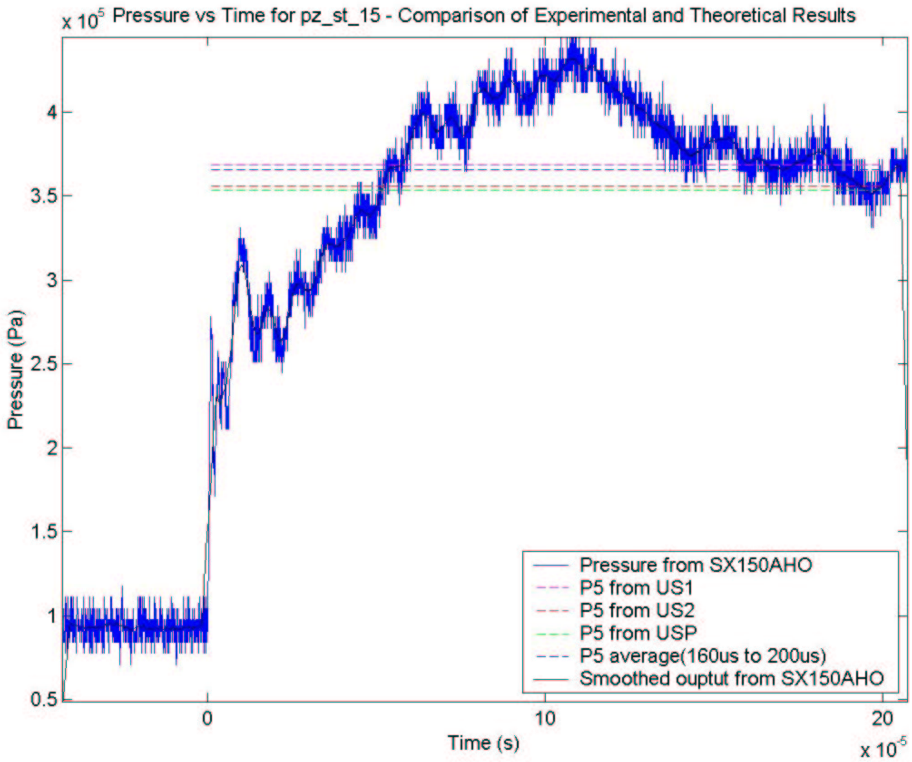

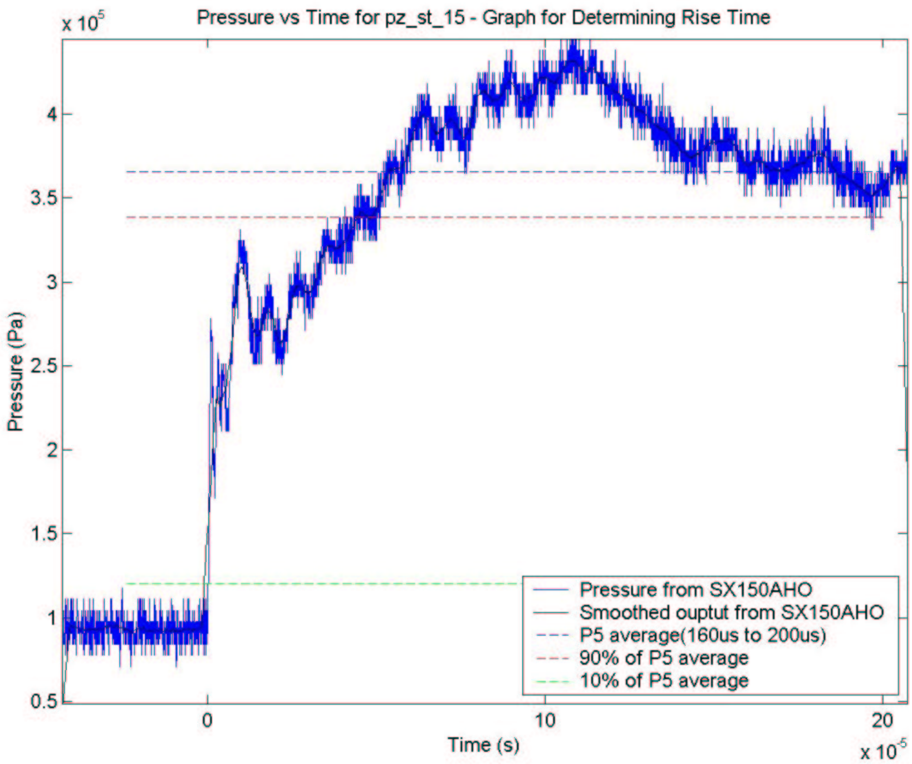

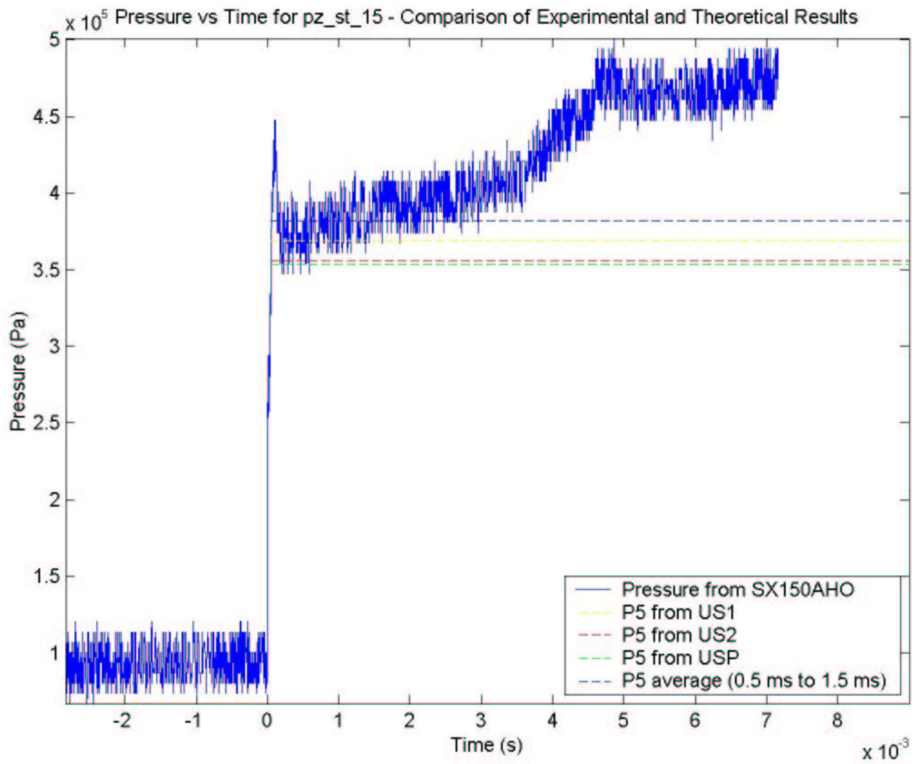
x 10^5 Pressure vs Time for pz_st_15 - Comparison of Experimental and Theoretical Results
Pressure (Pa)
Time (s)
x 10^-3
Pressure from SX150AHO
P5 from US1
P5 from US2
P5 from USP
P5 average (0.5 ms to 1.5 ms)
5
4.5
4
3.5
3
2.5
2
1.5
1
-2
-1
0
1
2
3
4
5
6
7
8

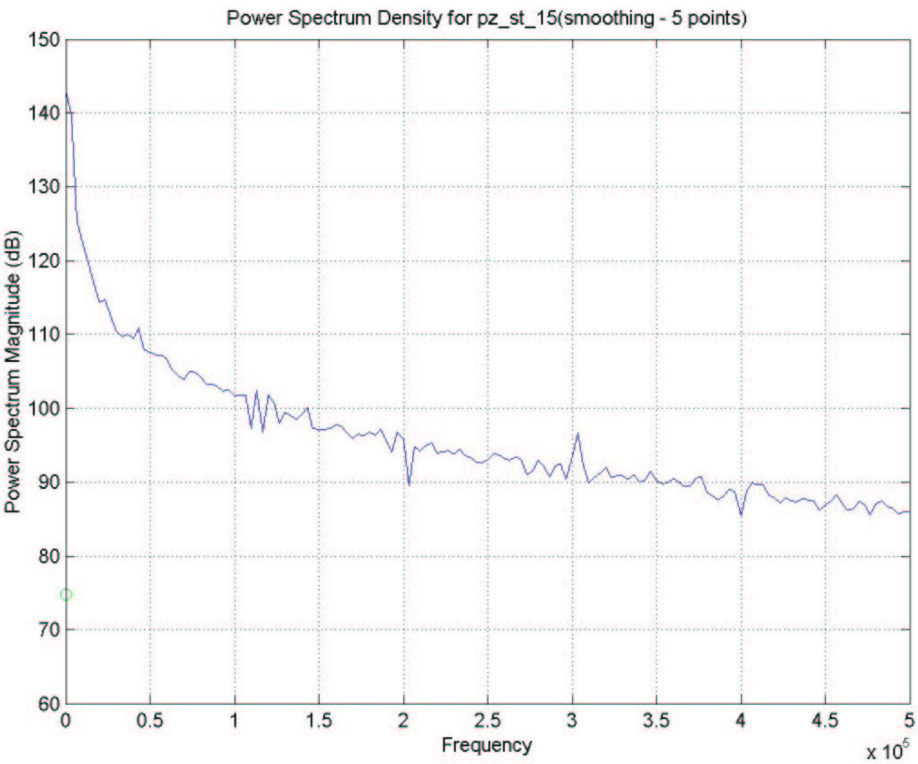
Power Spectrum Density for pz_st_15(smoothing - 5 points)
Power Spectrum Magnitude (dB)
Frequency
x 10^5
150
140
130
120
110
100
90
80
70
60
0
0.5
1
1.5
2
2.5
3
3.5
4
4.5
5

E.1.16 Shock Tube Test 16

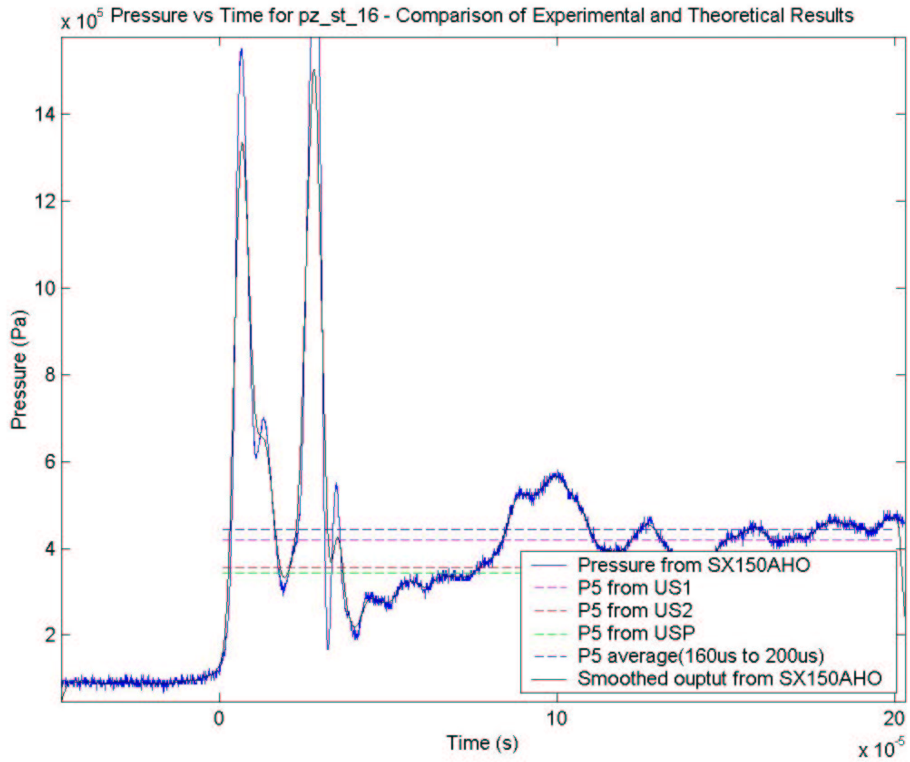

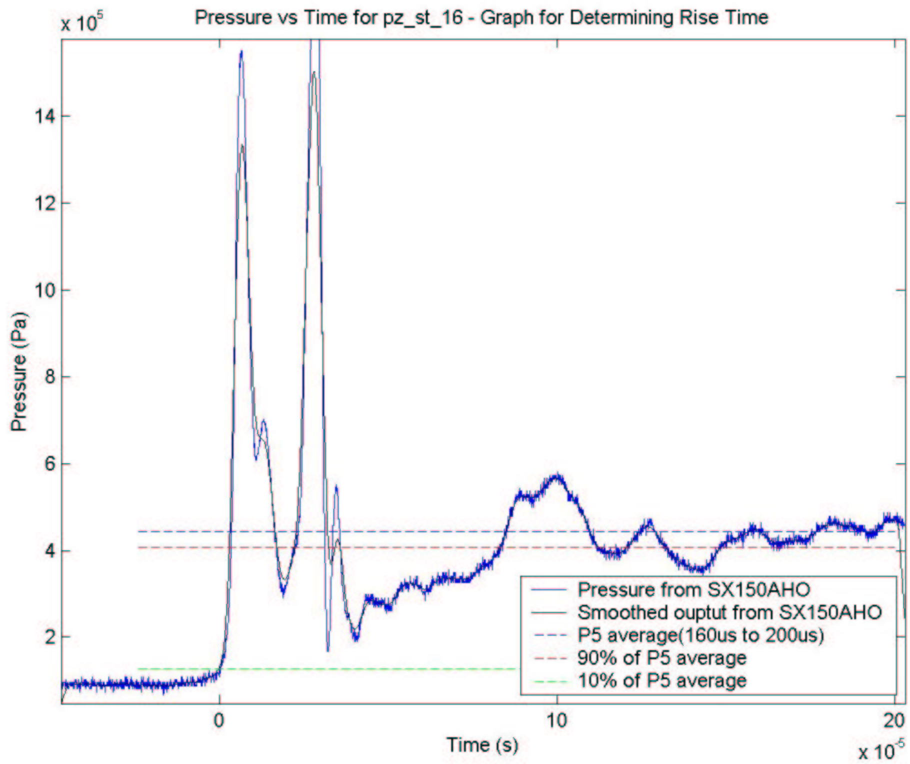

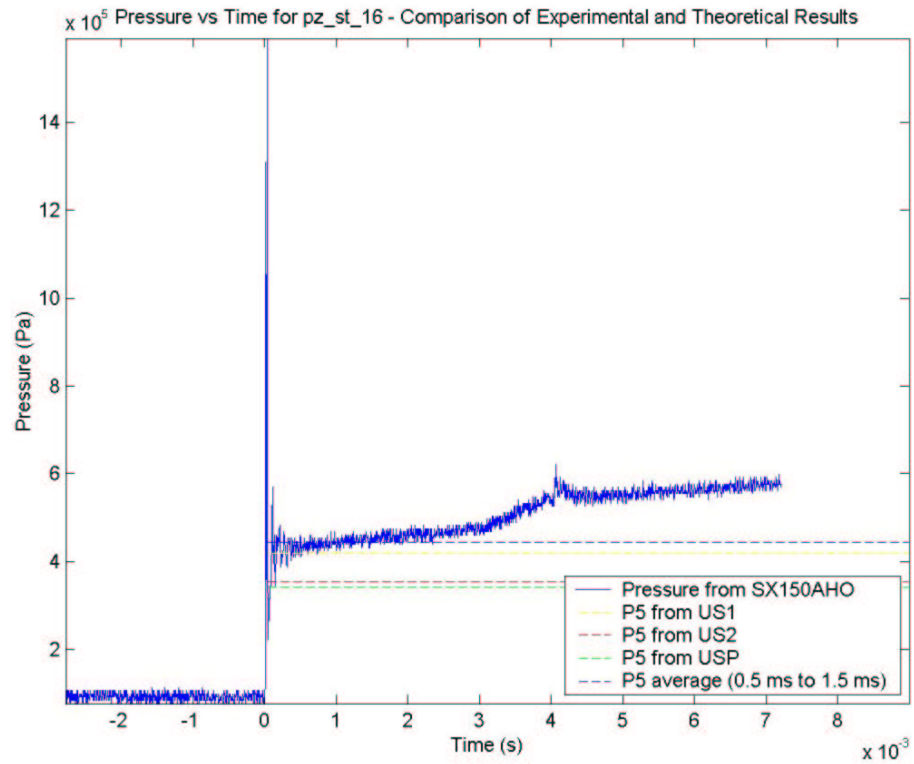
x 10^5 Pressure vs Time for pz_st_16 - Comparison of Experimental and Theoretical Results
Pressure (Pa)
Time (s)
x 10^-3
Pressure from SX150AHO
P5 from US1
P5 from US2
P5 from USP
P5 average (0.5 ms to 1.5 ms)

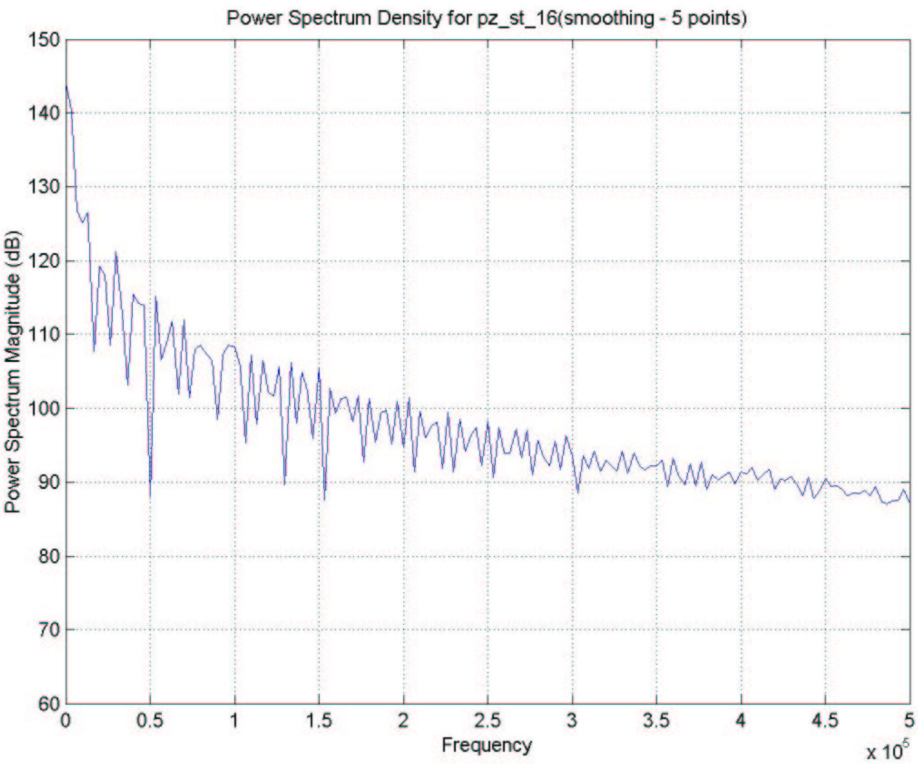
Power Spectrum Density for pz_st_16(smoothing - 5 points)
Power Spectrum Magnitude (dB)
Frequency
x 10^5

E.1.17 Shock Tube Test 17

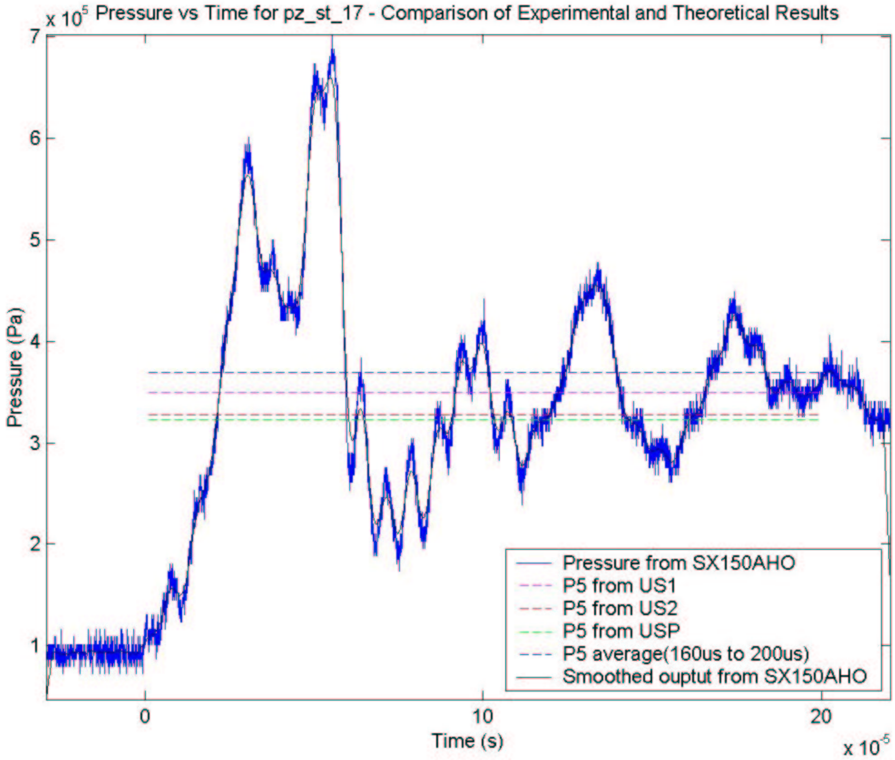

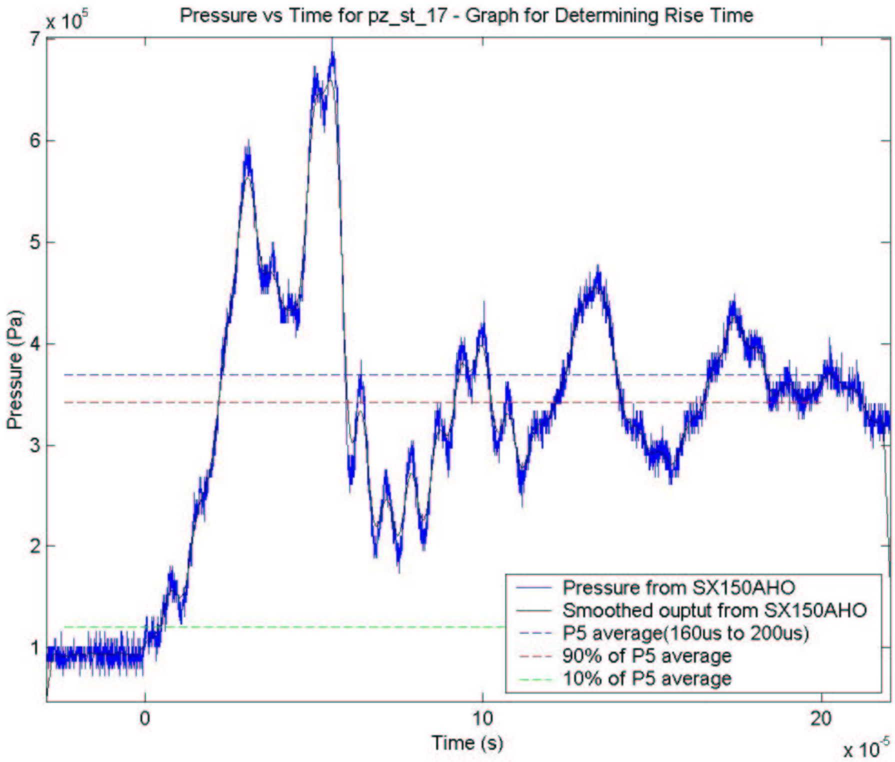

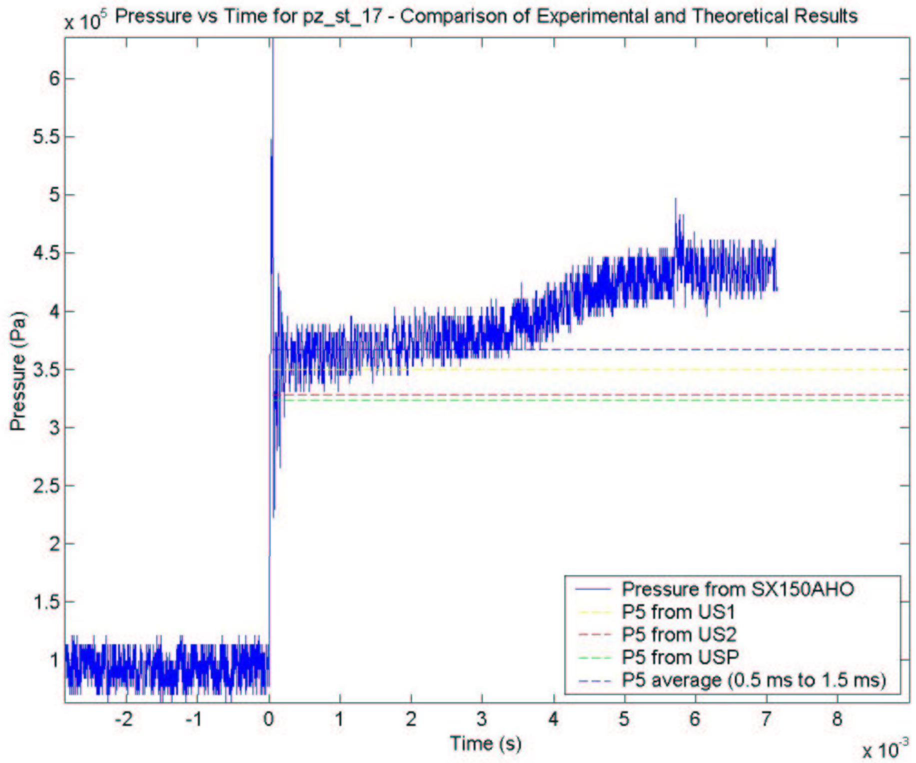
x 10^5 Pressure vs Time for pz_st_17 - Comparison of Experimental and Theoretical Results
Pressure (Pa)
Time (s)
x 10^-3
Pressure from SX150AHO
P5 from US1
P5 from US2
P5 from USP
P5 average (0.5 ms to 1.5 ms)

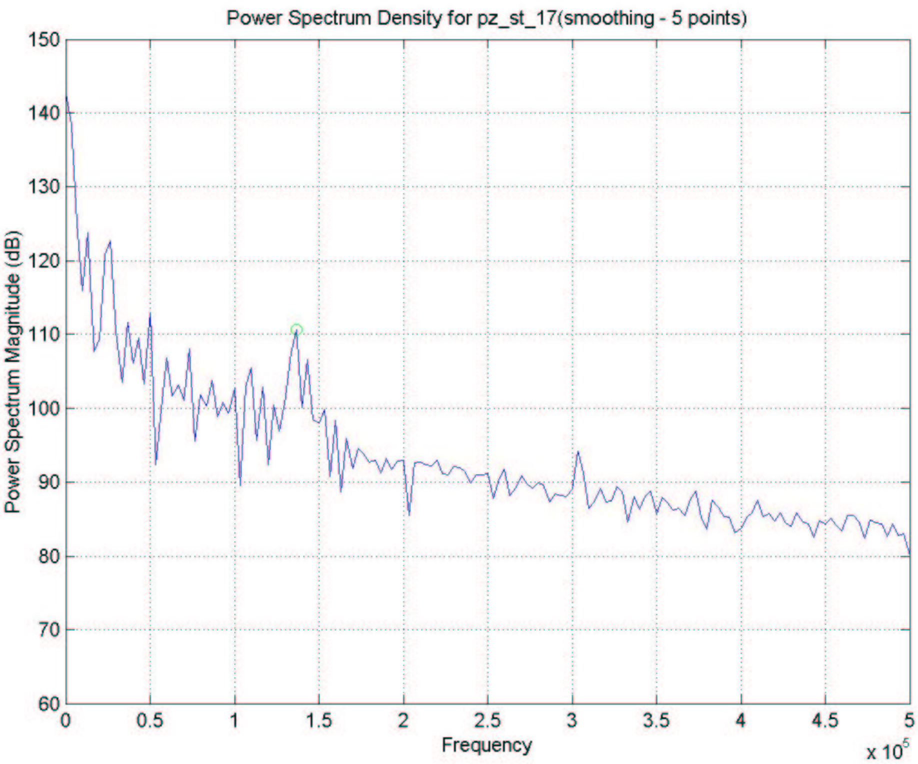
Power Spectrum Density for pz_st_17(smoothing - 5 points)
Power Spectrum Magnitude (dB)
Frequency
x 10^5